

**CRUCIFORM PI-SYSTEMS: NOVEL TWO-DIMENSIONAL CROSS-  
CONJUGATED CHROMOPHORES POSSESSING SPATIALLY SEPARATED  
FRONTIER MOLECULAR ORBITALS**

A Dissertation  
Presented to  
The Academic Faculty

By

Anthony Joseph Zucchero

In Partial Fulfillment  
Of the Requirements for the Degree  
Doctor of Philosophy in Chemistry

Georgia Institute of Technology

December, 2009

**CRUCIFORM PI-SYSTEMS: NOVEL TWO-DIMENSIONAL CROSS-  
CONJUGATED CHROMOPHORES POSSESSING SPATIALLY SEPARATED  
FRONTIER MOLECULAR ORBITALS**

Dr. Uwe H.F. Bunz, Advisor  
School of Chemistry and Biochemistry  
*Georgia Institute of Technology*

Dr. Laren M. Tolbert  
School of Chemistry and Biochemistry  
*Georgia Institute of Technology*

Dr. Joseph W. Perry  
School of Chemistry and Biochemistry  
*Georgia Institute of Technology*

Dr. David M. Collard  
School of Chemistry and Biochemistry  
*Georgia Institute of Technology*

Dr. Anselm Griffin  
School of Polymer, Textile, and Fiber Engineering  
*Georgia Institute of Technology*

Date Approved: December 3, 2009

## ACKNOWLEDGEMENTS

First, I must thank my advisor, Uwe Bunz, for his mentorship and friendship. His intellectual curiosity, creativity, and passion for science are an inspiration to me as a young researcher. He has worked tirelessly to create an unmatched environment for his graduate students, providing a wealth of stimulating projects as well as the intellectual freedom to explore them fully. I could not envision a more productive or supportive environment in which to spend a graduate career.

Thanks also to the current and former members of my committee – Laren Tolbert, David Collard, Joseph Perry, Anselm Griffin, and Marcus Weck – for graciously giving their time and advice whenever needed. Special thanks to Laren Tolbert, Joe Perry, and Marcus Weck for being productive and supportive collaborators. Without your efforts, much of the work presented in thesis would not have been possible.

Also, I must thank the members of the Bunz group – past and present – who have made my stay in the Bunz group memorable and productive: Shaobin Miao, Ik-Bum Kim, James Wilson, Carlito Bangcuyo, Brian Englert, Jake Leech, Sandra Shotwell, Selma Bakbak, Yiquing Wang, Ronnie Phillips, Scott Brombosz, Psaras McGrier, Juan Tolosa, Drew Zappas, Chris Kub, Ewelina Kielely, Jonny Bryant, Steven Hayden, Anthony Appleton, Nancy Berger, and Imani Jones. In particular, I owe a debt of gratitude to James who began our group's exploration of cruciform fluorophores and provided me with a jump start on my graduate research. Special thanks to Ronnie who entered the Bunz group with me – I could not imagine a better lab mate to overlap with. Thanks also to Scott; I will miss our long lunches and conversations when I move on.

Thanks to Psaras and Juan for their hard work which has contributed so much to our understanding of cruciforms. I wish all of you continued success in whatever paths you may choose.

My research at Georgia Tech has given me the opportunity to collaborate with an amazing group of students and faculty members. Thanks to Nisan Siegel and Joseph Perry for their in depth examination of the two-photon absorption of cruciform chromophores. Warren Gerhardt, Clint South, and Marcus Weck also deserve recognition for their work constructing coordination polymers using cruciforms as monomers. Thanks to Rebecca Shiels and Chris Jones for providing me with the silica materials used as solid supports for proof-of-principle sensory investigations. Thanks also to Martina Hauck, Jan Schönhaber, and Thomas Müller – their efforts made possible our examination of phenothiazine-substituted cruciforms. Finally, I have to recognize the substantial contributions of Kyril Solntsev and Laren Tolbert; your thoughtful suggestions, helpful discussions, and research efforts have greatly expanded my personal understanding of photophysics as well as our understanding of the cruciforms.

As I complete my work at Georgia Tech, I cannot help but recall the many formative experiences which made it possible for me to be where I am today. My years at Saint Louis Priory School shaped my character and taught me the fundamental skills of writing, public speaking, and critical thinking. In particular, I am grateful for the many members of the monastic community – especially Father Bede Price, OSB – who demonstrate daily through their life the importance of dedication, learning, and moral character. Also, special thanks to Thomas Tuthill, an unforgivable classics teacher and model *homo universalis*; in my six years at Priory, I witnessed a classics teacher derive

the quadratic formula, build a harpsichord, and study the wildflowers on the slopes of Cadillac Mountain. Though I may not remember all the Latin he taught me, I'll never forget his passion for knowledge and his efforts to make my stay at Priory as meaningful as possible.

I am also grateful for my years as an undergraduate at the University of the South. The Mountain gave me a strong liberal arts education along with a wealth of friends and memories. I am deeply grateful to my undergraduate research advisor, Robert Bachman, who encouraged me, shared his love for learning, and taught me how to be a successful researcher. I also have to thank the late Edward Kirven, my organic chemistry professor and academic advisor at Sewanee. Without them, I would not be where I am today. Thanks also to John Shibata, Deon Miles, and Richard Summers in the Department of Chemistry for all of their encouragement and support.

To my many friends who have supported me at Sewanee and at Tech. To Scott Knittle, Charles Jenkins, Jimmy Salter, Erle Newton, Stuart Chapman, Brett Bares, Todd Wass, Matt Pitner, Justin Gardner, Jay Kington, and all others whose names escape me at this moment. Special thanks also to my cousin Steve Sumner who has always been like a brother to me.

I am also eternally thankful for my family which instilled in me from an early age a love and respect for education. I am grateful to my mother and father, both of whom selflessly sacrificed to provide me every advantage and are always there in times of need. My father - a chemist and pharmacist by training - certainly inspired me to explore science. It is fair to say that I have inherited his diverse intellectual curiosity. My mother - always there on good days and bad - has given everything for me; I can never express

my gratitude for all she has done. My sister Theresa, who holds a Ph.D. in genetics, isn't as bad as our childhood squabbles would suggest. She famously predicted in 2005 that “this would be me someday” – I guess she was right.

Finally, thanks to my wife Elizabeth Wolf Zuccherro. You deserve my undying gratitude for standing by my side through all my trials over the last seven years. I could never have made it without you. I only hope I can be as supportive of you in the future.

## TABLE OF CONTENTS

ACKNOWLEDGEMENTS.....	iii
LIST OF TABLES.....	xi
LIST OF FIGURES.....	xiii
LIST OF SCHEMES.....	xviii
LIST OF ABBREVIATIONS.....	xix
SUMMARY.....	xxiii
CHAPTER 1 Cruciforms in Context.....	1
1.1 Introduction.....	1
1.2 Serendipity at Work: The PPE Problem.....	2
1.3 From Polymers to Small Molecules.....	3
1.4 Scope of Dissertation.....	5
1.5 References and Notes.....	6
CHAPTER 2 Synthesis and Photophysical Properties of Cruciforms.....	11
2.1 Introduction.....	11
2.2 Synthetic Methodology.....	12
2.3 Photophysical Properties of <b>2.1-2.8a</b> .....	14
2.4 FMO Structure of XFs.....	20
2.5 Conclusions.....	22
2.6 Experimental.....	23
2.7 References and Notes.....	35

CHAPTER 3 Cruciforms as Functional Fluorophores.....	37
3.1 Introduction.....	37
3.2 The Importance of FMO separation.....	40
3.3 XFs Exhibiting a Two-Stage Fluorescence Response: A Case Study.....	41
3.4 Response of XFs towards Metal Cations and TFA.....	45
3.4.1 Spectroscopic Data for <b>3.1-3.7</b> upon Addition of Trifluoroacetic Acid.....	45
3.4.2 Comparing Zn <sup>2+</sup> and TFA – Elucidating the Nature of Analyte Interactions.....	49
3.4.3 Fluorescence Response of XFs to the Triflates of Mg <sup>2+</sup> , Ca <sup>2+</sup> , and Mn <sup>2+</sup> .....	54
3.5 Conclusions.....	57
3.6 Experimental.....	58
3.7 References and Notes.....	60
 CHAPTER 4 Phenothiazine-Substituted Cruciforms: Synthesis and Metallochromic Properties.....	 63
4.1 Introduction.....	63
4.2 Results and Discussion.....	63
4.2.1 Synthesis.....	63
4.2.2 Spectroscopic properties and quantum chemical calculations.....	65
4.2.3 Titration studies of <b>4.5-4.7</b> using trifluoroacetic acid in CH <sub>2</sub> Cl <sub>2</sub> .....	72
4.2.4 Interaction of the XFs with metal salts.....	78
4.3 Conclusions.....	83
4.4 Experimental.....	85
4.5 References and Notes.....	94

CHAPTER 5 Synthesis and Characterization of Water-Soluble XFs.....	96
5.1 Introduction.....	96
5.2 Results and Discussion.....	98
5.2.1 Synthesis of XFs.....	98
5.2.2 Spectroscopic properties of cruciforms <b>5a-7a</b> and <b>8</b> in CH <sub>2</sub> Cl <sub>2</sub> .....	99
5.2.3 Spectroscopic properties of cruciforms <b>5.5b-5.7b</b> in water.....	104
5.2.4 Investigation of the pH dependency of absorption and emission in <b>5.5b-5.7b</b> .....	109
5.2.5 Metal-responsive properties of <b>5.5b-5.7b</b> in aqueous buffered solution.....	111
5.3 Conclusions.....	116
5.4 Experimental.....	117
5.5 References and Notes.....	123
CHAPTER 6 Supramolecular Cruciforms.....	129
6.1 Introduction.....	129
6.2 Results and Discussion.....	134
6.3 Conclusions.....	149
6.4 Experimental.....	150
6.5 References and Notes.....	158
CHAPTER 7 Cruciform-Silica Hybrid Materials.....	164
7.1 Introduction.....	164
7.2 Results and Discussion.....	165
7.2.1 Synthesis of mesoporous silica supports.....	165

7.2.2 Spectroscopic properties of cruciforms <b>7.1-7.7</b> in the presence of microstructured functionalized silica supports.....	167
7.2.3 Sensory responses of XF-functionalized silica microstructures towards representative volatile organic compounds (VOCs).....	177
7.3 Conclusions.....	179
7.4 Experimental.....	179
7.5 References and Notes.....	186
 CHAPTER 8 Conclusions and Future Directions.....	 189
8.1 Summary and Conclusions.....	189
8.2 Current and Future Research Directions.....	192
8.2.1 Expanding the color palate: Achieving new fluorescence responses.....	192
8.2.2 Photophysical behavior and sensory responses of distyrylbenzenes and arylethynylbenzenes: Probing the properties of XF building blocks.....	194
8.2.3 Incorporation of cross-conjugated motifs into water soluble PPEs: Towards red emissive PPEs.....	196
8.3 References and Notes.....	198

## LIST OF TABLES

Table 2.1. Absorption and emission data of XFs <b>2.1-2.8a</b> in CH <sub>2</sub> Cl <sub>2</sub> and hexanes.....	15
Table 2.2. Quantum yield and fluorescence lifetime of <b>2.1-2.7</b> in CHCl <sub>3</sub> .....	16
Table 3.1. Effect of TFA on the photophysical properties of <b>3.1-3.7</b> .....	47
Table 3.2. Photophysical properties of <b>3.1-3.7</b> upon addition of TFA and Zn(OTf) <sub>2</sub> .....	50
Table 3.3. Photophysical properties of <b>3.1-3.7</b> upon addition of Mg <sup>2+</sup> , Mn <sup>2+</sup> , and Ca <sup>2+</sup> .....	55
Table 4.1. Spectroscopic and quantum chemical data for the cruciforms <b>4.5-4.9</b> in dichloromethane.....	67
Table 4.2. Spectroscopic data of <b>4.5-4.9</b> in the presence of divalent metal ions in dichloromethane.....	81
Table 5.1. Absorption and emission data of XFs <b>5.5a-5.7a</b> and <b>5.8</b> in CH <sub>2</sub> Cl <sub>2</sub> in neutral, acid, and basic conditions.....	100
Table 5.2. Absorption and emission data of XFs <b>5.5b-5.7b</b> in water (Phosphate Buffer, pH = 7.0).....	108
Table 5.3. Emissive lifetime data of cruciforms <b>5.5b-5.7b</b> .....	112
Table 6.1. ITC <i>K<sub>a</sub></i> values and approximate degree of polymerization (DP) of each supramolecular complex.....	137
Table 6.2. Summary of the changes in emission observed upon the addition of increasing equivalents of <b>6.2</b> or <b>6.4</b> to <b>6.1</b> or <b>6.3</b> . The concentration of XF in all samples was 0.0445 mM in a mixture of CHCl <sub>3</sub> and DMSO (95:5).....	141
Table 6.3. Summary of the changes in emission observed upon the addition of <b>6.5</b> or <b>6.6</b> to <b>6.1</b> or <b>6.3</b> . The concentration of the cruciform in all samples was 0.0445 mM in a mixture of CHCl <sub>3</sub> : DMSO (95:5).....	141
Table 6.4. Preparation of spectroscopic solutions of <b>6.1•6.2</b> .....	153
Table 6.5. Preparation of spectroscopic solutions of <b>6.3•6.2</b> .....	154
Table 6.6. Preparation of spectroscopic solutions of <b>6.1•6.4</b> .....	155

Table 6.7. Preparation of spectroscopic solutions of <b>6.3•6.4</b> .....	155
Table 6.8. Preparation of spectroscopic solutions of <b>6.1•6.5</b> .....	156
Table 6.9. Preparation of spectroscopic solutions of <b>6.1•6.6</b> .....	156
Table 6.10. Preparation of spectroscopic solutions of <b>6.3•6.5</b> .....	157
Table 6.11. Preparation of spectroscopic solutions of <b>6.3•6.6</b> .....	158
Table 7.1. Tabulated emission data of XFs <b>7.1-7.7</b> in the solid state, solution, and complexed with functionalized silica. For reference, emissions of <b>7.1-7.7</b> upon exposure to trifluoroacetic acid and n-hexylamine in toluene solution.....	170

## LIST OF FIGURES

Figure 1.1. Structure of several classes of conjugated polymers.....	3
Figure 1.2. Generalized structure of an XF.....	4
Figure 2.1. Structure of XFs <b>2.1-2.8</b> .....	12
Figure 2.2. Emission of XFs in dichloromethane under blacklight irradiation.....	14
Figure 2.3. Normalized absorption and emission of <b>2.1-2.7</b> in hexanes and dichloromethane.....	17
Figure 2.4. Normalized absorption and emission spectra of XFs in hexanes.....	18
Figure 2.5. Frontier molecular orbitals of <b>2.8b</b> and <b>2.7b</b> .....	21
Figure 2.6. Normalized absorption and emission spectra of a Class C and Class D XF.....	22
Figure 3.1. Structure of XFs <b>3.1-3.7</b> .....	39
Figure 3.2. Emission of <b>3.7</b> in CHCl <sub>3</sub> , upon addition of a small amount of Zn(OTf) <sub>2</sub> , and upon addition of a large excess of Zn(OTf) <sub>2</sub> .....	41
Figure 3.3. Absorption and emission of <b>3.7</b> in CH <sub>2</sub> Cl <sub>2</sub> upon exposure to increasing equivalents of Zn(OTf) <sub>2</sub> .....	42
Figure 3.4. Absorption and emission of <b>3.3</b> in CH <sub>2</sub> Cl <sub>2</sub> upon exposure to increasing equivalents of Zn(OTf) <sub>2</sub> .....	43
Figure 3.5. Absorption and emission of <b>3.2</b> in CH <sub>2</sub> Cl <sub>2</sub> upon exposure to increasing equivalents of Zn(OTf) <sub>2</sub> .....	43
Figure 3.6. Effect of metallation or protonation upon the FMOs and emission of <b>3.3</b> and <b>3.2</b> .....	44
Figure 3.7. Effect of metallation or protonation upon the FMOs and emission of <b>3.7</b> .....	44
Figure 3.8. Emission of <b>3.1-3.7</b> in CH <sub>2</sub> Cl <sub>2</sub> and upon addition of TFA, Mg(OTf) <sub>2</sub> , Zn(OTf) <sub>2</sub> , Mn(OTf) <sub>2</sub> , and Ca(OTf) <sub>2</sub> .....	46
Figure 3.9. Protonation of <b>3.7</b> in a THF/methanol mixture with TFA.....	48

Figure 3.10. Comparison of the observed photophysical responses of XFs <b>3.1-3.7</b> towards TFA and Zn(OTf) <sub>2</sub> .....	51
Figure 3.11. <sup>1</sup> H NMR spectra of <b>3.3</b> in CDCl <sub>3</sub> upon addition of Zn(OTf) <sub>2</sub> and TFA.....	53
Figure 3.12. Fluorescence of <b>3.1-3.7</b> in CHCl <sub>3</sub> upon addition of Zn(OTf) <sub>2</sub> and TFA.....	57
Figure 4.1. Synthesized phenothiazine-substituted XFs <b>4.5-4.9</b> .....	65
Figure 4.2. Structure and the packing of XF <b>4.5</b> in the solid state.....	66
Figure 4.3. Normalized absorption and emission spectra of the XFs <b>4.5-4.9</b> in dichloromethane.....	66
Figure 4.4. Molecular orbital plots of cruciforms <b>4.5'-4.7'</b> .....	69
Figure 4.5. Molecular orbital plots of the bisprotonated species <b>4.5'-(2H)<sup>+</sup></b> , <b>4.6'-(2H)<sup>+</sup></b> , and <b>4.7'-(2H)<sup>+</sup></b> .....	70
Figure 4.6. Absolute HOMO-LUMO positions from (B3LYP/6-31G**//6-31G*) calculations.....	71
Figure 4.7. Structure of XFs <b>4.10</b> and <b>4.11</b> .....	72
Figure 4.8. Absorption and emission spectra of XF <b>4.5</b> in the presence of increasing amounts of TFA.....	74
Figure 4.9. Absorption and emission spectra of XF <b>4.6</b> in the presence of increasing amounts of TFA.....	75
Figure 4.10. Absorption and emission spectra of XF <b>4.7</b> in the presence of increasing amounts of TFA.....	76
Figure 4.11. Normalized absorption and emission spectra of XF <b>4.5</b> in the presence of different metal cations.....	78
Figure 4.12. Normalized absorption and emission spectra of XF <b>4.6</b> in the presence of different metal cations.....	79
Figure 4.13. Normalized absorption and emission spectra of XF <b>4.7</b> in the presence of different metal cations.....	79
Figure 4.14. Normalized absorption and emission spectra of XF <b>4.8</b> in the presence of different metal cations.....	79

Figure 4.15. Normalized absorption and emission spectra of XF <b>4.9</b> in the presence of different metal cations.....	80
Figure 4.16. Interaction of <b>4.7</b> and <b>4.5</b> with increasing amounts of Mg(OTf) <sub>2</sub> .....	81
Figure 4.17. Emission of <b>4.5-4.9</b> in CH <sub>2</sub> Cl <sub>2</sub> upon addition of various metal cations.....	84
Figure 5.1. Normalized absorption and emission spectra of <b>5.5a</b> , <b>5.6a</b> , <b>5.7a</b> , and <b>5.8</b> in CH <sub>2</sub> Cl <sub>2</sub> and after addition of TFA.....	101
Figure 5.2. Proposed excited state planarization of <b>5.7</b> .....	103
Figure 5.3. Overlaid normalized absorption and emission spectra of <b>5.5b</b> , <b>5.6b</b> , and <b>5.7b</b> in phosphate buffered aqueous solution and <b>5.8</b> in CH <sub>2</sub> Cl <sub>2</sub> .....	105
Figure 5.4. Absorption spectra of <b>5.6b</b> at concentrations of 1, 10 and 100 μmolL <sup>-1</sup> concentration in phosphate buffered aqueous solution.....	105
Figure 5.5. Emission of <b>5.5b</b> , <b>5.6b</b> , and <b>5.7b</b> in phosphate buffer at 1, 2, 5, 10, 25, 50 and 100 μmolL <sup>-1</sup> concentrations.....	106
Figure 5.6. Left: Emission spectra of <b>5.6b</b> under excitation at 325, 350, 375, 400, 425, 450, and 475 nm in phosphate buffered aqueous solution. Right: Normalized excitation spectra of <b>5.6b</b> at different wavelengths.....	107
Figure 5.7. Normalized absorption and emission spectra of <b>5.5b</b> , <b>5.6b</b> , and <b>5.7b</b> under neutral, acidic, and basic conditions.....	110
Figure 5.8. Qualitative results of the sensing of metal cations by the three XFs <b>5.5b-5.7b</b> in PIPES solution.....	111
Figure 5.9. Interaction of metal cations with XFs <b>5b-7b</b> (5 μmolL <sup>-1</sup> ) in PIPES solution.....	113
Figure 5.10. Interaction of metal cations with XFs <b>5b-7b</b> (50 μmolL <sup>-1</sup> ) in PIPES solution.....	114
Figure 6.1. Examples of mono- and bimetallic pincer complexes as supramolecular synthons in which E is a neutral two-electron donor and L can be a functional recognition unit.....	130
Figure 6.2. <sup>1</sup> H NMR spectra ( <i>d</i> <sub>7</sub> -DMF, 0.006 M) of the aromatic region depicting supramolecular assembly of <b>6.1</b> and <b>6.4</b> .....	135

Figure 6.3. Isotherm generated from the titration of <b>6.4</b> into <b>6.1</b> in DMF to yield <b>6.3P</b> .....	136
Figure 6.4. Monotopic Pd pincer complex <b>6.5</b> and monotopic Pt pincer complex <b>6.6</b> .....	138
Figure 6.5. Top: Plot of relative viscosity of bis-Pd pincer complexed materials <b>6.1P</b> and <b>6.2P</b> . Bottom: Plot of relative viscosity of bis-Pt pincer complexed materials <b>6.3P</b> and <b>6.4P</b> in DMF.....	139
Figure 6.6. Normalized emission of XFs <b>6.1</b> and <b>6.3</b> , and $\lambda_{\text{max}}$ of the furthest redshifted emissions of polymers <b>6.1P-6.4P</b> (precipitation seen at these maximum DPs) all at 0.0445mM. A) Emission of XF <b>6.1</b> (black trace), and Pd coordination polymers <b>6.1P</b> (blue trace) and <b>6.3P</b> (green trace). B) Emission of XF <b>6.3</b> (maroon trace), and Pt coordination polymers <b>6.2P</b> (yellow trace) and <b>6.4P</b> (orange trace).....	142
Figure 6.7. Emission spectra of <b>6.1</b> upon the addition of increasing equivalents of <b>6.2</b> .....	144
Figure 6.8. Emission spectra of <b>6.1</b> upon the addition of increasing equivalents of mono-Pd-pincer <b>6.5</b> .....	144
Figure 6.9. Emission of thin films of polymers <b>6.1P</b> , <b>6.2P</b> , and <b>6.4P</b> after the baseline-subtraction of a glass slide.....	145
Figure 6.10. Emission spectra of <b>6.3</b> upon the addition of increasing equivalents of <b>6.2</b> .....	145
Figure 6.11. Emission spectra of <b>6.3</b> upon the addition of increasing equivalents of mono-Pd-pincer <b>6.5</b> .....	146
Figure 6.12. Emission spectra of <b>6.3</b> upon the addition of increasing equivalents of <b>6.4</b> .....	147
Figure 6.13. Emission spectra of <b>6.3</b> upon the addition of increasing equivalents of mono-Pt-pincer <b>6.6</b> .....	148
Figure 6.14. Emission spectra of <b>6.1</b> upon the addition of increasing equivalents of <b>6.4</b> .....	148
Figure 6.15. Emission spectra of <b>6.1</b> upon the addition of increasing equivalents of mono-Pt-pincer <b>6.6</b> .....	149
Figure 7.1. Normalized emission spectra of <b>7.1-7.7</b> in toluene (top) and the solid state (bottom).....	168

Figure 7.2. Vials containing XFs <b>7.1-7.7</b> in toluene incubated with silicas ( <b>D</b> = Bare silica, <b>C</b> = Capped Silica, <b>A</b> = Acidic Silica, <b>B</b> = Basic Silica) for 24 hours. For comparison, column F shows XFs <b>7.1-7.7</b> in toluene exposed to TFA ( <b>7.1-7.5</b> ) or <i>n</i> -hexylamine ( <b>7.6, 7.7</b> ). Column E shows XFs <b>7.1-7.7</b> in a toluene solution.....	169
Figure 7.3. Normalized emission spectra of <b>7.1-7.7</b> supported on bare, capped, acidic, and basic silica. For comparison, the emission of XFs <b>7.1-7.7</b> in toluene, <b>7.1-7.5</b> with TFA, and <b>7.6-7.7</b> with <i>n</i> -hexylamine are shown.....	171
Figure 7.4. Schematic representation of the effect of protonation upon the FMOs and emission of XFs <b>7.1</b> (A, top left) and <b>7.3</b> (B, top right). C (bottom) shows the effect of deprotonation on the FMOs and emission of <b>7.6</b> .....	172
Figure 7.5. Fluorescence response of <b>7.1</b> supported on functionalized silica scaffold upon exposure to vapor analytes. The top spectra displays the emission of <b>7.1</b> supported on bare (green), capped (dark blue), acidic (orange), and basic (blue) silicas. Upon exposure to NEt <sub>3</sub> (middle) and trifluoroacetic acid (bottom) vapors, notable fluorescence responses are observed.....	176
Figure 8.1. Schematic representation of the potential sensory responses elicited by the binding of cationic and/or anionic species to symmetrically-functionalized XFs. Eight different binding scenarios are conceivable resulting in five unique fluorescence responses. The dotted lines indicate the position of the frontier molecular orbitals of the parent XF, while the solid lines indicate the changes to the FMOs upon binding of a cation or an anion to the XF.....	193
Figure 8.2. Top: Serial protonation or methylation of <b>8.1</b> and change in its emission color. Bottom: Fluorescence color of <b>8.1</b> after addition of TFA in dichloromethane.....	196
Figure 8.3. Structure of <b>8.2</b> and <b>8.3</b> .....	197

## LIST OF SCHEMES

Scheme 2.1. Synthesis of XFs <b>2.1-2.8a</b> .....	13
Scheme 4.1. Synthesis of phenothiazine XFs.....	64
Scheme 5.1. Interaction of cruciform fluorophores with metal cations.....	98
Scheme 5.2. Synthesis of cruciforms <b>5.5-5.7</b> by a combination of Horner and Sonogashira methods.....	99
Scheme 6.1. Coordination polymer <b>6.1P</b> , a fluorescent supramolecular assembly formed through the coordination of XF <b>6.1</b> with bis-Pd pincer <b>6.2</b> .....	133
Scheme 6.2. Pyridyl XF <b>6.3</b> , bis-Pt pincer complex <b>6.4</b> , and the three additional supramolecular assemblies ( <b>6.2P-6.4P</b> ) synthesized using monomers <b>6.1-6.4</b> .....	134
Scheme 7.1. Structure of XFs <b>7.1-7.7</b> and a schematic representation of the surface functionality of silicas <b>A-D</b> .....	166
Scheme 7.2. Synthetic pathway providing access to XFs <b>7.6-7.7</b> .....	183

## LIST OF ABBREVIATIONS

Å	angstrom
A	absorbance
AcOH	acetic acid
Ar	aryl
°C	degrees Celsius
cm <sup>-1</sup>	wavenumber
δ	chemical shift
d	days
DCM	dichloromethane
DI	deionized
DMF	dimethylformamide
DMSO	dimethylsulfoxide
DNA	deoxyribonucleic acid
DP	degree of polymerization
EDTA	ethylenediaminetetraacetic acid
EI	electrospray ionization
ε	molar absorptivity
Et <sub>2</sub> O	diethyl ether
EtOAc	ethyl acetate
EtOH	ethanol
Eq	equivalents
ex	excitation

FMO	frontier molecular orbital
g	gram
HRMS	high resolution mass spectrometry
HOMO	highest occupied molecular orbital
h	hour
ITC	isothermal titration calorimetry
IR	infrared
J	coupling constant
K <sub>a</sub>	association constant
L	liter
LED	light emitting device
LUMO	lowest unoccupied molecular orbital
m/z	mass-to-charge ratio
MP	melting point
MeOH	methanol
mg	milligram
MHz	megaHertz
min	minute
mL	milliliter
mmol	millimole
μL	microliter
μm	micrometer
M	molarity

MSOA	multistage open association
nm	nanometer
NBS	<i>N</i> -Bromosuccinimide
NLO	non-linear optical
NMR	nuclear magnetic resonance
OTf	trifluoromethanesulfonate
%	percent
$\Phi_F$	fluorescence quantum yield
PIPES	piperazine-1,4-bis(2-ethanesulfonic acid)
Ppb	parts per billion
PPE	poly( <i>para</i> -phenyleneethynylene)
Ppm	parts per million
PPV	poly( <i>para</i> -phenylenevinylene)
rt	room temperature
TBAF	tetrabutylammonium fluoride
TEA	triethylamine
TFA	trifluoroacetic acid
THF	tetrahydrofuran
THP	tetrahydropyranyl
TIPS	triisopropylsilane
TLC	thin layer chromatography
TMS	trimethylsilane
Triflate	trifluoromethanesulfonate

UV	ultra-violet
VOC	volatile organic compound
XF	cruciform

## SUMMARY

The design of chromophores targets materials with optoelectronic properties necessary for advanced applications. Organic materials possess properties which emerge from the collective impact of the constituent backbone and substituents as well as their connectivity (i.e. molecular architecture), necessitating the exploration of novel conjugated architectures. This thesis chronicles our examination of 1,4-distyryl-2,5-bis(arylethynyl)benzenes (cruciforms, XFs). Electronic substitution of this ‘X-shaped’ cross-conjugated scaffold tunes *both the energy levels and the spatial distribution* of the frontier molecular orbitals (FMOs) in XFs. The resulting fluorophores exhibit FMO separation, imbuing XFs with desirable properties for sensory applications. Using model analytes, we examine how the underlying FMO arrangement and the nature of analyte interaction elicit observable responses. These studies provide a foundation for future access of functional responsive ratiometric cores. This case study demonstrates the importance and unique potential of FMO-separated fluorophores.

## CHAPTER 1

### Cruciforms in Context

#### 1.1 Introduction

Conjugated organic materials have attracted interest as fluorescent sensors and components in organic electronic devices. Chromophore design targets materials with the electronic and optical properties necessary for these advanced applications. The properties of organic materials emerge from the collective impact of the constituent backbone and substituents as well as their connectivity (i.e. molecular architecture). Thus, the development of advanced materials necessitates the exploration of novel conjugated architectures.

Motivated by a desire to develop novel functional materials, the Bunz group has actively engaged in the exploration of new molecular architectures. Many of these efforts have probed the suitability of organic materials to exhibit sensory responses. There is tremendous interest in the development of fluorescent sensors for a variety of a variety of targets, including metal ions,<sup>1</sup> chemical warfare agents,<sup>2</sup> explosives,<sup>3</sup> biomolecules,<sup>4</sup> and bacteria.<sup>5</sup> For dyes to serve as sensors and exhibit ratiometric responses, the interaction of an analyte must elicit a change in fluorophore's the HOMO-LUMO gap. This necessitates that one frontier molecular orbitals (FMO) must be disproportionately affected by analyte interaction. In the majority of organic fluorophores, HOMO and LUMO are 'congruent', i.e. the orbital coefficients are similar in the respective FMOs. One would not expect large shifts in color or emission wavelength upon binding to an analyte; the

position of HOMO and LUMO should be more or less equally affected, resulting in only small changes in the HOMO-LUMO gap.

A seductive strategy to develop fluorescent cores with more impressive responsivity is to design molecular architectures possessing spatially separated FMOs. In these systems, electronic information becomes spatially encoded; recognition elements can be incorporated into the fluorophore such that analyte binding independently influences the FMOs. Therefore, binding largely stabilizes either the HOMO or LUMO, inducing a significant change in emission and absorption spectra. As a result, the design of fluorophores possessing spatially separated FMOs has important implications for the design of advanced sensory cores.

## 1.2 Serendipity at Work: The PPE Problem

In spite of the obvious potential of FMO-separated fluorophores in sensory applications, relatively few organic materials have been described possessing these orbital arrangements. As is often the case in the development of functional materials, a serendipitous discovery led to our investigation of FMO-separated fluorophores. The Bunz group has long maintained an active research interest in poly(*para*-phenyleneethynylene)s (PPEs, **1.1**, Figure 1.1), a class of conjugated polymers related to PPVs (**1.2**).<sup>6</sup> Though PPEs possess many desirable properties, they do not share the balanced performance of PPVs in organic device applications; hole injection is a particular problem. Attempts to remedy this shortcoming by introducing vinyl groups into the main chain did not significantly improve performance; **1.3** resembles **1.1** much more than **1.2** with respect to its optical and solid state semiconducting properties.<sup>7</sup> In a

second attempt to induce PPV-character in PPEs, we synthesized a series of cross-conjugated polymers of the type **1.4a-c**, incorporating styryl groups in the sidechain.<sup>8</sup> In these systems, the solution and solid state band gap shrinks from **1.4a**→**1.4c**. Hole injection is considerably facilitated, particularly in **1.4c** which was explored in a photodiode-type application; **1.4c** is more electron rich than PPV.<sup>8,9</sup> Cyclic voltammetry revealed that increasing donor strength in the distyrylbenzene arms (from **1.4a** to **1.4c**) exclusively affects the HOMO position. Only later would we come to fully appreciate the significance of this discovery: *these cross-conjugated architectures permit the spatial separation of FMOs*.

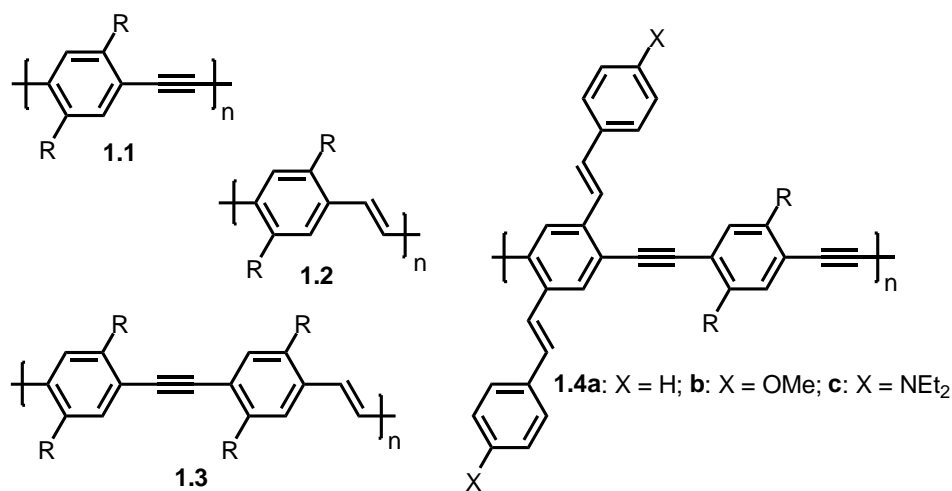


**Figure 1.1.** Structure of several classes of conjugated polymers, including PPEs (**1.1**), PPVs (**1.2**), and hybrid polymers **1.3** and **1.4a-c**.

### 1.3 From Polymers to Small Molecules

To better understand PPE-PPV hybrid polymers **1.4a-1.4c**, we prepared a series of ‘x-shaped’ 1,4-distyryl-2,5-bisarylethynylbenzenes (cruciforms, XFs). Though initially intended as model compounds, we quickly discovered these XFs are fascinating and useful in their own right.

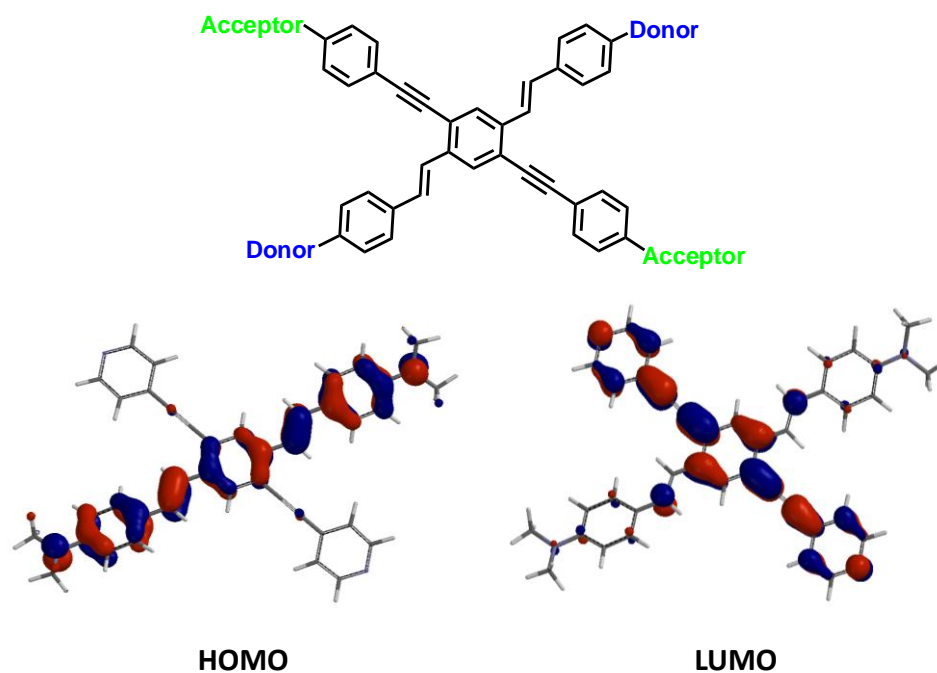


**Figure 1.2.** Generalized structure of an XF (top). The bottom depicts the FMO distribution of a donor-acceptor substituted XF, illustrating the FMO separation induced upon donor-acceptor substitution of the XF scaffold.

There has long been an interest in chromophores possessing linear 1-dimensional  $\pi$ -systems, ranging from small molecules (i.e. distyrylbenzenes or oligophenylene ethynyls) to conjugated polymers. However, the exploration of new conjugated architectures has recently yielded a variety of 2-dimensional, ‘X-shaped’, conjugated materials, including spiro compounds,<sup>10</sup> paracyclophanes,<sup>11</sup> swivel-type cruciforms,<sup>12</sup> bisoxazole-derived cruciforms,<sup>13</sup> tetraethynylethenes,<sup>14</sup> tetrasubstituted tolans,<sup>15</sup> etc.<sup>16,17</sup> A subset of these compounds are constructed from two ‘perpendicular’  $\pi$ -conjugated linear arms connected through a central aromatic core; examples include tetrakis(arylethynyl)benzenes,<sup>18,19</sup> tetrakis(styryl)benzenes,<sup>20,21</sup> and tetrasubstituted thiophenes.<sup>22</sup>

Our 1,4-distyryl-2,5-bis(arylethynyl)benzenes are another fascinating example of such a 2-dimensional cross-conjugated architecture increasingly investigated for their attractive electro-optical properties (Figure 1.2). XFs are composed of two linear  $\pi$ -conjugated segments – a perpendicular distyryl branch and an arylethynyl branch – connected via a central benzene core. Analysis of the electronic structure of XFs has revealed that donor and acceptor substitution results in compounds possessing FMOs spatially disjoint from one another; in these cases the HOMO and LUMO localize on the ‘orthogonal’ arms of XFs. This induced separation of the FMOs in XFs has significant consequences for their photophysics and has led to their use as building blocks in supramolecular assemblies,<sup>23</sup> components in molecular electronics,<sup>24</sup> and most notably as responsive cores in the sensory schemes.<sup>25</sup>

It is worth noting that spectroscopy clearly indicates the contribution of other transitions contributing to the photophysical behavior of XFs – particularly in the case of donor-acceptor substituted XFs. For the purposes of simplicity and clarity, this thesis will discuss spectroscopic transitions exclusively as transitions from HOMO to LUMO. The thesis of Nisan Siegel (Perry Group, School of Chemistry and Biochemistry, Georgia Institute of Technology) as well as a manuscript in preparation will more rigorously examine the photophysics of these molecules. However, for the purposes of understanding the responsive behavior of these cores, the simplified model of HOMO-LUMO transitions will be used.

## 1.4 Scope of Dissertation

This dissertation comprises a preliminary examination of XFs, including their synthesis, investigation of their photophysical properties, and evaluation of their sensory responses. Several distinct projects will form the body of my thesis:

- Synthesis and photophysical properties of XFs
- Cruciforms as functional fluorophores: response to protons and selected metal ions
- Synthesis and characterization of phenothiazine-substituted cruciforms
- Water-soluble cruciforms
- Self-assembled supramolecular cruciforms
- Cruciform-silica hybrid materials

These research efforts have probed the responsivity of XFs, highlighting the utility of FMO-separated materials as ratiometric cores in sensory applications.

## 1.5 References and Notes

1. (a) Guo, X.; Qian, X.; Jia, L. Highly selective and sensitive fluorescent chemosensor for  $\text{Hg}^{2+}$  in neutral buffer aqueous solution. *J. Am. Chem. Soc.* **2004**, *126*, 2272-2273. (b) Prodi, L.; Bargossi, C.; Montalti, M.; Zaccheroni, N.; Su, N.; Bradshaw, J. S.; Izatt, R. M.; Savage, P. B. An effective fluorescent chemosensor for mercury ions. *J. Am. Chem. Soc.* **2000**, *122*, 6769-6770. (c) Deo, S.; Godwin, H. A. A Selective, Ratiometric Fluorescent Sensor for  $\text{Pb}^{2+}$ . *J. Am. Chem. Soc.* **2000**, *122*, 174-175. (d) Gunnlaugsson, T.; Lee, T. C.; Parkesh, R. Highly selective fluorescent chemosensors for cadmium in water. *Tetrahedron.* **2004**, *60*, 11239-11249. (e) Walkup, G. K.; Burdette, S. C.; Lippard, S. J.; Tsien, R. Y. A new cell-permeable fluorescent probe for  $\text{Zn}^{2+}$ . *J. Am. Chem. Soc.* **2000**, *122*, 5644-5645. (f) Burdette, S. C.; Walkup, G. K.; Spingler, B.; Tsien, R. Y.; Lippard, S. J. Fluorescent sensors for  $\text{Zn}^{2+}$  based on a fluorescein platform: Synthesis, properties and intracellular distribution. *J. Am. Chem. Soc.* **2001**, *123*, 7831-7841. (g) Jiang, P. J.; Guo, Z. J. Fluorescent detection of zinc in biological systems: recent development on the design of chemosensors and biosensors. *Coord. Chem. Rev.* **2004**, *248*, 205-229.

2. (a) Burnworth, M.; Rowan, S. J.; Weder, C. Fluorescent sensors for the detection of chemical warfare agents. *Chem. Eur. J.* **2007**, *13*, 7828-7836. (b) Zhang, S. W.; Swager, T. M. Fluorescent detection of chemical warfare agents: Functional group specific ratiometric chemosensors. *J. Am. Chem. Soc.* **2003**, *125*, 3420-342.
3. Yang, J. S.; Swager, T. M. Fluorescent porous polymer films as TNT chemosensors: Electronic and structural effects. *J. Am. Chem. Soc.* **2003**, *120*, 11864-11873.
4. (a) Kim, I. B.; Wilson, J. N.; Bunz, U. H. F. Mannose-substituted PPEs detect lectins: A model for Ricin sensing. *Chem. Commun.* **2005**, 1273-1275. (b) Gaylord, B. S.; Heeger, A. J.; Bazan, G. C. DNA detection using water-soluble conjugated polymers and peptide nucleic acid probes. *Proc. Natl. Acad. Sci.* **2002**, *99*, 10954-10957. (c) Kumaraswamy, S.; Bergstedt, T.; Shi, X. B.; Rininsland, F.; Kushon, S.; Xia, W. S.; Ley, K.; Achyuthan, K.; McBranch, D.; Whitten, D. Fluorescent-conjugated polymer superquenching facilitates highly sensitive detection of proteases. *Proc. Natl. Acad. Sci.* **2004**, *101*, 7511-7515
5. (a) Disney, M. D.; Zheng, J.; Swager, T. M.; Seeberger, P. H. Detection of bacteria with carbohydrate-functionalized fluorescent polymers. *J. Am. Chem. Soc.* **2004**, *126*, 13343-13346. (b) Phillips, R. L.; Miranda, O. R.; You, C.-C.; Rotello, V. M.; Bunz, U. H. F. Rapid and efficient identification of bacteria using gold-nanoparticle-poly(*para*-phenyleneethynylene) constructs. *Angew. Chem. Int. Ed.* **2008**, *47*, 2590-2594.
6. Bunz, U. H. F. Poly(aryleneethynylene)s: Syntheses, properties, structures, and applications. *Chem. Rev.* **2000**, *100*, 1605-1644.
7. Tekin, E.; Egbe, D. A. M.; Kranenburg, J. M.; Ulbricht, C.; Rathgeber, S.; Birckner, E.; Rehmann, N.; Meerholz, K.; Schubert, U. S. Effect of Side Chain Length Variation on the Optical Properties of PPE - PPV Hybrid Polymers. *Chem. Mater.* **2008**, *20*, 2727-2735.
8. (a) Wilson, J. N.; Windscheif, P. M.; Evans, U.; Myrick, M. L.; Bunz, U. H. F. Band gap engineering of poly(*p*-phenyleneethynylene)s: cross-conjugated PPE-PPV hybrids. *Macromolecules.* **2002**, *35*, 8681-8683. (b) Wilson, J. N.; Josowicz, M.; Wang, Y.; Bunz, U. H. F. Cruciform  $\pi$ -systems: hybrid phenylene-ethynylene/phenylene-vinylene oligomers. *Chem. Commun.* **2003**, 2962-2963.
9. Xu, Y.; Berger, P. R.; Wilson, J. N.; Bunz, U. H. F. Photoresponsivity of polymer thin-film transistors based on polyphenyleneethynylene derivative with improved hole injection. *Appl. Phys. Lett.* **2004**, *85*, 4219-4221.
10. (a) Saragi, T. P. I.; Spehr, T.; Siebert, A.; Fuhrmann-Lieker, T.; Salbeck, J. Spiro compounds for organic optoelectronics. *Chem. Rev.* **2007**, *107*, 1011-1065. (b) Shirota, Y.; Kageyama, H. Charge carrier transporting molecular materials and their applications in devices. *Chem. Rev.* **2007**, *107*, 953-1010. (c) Müller, C. D.; Falcou,

- A.; Reckefuss, N.; Rojahn, M.; Wiederhirn, V.; Rudati, P.; Frohne, H.; Nuyken, O.; Becker, H.; Meerholz, K. Multi-colour organic light-emitting displays by solution processing. *Nature*. **2003**, *421*, 829-833.
11. (a) Bartholomew, G. P.; Bazan, G. C. *Acc. Chem. Res.* **2001**, *34*, 30-39. (b) Bartholomew, G. P.; Rumi, M.; Pond, S. J. K.; Perry, J. W.; Tretiak, S.; Bazan, G. C. Two-photon absorption in three-dimensional chromophores based on [2.2]-paracyclophane. *J. Am. Chem. Soc.*, **2004**, *126*, 11529-11542. (c) Bartholomew, G. P.; Bazan, G. C. Synthesis, characterization, and spectroscopy of 4,7,12,15-[2.2]paracyclophane containing donor and acceptor groups: impact of substitution patterns on through-space charge transfer. *J. Am. Chem. Soc.*, **2002**, *124*, 5183-5196.
12. (a) Zen, A.; Pingel, P.; Jaiser, F.; Neher, D.; Grenzer, J.; Zhuang, W.; Rabe, J. P.; Bilge, A.; Galbrecht, F.; Nehls, B. S.; Farrell, T.; Scherf, U.; Abellon, R. D.; Grozema, F. C.; Siebbeles, L. D. A. Organic field-effect transistors utilizing solution-deposited oligothiophene-based swivel cruciforms. *Chem. Mater.* **2007**, *19*, 1267-1276. (b) Bilge, A.; Zen, A.; Forster, M.; Li, H.; Galbrecht, F.; Nehls, B. S.; Farrell, T.; Neher, D.; Scherf, U. Swivel-cruciform oligothiophene dimers. *J. Mater. Chem.*, **2006**, *16*, 3177-3182.
13. (a) Klare, J. E.; Tulevski, G. S.; Sugo, K.; de Picciotto, A.; White, K. A.; Nuckolls, C. Cruciform pi-systems for molecular electronics applications. *J. Am. Chem. Soc.* **2003**, *125*, 6030-6031. (b) Klare, J. E.; Tulevski, G. S.; Nuckolls, C. Chemical reactions with upright monolayers of cruciform pi-systems. *Langmuir*. **2004**, *20*, 10068-10072. (c) Florio, G. M.; Klare, J. E.; Pasamba, M. O.; Werblowsky, T. L.; Hyers, M.; Berne, B. J.; Hybertsen, M. S.; Nuckolls, C.; Flynn, G. W. Frustrated Ostwald ripening in self-assembled monolayers of cruciform pi-systems. *Langmuir*. **2006**, *22*, 10003-10008. (d) Tang, J.; De Poortere, E. P.; Klare, J. E.; Nuckolls, C.; Wind, S. J. Single-molecule transistor fabrication by self-aligned lithography and in situ molecular assembly. *Microelectron. Eng.* **2006**, *83*, 1706-1709.
14. (a) Nielsen, M. B.; Diederich, F. Conjugated oligoenynes based on the diethynylethene unit. *Chem. Rev.* **2005**, *105*, 1837-1867. (b) Kivala, M.; Diederich, F. Acetylene-derived strong organic acceptors for planar and nonplanar push-pull chromophores. *Acc. Chem. Res.* **2009**, *42*, 235-248.
15. Tolosa, J.; Díez-Barra, E.; Sánchez-Verdú, P.; Rodríguez-López, J. Unsymmetrically substituted four-armed tolans: new multichromophoric molecules. *Tetrahedron Lett.* **2006**, *47*, 4647-4651.
16. (a) Zhao, C.-H.; Wakamiya, A.; Inukai, Y.; Yamaguchi, S. Highly emissive organic solids containing 2,5-diboryl-1,4-phenylene unit. *J. Am. Chem. Soc.* **2006**, *128*, 15934-15935. (b) Blaszczyk, A.; Fischer, M.; von Hanisch, C.; Mayor, M. The synthesis of molecular rods with a transversal push-pull system. *Eur. J. Org. Chem.* **2007**, *16*, 2630-2642. (c) Li, Z. H.; Wong, M. S.; Tao, Y. Two-dimensional

- oligoarylenes: synthesis and structure-properties relationships. *Tetrahedron*. **2005**, *61*, 5277-5285.
17. (a) Opsitnick, E.; Lee, D. Two-dimensional electronic conjugation: statics and dynamics at structural domains beyond molecular wires. *Chem. Eur. J.* **2007**, *13*, 7040-7049. (b) Galbrecht, F.; Bünnagel, T.; Bilge, A.; Scherf, U.; Farrell, T. Cruciform-Conjugated Oligomers. In *Functional Organic Materials – Syntheses, Strategies, and Applications*; Müller, T. J. J., Bunz, U. H. F., Eds.; Wiley-VCH: Heidelberg, **2007**, 83-118.
18. (a) Marsden, J. A.; Miller, J. J.; Shirtcliff, L. D.; Haley, M. M. Structure-property relationships of donor/acceptor-functionalized tetrakis(phenylethynyl)benzenes and bis(dehydrobenzoannuleno)benzenes. *J. Am. Chem. Soc.* **2005**, *127*, 2464-2476. (b) Spitler, E. L.; Shirtcliff, L. D.; Haley, M. M. Dynamic proton-induced two-stage emission switching in donor-functionalized bis(dehydrobenzo[n]annuleno)benzenes and 1,2,4,5-tetrakis(phenylethynyl)benzene. *J. Org. Chem.* **2007**, *72*, 86-96. (c) Slepko, A. D.; Hegmann, F. A.; Tykwinski, R. R.; Kamada, K.; Ohta, K.; Marsden, J. A.; Spitler, E. L.; Miller, J. J.; Haley, M. H. *Opt. Lett.* **2006**, *31*, 3315-3317. (d) Spitler, E. L.; Haley, M. M. Dynamic proton-induced two-stage emission switching in donor-functionalized bis(dehydrobenzo[n]annuleno)benzenes and 1,2,4,5-tetrakis(phenylethynyl)benzene. *Tetrahedron*. **2008**, *64*, 11469-11474.
19. Moore, A. M.; Dameron, A. A.; Mantooh, B. A.; Smith, R. K.; Fuchs, D. J.; Cizek, J. W.; Maya, F.; Yao, Y.; Tour, J. M.; Weiss, P. S. Molecular engineering and measurements to test hypothesized mechanisms in single molecule conductance switching. *J. Am. Chem. Soc.* **2006**, *128*, 1959-1967.
20. (a) Fratiloiu, S.; Senthilkumar, K.; Grozema, F. C.; Christian-Pandya, H.; Niazimbetova, Z. I.; Bhandari, Y. J.; Galvin, M. E.; Siebbeles, L. D. Two-dimensional charge delocalization in X-shaped phenylenevinylene oligomers. *Chem. Mater.* **2006**, *18*, 2118-2129. (b) Niazimbetova, Z. I.; Christian, H. Y.; Bhandari, Y. J.; Beyer, F. L.; Galvin, M. E. Design and development of novel 2-D oligomers for electroactive device application. *J. Phys. Chem. B.* **2004**, *108*, 8673-8681. (c) Christian-Pandya, H. K.; Niazimbetova, Z. I.; Beyer, F. L.; Galvin, M. E. Role of symmetry and charge delocalization in two-dimensional conjugated molecules for optoelectronic applications. *Chem. Mater.* **2007**, *19*, 993-1001.
21. (a) Kang, H.; Facchetti, A.; Jiang, H.; Cariati, E.; Righetto, S.; Ugo, R.; Zuccaccia, C.; Macchioni, A.; Stern, C. L.; Liu, Z.; Ho, S.-T.; Brown, E. C.; Ratner, M. A.; Marks, T. J. Ultralarge hyperpolarizability twisted pi-electron system electro-optic chromophores: Synthesis, solid-state and solution-phase structural characteristics, electronic structures, linear and nonlinear optical properties, and computational studies. *J. Am. Chem. Soc.* **2007**, *129*, 3267-3286. (b) Kang, H.; Evmenenko, G.; Dutta, P.; Clays, K.; Song, K.; Marks, T. J. X-shaped electro-optic chromophore with remarkably blue-shifted optical absorption. synthesis, characterization, linear/nonlinear optical properties, self-assembly, and thin film microstructural characteristics. *J. Am. Chem. Soc.* **2006**, *128*, 6194-6205. (c) Hu, K.; Zhu, P. W.;

- Yu, Y.; Facchetti, A.; Marks, T. J. Self-assembled electrooptic thin films with remarkably blue-shifted optical absorption based on an X-shaped chromophore. *J. Am. Chem. Soc.* **2004**, *126*, 15974-15975.
22. (a) Hsu, H.-F.; Kuo, C.-H.; Chen, C.-F.; Lin, Y.-H.; Huang, L.-Y.; Chen, C.-H.; Cheng, K.-C.; Chen, H.-H. Synthesis and mesomorphic properties of multiynylthiophenes: 2,3,4,5-tetrakis(4-alkoxyphenylethynyl)thiophenes and 2,3,5-tris(4-alkoxyphenylethynyl)thiophenes. *Chem. Mater.* **2004**, *16*, 2379-2385. (b) Sun, X. B.; Zhou, Y. H.; Wu, W. C.; Liu, Y. Q.; Tian, W. J.; Yu, G.; Qiu, W. F.; Chen, S. Y.; Zhu, D. B. X-shaped oligothiophenes as a new class of electron donors for bulk-heterojunction solar cells. *J. Phys. Chem. B.* **2006**, *110*, 7702-7707. (c) Sun, X. B.; Liu, Y. Q.; Chen, S. Y.; Qiu, W. F.; Yu, G.; Ma, Y. Q.; Qi, T.; Zhang, H. J.; Xu, X. J.; Zhu, D. B. X-shaped electroactive molecular materials based on oligothiophene architectures: Facile synthesis and photophysical and electrochemical properties. *Adv. Funct. Mater.* **2006**, *16*, 917-925.
23. (a) Gerhardt, W. W.; Zuccherro, A. J.; Wilson, J. N.; South, C. R.; Bunz, U. H. F.; Weck, M. Supramolecular cruciforms. *Chem. Commun.* **2006**, 2141-2143. (b) Gerhardt, W. W.; Zuccherro, A. J.; South, C. R.; Bunz, U. H. F.; Weck, M. Controlling polymer properties through dynamic metal-ligand interactions: supramolecular cruciforms made easy. *Chem. Eur. J.* **2007**, *13*, 4467-4474.
24. Grunder, S.; Huber, R.; Horhoiu, V.; González, M. T.; Schönenberger, C.; Calame, M.; Mayor, M. New cruciform structures: towards coordination induced single molecule switches. *J. Org. Chem.* **1997**, *72*, 8337-8344.
25. (a) Wilson, J. N.; Bunz, U. H. F. Switching of intermolecular charge-transfer in cruciforms: metal ion sensing. *J. Am. Chem. Soc.* **2005**, *127*, 4124-4125. (b) Zuccherro, A. J.; Wilson, J. N.; Bunz, U. H. F. Cruciforms as functional fluorophores: response to protons and selected metal ions. *J. Am. Chem. Soc.* **2006**, *128*, 11872-11881. (c) Tolosa, J.; Zuccherro, A. J.; Bunz, U. H. F. Water-soluble cruciforms: response to protons and selected metal ions. *J. Am. Chem. Soc.* **2008**, *130*, 6498-6506. (d) Brombosz, S. M.; Zuccherro, A. J.; Phillips, R. L.; Vazquez, D.; Wilson, A.; Bunz, U. H. F. Terpyridine-based cruciform-Zn<sup>2+</sup> complexes as anion-responsive fluorophores. *Org. Lett.* **2007**, *22*, 4519-4522. (e) Hauck, M.; Schönhaber, J.; Zuccherro, A. J.; Hardcastle, K. I.; Müller, T. J. J.; Bunz, U. H. F. Phenothiazine cruciforms: synthesis and metallochromic properties. *J. Org. Chem.* **2007**, *72*, 6714-6725. (f) McGrier, P. L.; Solntsev, K. M.; Schönhaber, J.; Brombosz, S. M.; Tolbert, L. M.; Bunz, U. H. H. Hydroxy-cruciforms. *Chem. Commun.* **2007**, 2127-2129. (g) McGrier, P. L.; Solntsev, K. M.; Miao, S.; Tolbert, L. M.; Miranda, O. R.; Rotello, V. M.; Bunz, U. H. F. Hydroxycruciforms: Amine-responsive fluorophores. *Chem. Eur. J.* **2008**, *14*, 4503-4510.

## CHAPTER 2

### Synthesis and Photophysical Properties of Cruciforms

#### 2.1. Introduction

Organic materials possess properties which emerge from the collective impact of the constituent backbone and substituents as well as their connectivity (i.e. molecular architecture), necessitating the exploration of novel conjugated architectures. The construction of novel molecular geometries provide the opportunity to develop advanced functional materials with new and unique properties. Though initially envisioned exclusively as model compounds, 1,4-bisarylethynyl-2,5-distyrylbenzenes are in fact a class of remarkable and versatile fluorophores.

To examine the properties and potential of these XFs, we elected to prepare a series of XFs with varied donor and acceptor substitution of the aromatic periphery. Herein, we detail the synthesis and study of a small library of XFs containing Lewis basic functionalities (Figure 2.1). We elected to prepare this series of these fluorophores to probe the photophysical properties of XFs possessing variable electronic substitution. In addition, these Lewis basic XFs are quintessential examples of functional chromophores, as they contain embedded recognition elements as integral parts of their  $\pi$ -system.<sup>1</sup> As such, these chromophores are innately qualified to serve as active elements in sensors or sensor arrays and in advanced materials applications. To fully understand and appreciate the subtleties of these cruciform chromophores and lay the groundwork for future study, we examined the steady state photophysics of **2.1-2.8a**. The observed photophysics can

be explained by the position and the spatial arrangement of the FMOs in these fluorophores.

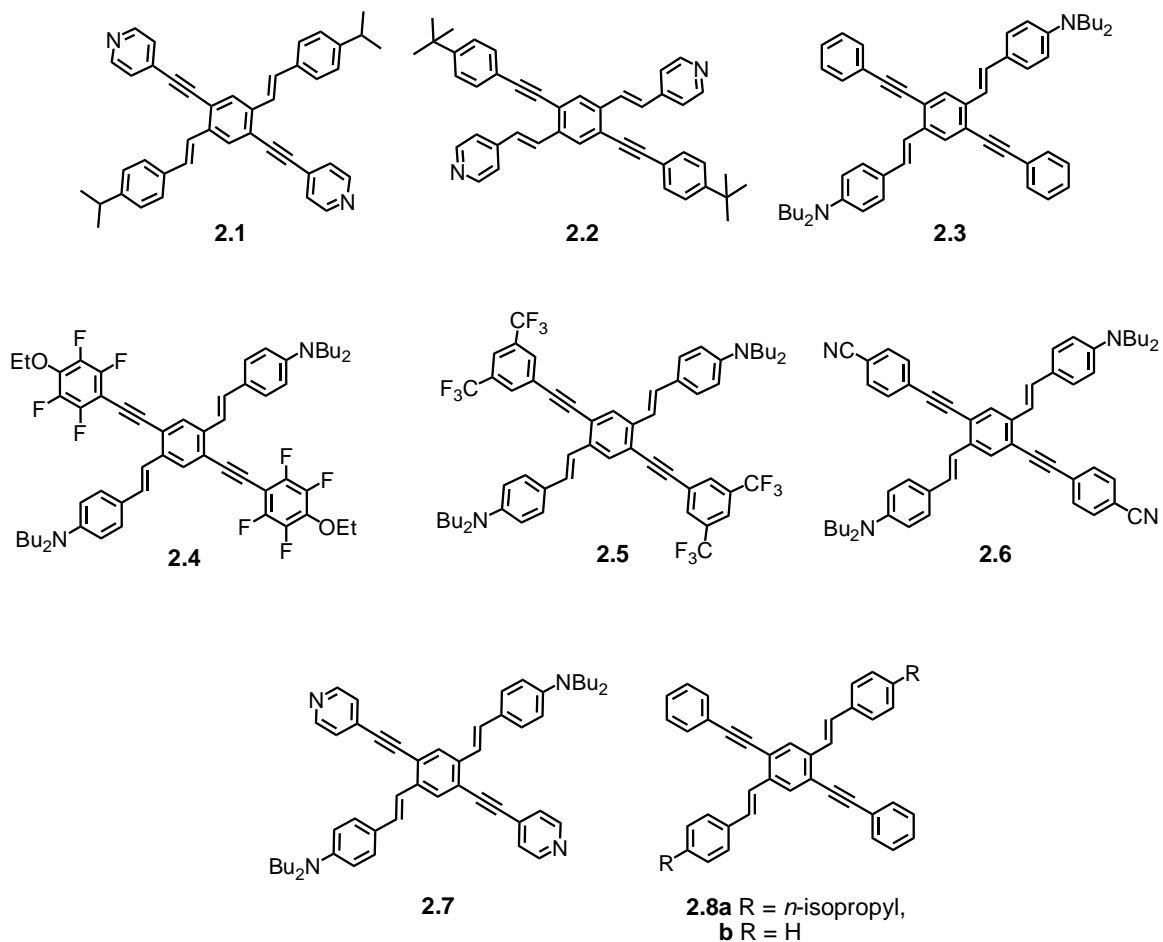
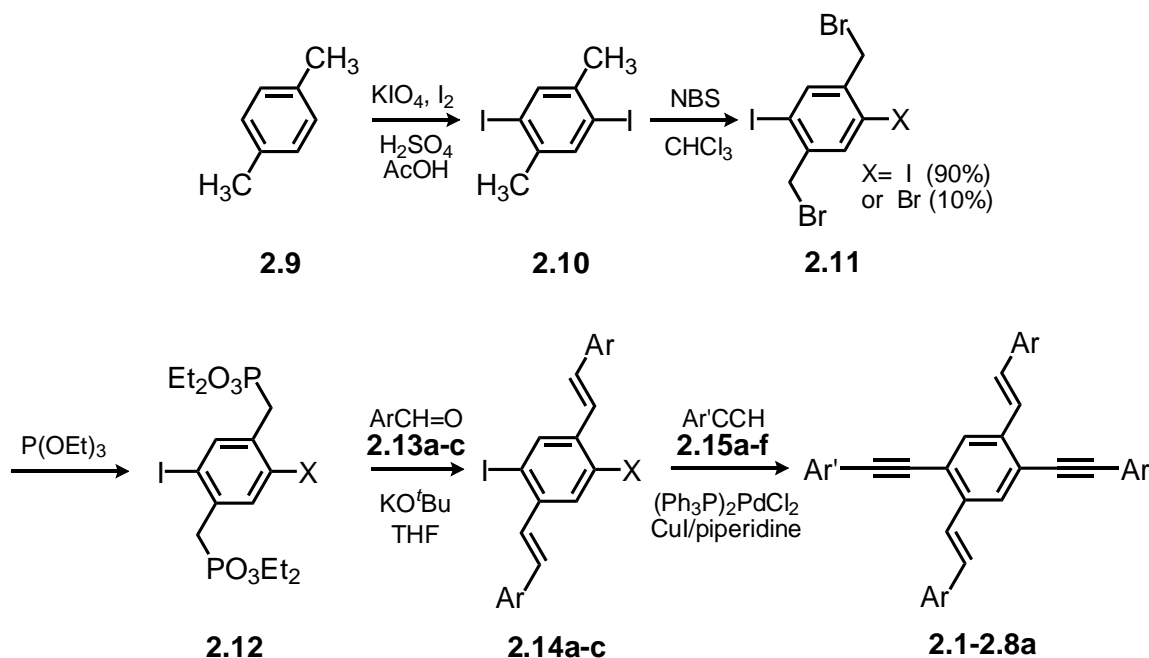


**Figure 2.1.** Structure of XFs 2.1-2.8.

## 2.2. Synthetic Methodology

Cruciform fluorophores are  $\pi$ -systems in which two alkene and two alkyne arms are placed in a 1,4-2,5-relationship on a central benzene ring. All XFs are constructed from a common tetrahalide precursor, 2,5-bis(bromomethyl)-1,4-diiodobenzene (**2.11**, Scheme 2.1). This was furnished in a two step synthetic sequence from *para*-xylene.

Iodination<sup>2</sup> of **2.9** provided **2.10** in a 78 % yield; subsequent bromination with *N*-bromosuccinimide yielded tetrahalide **2.11**.<sup>2</sup> These radical bromination conditions afforded an inseparable mixture of 2,5-bis(bromomethyl)-1,4-diiodobenzene (90 %) and the halogen-exchanged 1-iodo-4-bromo-2,5-bis(bromomethyl)benzene (10 %). This mixture was successfully used for all subsequent reactions as both materials are reactive under the coupling conditions employed for XF synthesis.



**Scheme 2.1.** Synthesis of XFs **2.1-2.8a**.

**2.11** was reacted with triethylphosphite in an Arbuzov reaction, forming phosphonate **2.12** in nearly quantitative yield. A Horner<sup>3</sup> olefination of bisphosphonate **2.12** with aromatic aldehydes **2.13a-c** and potassium *tert*-butoxide in THF formed the arylenevinylene branch of the XFs. Diiodides **2.14a-c** were obtained as brilliant yellow-to-orange crystalline powders; <sup>1</sup>H NMR confirmed the stilbenoid double bonds were exclusively *trans*-configured, as expected for Horner olefinations.<sup>3</sup> Subsequently, a

Sonogashira-Hagihara coupling<sup>4</sup> was performed to form the aryleneethynylene arm. 1,4-diiodo-2,5-distyrylbenzenes **2.14a-c** were reacted with alkynes **2.15a-f** in piperidine/THF with a (Ph<sub>3</sub>P)<sub>2</sub>PdCl<sub>2</sub>/CuI catalyst system to give XFs **2.1-2.8a** in good-to-excellent yields. It is noteworthy that as both Horner and Sonogashira reactions are robust, this synthetic sequence allows the construction of virtually any conceivable XF, as long as the necessary aldehydes and alkynes are accessible.

### 2.3. Photophysical Properties of 2.1-2.8a

Cruciforms **2.1-2.8a** were obtained as yellow-to-red crystalline powders; when dissolved, all XFs are vibrantly fluorescent in organic solvents. Figure 2.2 displays the distinct emission colors, ranging from blue to orange, of representative XFs in dichloromethane as obtained by digital photography.



**Figure 2.2.** Emission of XFs in dichloromethane under blacklight irradiation ( $\lambda_{\text{max}}$  365 nm).

**Table 2.1.** Absorption and Emission Data of XFs **2.1-2.8a** in Dichloromethane and Hexanes.

XF	Dichloromethane		Hexanes		
	$\lambda_{\max}$ absorption (nm)	$\lambda_{\max}$ emission (nm)	$\lambda_{\max}$ absorption (nm)	$\lambda_{\max}$ emission (nm)	Vibronic progression ( $\text{cm}^{-1}$ )
<b>2.1</b>	330	456	324	427	1097
	370		365	448	
	395 sh		390 sh		
<b>2.2</b>	330	444	325	422	1225
	361 sh		353	445	
<b>2.3</b>	336	519	332	469	1242
	436		422	498	
<b>2.4</b>		561	447 sh		-
	337		334	509	
	352		348		
	443		418		
<b>2.5</b>	479 sh	567	470 sh		-
	296		296	516	
	331		333		
	348		345		
	433		416		
<b>2.6</b>	472 sh	590	461 sh		-
	340		321	514	
	361		344		
	427		355		
	478 sh		415		
<b>2.7</b>		567	460		-
	295		288	496	
	333		330		
	346		341		
	437		425		
<b>2.8a</b>	472 sh	419	460 sh		1302
	331		327	409	
	374		369	432	
	396 sh		390 sh		

**Table 2.2.** Quantum yield and fluorescence lifetime of **2.1-2.7** in chloroform. All fluorescence lifetimes were monoexponential and fitted with a single decay function.

<b>XF</b>	Quantum Yield CHCl <sub>3</sub>	Fluorescence Lifetime $\tau$ (ns) CHCl <sub>3</sub>
<b>2.1</b>	0.70	4.1
		3.9
		3.9
<b>2.2</b>	0.67	3.8
<b>2.3</b>	0.31	1.7
<b>2.4</b>	0.15	4.2
		4.4
<b>2.5</b>	0.09	4.4
		4.2
<b>2.6</b>	0.05	3.9
		4.0
<b>2.7</b>	0.11	4.3
		4.3

The steady state photophysics of **2.1-2.8a** were carefully probed. The absorption and emission spectra and the radiative lifetimes of **2.1-2.3**, **2.5** and **2.7** are discussed here in detail. The spectra and results for **2.4** and **2.6** are included but are similar to those of **2.5** and do not warrant separate discussion. Figure 2.3 displays the absorption and emission spectra of **2.1-2.7** in dichloromethane and hexanes. The absorption spectra of the either donor or acceptor-substituted cruciforms **2.1-2.2** are similar in shape, possessing one main transition at 300-350 nm and a second one at higher wavelengths that appears as a shoulder. The donor and the donor-acceptor cruciforms **2.3-2.7** (discussed here are **2.3**, **2.5**, and **2.7**) show a prominent, broad absorption feature around 450 nm and a second one with an additional shoulder at lower wavelengths. The low energy band is intense in **2.4-2.7** and is due to a charge-transfer interaction of the donor

and the acceptor groups. The emission spectra of cruciforms **2.1-2.7** in dichloromethane are broad and featureless with emission maxima ranging from 444-590 nm. The strongly donor-acceptor substituted cruciforms **2.4-2.7** show red-shifted emission (561-590 nm) when compared to that of **2.1-2.3** (444-519 nm).

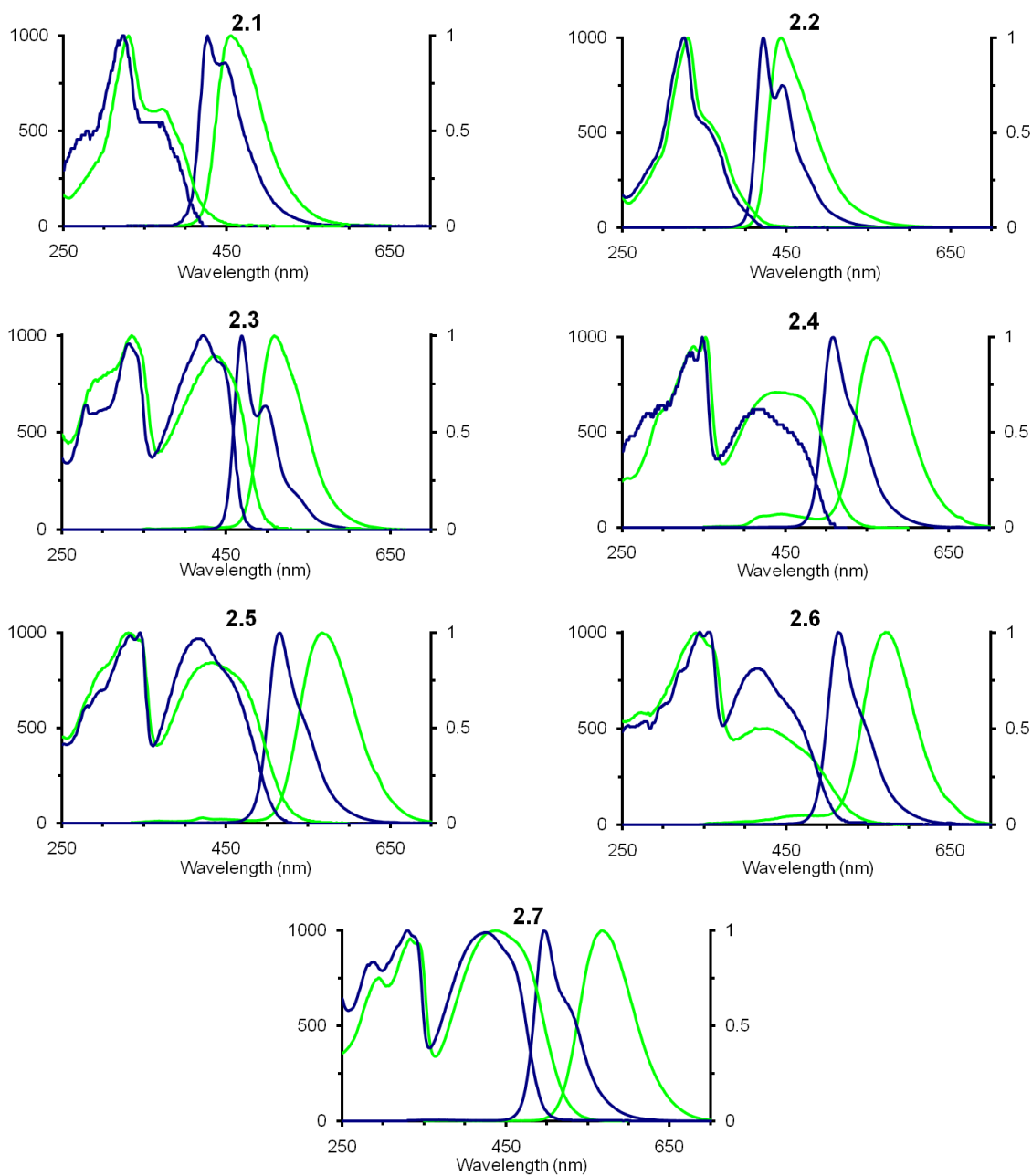


**Figure 2.3.** Normalized absorption and emission spectra of **2.1-2.7** in hexanes (blue) and dichloromethane (green).

The quantum yield (Table 2.2) of **2.1-2.3** in halogenated solvents is in the range of 0.3-0.7, while the donor- acceptor substituted cruciforms **2.4-2.7** display quantum yields that are lower and range from 0.05-0.11. The quantum yield is qualitatively inversely correlated with  $\lambda_{\text{max}}$  emission in these species – the lower energy the emission, the lower the quantum yield. The decrease of emission quantum yield upon red shift of the emission is not unexpected, as nonradiative pathways by vibronic coupling are more accessible in compounds with a smaller band gap.<sup>5</sup> However, in **2.1-2.7**, there is no clear numerical correlation between gap and emission quantum yields.

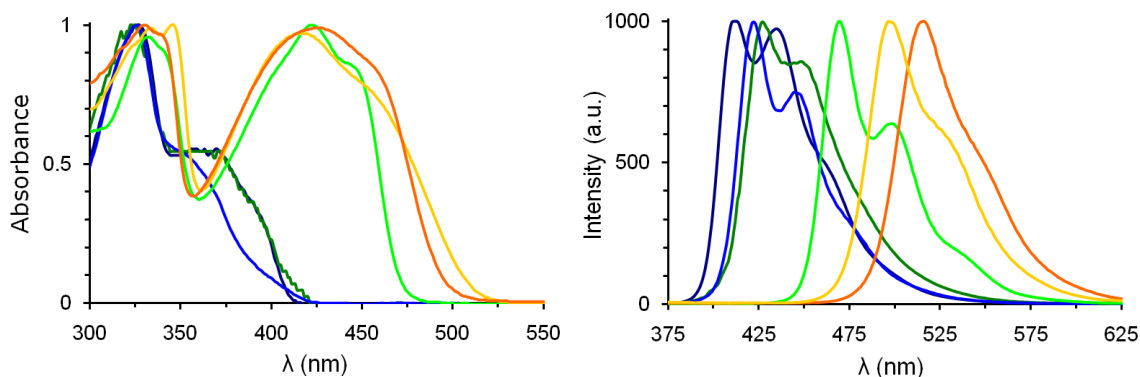


**Figure 2.4.** Normalized absorption (left) and emission (right) of XF **2.8a**(dark blue), **2.2**(light blue), **2.1**(dark green), **2.3**(light green), **2.5**(yellow), and **2.7**(orange) in hexanes.

The normalized absorption and emission spectra of **2.1-2.3**, **2.5**, **2.7**, and **2.8a** in hexanes are displayed in Figure 2.4. Their emissions appear blue-shifted in hexanes relative to those recorded in dichloromethane; their Stokes shifts are also smaller than the corresponding Stokes shifts in dichloromethane. Increasing positive solvatochromism is observed upon increasing donor-acceptor substitution.

The cruciforms **2.1-2.3** and **2.8a** show a vibronic progression ranging from 1097-1302  $\text{cm}^{-1}$ , associated with the C=C-stretching mode of the distyrylbenzene arms. In these cruciforms, this numerical value is somewhat smaller than in simple aminostilbenes ( $1300\pm 80 \text{ cm}^{-1}$ ), probably due to increased conjugation.<sup>6</sup> In **2.1-2.3**, the intensity of the main band is larger than the intensity of the vibronic progression while in **2.8a**. A classic interpretation would assert that the 0,0 transition is more prevalent than the 0,1 transition; concomitantly, in the excited state the distortion around the stilbene double bonds would be only modest, because distortion correlates with an increased intensity of the vibronic progression. It is not clear if the classic picture holds for **2.1-2.3** and **2.8a**; their Stokes shifts are quite large and the main band might already be the vibronic 0,1 or 0,2 transition. Cruciforms **2.1-2.3** and **2.8a** feature spatially delocalized HOMOs and LUMOs and the emission spectra in hexanes are similar to those observed for stilbenes with analogous substituent patterns.

Upon examination of the emission spectra of **2.5** and **2.7** in hexanes, one notices a bathochromic shift and a loss of the vibronic fine structure. The more red shifted the emission, the less vibronic fine structure is visible. The increasing donor-acceptor character in **2.4-2.7** and the concomitantly increased internal charge transfer character of the excited state renders it more distorted and explains the observed features (or the lack thereof). We hypothesize that the local separation of the FMOs in **2.4-2.7** is characterized by a loss of fine structure in their fluorescence spectra taken in nonpolar solvents – a convenient heuristic instrument to characterize novel cruciforms.

The fluorescence lifetimes of **2.1-2.7** were determined in chloroform. In all cases, lifetimes were found to be mono-exponential and were fitted with a single decay function

(Table 2.2). With the exception of **2.3**, ( $\tau = 1.7$  ns) the emissive lifetimes of the cruciforms are  $\tau \approx 4$  ns. These lifetimes are atypical for distyrylbenzene derivatives which normally show shorter lifetimes of approximately  $\tau \approx 1$  ns.<sup>7</sup> The same is true for bis(phenylethynyl)benzenes, which also feature short radiative lifetimes.<sup>8</sup>

#### 2.4. FMO Structure of XFs

Varying substitution of the XF framework results in differentiated spectroscopic properties. To rationalize the optical properties of these XFs, we performed quantum chemical calculations on simplified analogues of XFs **2.8a** and **2.7** (**2.8b** and **2.7b**). B3LYP 6-31G\*\*//6-31G\*\* calculations provide an understanding of ground state properties and HOMO-LUMO gaps when examining trends in a series of related compounds. In the unsubstituted parent XF **2.8b**, the HOMO and LUMO are evenly distributed over the  $\pi$ -system, with larger coefficients on the central benzene ring and smaller ones on the peripheral phenyl rings (Figure 2.5). This distribution is typical of  $\pi$ -conjugated hydrocarbons. Donor-acceptor substitution of the XF framework elicits a large change in the coefficient distribution of the FMOs. In the case of **20b**, possessing donor substituents on the distyryl axis of the XF and acceptor substituents on the arylethynyl axis of the XF, HOMO and LUMO show a spatially *disjoint* distribution. *The donor and acceptor substituents localize the FMOs on the respective arylethynyl and styryl branches.*

The ability of substitution to tune the FMO distribution – and as a result the optical properties – of XFs allows us to divide these chromophores into two subsets. *Class D* XFs show a *disjoint* FMO structure as a consequence of donor-acceptor

substitution of the framework. On the other hand, cruciforms that are not significantly donor/acceptor substituted possess spatially superimposable FMOs; we propose to call these *Class C* XFs in reference to their spatially *congruent* FMO arrangement. The distinction between Class C and Class D XFs is rigidly defined; however, the gradual transition between the two coincides with the appearance of a charge transfer band in the absorption spectra and a loss of vibronic features in the emission spectra. The stark spectroscopic differences in Class C and Class D XFs is highlighted in Figure 2.6.

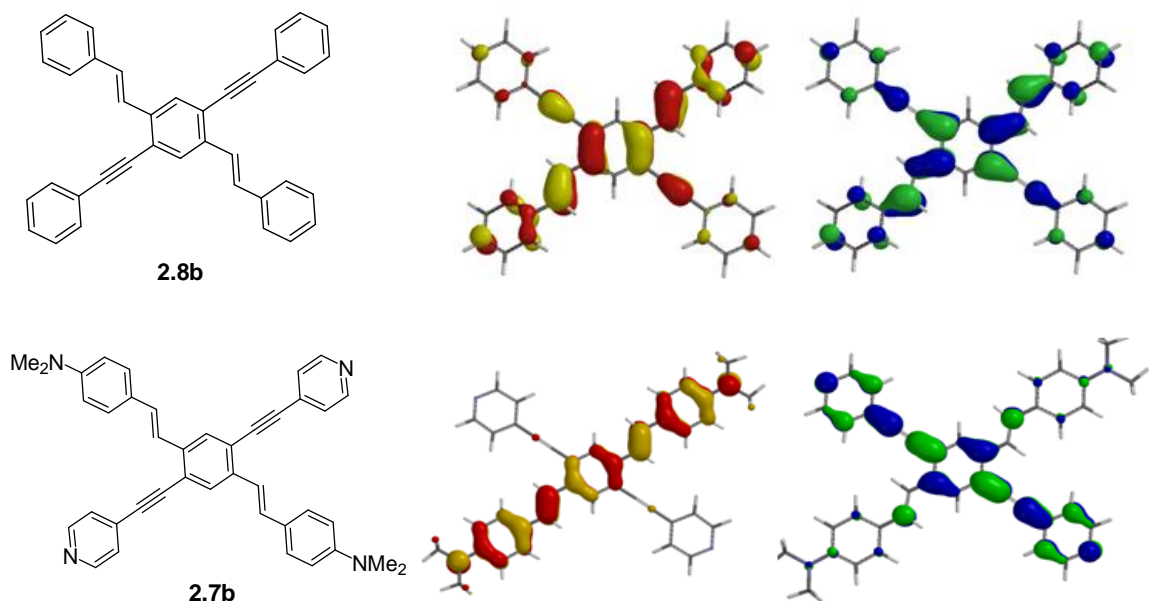


**Figure 2.5.** Top: Frontier molecular orbitals of **2.8b** (Spartan, B3LYP 6-31G\*\*//6-31G\*\*); left: HOMO (-5.17 eV), right: LUMO (-2.00 eV). Bottom: Frontier orbitals of **2.7b** (Spartan, B3LYP 6-31G\*\*//6-31G\*\*); left: HOMO (-4.63 eV) and right: LUMO (-2.07 eV) are now localized on the different branches of the molecule.

Generally, a disjoint FMO structure permits the independent tuning of the oxidation and reduction potential (or HOMO and LUMO) of such fluorophores. If one examines pars pro toto the disjoint FMOs of **2.7**, one notes that there is orbital overlap in

the central benzene ring, but the overall overlap integral is not large; the HOMO-LUMO transition is symmetry-allowed and not degenerate in the one electron approximation. The disjoint FMOs explain the unusually long emissive lifetime as a consequence of a weakly Franck-Condon allowed transition. The large Stokes shifts in the disjoint cruciforms likewise support the assumption of a poor overlap of the ground with the excited state, and corroborate the results obtained from the lifetime measurements.

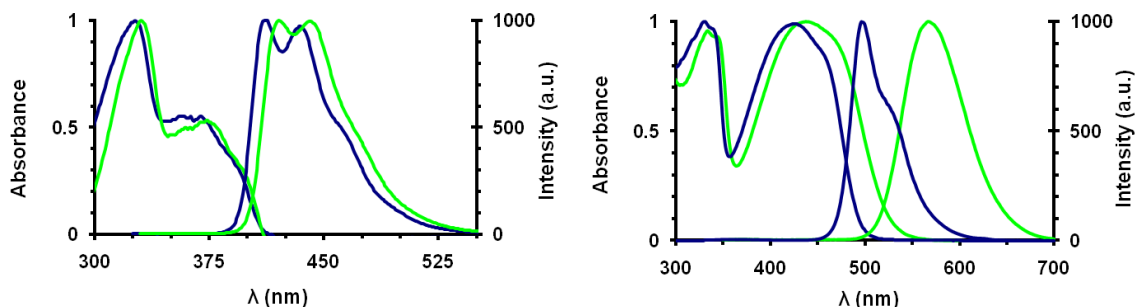


**Figure 2.6.** Normalized absorption and emission spectra of Class C XF **2.8a** (left) and Class D XF **2.7** (right) in hexanes (blue trace) and dichloromethane (green trace).

## 2.5. Conclusions

Moving beyond one-dimensional molecular wire-type fluorophores to two-dimensional ‘X-shaped’ materials provides access to conjugated architectures with unexpected and exciting properties.<sup>9</sup> XFs represent a prime example of such novel conjugated architectures; 1,4-bisarylethynyl-2,5-distyrylbenzenes are in a class of remarkable and versatile fluorophores.

The herein investigated cruciforms **2.1-2.8a** are substituted 1,4-distyrylbenzenes; however, their photophysical behavior is distinct as a result of their 2-dimensional molecular architecture. Varied substitution of the XF periphery dramatically influences the FMO distribution in these cores, inducing spatial separation of HOMO and LUMO on

the XF scaffold. As a result, cruciforms can be categorized as possessing either a *congruent* (Class C) or *disjoint* (Class D) FMO arrangement. These classes exhibit dramatically different photophysical behavior.

Organic chromophores exhibiting FMO separation are quite rare; however, they are of increasing interest owing to their unique photophysical behavior and potential in sensory applications. Examples of other FMO-separated materials include 1,2,4,5-tetraarylethynylbenzenes,<sup>10</sup> donor-acceptor biphenyls (swivel-cruciforms),<sup>11</sup> and certain pyrazoline derivatives.<sup>12</sup> With this fundamental understanding in place, we move forward to examine the sensory potential of these functional fluorophores.

This work has been published in the *Journal of the American Chemical Society*:  
Zuccherro, A. J.; Wilson, J. N.; Bunz, U. H. F. Cruciforms as functional fluorophores: response to protons and selected metal ions. *J. Am. Chem. Soc.* **2006**, *128*, 11872-11881.

## 2.6 Experimental

**General Methods.** All chemicals were purchased from Aldrich Chemical, Acros, TCI America, or Fischer Scientific and used without purification unless otherwise specified. Column chromatography was performed using Standard Grade silica gel 60 Å, 32-63 µm (230 x 450 mesh) from Sorbent Technologies and the indicated eluent. Elution of cruciforms was readily monitored using a handheld UV lamp (365 nm). Melting points were obtained using a Mel-Temp apparatus fitted with a Fluke 51<sup>K/J</sup> digital thermometer. All IR spectra were obtained using a Simadzu FTIR-8400s spectrometer. Unless otherwise specified, NMR spectra were recorded at 298 K on a Varian Mercury spectrometer (300 MHz). Chemical shifts are reported in parts per million (ppm), using

residual solvent (chloroform-*d*) as an internal standard. Data Reported as follows: chemical shift, multiplicity (s = singlet, d = doublet, t = triplet, q = quartet, m = multiplet), coupling constant, and integration. Mass spectral analyses were provided by the Georgia Institute of Technology Mass Spectrometry Facility.

All absorption spectra were collected using a Shimadzu UV-2401PC spectrophotometer. All emission spectra were acquired using a Shimadzu RF-5301PC spectrofluorophotometer. Lifetime data were collected using a Lifespec-ps (Edinburgh Instruments), pulsed diode laser (PicoQuant, 372 nm excitation), and PMT detector (Hamamatsu). Data were fit to single exponential decay so as to optimize chi-squared values. Quantum yields for all cruciforms were measured using standard procedures using quinine sulfate as a standard.

**Synthesis of 2.10. 1,4-Diiodo-2,5-dimethylbenzene.** *p*-xylene (40 mL, 0.324 mol), acetic acid (300 mL), KIO<sub>4</sub> (43 g, 0.187 mol), and ground I<sub>2</sub> (86 g, 0.339 mol) were placed in a 1000 mL three neck round bottom flask fitted with an addition funnel and reflux condenser. The mixture was stirred at 40°C for 15 min after which H<sub>2</sub>SO<sub>4</sub> (6.5 mL, 0.122 mol) was added dropwise. The mixture was then allowed to stir for 20 hours at 90°C. The reaction was then allowed to cool to room temperature. Aqueous sodium sulfite was added and the reaction was stirred until colorless. The reaction mixture was then extracted three times with dichloromethane. The organic layers were washed three times with water and dried with magnesium sulfate. The solvent was removed by vacuum and the resulting solid was recrystallized from chloroform, isolating **2.10** (90.57 g, 78 %) as colorless crystals. MP: 83°C. <sup>1</sup>H NMR (300 MHz, CDCl<sub>3</sub>): δ = 7.589 (s, 2H), 2.278 (s, 6H). IR: ν [cm<sup>-1</sup>] = 3062.75, 3014.53, 2973.07, 2945.1, 2911.35, 2893.99,

2843.84, 2801.41, 2730.05, 2553.58, 2456.18, 2307.67, 2055.98, 1904.57, 1747.39, 1467.73, 1445.55, 1433.98, 1417.58, 1372.26, 1331.76, 1314.4, 1258.47, 1246.89, 1190.00, 1118.64, 1077.17, 1030.88, 980.74, 980.74, 962.41, 876.59, 742.54, 718.43.

**Synthesis of 2.11. 2,5-bis(bromomethyl)-1,4-diiodobenzene. 2.10** (20 g, 0.056 mol) was dissolved in 500 mL chloroform in a 1000 mL round bottom flask equipped with a reflux condenser. *N*-Bromosuccinimide (22 g, 0.124 mol) was added and the solution was heated for 15 min using two 120 watt sun lamps. After 15 min, another 22 g of NBS was added. The reaction was stirred for 4 hours at reflux while being irradiated with the sun lamps. The reaction mixture was allowed to cool to room temperature and was quenched with sodium sulfite until colorless. The organics were washed three times with water then dried with magnesium sulfate. The solvent was removed in vacuo and the resulting solids were recrystallized from chloroform, yielding **2.11** (7.48 g, 26 %) as colorless needles. The product proved to be an inseparable mixture of 2,5-bis(bromomethyl)-1,4-diiodobenzene (90 %) and the halogen-exchanged 1-iodo-4-bromo-2,5-bis(bromomethyl)benzene (10 %). MP: 211°C. <sup>1</sup>H NMR (300 MHz, CDCl<sub>3</sub>): δ = 7.834 (s, 2H), 4.483 (s, 6H). <sup>13</sup>C NMR (300 MHz, CDCl<sub>3</sub>): δ = 140.779, 139.413, 100.859, 27.241. IR: ν [cm<sup>-1</sup>] = 3908.48, 3889.19, 3697.29, 3245.01, 3191.97, 3063.71, 3027.07, 3003.92, 2972.1, 2951.85, 2862.17, 2844.81, 2736.8, 2645.19, 2623.01, 2465.82, 2416.64, 2315.38, 2288.38, 2102.26, 1993.29, 1779.21, 1730.99, 1466.76, 1433.01, 1347.19, 1332.72, 1275.82, 1256.54, 1214.11, 1190.96, 1171.68, 1161.07, 1069.45, 1057.88, 1039.56, 1002.92, 951.81, 898.77, 866.94, 810.05, 784.97, 773.4, 668.29.

**Synthesis of 2.12.** 2,5-bis(bromomethyl)-1,4-diiodobenzene (10 g, 0.019 mol) and triethylphosphite (30 mL, 0.175 mol) were combined in a round bottom flask and stirred for 12 hours at 125°C under reflux. After 12 hours, the reaction was allowed to cool to room temperature, at which point a colorless precipitate formed. The precipitate was collected by vacuum filtration and washed thoroughly with hexanes, isolating bisphosphonate **2.12** (12.232 g, 97 %) as a colorless powder. MP: 133°C. <sup>1</sup>H NMR (300 MHz, CDCl<sub>3</sub>): δ = 7.853 (s, 2H), 4.053 (q, 8H), 3.253 (d, 4H), 1.242 (t, 12H). <sup>13</sup>C NMR (300 MHz, CDCl<sub>3</sub>): δ = 141.9, 137.6, 103.3, 63.8, 38.0, 37.5, 18.6. IR: ν [cm<sup>-1</sup>] = 3094.57, 2992.35, 2968.24, 2929.67, 2914.24, 2866.02, 2773.45, 2741.62, 2494.75, 2267.17, 1835.14, 1769.57, 1479.3, 1413.72, 1392.51, 1358.76, 1305.72, 1286.43, 1251.72, 1237.25, 1186.14, 1163.00, 1064.63, 1046.31, 1017.38, 936.38, 892.98, 859.23, 819.69, 811.98, 788.83, 764.72, 725.18, 614.29. ES<sup>+</sup> MS calculated for [C<sub>16</sub>H<sub>26</sub>O<sub>6</sub>P<sub>2</sub>], 630.13; C, 30.50; H, 4.89; found C, 31.23; H, 4.45.

**Synthesis of diiodide 2.14a.** **2.12** (2.00 g, 3.17 mmol) was placed in a dry 500 mL Schlenk flask under nitrogen purge. 100 mL of dry THF was added, followed by an excess of potassium *tert*-butoxide. Upon addition of base, the reaction turned a deep maroon. The reaction was capped under nitrogen and stirred for 10 minutes. 4-isopropylbenzaldehyde (1.18 g, 7.90 mmol) was added dropwise via syringe. The reaction was heated to 35°C for 8 hours. After 8 hours, the reaction was cooled to room temperature and 100 mL of water was added. The reaction was filtered and rinsed with water. The crude solid was dissolved in 50 mL of dichloromethane and precipitated into 300 mL of hexane. **2.14a** (1.54 g, 79 %) was isolated via filtration as bright yellow-green crystals. MP: 205-206°C. <sup>1</sup>H NMR (300 MHz, CDCl<sub>3</sub>): δ = 8.06 (s, 2H), 7.49 (d, J<sub>3H,H</sub> =

8.2 Hz, 4H), 7.25 (d,  $J_{3\text{H,H}} = 8.2$  Hz, 4H), 7.15 (d,  $J_{3\text{H,H}} = 16.2$  Hz, 2H), 6.96 (d,  $J_{3\text{H,H}} = 16.2$  Hz, 2H), 3.01-2.87 (m, 2H), 1.28 (d,  $J_{3\text{H,H}} = 6.87$  Hz, 12H).  $^{13}\text{C}$  NMR (300 MHz,  $\text{CDCl}_3$ ):  $\delta = 149.52, 140.87, 136.30, 134.43, 132.34, 129.84, 127.23, 127.10, 100.65, 34.35, 24.32$ . IR:  $\nu$  [ $\text{cm}^{-1}$ ] = 3004, 2950, 2929, 2856, 1628, 1512, 1454, 1355, 1329, 1243, 1052, 1041, 962, 890, 864, 854, 824, 816.

**Synthesis of diiodide 2.14b.** **2.12** (0.63 g, 1.00 mmol) was placed in a dry 250 ml Schlenk flask under nitrogen purge. 50 mL of dry THF was added, followed by an excess of potassium *tert*-butoxide. Upon addition of base, the reaction turned a deep maroon. The reaction was capped under nitrogen and stirred for 10 minutes. 4-pyridine carboxaldehyde (0.236 g, 2.20 mmol) was added dropwise via syringe. The reaction was heated to 35°C for 8 hours. After 8 hours, the reaction was cooled to room temperature and 100 mL of water was added. The reaction was extracted with chloroform, rinsed with brine, and dried with magnesium sulfate. The organics were reduced in vacuo isolating a crude solid. The crude solid was recrystallized from chloroform/hexanes, isolating **2.14b** (0.413 g, 77 %) as pale yellow crystals. MP: 273°C.  $^1\text{H}$  NMR (300 MHz,  $\text{CDCl}_3$ ):  $\delta = 8.62$  (d,  $J_{3\text{H,H}} = 3.84$  Hz, 4H), 8.09 (s, 2H), 7.40 (m, 6H), 6.93 (d,  $J_{3\text{H,H}} = 16.2$  Hz, 2H).  $^{13}\text{C}$  NMR (300 MHz,  $\text{CDCl}_3$ ):  $\delta = 150.40, 143.56, 140.62, 136.91, 130.13, 128.32, 121.13, 100.42$ . IR:  $\nu$  [ $\text{cm}^{-1}$ ] = 3047.4, 3030.7, 3026.6, 1560.1, 1555.6, 1051.9, 956.1, 856.1, 801.9, 731.1, 672.8.

**Synthesis of diiodide 2.14c.** **2.12** (5.65 g, 8.57 mmol) was placed in a dry 500 ml Schlenk flask under nitrogen purge. 200 mL of dry THF was added, followed by an excess of potassium *tert*-butoxide. Upon addition of base, the reaction turned a deep maroon. The reaction was capped under nitrogen and stirred for 10 minutes. 4-

dibutylaminobenzaldehyde (5.00 g, 21.4 mmol) was added dropwise via syringe. The reaction was heated to 35°C for 8 hours. After 8 hours, the reaction was cooled to room temperature and 200 mL of water was added. The reaction was filtered and rinsed with water. The crude solid was recrystallized from chloroform/hexanes isolating **2.14c** (5.18 g, 72 %) as brilliant orange crystals. MP: 165°C. <sup>1</sup>H NMR (300 MHz, CDCl<sub>3</sub>): δ = 8.00 (s, 2H), 7.40 (d, J<sub>3H,H</sub> = 8.78 Hz, 4H), 6.92-6.85 (dd, J<sub>3H,H</sub> = 16.2 Hz, 4H), 6.63 (d, J<sub>3H,H</sub> = 8.79 Hz, 4H), 3.28 (t, J<sub>3H,H</sub> = 7.41 Hz, 8H), 1.60-1.52 (m, 8H), 1.39-1.31 (m, 8H), 0.95 (t, J<sub>3H,H</sub> = 7.13 Hz, 12H). <sup>13</sup>C NMR (300 MHz, CDCl<sub>3</sub>): δ = 148.16, 140.42, 135.40, 131.89, 128.27, 125.39, 123.78, 111.49, 100.15, 50.77, 29.42, 20.32, 14.01. IR: ν [cm<sup>-1</sup>] = 2947.0, 2925.8, 2866.0, 1596.9, 1521.7, 1456.2, 1369.4, 1355.9, 1284.5, 1220.9, 1186.1, 1149.5, 1041.5, 954.7, 925.8, 802.3.

**Synthesis of alkyne 2.15e. TMS-protected 1-ethynyl-3,5bis(trifluoromethyl)benzene.**

3,5-Bis(trifluoromethyl)iodobenzene (2.00 g, 5.88 mmol) was combined with (PPh<sub>3</sub>)<sub>2</sub>PdCl<sub>2</sub> (50.0 mg, 72.1 μmol), CuI (50.0 mg, 333 μmol), 2.0 mL THF, and 2.0 mL piperidine in a nitrogen-purged Schlenk flask. The mixture was degassed and capped with a septum. Trimethylsilylacetylene (0.635 g, 6.47 mmol) was added via syringe. The reaction was then heated gently with a heat gun until precipitates formed; the reaction was then stirred in a warm water bath for 12 hours. The crude reaction mixture was eluted through a silica plug with hexanes. The hexanes were reduced in vacuo and **2.15e** (1.83 g, 83 %) was conveniently crystallized by sublimation in its own container at ambient temperature. <sup>1</sup>H NMR (300 MHz, CDCl<sub>3</sub>): δ = 7.87 (s, 2H), 7.78 (s, 1H), 0.25 (s, 9H). <sup>13</sup>C NMR (300 MHz, CDCl<sub>3</sub>): δ = 132.54-131.53 (q, J<sub>2C,F</sub> = 33.8 Hz), 132.06-132.03 (q, J<sub>3C,F</sub> = 3.0 Hz), 127.19-119.06 (q, J<sub>1C,F</sub> = 272.9 Hz), 125.66, 122.02-121.9 (q,

$J_{3C,F} = 3.76$  Hz), 101.7, 98.97, 0.14. IR:  $\nu$  [ $\text{cm}^{-1}$ ] = 3087.8, 2960.5, 2900.7, 2173.6, 1834.2, 1807.2, 1786.0, 1608.5, 1460.0, 1409.9, 1373.2, 1300.8, 1249.8, 1181.2, 1130.2, 1107.1, 912.3, 907.7, 896.8, 891.1, 763.8.

**Synthesis of XF 2.1.** The diiodide precursor **2.13a** (500 mg, 0.809 mmol) was combined with 4-ethynylpyridine (**2.15a**, 209 mg, 2.02 mmol),  $(\text{PPh}_3)_2\text{PdCl}_2$  (5.0 mg, 7.1  $\mu\text{mol}$ ), CuI (5.0 mg, 33  $\mu\text{mol}$ ), 2 mL Hünig's base, and 2 mL THF in a Schlenk tube under nitrogen purge. The reaction was capped with a septum, placed in a 45°C water bath, and allowed to react for 24 hours. The crude reaction was poured into a 1 L flask containing 250 mL 5 % aqueous  $\text{NH}_4\text{OH}$  and 250 mL of hexanes. The mixture was vigorously stirred, then filtered, isolating a yellow solid. The solid was collected by filtration, dissolved in a minimum volume of chloroform, and precipitated into 250 mL of rapidly stirring hexanes. The solid was collected by vacuum filtration, yielding XF **2.1** (322 mg, 70 %) as a yellow needles. MP: 273-275°C (decomposition).  $^1\text{H}$  NMR (300 MHz,  $\text{CDCl}_3$ ):  $\delta$  = 8.67 (bs, 4H), 7.91 (s, 2H), 7.55 (d,  $J_{3\text{H,H}} = 16.5$  Hz), 7.54 (d, 4H,  $J_{3\text{H,H}} = 8.24$  Hz), 7.45 (d, 4H,  $J_{3\text{H,H}} = 5.5$  Hz), 7.25 (m, 6H), 2.99-2.90 (m, 2H), 1.39 (d, 12H,  $J_{3\text{H,H}} = 6.9$  Hz).  $^{13}\text{C}$  NMR (300 MHz,  $\text{CDCl}_3$ ):  $\delta$  = 150.1, 149.6, 137.9, 134.7, 131.5, 129.2, 127.2, 127.0, 125.7, 124.2, 121.9, 93.0, 92.4, 34.3, 24.3. IR:  $\nu$  [ $\text{cm}^{-1}$ ] = 3044, 3023, 2957, 2869, 1591, 1538, 1514, 1458, 1404, 1249, 1214, 967, 864, 817, 625. Analysis: calculated C = 88.69, H = 6.38; found C = 88.41, H = 6.28.

**Synthesis of XF 2.2.** The diiodide precursor **2.13b** (250 mg, 0.466 mmol) was combined with 1-*tert*-butyl-4-ethynylbenzene (**2.15b**, 184 mg, 1.17 mmol),  $(\text{PPh}_3)_2\text{PdCl}_2$  (5.0 mg, 7.1  $\mu\text{mol}$ ), CuI (5.0 mg, 33  $\mu\text{mol}$ ), 4 mL THF/piperidine (1:1) in a Schlenk tube under nitrogen purge. The reaction was capped with a septum, placed in a 45°C water bath, and

allowed to react for 24 hours. The crude reaction was poured into a 1 L flask containing 250 mL 5 % aqueous  $\text{NH}_4\text{OH}$  and 250 mL of hexanes. The mixture was vigorously stirred, then filtered, isolating a yellow solid. The solid was collected by filtration, dissolved in a minimum volume of chloroform, and precipitated into 250 mL of rapidly stirring hexanes. The solid was collected by vacuum filtration, yielding XF **2.2** (214 mg, 77 %) as a pale yellow solid. MP: 264°C.  $^1\text{H}$  NMR (300 MHz,  $\text{CDCl}_3$ ):  $\delta$  = 8.61 (bs, 4H), 7.91 (s, 2H), 7.87 (d, 2H,  $J_{\text{H,H}} = 16.5$  Hz), 7.54 (d, 4H,  $J_{\text{H,H}} = 8.51$  Hz), 7.44 (m, 8H), 7.22 (d, 2H,  $J_{\text{H,H}} = 16.5$  Hz), 1.34 (s, 18H).  $^{13}\text{C}$  NMR (300 MHz,  $\text{CDCl}_3$ ):  $\delta$  = 152.34, 150.22, 144.23, 136.76, 131.31, 129.85, 129.18, 128.06, 125.62, 122.90, 121.20, 119.62, 96.55, 86.53, 34.88, 31.14. IR:  $\nu$  [ $\text{cm}^{-1}$ ] = 2960.5, 2868.0, 2358.8, 2208.3, 1593.1, 1506.3, 1461.9, 1363.6, 1267.1, 1217.0, 1103.2, 1016.4, 962.4, 866.0, 833.2, 800.4. MS (DEP,  $\text{C}_{44}\text{H}_{40}\text{N}_2$ ):  $m/z$  = 596.

**Synthesis of XF 2.3.** The diiodide precursor **2.13c** (330 mg, 0.418 mmol) was placed into a Schlenk tube and purged with nitrogen.  $(\text{PPh}_3)_2\text{PdCl}_2$  (5.0 mg, 7.1  $\mu\text{mol}$ ) and  $\text{CuI}$  (5.0 mg, 33  $\mu\text{mol}$ ) were added, and the reaction mixture was dissolved in 4 mL of piperidine/THF (1:1). The reaction was stirred under nitrogen at room temperature for 15 minutes. Phenyl acetylene (**2.15c**, 107 mg, 1.05 mmol) was then added. The reaction was then allowed to stir at room temperature for 24 hours. The crude reaction mixture was poured into water and extracted into  $\text{CHCl}_3$ . This was then added dropwise to rapidly stirring methanol, precipitating an orange solid. Recrystallization from methanol yielded cruciform **2.3** (280 mg, 91 %) as orange crystals. MP: 164-168°C.  $^1\text{H}$  NMR (300 MHz,  $\text{CDCl}_3$ ):  $\delta$  = 7.84 (s, 2H), 7.84 (d, 4H,  $J_{\text{H,H}} = 7.7$  Hz), 7.44 (m, 12H), 7.19 (d, 2H,  $J_{\text{H,H}} = 16.5$  Hz), 6.64 (d, 4H,  $J_{\text{H,H}} = 8.8$  Hz), 3.31 (t, 8H,  $J_{\text{H,H}} = 7.41$  Hz), 1.63

(m, 8H), 1.39 (m, 8H), 0.97 (t, 12H,  $J_{3\text{H,H}} = 7.4$  Hz).  $^{13}\text{C}$  NMR (300 MHz,  $\text{CDCl}_3$ ):  $\delta = 147.97, 137.29, 131.57, 130.38, 128.38, 128.25, 128.09, 128.07, 124.49, 123.48, 121.41, 120.50, 111.59, 94.78, 88.51, 50.74, 29.46, 20.32, 14.00$ . IR:  $\nu [\text{cm}^{-1}] = 3033.8, 2929.7, 1795.6, 1600.8, 1521.7, 1461.9, 1400.2, 1367.4, 1257.5, 1220.9, 1147.9, 1109.0, 925.8, 804.3, 752.2, 688.5$ . MS (DEP,  $\text{C}_{54}\text{H}_{60}\text{N}_2$ ):  $m/z = 736$ .

**Synthesis of XF 2.4.** The diiodide precursor **2.13c** (1.00 g, 3.78 mmol) was combined with 2.0 mL of ethanol and 1.0 g of potassium hydroxide. After 10 minutes, pentafluorophenylethynyl-trimethylsilane (**2.15d**, 789 mg, 1.00 mmol),  $(\text{PPh}_3)_2\text{PdCl}_2$  (5.0 mg, 7.1  $\mu\text{mol}$ ), CuI (5.0 mg, 33  $\mu\text{mol}$ ) and 6.0 mL of triethylamine/THF 1:1 were added while under nitrogen purge. The reaction was allowed to progress over 24 hours. The crude reaction mixture was precipitated from dichloromethane into hexane and a second time from dichloromethane into cold methanol.  $^1\text{H}$  NMR determined the product still contained impurities (deemed later to be the addition of ethoxide to the fluorinated aromatic ring), so the product was purified by flash chromatography (dichloromethane/hexane, 1:1 as eluent). The resulting brilliant orange powder was recrystallized by evaporation of dichloromethane from methanol yielding crystals of XF **2.4** (2.38 g, 65 %) suitable for crystallographic analysis which ultimately determined the source of the additional peaks in the NMR spectrum.  $^{13}\text{C}$  NMR was not feasible due to the highly fluorinated ring system producing a forest of peaks. MP: 173-174°C.  $^1\text{H}$  NMR (300 MHz,  $\text{CDCl}_3$ ):  $\delta = 7.88$  (s, 2H), 7.47 (m, 6H,  $J_{3\text{H,H}} = 16.15$  Hz), 6.67 (d, 2H,  $J_{3\text{H,H}} = 8.57$  Hz), 4.42 (q, 4H,  $J_{3\text{H,H}} = 7.02$  Hz), 3.34 (t, 8H,  $J_{3\text{H,H}} = 7.27$  Hz), 1.63-1.56 (m, 8H), 1.46-1.32 (m, 14H), 0.98, 0.93 (t, 12H,  $J_{3\text{H,H}} = 7.34$  Hz). IR:  $\nu [\text{cm}^{-1}] = 3034.8, 2965.4, 2860.2, 2210.3, 1603.7, 1578.6, 1521.7, 1497.6, 1442.7, 1400.2, 1390.6, 1365.5,$

1274.9, 1217.0, 1196.8, 1186.1, 1127.3, 1026.1, 983.6, 956.66, 893.0, 805.2, 683.7.

Analysis for  $C_{58}H_{60}F_8N_2O_2$ : calculated C = 71.88, H = 6.24; found C = 71.68, H = 6.19.

**Synthesis of XF 2.5.** The diiodide precursor **2.13c** (182 mg, 0.250 mmol) was placed into a Schlenk tube and purged with nitrogen.  $(PPh_3)_2PdCl_2$  (5.0 mg, 7.1  $\mu$ mol) and CuI (5.0 mg, 33  $\mu$ mol) were added, and the reaction mixture was dissolved in 4 mL of piperidine/THF (1:1). The reaction was stirred under nitrogen at room temperature for 15 minutes. 1-ethynyl-3,5bis(trifluoromethyl)benzene (**2.15e**, 177 mg, 0.624 mmol) was then added. The reaction was then allowed to stir at room temperature for 24 hours. The crude reaction mixture was poured into water and extracted into  $CHCl_3$ . This was then added dropwise to rapidly stirring methanol, precipitating an orange solid. Recrystallization from methanol yielded cruciform **2.5** (192 mg, 76 %) as orange crystals. MP: 191°C.  $^1H$  NMR (300 MHz,  $CDCl_3$ ):  $\delta$  = 8.02 (s, 4H), 7.86 (s, 2H), 7.84 (s, 2H), 7.43 (d, 4H,  $J_{3H,H} = 8.78$  Hz), 7.37 (d, 2H,  $J_{3H,H} = 16.2$  Hz), 7.19 (d, 2H,  $J_{3H,H} = 16.3$  Hz), 6.65 (d, 4H,  $J_{3H,H} = 8.51$  Hz), 3.32 (t, 8H,  $J_{3H,H} = 6.59$  Hz), 1.58 (m, 8H), 1.39 (m, 8H), 0.97 (t, 12H,  $J_{3H,H} = 7.14$  Hz).  $^{13}C$  NMR (300 MHz,  $CDCl_3$ ):  $\delta$  = 148.29, 137.80, 132.53-131.53 (m), 131.30, 131.21, 128.22, 128.13, 127.06-118.9 (m), 125.70, 123.98, 121.62, 120.82, 119.66, 111.59, 92.07, 91.94. MS (DEP,  $C_{56}H_{56}F_{12}N_2$ ):  $m/z = 1008$ .

**Synthesis of XF 2.6.** The diiodide precursor **2.13c** (683 mg, 0.866 mmol) was combined with 4-ethynylbenzotrile (**2.15f**, 330 mg, 2.60 mmol),  $(PPh_3)_2PdCl_2$  (5.0 mg, 7.1  $\mu$ mol), CuI (5.0 mg, 33  $\mu$ mol) and dissolved in 4.0 mL of triethylamine/THF 1:1. The reaction was stirred for 24 hours at 40°C. The crude reaction mixture was precipitated twice from dichloromethane into hexane. The resulting orange-red powder was purified by flash chromatography beginning with hexane and gradually switching to 1:2

dichloromethane:hexane isolating XF **2.6** (0.532 g, 78 %). MP: 239-241°C.  $^1\text{H}$  NMR (300 MHz,  $\text{CDCl}_3$ ):  $\delta$  = 7.84 (s, 2H), 7.68 (m, 8H), 7.42 (d, 4H,  $J_{3\text{H,H}} = 8.71$  Hz), 7.36 (d, 2H,  $J_{3\text{H,H}} = 16.16$  Hz), 7.19 (d, 2H,  $J_{3\text{H,H}} = 16.21$  Hz), 6.66 (d, 4H,  $J_{3\text{H,H}} = 8.81$  Hz), 3.34 (d, 8H,  $J_{3\text{H,H}} = 7.15$  Hz), 1.63 (m, 8H), 1.41 (m, 8H), 1.00 (t, 12H,  $J_{3\text{H,H}} = 7.31$  Hz).  $^{13}\text{C}$  NMR ( $\text{CDCl}_3$ ):  $\delta$  = 148.37, 137.84, 132.33, 132.21, 131.35, 128.63, 128.42, 128.34, 124.24, 121.22, 119.92, 118.76, 111.80, 93.06, 51.11, 29.84, 20.74, 14.43. IR:  $\nu$  [ $\text{cm}^{-1}$ ] = 3037.7, 2952.8, 2927.7, 2925.8, 2918.1, 2859.2, 2222.8, 2205.4, 1600.8, 1550.6, 1521.7, 1509.1, 1465.8, 1457.1, 1427.2, 1399.2, 1367.4, 1314.4, 1284.5, 1252.6, 1221.8, 1183.2, 1149.5, 1109.9, 1104.1, 983.6, 954.7, 924.8, 887.1, 846.6, 835.1, 822.5, 801.3. MS (EI, 70 eV):  $\text{M}^+$  786.6 (36), 434.4 (62), 289.2 (68), 162.1 (100), 106.1 (49), 41.1 (95). HRMS (EI, 70 eV): calculated for  $\text{C}_{56}\text{H}_{58}\text{N}_4$ : 786.46615, found 786.46568.

**Synthesis of XF 2.7.** The diiodide precursor **2.13c** (560 mg, 0.758 mmol) was combined with 4-ethynylpyridine (**2.15a**, 300 mg, 2.91 mmol),  $(\text{PPh}_3)_2\text{PdCl}_2$  (5.0 mg, 7.1  $\mu\text{mol}$ ), CuI (5.0 mg, 33  $\mu\text{mol}$ ), 2 mL Hünig's base, and 2 mL THF in a Schlenk tube under nitrogen purge. The reaction was capped with a septum, placed in a 45°C water bath, and allowed to react for 24 hours. The crude reaction was poured into a 1 L flask containing 250 mL 5 % aqueous  $\text{NH}_4\text{OH}$  and 250 mL of hexanes. The mixture was vigorously stirred, then filtered, isolating a bright orange solid. The solid was collected by filtration, dissolved in a minimum volume of chloroform, and precipitated into 250 mL of rapidly stirring hexanes. The solid was collected by vacuum filtration, yielding XF **2.7** (347 mg, 62 %) as a bright orange solid. MP: 201-203°C.  $^1\text{H}$  NMR (300 MHz,  $\text{CDCl}_3$ ):  $\delta$  = 8.66 (bs, 4H), 7.87 (s, 2H), 7.46-7.41 (m, 8H), 7.35 (d, 2H,  $J_{3\text{H,H}} = 16.2$  Hz), 7.18 (d, 2H,  $J_{3\text{H,H}} = 16.2$  Hz), 6.65 (bd, 4H), 3.32 (t, 8H,  $J_{3\text{H,H}} = 7.7$  Hz), 1.75-1.52 (m, 8H), 1.38-1.33 (m,

8H), 0.96 (t, 12H,  $J_{3\text{H,H}} = 7.4$  Hz).  $^{13}\text{C}$  NMR (300 MHz,  $\text{CDCl}_3$ ):  $\delta = 149.95, 148.31, 137.85, 131.63, 128.65, 125.74, 124.34, 121.14, 119.92, 111.86, 93.24, 92.51, 51.15, 29.85, 20.75, 14.45$ . IR:  $\nu$  [ $\text{cm}^{-1}$ ] = 2956, 2869, 1600, 1589, 1517, 1399, 1366, 1313, 1281, 1218, 1184, 1151, 955, 821, 804. Analysis: calculated C = 84.51, H = 7.91; found C = 84.33, H = 7.78.

**Synthesis of XF 2.8a.** The diiodide precursor **2.13a** (1.01 g, 1.63 mmol) was placed into a Schlenk tube and purged with nitrogen.  $(\text{PPh}_3)_2\text{PdCl}_2$  (5.0 mg, 7.1  $\mu\text{mol}$ ) and CuI (5.0 mg, 33  $\mu\text{mol}$ ) were added, and the reaction mixture was dissolved in 10.0 mL of piperidine/THF (1:1). The reaction was stirred under nitrogen at room temperature for 15 minutes. Phenyl acetylene (**2.15c**, 415 mg, 4.06 mmol) was then added. The reaction was then allowed to stir at room temperature for 24 hours. The crude reaction mixture was poured into water and extracted three times into  $\text{CHCl}_3$ . The combined organics were then washed three times with water, three times with brine, and dried with  $\text{MgSO}_4$ . The crude product was isolated in vacuo as a greenish yellow powder. Recrystallization from dichloromethane/hexanes yielded cruciform **2.8a** (0.61 g, 66 %) as greenish yellow needles. MP: 234-236°C under decomposition.  $^1\text{H}$  NMR (300 MHz,  $\text{CDCl}_3$ ):  $\delta = 7.91$  (s, 2H), 7.67-7.61 (m, 6H), 7.52 (d, 4H,  $J_{3\text{H,H}} = 8.1$  Hz), 7.44-7.39 (m, 6H), 7.29-7.24 (m, 6H), 2.99-2.89 (m, 2H), 1.29 (d, 12H,  $J_{3\text{H,H}} = 6.9$  Hz).  $^{13}\text{C}$  NMR (300 MHz,  $\text{CDCl}_3$ ):  $\delta = 149.24, 137.62, 135.16, 131.85, 130.78, 128.95, 128.80, 128.74, 127.14, 127.05, 124.99, 123.42, 122.40, 95.67, 88.15, 34.21, 24.18$ . IR:  $\nu$  [ $\text{cm}^{-1}$ ] = 3082.0, 3024.2, 2952.8, 2869.9, 1627.8, 1595.0, 1508.2, 1496.7, 960.5, 860.2, 813.9, 752.2, 686.6.

## 2.5. References and Notes

26. (a) Wilson, J. N.; Bunz, U. H. F. Switching of intermolecular charge-transfer in cruciforms: metal ion sensing. *J. Am. Chem. Soc.* **2005**, *127*, 4124-4125. (b) Zuccherro, A. J.; Wilson, J. N.; Bunz, U. H. F. Cruciforms as functional fluorophores: response to protons and selected metal ions. *J. Am. Chem. Soc.* **2006**, *128*, 11872-11881.
27. Wheland, R. C.; Martin, E. L. Synthesis of substituted 7,7,8,8-tetracyanoquinodimethanes. *J. Org. Chem.* **1975**, *40*, 3101-3109.
28. (a) Horner, L.; Hoffmann, H.; Wippel, H. G.; Klahre, G. Phosphororganische verbindungen .20. Phosphinoxyde als olefinierungsreagenzien. *Chem. Ber.* **1959**, *92*, 2499-2505. (b) Horner, L.; Klink, W. Phosphororganische verbindungen .43. Untersuchungen zum sterischen verlauf der po-aktivierten olefinierung. *Tetrahedron Lett.* **1964**, *36*, 2467-2473.
29. (a) Sonogashira, K. Development of Pd-Cu catalyzed cross-coupling of terminal acetylenes with sp<sup>2</sup>-carbon halides. *J. Organomet. Chem.* **2002**, *653*, 46-49. (b) Bunz, U. H. F. Poly(aryleneethynylene)s: Syntheses, properties, structures, and applications. *Chem. Rev.* **2000**, *100*, 1605-1645.
30. (a) Tolbert, L. M.; Nesselroth, S. M.; Netzel, T. L.; Raya, N.; Stapleton, M. Substituent effects on carbanion photophysics – 9-arylfluorenyl anions. *J. Phys. Chem.* **1992**, *96*, 4492-4496. (b) Englman, R.; Jortner, J. Energy gap law for radiationless transitions in large molecules. *Molecular Physics* **1970**, *18*, 145-154. (c) Caspar, J. V.; Meyer, T. J. Application of the energy-gap law to nonradiative, excited-state decay. *J. Phys. Chem.* **1983**, *87*, 952-957.
31. (a) Yang, J. S.; Chiou, S. Y.; Liao, K. L. Fluorescence enhancement of trans-4-aminostilbene by N-phenyl substitutions: The "amino conjugation effect." *J. Am. Chem. Soc.* **2004**, *126*, 2518-2527. (b) Yang, J. S.; Liao, K. L.; Wang, C. M.; Hwang, C. Y. Substituent-dependent photoinduced intramolecular charge transfer in N-aryl-substituted trans-4-aminostilbenes. *J. Am. Chem. Soc.* **2004**, *126*, 12325-12335. (c) Yang, J. S.; Liao, K. L.; Tu, C. W.; Hwang, C. Y. Excited-state behavior of N-phenyl-substituted trans-3-aminostilbenes: Where the "m-amino effect" meets the "amino-conjugation effect." *J. Phys. Chem. A.* **2005**, *109*, 6450-6456. (d) Yang, J. S.; Lin, Y. D.; Chang, Y. H.; Wang, S. S. Synthesis, dual fluorescence, and fluoroionophoric behavior of dipyrindylaminomethylstilbenes. *J. Org. Chem.* **2005**, *70*, 6066-6073.
32. (a) Marri, E.; Pannacci, D.; Galiazzo, G.; Mazzucato, U.; Spalletti, A. Effect of the nitrogen heteroatom on the excited state properties of 1,4-distyrylbenzene. *J. Phys. Chem. A.* **2003**, *107*, 11231-11238. (b) Sancho-Garcia, J. C.; Bredas, J. L.; Beljonne, D.; Cornil, J.; Martinez-Alvarez, R.; Hanack, M.; Poulsen, L.; Gierschner, J.; Mack, H. G.; Egelhaaf, H. J.; Oelkrug, D. Design of pi-conjugated organic materials for

- one-dimensional energy transport in nanochannels. *J. Phys. Chem. B.* **2005**, *109*, 4872-4880. (c) Pond, S. J. K.; Tsutsumi, O.; Rumi, M.; Kwon, O.; Zojer, E.; Bredas, J. L.; Marder, S. R.; Perry, J. W. Metal-ion sensing fluorophores with large two-photon absorption cross sections: Aza-crown ether substituted donor-acceptor-donor distyryl benzenes. *J. Am. Chem. Soc.* **2004**, *126*, 9291-9306. (d) Hong, J. W.; Woo, H. Y.; Liu, B.; Bazan, G. C. Solvatochromism of distyrylbenzene pairs bound together by [2.2]paracyclophane: Evidence for a polarizable "Through-Space" delocalized state. *J. Am. Chem. Soc.* **2005**, *127*, 7435-7443. (e) Gierschner, J.; Egelhaaf, H. J.; Mack, H. G.; Oelkrug, D.; Martinez Alvarez, R.; Hanack M. Luminescence of conjugated molecules confined in nanochannels. *Synth. Met.* **2003**, *137*, 1449-1450. (f) Holzer, W.; Penzkofer, A.; Gong, S. H.; Bradley, D. D. C.; Long, X.; Blau, W. J.; Davey, A. P. Excitation intensity-dependent fluorescence behaviour of some luminescent polymers. *Polymer.* **1998**, *39*, 3651-3656.
33. (a) Birckner, E.; Grummt, U.-W.; Göller, A. H.; Pautzsch, T.; Egbe, D. A. M.; Al-Higari, M.; Klemm, E. Photophysics of arylene and heteroaryleneethylenes. *J. Phys. Chem. A.* **2001**, *105*, 10307-10315. (b) Biswas, M.; Nguyen, P.; Marder, T. B.; Khundkar, L. R. Unusual size dependence of nonradiative charge recombination rates in acetylene-bridged compounds. *J. Phys. Chem. A.* **1997**, *101*, 16897-1695. (c) Collings, J. C.; Parsons, A. C.; Porres, L.; Beeby, A.; Basanov, A. S.; Howard, J. A. K.; Lydon, D. B.; Low, P. J.; Fairlamb, J. S.; Marder, T. B. Optical properties of donor-acceptor phenylene-ethynylene systems containing the 6-methylpyran-2-one group as an acceptor. *Chem. Commun.* **2005**, 2666-2668. (d) Sun, S.-S.; Lees, A. J. Photophysics and evidence of excimer formation, linear bipyridines in solution and solid films. *J. Photochemistry, Photobiology A.* **2001**, *140*, 157-161.
34. Opsitnick, E.; Lee, D. Two-dimensional electronic conjugation: statics and dynamics at structural domains beyond molecular wires. *Chem. Eur. J.* **2007**, *13*, 7040-7049.
35. (a) Marsden, J. A.; Miller, J. J.; Shirtcliff, L. D.; Haley, M. M. Structure-property relationships of donor/acceptor-functionalized tetrakis(phenylethynyl)benzenes and bis(dehydrobenzoannuleno)benzenes. *J. Am. Chem. Soc.* **2005**, *127*, 2464-2476. (b) Spitler, E. L.; Shirtcliff, L. D.; Haley, M. M. Dynamic proton-induced two-stage emission switching in donor-functionalized bis(dehydrobenzo[n]annuleno)benzenes and 1,2,4,5-tetrakis(phenylethynyl)benzene. *J. Org. Chem.* **2007**, *72*, 86-96. (c) Slepko, A. D.; Hegmann, F. A.; Tykwinski, R. R.; Kamada, K.; Ohta, K.; Marsden, J. A.; Spitler, E. L.; Miller, J. J.; Haley, M. M. *Opt. Lett.* **2006**, *31*, 3315-3317. (d) Spitler, E. L.; Haley, M. M. Dynamic proton-induced two-stage emission switching in donor-functionalized bis(dehydrobenzo[n]annuleno)benzenes and 1,2,4,5-tetrakis(phenylethynyl)benzene. *Tetrahedron.* **2008**, *64*, 11469-11474.
36. (a) Zen, A.; Pingel, P.; Jaiser, F.; Neher, D.; Grenzer, J.; Zhuang, W.; Rabe, J. P.; Bilge, A.; Galbrecht, F.; Nehls, B. S.; Farrell, T.; Scherf, U.; Abellon, R. D.; Grozema, F. C.; Siebbeles, L. D. A. Organic field-effect transistors utilizing solution-deposited oligothiophene-based swivel cruciforms. *Chem. Mater.* **2007**, *19*, 1267-1276. (b) Bilge, A.; Zen, A.; Forster, M.; Li, H.; Galbrecht, F.; Nehls, B. S.; Farrell,

- T.; Neher, D.; Scherf, U. Swivel-cruciform oligothiophene dimers. *J. Mater. Chem.*, **2006**, *16*, 3177–3182.
37. Henary, M. M.; Wu, Y. G.; Fahrni, C. J. Zinc(II)-selective ratiometric fluorescent sensors based on inhibition of excited-state intramolecular proton transfer. *Chem. Eur. J.* **2004**, *10*, 3015-3025.

## CHAPTER 3

### Cruciforms as Functional Fluorophores

#### 3.1. Introduction

Functional chromophores contain embedded recognition elements as integral parts of their  $\pi$ -system. Such chromophores are innately qualified to serve as active elements in sensors or sensor arrays and in advanced materials applications. *Functional* chromophores are different from *functionalized* chromophores, where recognition elements are merely appendages affixed to a fluorescent core. Functional chromophores undergo analyte-induced shifts in absorption and emission; the binding modulates electronic properties due to the interweaving of  $\pi$ -system and recognition element. Prominent examples are Zn-ESIPT sensors and related phores,<sup>1</sup> bipyridine-containing conjugated polymers,<sup>2</sup> tetraethynylethenes (TEEs) and diethynylethenes (DEEs),<sup>3</sup> and oligophenyleneethynylene-embedded 2,6-bis(1,9-methylbenzimidazolyl)pyridines.<sup>4</sup> Whenever basic nitrogens or phenolates are integral part of a dye, functional chromophores result. Pyridines, bipyridines and terpyridines as well as aromatic dialkylamines, phenolates, and phosphines, inter alia, are good candidates to render a chromophore “functional”. Embedded bases can be either strongly electron accepting, such as pyridines, or strongly electron donating, such as dialkylanilines, permitting the rational design of functional chromophores with modular photophysical responses. If donor and acceptor units are spatially separated, it will be possible to address HOMO and LUMO independently by Lewis acids or metal cations. A chromophore system will result that naturally displays a substantial sensory response upon binding to an electron

deficient analyte. Cruciforms **3.1-3.7** are functional chromophores, with incorporated basic nitrogens; they should show potential in the fabrication of functional sensor arrays for metal ions.<sup>5</sup>

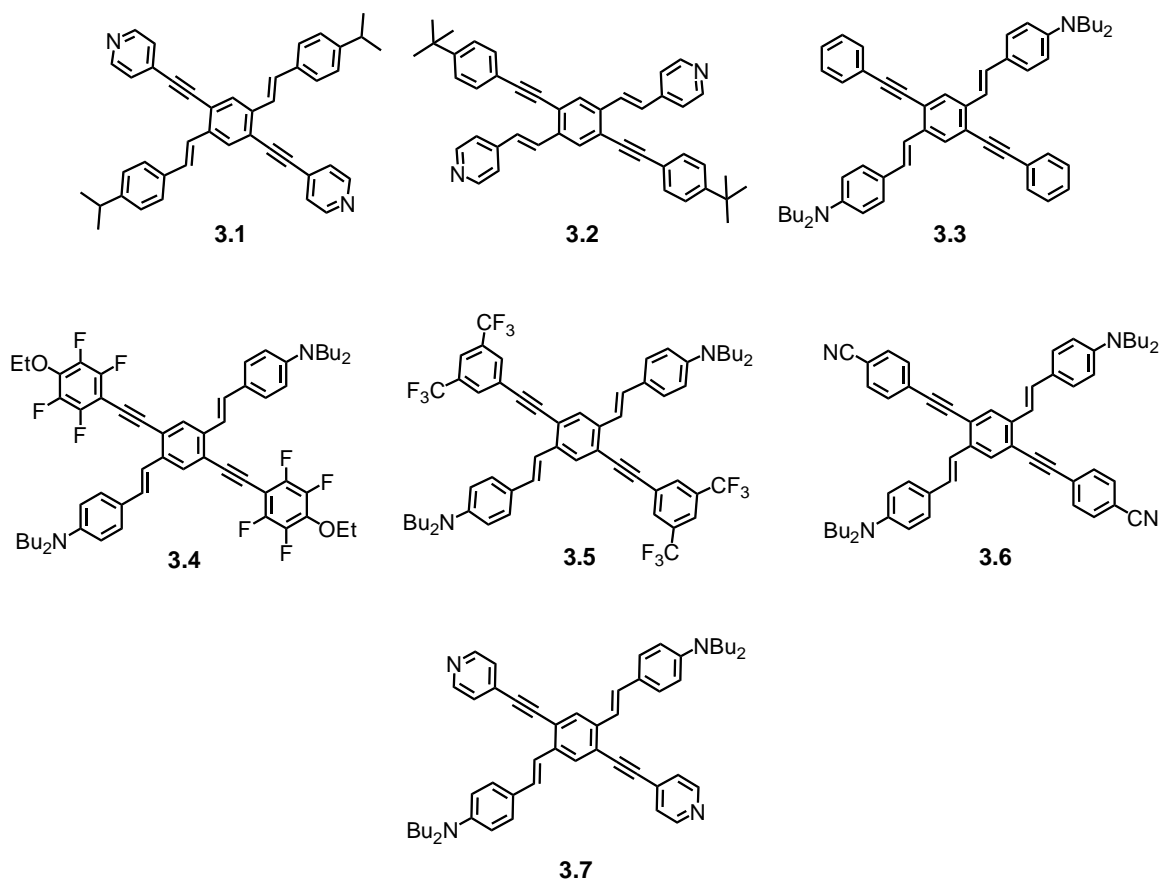


**Figure 3.1.** Structure of XFs **3.1-3.7**.

Our previous investigation of **3.1-3.7** revealed the unique photophysical properties of these Lewis basic XFs. Our examination revealed these properties emerge as a consequence of the XF skeleton's ability to exhibit FMO separation. We hypothesized that the substituent induced separation of the FMOs in XFs **3.1-3.7** might render these materials extremely responsive towards electron deficient analytes. To fully understand and appreciate the subtleties and issues associated with the sensory response

of these cruciform chromophores, we examined the response of XFs **3.1-3.7** to protons (trifluoroacetic acid, TFA) and the triflate salts of  $\text{Mg}^{2+}$ ,  $\text{Ca}^{2+}$ ,  $\text{Mn}^{2+}$  and  $\text{Zn}^{2+}$ . We selected these metal cations as they are all biologically active, +2 charged ions of similar size. Large shifts in absorption, fluorescence, quantum yields, and emissive lifetimes are observed upon the addition of protons or metal cations. The comparison of the results upon the addition of TFA and metal cation provides a convenient method to probe the locus and stereochemistry of metal binding. The observed photophysics can be explained by the position and the spatial arrangement of the frontier molecular orbitals and their interaction with cations.

### **3.2. The Importance of FMO Separation**

For dyes to exhibit ratiometric sensory responses, the interaction of an analyte must elicit a substantial change in the fluorophore's HOMO-LUMO gap. This necessitates that one frontier molecular orbital must be disproportionately affected by analyte interaction. In the majority of organic fluorophores, HOMO and LUMO are 'congruent', i.e. the orbital coefficients are similar in the respective FMOs. One would not expect large shifts in color or emission wavelength upon binding to an analyte; the position of HOMO and LUMO should be more or less equally affected, resulting in only small net changes in the HOMO-LUMO gap.

In molecular architectures exhibiting spatially separated FMOs, an alluring alternative is possible. In these situations, electronic information becomes spatially encoded; if recognition elements are incorporated into the fluorophore such that analyte binding independently influences the FMOs, large ratiometric sensory responses can be

observed. In such systems, binding largely stabilizes either the HOMO or LUMO, inducing a significant change in emission and absorption spectra. As a result, conjugated frameworks such as the XFs exhibiting FMO separation have intrinsic potential as responsive materials. XFs possessing Lewis-basic nitrogens incorporated into the  $\pi$ -electron system provide an opportunity to probe the sensory responses of XFs when exposed to model analytes such as TFA or metal cations.

### 3.3. XFs Exhibiting a Two-Stage Fluorescence Response: A Case Study

Our initial examination of the sensory responses of XFs began by exposing **3.7** to both  $\text{Zn}^{2+}$  and TFA.<sup>6</sup> Upon addition of increasing equivalents of  $\text{Zn}^{2+}$  ions to **3.7** in chloroform, a rare two-stage fluorescence response is observed: the emission color changes dramatically from orange to blue and then to green (Figure 3.2). A similar response is observed upon addition of TFA to **3.7**.

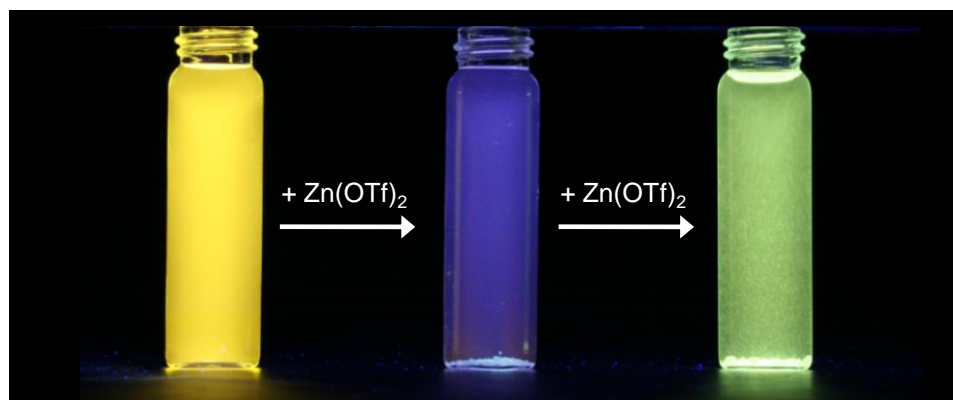


**Figure 3.2.** Emission of **3.7** in chloroform (left vial, orange emission), upon addition of a small amount of  $\text{Zn}(\text{OTf})_2$  (center vial, blue emission), and upon addition of a large excess of  $\text{Zn}(\text{OTf})_2$  (right vial, green emission).

To more carefully examine this effect, we performed a spectrophotometric titration of **3.7** with  $\text{Zn}(\text{OTf})_2$  in dichloromethane (Figure 3.3). The absorption of **3.7**

consists of a high energy band 335 nm and a charge transfer peak centered at 440 nm. Upon addition of  $\text{Zn}^{2+}$ , the charge transfer feature disappears accompanied by a small shift (335  $\rightarrow$  350 nm) in the high energy band. In the emission, upon addition of a small quantity of  $\text{Zn}(\text{OTf})_2$ , a large blue shift (570  $\rightarrow$  420 nm) occurs; subsequent addition of  $\text{Zn}^{2+}$  results in a bathochromic shift (420  $\rightarrow$  530 nm).

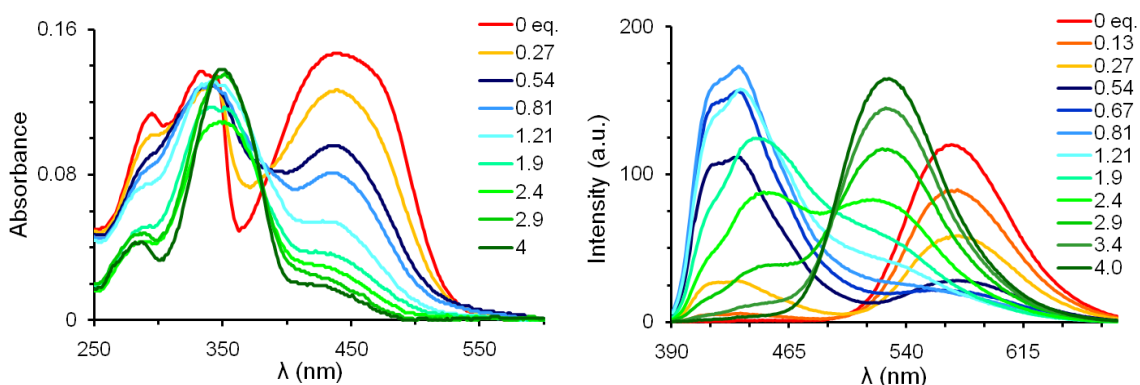


**Figure 3.3.** Absorption (left) and emission (right) of **3.7** in dichloromethane upon exposure to increasing equivalents of zinc triflate.

To rationalize this two-stage response, we elected to examine the sensory response of **3.2** and **3.3**; these XFs are bona fide models of **3.7** possessing either pyridyl or dibutylamino substituents. In the case of **3.3**, only a hypsochromic shift (527  $\rightarrow$  430 nm) is observed upon addition of  $\text{Zn}^{2+}$  (Figure 3.4). Consideration of the FMO arrangement in **3.3** offers an explanation for this result; B3LYP 6-31G\*\*//6-31G\*\* calculations suggest the HOMO is localized primarily on the distyryl axis of the XF. Binding of  $\text{Zn}^{2+}$  to the aniline nitrogens of **3.3** stabilizes the HOMO while leaving the LUMO largely unperturbed. As a result, a blue shift in emission is observed (Figure 3.6a). XF **3.2** contains exclusively the pyridyl binding functionalities on the arylethynyl axis. Upon reaction with zinc triflate, a redshift in emission (457  $\rightarrow$  564 nm) is observed

(Figure 3.5). Zinc coordination of the pyridyl nitrogens stabilizes the LUMO of **3.2** which lies along the arylethynyl axis of the XF scaffold while the HOMO is unaffected (Figure 3.6b).

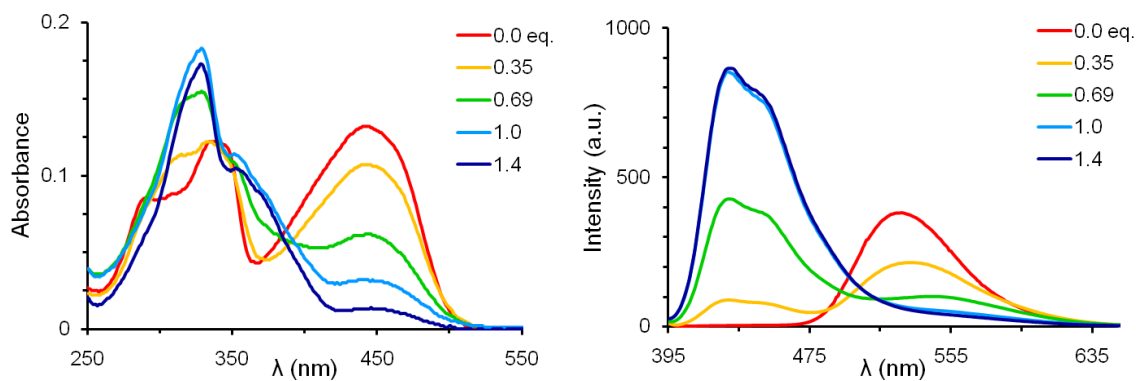


**Figure 3.4.** Absorption (left) and emission (right) of **3.3** in dichloromethane upon exposure to increasing equivalents of zinc triflate.

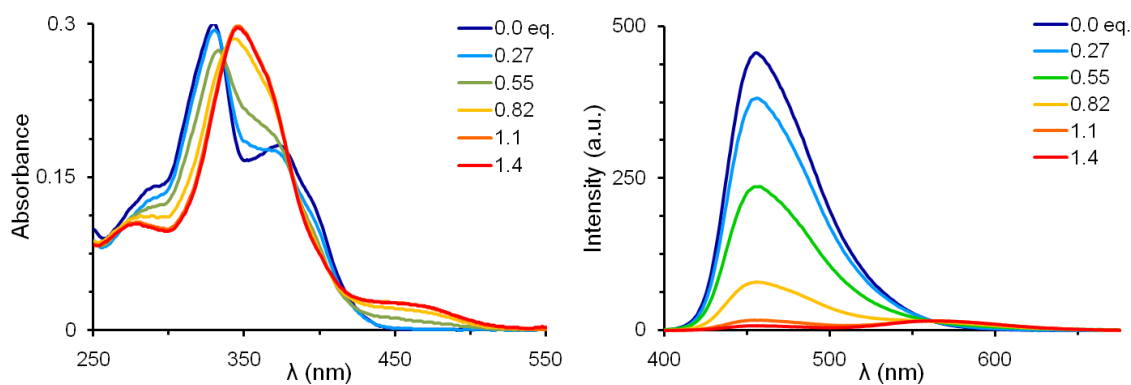


**Figure 3.5.** Absorption (left) and emission (right) of **3.2** in dichloromethane upon exposure to increasing equivalents of zinc triflate.

The two-stage fluorescence response of **3.7** can be understood in light of models **3.2** and **3.3** (Figure 3.7). Upon addition of  $\text{Zn}^{2+}$  to **3.7**, coordination first occurs at the anilines, stabilizing the HOMO while leaving the LUMO unaffected, generating the initial blue shift. Subsequent addition of  $\text{Zn}^{2+}$  coordinates the pyridyl nitrogens of **3.3**; this interaction stabilizes the LUMO, causing the second bathochromic shift.

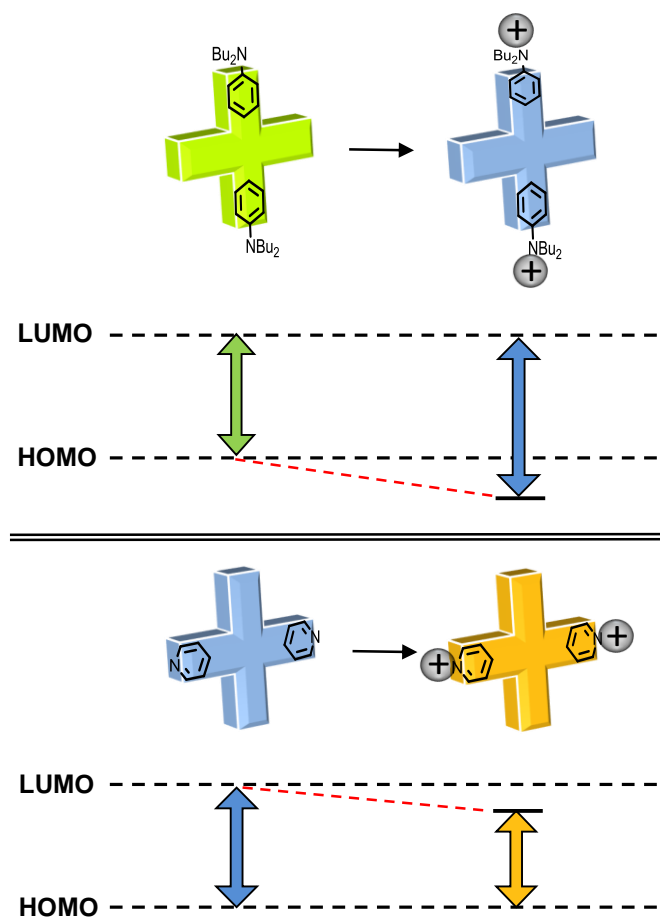


**Figure 3.6.** Schematic representation of the effect of metallation or protonation upon the FMOs and emission of XF **3.3** (A, top) and **3.2** (B, bottom).

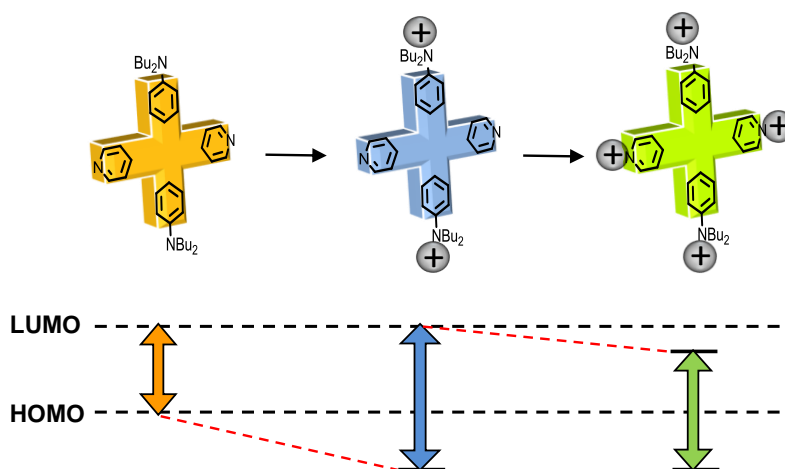


**Figure 3.7.** Schematic representation of the effect of metallation or protonation upon the FMOs and emission of XF **3.7**.

### 3.4. Response of XFs towards Metal Cations and TFA

Encouraged by the interesting sensory response obtained upon addition of  $\text{Zn}(\text{OTf})_2$  to **3.7**, we carefully examined photophysical properties of **3.1-3.7** upon addition of TFA and a variety of  $2^+$  metal triflates. Figure 3.8 displays the emission spectra of **3.1-3.7** in dichloromethane and upon addition of excess TFA,  $\text{Zn}(\text{OTf})_2$ ,  $\text{Mg}(\text{OTf})_2$ ,  $\text{Ca}(\text{OTf})_2$ , and  $\text{Mn}(\text{OTf})_2$ . Herein, the sensory responses of **3.1-3.3**, **3.5**, and **3.7** are discussed in detail. The responses observed in the cases of **3.4** and **3.6** are similar to those of **3.5** and do not warrant separate discussion.

#### 3.4.1. Spectroscopic data for 3.1-3.7 upon addition of trifluoroacetic acid.

As expected, protonation with excess TFA elicits large changes in the optical properties of **3.1-3.7** (Table 3.1). Upon protonation, the absorptions of **3.1** and **3.2** experience a red shift, while the absorptions of **3.3-3.7** undergo a significant blue shift ( $\approx 100$  nm). These shifts are mirrored in the emission spectra of XFs, where upon protonation of **3.1** and **3.2** large red shifts are observed, while in **3.3-3.7** blue shifts occur. In **3.3** and **3.7** the effect is moderate; however, in **3.4-3.6**, protonation results in a dramatic blue shift in excess of 150 nm. These shifts are all in accordance with the FMO model presented in Section 3.3. Protonation always disproportionately stabilizes one of the spatially segregated FMOs exclusively, generating large observable spectroscopic shifts.

The changes in the absorption and emission of the XFs are accompanied by changes in fluorescence quantum yield; in **3.1** and **3.2** the quantum yields drop from 0.7 to 0.06, while in **3.4-3.6** the quantum yields increase from 0.05-0.15 to 0.4-0.7 upon

protonation. In the most extreme cases, **3.5** and **3.6**, the quantum yields increase by a factor of 7.5 upon protonation. Overall, there is a crude and qualitative correlation with the energy gap law.<sup>7</sup>

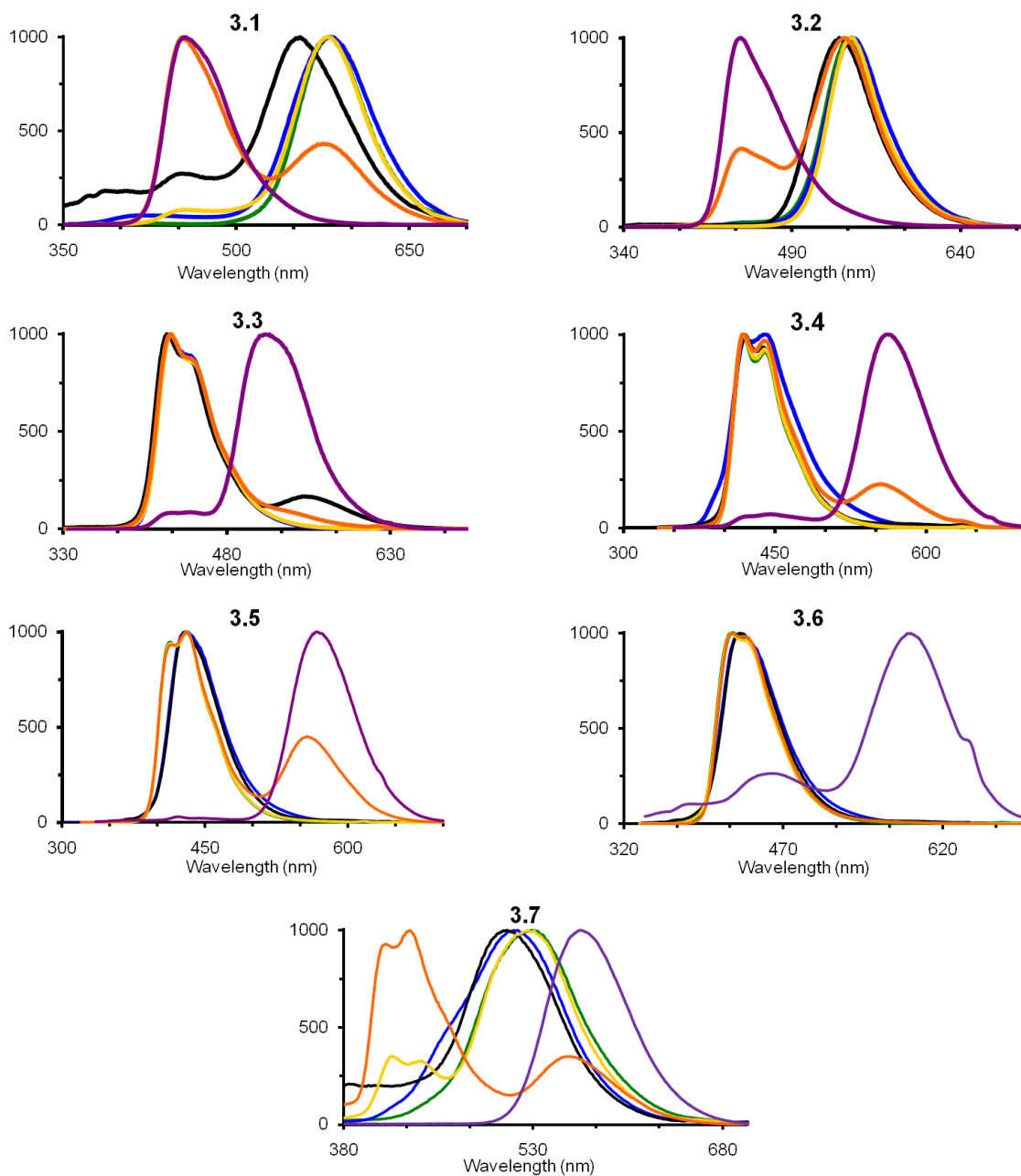


**Figure 3.8.** Normalized emission of **3.1-3.7** in dichloromethane (purple trace) and upon addition of excess TFA (black trace), Mg(OTf)<sub>2</sub> (green trace), Zn(OTf)<sub>2</sub> (blue trace), Mn(OTf)<sub>2</sub> (yellow trace), and Ca(OTf)<sub>2</sub>.

The change in radiative lifetime upon protonation varies from moderate for **3.5** (4.4 to 4.0 ns) to significant for **3.7** (4.4 to 1.8 ns). Both increase and decrease of the radiative lifetimes is observed. The compound **3.2** shows an increase in lifetime from 3.8 to 7.2 ns upon protonation. These significant changes make the cruciforms potentially useful for fluorescence lifetime imaging (FLIM) applications.<sup>8</sup> In a broadly general sense, the emissive lifetimes increase upon decreasing HOMO-LUMO gap and decreasing orbital overlap in the protonated species.

**Table 3.1.** Effect of TFA on the photophysical properties of **3.1-3.7**.

		<b>3.1</b>	<b>3.2</b>	<b>3.3</b>	<b>3.4</b>	<b>3.5</b>	<b>3.6</b>	<b>3.7</b>
XF	$\lambda_{\max}$ Abs (nm) <sup>a</sup>	330	330	436	443	433	427	437
	$\lambda_{\max}$ Em (nm) <sup>a</sup>	456	444	519	561	567	590	567
	Quantum Yield <sup>b</sup>	0.70	0.67	0.31	0.15	0.09	0.05	0.11
	Fluorescence Lifetime $\tau$ (ns) <sup>b,c</sup>	3.9 4.1 3.9	3.8	1.7	4.2 4.4	4.4 4.2	3.9 4.0	4.3 4.3
+ excess TFA	$\lambda_{\max}$ Abs (nm) <sup>a</sup>	339	350	330	336	337	338	343
	$\lambda_{\max}$ Em (nm) <sup>a</sup>	555	532	425	420	430	430	509
	Quantum Yield <sup>b</sup>	-	0.06	0.44	0.65	0.68	0.38	0.06
	Fluorescence Lifetime $\tau$ (ns) <sup>b,c</sup>	3.7 3.1 3.6	6.7 7.6	2.6 2.9	3.5 2.9 3.1	2.8 3.1	2.5 3.0 2.9	1.8 2.1 2.0

<sup>a</sup> measurements in CH<sub>2</sub>Cl<sub>2</sub>. <sup>b</sup> measurements in CHCl<sub>3</sub>. <sup>c</sup> lifetimes were monoexponential and fitted with a single decay function. Multiple trials are reported in some cases.

To investigate the effect of protonation on the spectra of **3.7** in more detail, we performed a titration in THF/methanol; **3.7** is attractive, it contains both pyridine and dibutylamino substituents (Figure 3.9). Upon adding acid, the emission of **3.7** ( $\lambda_{\max}$  em

= 598 nm – note that in THF/methanol, the emission of **3.7** is red-shifted when compared to the emission recorded in dichloromethane), diminishes and is replaced by an emission at 445 nm, corresponding to **3.7** with dibutylamino-protonated arms ( $\lambda_{\text{max em}} = 445 \text{ nm}$ ). At pH 3.6, an approximate 1:1 ratio of the dibutylamino-protonated species ( $\lambda_{\text{max em}} = 445 \text{ nm}$ ) and the non-protonated species (XF **3.7**) is found. At a pH of 2.7 all of the non-protonated **3.7** has disappeared, and only protonated species emitting at 445 nm are observed.<sup>9</sup> Diethylaniline has a  $\text{pK}_a$  of 6.67, while pyridine displays a  $\text{pK}_a$  of 5.25; from the pH-dependent optical data we conclude that a) the dibutylamino group is protonated first, and b) both dibutylamino groups are protonated independently. *If that were not the case, i.e. if monoprotonation would happen, one would expect the disappearance of 50% of the neutral species to be complete at pH 6.6 and not at 3.6.*

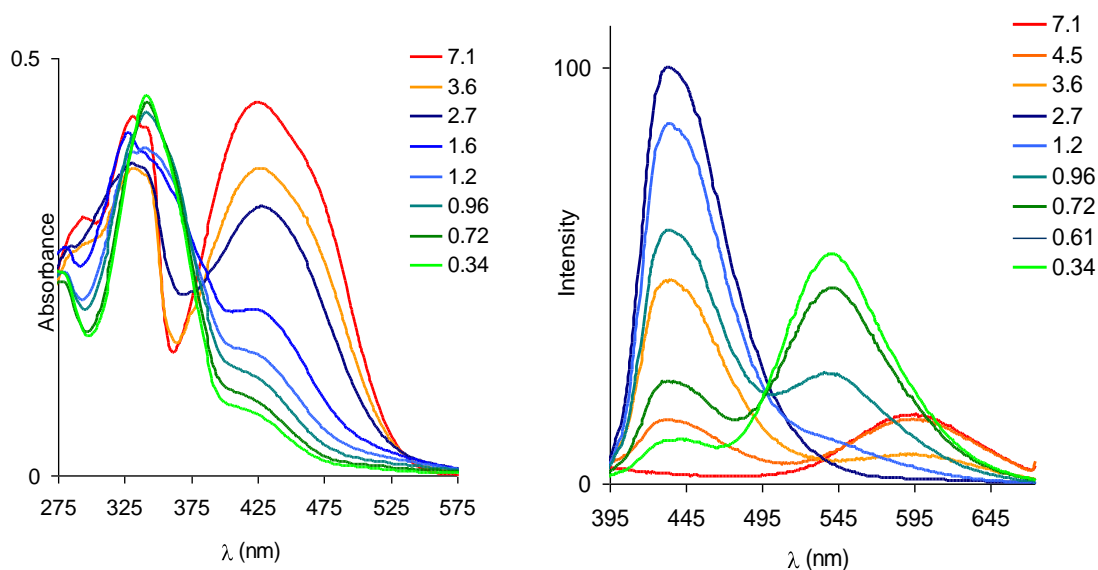


**Figure 3.9.** Protonation of **3.7** in a THF/methanol mixture with trifluoroacetic acid. Emission maxima are 598 nm at pH 7.1, 437 nm at pH 2.7 and 542 nm at pH 0.34.

Upon further protonation, a second isosbestic point is found and an emission centered at 542 nm grows in. We attribute this species to a cruciform **3.7** that is protonated at the dibutylamino arms *and* at the pyridine rings. From the above discussion we conclude that either one or both pyridine rings could be protonated, depending upon the difference in  $pK_a$  values of the mono-protonated pyridine and the di-protonated pyridine species. In the second case, the  $pK_a$  values of all four basic sites would be largely independent and successive double protonation of the dibutylamino and the pyridine group would occur. Due to our stoichiometric investigation detailed below (Section 3.4.2), we conclude that in **3.7** we first doubly protonate the dibutylamino groups, and then, in a second step, doubly protonate the pyridine units, suggesting that the  $pK_a$  values do not change much upon protonation of one end of the respective arm of the cruciform.

#### **3.4.2. Comparing $Zn^{2+}$ and TFA – Elucidating the nature of analyte interactions.**

The exposure of functional cruciforms towards zinc and other metal ions also elicits chromic changes in absorption and emission (Figure 3.8). It was of interest to examine more carefully the nature of the cation/cruciform interaction. More specifically, it was imperative to determine the locus of metal binding. In the case of the pyridines the binding site must be the lone electron pair. However, in case of cruciforms that contain dialkylaniline subunits, the metal cations could either bind to the electron-rich aromatic  $\pi$ -face or directly through the nitrogen of the dialkylamino group. Examples of metal cations binding to electron rich aromatic  $\pi$ -faces are known; therefore, the question for the location of the metal cations is not trivial.<sup>10</sup> We selected zinc, a metal of importance

in biology,<sup>11</sup> because it is in the d<sup>10</sup> configuration and without optical transition in the visible.

How could one distinguish between zinc binding through the aniline nitrogens or through the electron rich ring? Reacting cruciforms with TFA, the proton will bind to the free electron pair of the nitrogen, i.e. protonation will occur either at the pyridine-nitrogen or at the dibutylaniline. If the photophysical properties of the cruciforms upon exposure to protons and to zinc triflate are significantly different, one would conclude that zinc ions and protons would occupy different binding sites. Alternatively, if comparable spectroscopic responses are observed for Zn<sup>2+</sup> and TFA, we can conclude that a similar mode of analyte interaction with the XF exists.

**Table 3.2.** Photophysical properties of **3.1-3.7** upon addition of TFA and Zn(OTf)<sub>2</sub>.

		<b>3.1</b>	<b>3.2</b>	<b>3.3</b>	<b>3.4</b>	<b>3.5</b>	<b>3.6</b>	<b>3.7</b>
+ excess TFA	$\lambda_{\max}$ Abs (nm) <sup>a</sup>	339	350	330	336	337	338	343
	$\lambda_{\max}$ Em (nm) <sup>a</sup>	555	532	425	420	430	430	509
	Quantum Yield <sup>b</sup>	-	0.06	0.44	0.65	0.68	0.38	0.06
	Fluorescence Lifetime $\tau$ (ns) <sup>b,c</sup>	3.7 3.1 3.6	6.7 7.6	2.6 2.9	3.5 2.9 3.1	2.8 3.1	2.5 3.0 2.9	1.8 2.1 2.0
+ excess Zn(OTf) <sub>2</sub>	$\lambda_{\max}$ Abs (nm) <sup>a</sup>	356	339	328	326	336	336	340
	$\lambda_{\max}$ Em (nm) <sup>a</sup>	580	543	429	421	429	429	518
	Quantum Yield <sup>b</sup>	0.31	0.18	0.62	0.80	0.84	0.58	0.11
	Fluorescence Lifetime $\tau$ (ns) <sup>b,c</sup>	3.9 4.0	6.8 6.9	3.1 2.8	3.1 2.7 2.9	2.6 2.9	3.7 3.1 3.3	2.1 2.0

<sup>a</sup> measurements in CH<sub>2</sub>Cl<sub>2</sub>. <sup>b</sup> measurements in CHCl<sub>3</sub>. <sup>c</sup> lifetimes were monoexponential and fitted with a single decay function. Multiple trials are reported in some cases.

Table 3.2 details the photophysical properties of **3.1-3.7** upon addition of  $\text{Zn}(\text{OTf})_2$  and compares them to the responses observed upon addition of TFA. To further facilitate a comparison, Figure 3.10 graphically presents the changes in absorption, emission, quantum yield, and fluorescence lifetime upon addition of  $\text{Zn}^{2+}$  and TFA. In all cases, *the changes in spectroscopic properties, quantum yields and emissive lifetimes of 3.1-3.7 are similar upon addition of zinc triflate and of TFA.*

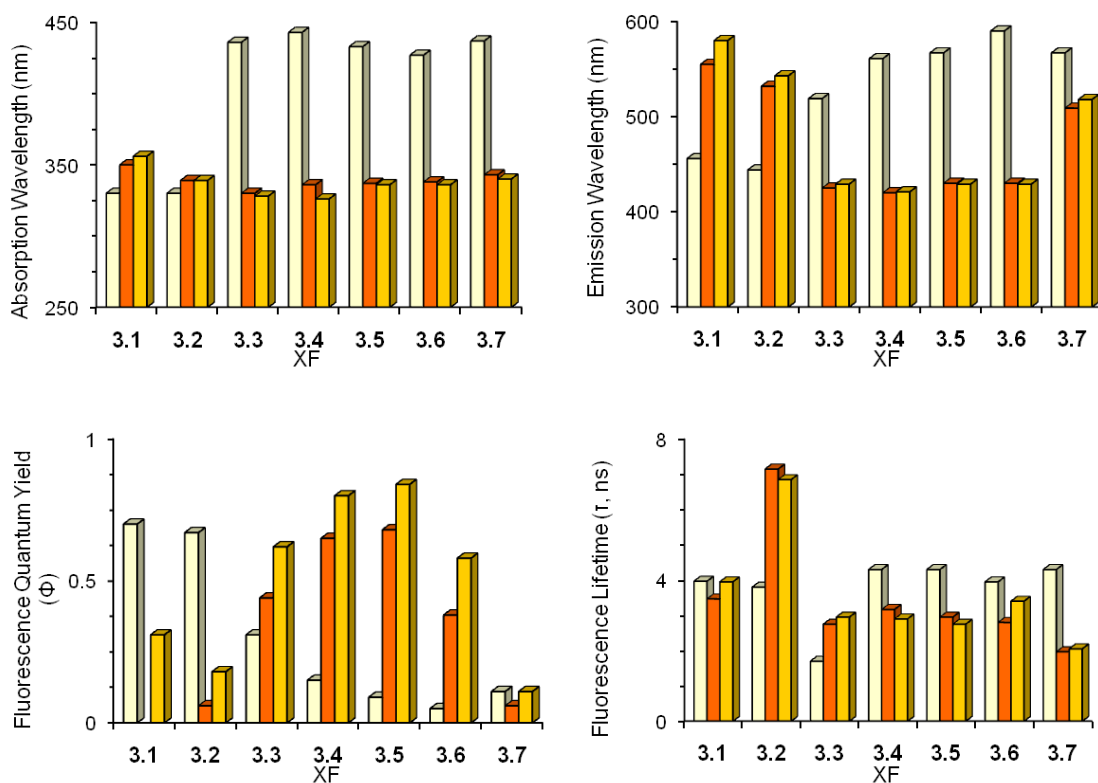


**Figure 3.10.** Comparison of the observed photophysical responses of XF**s** **3.1-3.7** (beige bar) towards TFA (dark orange bar) and  $\text{Zn}(\text{OTf})_2$  (light orange bar).

The shifts observed upon addition of zinc cations can be explained (as in the case of TFA) by considering the influence of analyte binding on the spatially segregated FMOs in **3.1-3.7**. In both cases, the positive charge is the determining issue. Addition of zinc triflate to the pyridine-containing cruciforms leads to a somewhat larger red-shift in

emission and to higher fluorescence quantum yields when compared to the values obtained for protonation of the cruciforms. These findings may indicate a stronger binding of the divalent zinc ions than of the protons to the pyridine units of the cruciforms. However, the overall similarities of the series of photophysical data, obtained for protonation vs. exposure to zinc ions, *suggests that the zinc ions bind directly through the aniline nitrogens.*

In addition to determining the locus of interaction, we also wished to determine the stereochemical interaction. We assume that addition of excess TFA to solutions of **3.1-3.7** results in the protonation of all available nitrogens. The similarity between the responses observed upon addition of zinc and TFA certainly suggest that if TFA protonates all nitrogens, the metal cations probably complex all available Lewis basic nitrogens as well.

To further address the issue of the stoichiometry, we investigated the  $^1\text{H}$  NMR spectra of **3.2** and **3.3**, in deuterated chloroform, upon addition of zinc triflate and TFA. The results obtained for **3.3** are included here as Figure 3.11; similar results were obtained for **3.2**. Upon addition of TFA to either of the cruciforms we see only *one* set of sharp signals assigned to a symmetrical structure, suggesting in both cases that the respectively formed species is doubly protonated at the aniline or at the pyridine. In the case of a putative mono-protonated species, we would have expected to see a complex and/or broadened NMR pattern. From the emission spectra of **3.2** and **3.3**, we know that protonation produces one discrete species each, i.e. the NMR spectra taken under identical conditions can not represent an equilibrium mixture of different protonated species. We therefore conclude addition of TFA protonates *both* Lewis nitrogens in **3.2**

and **3.3**. Upon addition of zinc triflate, we observe results that are comparable to those we have obtained for the protonation of these cruciforms, suggesting again the similarity of the processes involved. Chemical shifts are very similar in both cases (TFA and zinc), and greater changes in chemical shift are observed for hydrogens closer in proximity to the Lewis basic center. Binding of the zinc through the electron-rich aromatic  $\pi$ -face does *not* seem to be important in solution; however, in the solid state the situation could be different. Once again, the nature of the NMR spectra suggests coordination to both Lewis basic nitrogens.

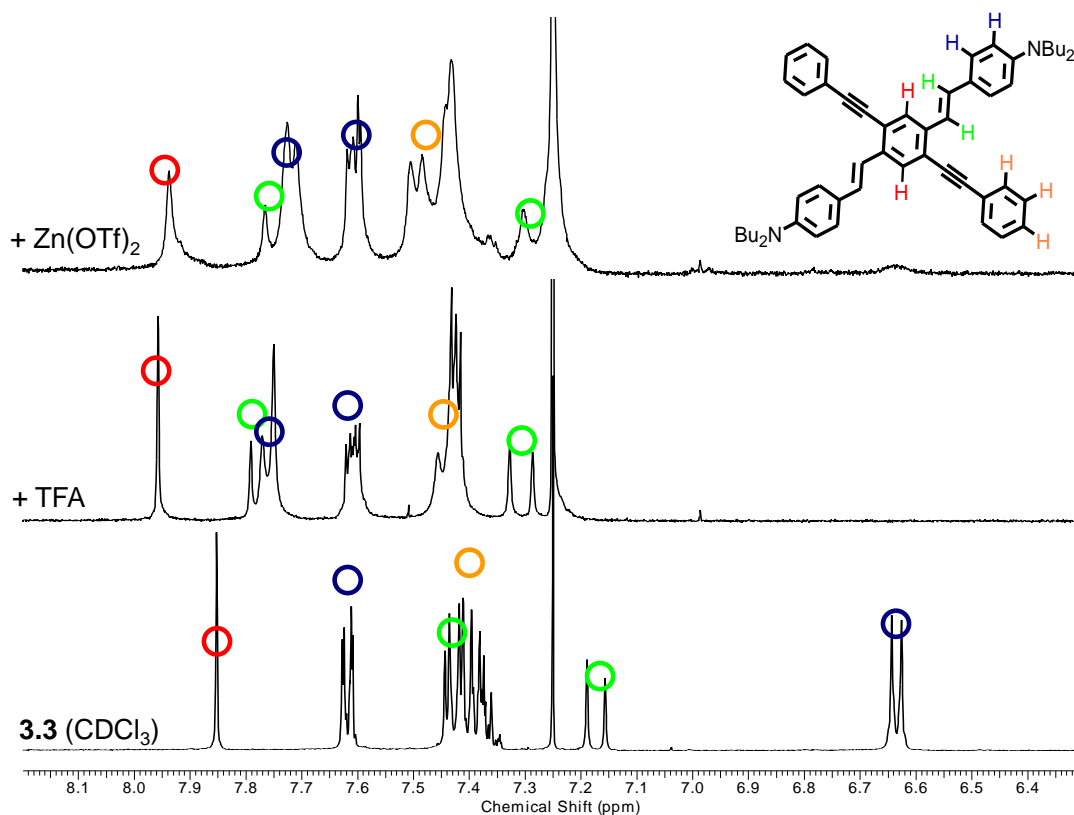


**Figure 3.11.**  $^1\text{H}$  NMR spectra of **3.3** ( $\text{CDCl}_3$ ). Top: After addition of an excess of zinc triflate. Middle: After addition of an excess of trifluoroacetic acid. Bottom: **3.3** in chloroform-*d*. All spectra were taken at 400 MHz.

### 3.4.3. Fluorescence response of XFs to the triflates of $Mg^{2+}$ , $Ca^{2+}$ , and $Mn^{2+}$ .

With the effects of the addition of proton acids and zinc ions secured, we were curious if other metal cations in their +2 oxidation state would affect the fluorescence of the cruciforms differently. We chose  $Mg^{2+}$ ,  $Ca^{2+}$  and  $Mn^{2+}$ , all as their triflates as suitable representatives because they are sufficiently similar in their overall properties to zinc ions. Manganese and magnesium ions have roughly the same size as zinc ions and only calcium is somewhat bigger ( $Zn^{2+}$  88 pm,  $d^{10}$ ;  $Mn^{2+}$  89 pm,  $d^5$ ;  $Mg^{2+}$  86 pm,  $d^0$ ;  $Ca^{2+}$  114 pm,  $d^0$ ).<sup>12</sup> The main difference is the increase in hardness when going from  $Zn^{2+}$  to  $Mg^{2+}$  and the presence of five unpaired electrons in  $Mn^{2+}$ . We were interested to see if the presence of the unpaired electrons would lead to a quenching of the fluorescence of the cruciforms and how increasing hardness and size would influence binding to the cruciforms.

Figure 3.8 and Table 3.3 show the pertinent results of the binding of all four metal cations to **3.1-3.7**. We will discuss the metal responses of the cruciforms **3.1-3.3**, **3.5**, and **3.7** in more detail. Upon exposure to the set of three metals, cruciforms **3.1-3.3** show large but metal independent shifts, similar to those obtained for zinc ions. In cruciform **3.2** the response is somewhat more varied with the emission maxima ranging from 536 nm to 543 nm upon addition of the metal cations. In **3.1** and **3.2** the addition of  $Mg^{2+}$ ,  $Mn^{2+}$ , and  $Zn^{2+}$  transforms all of the fluorophore into a metal bound species, while in the case of  $Ca^{2+}$  only partial binding occurs. One can observe bound and unbound species. The more electron rich **3.2** binds better to  $Ca^{2+}$  ions and the ratio of the emission intensity bound/unbound cruciform is considerably larger than in **3.1**

**Table 3.3.** Photophysical properties of **3.1-3.7** upon addition of Mg<sup>2+</sup>, Mn<sup>2+</sup>, and Ca<sup>2+</sup>.

		<b>3.1</b>	<b>3.2</b>	<b>3.3</b>	<b>3.4</b>	<b>3.5</b>	<b>3.6</b>	<b>3.7</b>
+ Mg(OTf) <sub>2</sub>	$\lambda_{\max}$ Em (nm) <sup>a</sup>	581	542	429	418	431	422	530
	Quantum Yield <sup>b</sup>	0.49	0.28	0.79	0.85	0.94	0.86	0.23
	Fluorescence Lifetime $\tau$ (ns) <sup>b,c</sup>	5.0	6.9	3.0	2.9	2.9	3.4	2.1
+ Mn(OTf) <sub>2</sub>	$\lambda_{\max}$ Em (nm) <sup>a</sup>	579	542	429	418	430	421	526
	Quantum Yield <sup>b</sup>	0.46	0.22	0.69	0.86	0.89	0.79	- <sup>d</sup>
	Fluorescence Lifetime $\tau$ (ns) <sup>b,c</sup>	4.9	7.0	2.9	2.8	2.9	3.0	1.3
+ Ca(OTf) <sub>2</sub>	$\lambda_{\max}$ Em (nm) <sup>a</sup>	576	536	429	419	431	422	433
	Quantum Yield <sup>b</sup>	- <sup>d</sup>	- <sup>d</sup>	0.76	- <sup>d</sup>	- <sup>d</sup>	- <sup>d</sup>	- <sup>d</sup>
	Fluorescence Lifetime $\tau$ (ns) <sup>b,c</sup>	3.4	6.4	2.8	2.7	2.7	2.9	2.6

<sup>a</sup> measurements in CH<sub>2</sub>Cl<sub>2</sub>. <sup>b</sup> measurements in CHCl<sub>3</sub>. <sup>c</sup> lifetimes were monoexponential and fitted with a single decay function. Multiple trials are reported in some cases. <sup>d</sup> not available due to the presence of two emitting species in solution

Compound **3.5** with its strongly electron withdrawing trifluoromethyl substituents shows a different response for Zn<sup>2+</sup> than for Mg<sup>2+</sup>, Mn<sup>2+</sup>, and Ca<sup>2+</sup>, as an additional blue-shifted feature is visible at 413-417 nm. The Zn<sup>2+</sup>-induced emission is broad, featureless and centered at 429 nm. Even saturated solutions of Ca(OTf)<sub>2</sub> leave a fraction of **3.5** unbound. The pyridine-dibutylamino cruciform **3.7** shows the most varied metal response. Both zinc and magnesium fully complex **3.7**, but with different emission maxima (Zn<sup>2+</sup> 518 nm, Mg<sup>2+</sup> 530 nm). Manganese only partly binds to **3.7**. A feature at 418 nm is due to complexation of the dibutylamino groups while the second feature at 526 nm represents the fully, fourfold complexed **3.7**. In the case of Ca<sup>2+</sup> we also see two different features. One corresponds to the uncomplexed cruciform, while the second one

is observed at 414 nm and represents **3.7** in which only the two dibutylamino units are calcium-bound.

All of the cruciform-metal ion complexes are fluorescent. Their quantum yields are also shown in Table 3.3. We were not able to determine the emission quantum yield of the Ca-complexes, because we always (with exception of **3.3**) observe bound and unbound species. Generally, the  $\text{Mg}^{2+}$ -complexes show the highest quantum yields, followed by the  $\text{Mn}^{2+}$ -complexes. The  $\text{Zn}^{2+}$ -complexes are the least fluorescent, only to be undercut by the protonated cruciforms. The reason for the metal-based variations in the fluorescence quantum yield is not clear, and it is not reflected by changes in the radiative lifetimes. Here all of the different metal complexes of one cruciform show similar fluorescence lifetimes.

From these results a self-consistent picture emerges. The cruciforms can be ordered in their metal binding power as **3.3** > **3.2**  $\approx$  **3.5**  $\approx$  **3.7** > **3.1**. The electron releasing quality of the binding element seems to play the largest role. The metals can also be ranked in the power in which they bind the cruciforms;  $\text{Mg}^{2+} \approx \text{Zn}^{2+} > \text{Mn}^{2+} > \text{Ca}^{2+}$ . The lesser binding ability of  $\text{Ca}^{2+}$  as compared to the other metal cations is due to its increased size and decreased charge density.  $\text{Mg}^{2+}$ ,  $\text{Zn}^{2+}$  and  $\text{Mn}^{2+}$  have all the same size and charge but are  $d^0$ ,  $d^5$  and  $d^{10}$  configured respectively.  $\text{Zn}^{2+}$ , the softer metal ion, binds better to the pyridines than  $\text{Mn}^{2+}$  as expected. The second row ion,  $\text{Mg}^{2+}$ , the smallest and the hardest of all of the investigated ones, binds well both to the pyridine as well as to the dibutylamino groups. It was surprising for us that the  $d^5$ -configured  $\text{Mn}^{2+}$  did not lead to quenching of the fluorescence of any of the cruciforms, because we expected that unpaired electrons lead to spin-orbit coupling in the metal-cruciform

complexes. Overall, the responses of the different metal cations to the different cruciforms are varied and the four cations can be discerned under ideal conditions. This is surprising, because the cruciforms were not designed to be metal sensory compounds.

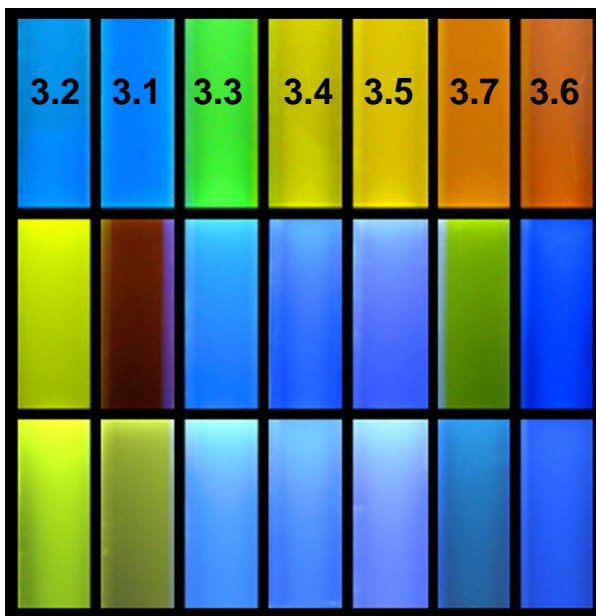


**Figure 3.12.** Fluorescence of **3.1-3.7** in chloroform. Top row displays **3.1-3.7** without any additive. Middle row: After addition of trifluoroacetic acid. Bottom row: After addition of zinc triflate. The difference in the appearance of **3.7** and **3.1** in the presence of zinc triflate as compared to the pictures taken in the presence of trifluoroacetic acid is due to the inherent sensitivity profile of the camera. All pictures were taken under a blacklight at a maximum emission wavelength of 365 nm.

### 3.5. Conclusions

Having previously examined the photophysical properties of **3.1-3.7** and uncovered the ability of XFs to exhibit spatially separated FMOs, we elected to examine the sensory behavior of these chromophores. As **3.1-3.7** are functional fluorophores possessing Lewis basic nitrogens, we decided to probe the sensory potential of these novel fluorescent cores by examining their response to TFA and to the triflates of  $\text{Mg}^{2+}$ ,

$\text{Ca}^{2+}$ ,  $\text{Mn}^{2+}$  and  $\text{Zn}^{2+}$ . Spectacular sensory responses occur in all cases, as is graphically demonstrated in Figure 3.12. The locus and stoichiometry of interactions were also determined. Addition of protons or metal ions results in similar changes in the optical and NMR spectroscopic properties of all of the investigated cruciforms, suggesting that the metal ions and the protons bind to the same sites, *viz.* the free electron pairs of both dialkylaniline and pyridine nitrogens. The parallel results observed for the addition of protons and metal ions suggests that protons can be used to qualitatively and conveniently assess the photophysical sensory responses observed in operationally functional fluorophores such as cruciforms, when positive charge is the major contributor to the change in fluorescence. These cruciforms indeed display a wealth of unexpected photophysical properties which makes them attractive objects of study.

This work has been published in the *Journal of the American Chemical Society*:  
Zuccherro, A. J.; Wilson, J. N.; Bunz, U. H. F. Cruciforms as functional fluorophores: response to protons and selected metal ions. *J. Am. Chem. Soc.* **2006**, *128*, 11872-11881.

### 3.6. Experimental

**General Methods.** All chemicals were purchased from Aldrich Chemical, Acros, TCI America, or Fischer Scientific and used without purification unless otherwise specified. Column chromatography was performed using Standard Grade silica gel 60 Å, 32-63 µm (230 x 450 mesh) from Sorbent Technologies and the indicated eluent. Elution of cruciforms was readily monitored using a handheld UV lamp (365 nm). Melting points were obtained using a Mel-Temp apparatus fitted with a Fluke 51<sup>K/J</sup> digital thermometer. All IR spectra were obtained using a Simadzu FTIR-8400s spectrometer. Unless

otherwise specified, NMR spectra were recorded at 298 K on a Varian Mercury spectrometer (300 MHz). Chemical shifts are reported in parts per million (ppm), using residual solvent (chloroform-*d*) as an internal standard. Data Reported as follows: chemical shift, multiplicity (s = singlet, d = doublet, t = triplet, q = quartet, m = multiplet), coupling constant, and integration. Mass spectral analyses were provided by the Georgia Institute of Technology Mass Spectrometry Facility.

All absorption spectra were collected using a Shimadzu UV-2401PC spectrophotometer. All emission spectra were acquired using a Shimadzu RF-5301PC spectrofluorophotometer. Lifetime data were collected using a Lifespec-ps (Edinburgh Instruments), pulsed diode laser (PicoQuant, 372 nm excitation), and PMT detector (Hamamatsu). Data were fit to single exponential decay so as to optimize chi-squared values. Quantum yields for all cruciforms were measured using standard procedures using quinine sulfate as a standard.

**Synthesis of Calcium and Manganese Trifluoromethanesulfonate.** The procedure utilized to prepare calcium and manganese triflate was adapted from a previously published method.<sup>13</sup> The corresponding carbonate salts were suspended in deionized water and stirred at room temperature.  $\text{CF}_3\text{SO}_3\text{H}$  (2 molar equivalents) was added dropwise to the stirring suspension. The reaction was then allowed to stir overnight at room temperature. The reaction mixtures were filtered and the triflate salts were isolated in vacuo. These were subsequently heated to obtain the anhydrous triflate salts. The resulting triflates were carefully washed multiple times with dichloromethane to remove any residual triflic acid. The pH of aqueous solutions of both triflate salts was checked to confirm no triflic acid remained.

**<sup>1</sup>H NMR Spectra Upon Addition of Zinc Triflate and TFA.** A solution of cruciform **3.3** (4 mg/mL) in chloroform-*d* was prepared. Excess trifluoroacetic acid and zinc triflate was added to the sample as required. The sample were allowed to equilibrate for 8 hours before measurement. In order to determine peak assignments, spectra of **3.3** alone and with excess trifluoroacetic acid were collected using a Bruker DRX 500 MHz NMR. All other spectra were collected using a Bruker AMX 400 MHz NMR.

**Titration of 3.7 with Trifluoroacetic Acid.** A stock solution of **3.7** in a methanol/THF mixture was prepared. A stock solution of trifluoroacetic acid in methanol was also prepared. All pH measurements were made using a calibrated VWR symPHony SP20 digital pH meter. Upon addition of trifluoroacetic acid in methanol to **3.7**, the resulting pH was measured and absorption/emission spectra were collected.

### 3.7. References and Notes

1. (a) Henary, M. M.; Wu, Y.G.; Fahrni, C. J. Zinc(II)-selective ratiometric fluorescent sensors based on inhibition of excited-state intramolecular proton transfer. *Chemistry Eur. J.* **2004**, *10*, 3015-3025. (b) Pond, S. J. K.; Tsutsumi, O.; Rumi, M.; Kwon, O.; Zojer, E.; Bredas, J. L.; Marder, S. R.; Perry, J. W. Metal-ion sensing fluorophores with large two-photon absorption cross sections: Aza-crown ether substituted donor-acceptor-donor distyryl benzenes. *J. Am. Chem. Soc.* **2004**, *126*, 9291-9306.
2. (a) Wang, B.; Wasielewski, M. R. Design and synthesis of metal ion-recognition-induced conjugated polymers: An approach to metal ion sensory materials. *J. Am. Chem. Soc.* **1997**, *119*, 12-21. (b) Bangcuyo, C. G.; Rampey-Vaughn, M. E.; Quan, L. T.; Angel, S. M.; Smith, M. D.; Bunz, U. H. F. Quinoline-containing, conjugated poly(aryleneethynylene)s: Novel metal and H<sup>+</sup>-responsive materials. *Macromolecules* **2002**, *35*, 1563-1568. (c) Pautzsch, T.; Klemm, E. Ruthenium-chelating poly(heteroaryleneethynylene)s: Synthesis and properties. *Macromolecules* **2002**, *35*, 1569-1575.
3. Gobbi, L.; Seiler, P.; Diederich, F. A novel three-way chromophoric molecular switch: pH and light controllable switching cycles. *Angew. Chem. Int. Ed.* **1999**, *38*, 674-678. (b) Diederich, F. Carbon-rich acetylenic scaffolding: rods, rings and switches. *Chem. Commun.* **2001**, 219-227. (c) Tykwinski, R. R.; Gubler, U.; Martin,

- R. E.; Diederich, F.; Bosshard, C.; Gunter, P. Structure-property relationships in third order nonlinear optical chromophores. *J. Phys. Chem. B* **1998**, *102*, 4451-4465. (d) Tykwinski, R. R.; Schreiber, M.; Carlon, R. P.; Diederich, F.; Gramlich, V. Donor/acceptor-substituted tetraethynylethenes: Systematic assembly of molecules for use as advanced materials. *Helv. Chim. Acta* **1996**, *79*, 2249-2281. (e) Hilger, A.; Gisselbrecht, J. P.; Tykwinski, R.; Boudon, C.; Schreiber, M.; Martin, R.; Lüthi, H. P.; Gross, M.; Diederich, F. Electronic characteristics of arylated tetraethynylethenes: A cooperative computational and electrochemical investigation. *J. Am. Chem. Soc.* **1997**, *119*, 2069-2078. (f) Mitzel, F.; Boudon, C.; Gisselbrecht, J. P.; Seiler, P.; Gross, M.; Diederich, F. Donor-substituted perethynylated dehydroannulenes and radiannulenes: Acetylenic carbon sheets featuring intense intramolecular charge transfer. *Helv. Chim. Acta* **2004**, *87*, 1130-1157. (g) Gisselbrecht, J. P.; Moonen, N. N. P.; Boudon, C.; Nielsen, M. B.; Diederich, F.; Gross, M. Redox properties of linear and cyclic scaffolds based on Di- and tetraethynylethene. *Eur. J. Org. Chem.* **2004**, 2959-2972.
4. (a) Knapton, D.; Rowan, S. J.; Weder, C. Synthesis and properties of metallo-supramolecular poly(p-phenylene ethynylene)s. *Macromolecules* **2006**, *39*, 651-657. (b) Iyer, P. K.; Beck, J. B.; Weder, C.; Rowan, S. J. Synthesis and optical properties of metallo-supramolecular polymers. *Chem. Commun.* **2005**, 319-321.
  5. (a) Lavigne, J. J.; Anslyn, E. V. Teaching old indicators new tricks: A colorimetric chemosensing ensemble for tartrate/malate in beverages. *Angew. Chem. Int. Ed.* **1999**, *38*, 3666-3669. (b) Wright, A. T.; Anslyn, E. V.; McDevitt, J. T. A differential array of metalated synthetic receptors for the analysis of tripeptide mixtures. *J. Am. Chem. Soc.* **2005**, *127*, 17405-17411. (c) Rakow, N. A.; Suslick, K. S. A colorimetric sensor array for odour visualization. *Nature* **2000**, *406*, 710-713. (d) Rakow, N. A.; Sen, A. Colorimetric sensor arrays for molecular recognition. *Tetrahedron* **2004**, *60*, 11133-11138. (e) Albert, K. J.; Lewis, N. S.; Schauer, C. L.; Sotzing, G. A.; Stitzel, S. E.; Vaid, T. P.; Walt, D. R. Cross-reactive chemical sensor arrays. *Chem. Rev.* **2000**, *100*, 2595-2626.
  6. (a) Wilson, J. N.; Bunz, U. H. F. Switching of intermolecular charge-transfer in cruciforms: metal ion sensing. *J. Am. Chem. Soc.* **2005**, *127*, 4124-4125. (b) Zuccherro, A. J.; Wilson, J. N.; Bunz, U. H. F. Cruciforms as functional fluorophores: response to protons and selected metal ions. *J. Am. Chem. Soc.* **2006**, *128*, 11872-11881.
  7. (a) Tolbert, L. M.; Nesselroth, S. M.; Netzel, T. L.; Raya, N.; Stapleton, M. Substituent effects on carbanion photophysics – 9-arylfluorenyl anions. *J. Phys. Chem.* **1992**, *96*, 4492-4496. (b) Englman, R.; Jortner, J. Energy gap law for radiationless transitions in large molecules. *Molecular Physics* **1970**, *18*, 145-154. (c) Caspar, J. V.; Meyer, T. J. Application of the energy-gap law to nonradiative, excited-state decay. *J. Phys. Chem.* **1983**, *87*, 952-957.

8. (a) Bastiaens, P. I. H.; Squire, A. Fluorescence lifetime imaging microscopy: spatial resolution of biochemical processes in the cell. *Trends Cell Biol.* **1999**, *9*, 48-52. (b) Lakowicz, J. R.; Szmajcinski, H.; Nowaczyk, K.; Berndt, K. W.; Johnson, M. Fluorescence Lifetime Imaging. *Anal. Biochem.* **1992**, *202*, 316-330. (c) Pepperkok, R.; Squire, A.; Geley, S.; Bastiaens P. I. H. Simultaneous detection of multiple green fluorescent proteins in live cells by fluorescence lifetime imaging microscopy. *Curr. Biol.* **1999**, *9*, 269-272. (d) Mayr, T.; Igel, C.; Liebsch, G.; Klimant, I.; Wolfbeis, O. S. Cross-reactive metal ion sensor array in a micro titer plate format. *Anal. Chem.* **2003**, *75*, 4389-4396.
9. For a collection of pK<sub>a</sub> values see: <http://www.zirchrom.com/organic.htm>.
10. (a) Hirsch, K. A.; Wilson, S. R.; Moore, J. S. Coordination networks of 3,3'-dicyanodiphenylacetylene and silver(I) salts: Structural diversity through changes in ligand conformation and counterion. *Inorg. Chem.* **1997**, *36*, 2960-2968. (b) Venkataraman, D.; Lee, S.; Moore, J. S.; Zhang, P.; Hirsch, K. A.; Gardner, G. B.; Covey, A. C.; Prentice, C. L. Coordination networks based on multitopic ligands and silver(I) salts: A study of network connectivity and topology as a function of counterion. *Chem. Mater.* **1996**, *8*, 2030-2040. (c) Hirsch, K. A.; Wilson, S. R.; Moore, J. S. Association of dicyanodiphenylacetylenes with silver(I) salts in solution and solid state: Electrospray ionization mass spectrometry samples aggregates at subsaturated concentrations. *J. Am. Chem. Soc.* **1997**, *119*, 10401-10412.
11. Suh, S. W.; Jensen, K. B.; Jensen, M. S.; Silva, D. S.; Kessler, P. J.; Danscher, G.; Frederickson, C. J. Histochemically-reactive zinc in amyloid plaques, angiopathy, and degenerating neurons of Alzheimer's diseased brains. *Brain Res.* **2000**, *852*, 274-278.
12. Values taken from <http://www.scescape.net/~woods/>.
13. Inada, Y.; Nakano, Y.; Inamo, M.; Funahashi, S. Structural characterization and formation mechanism of sitting-atop (SAT) complexes of 5,10,15,20-tetraphenylporphyrin with divalent metal ions. Structure of the Cu(II)-SAT complex as determined by fluorescent extended x-ray absorption fine structure. *Inorg. Chem.* **2000**, *39*, 4793-4801.

## CHAPTER 4

### Phenothiazine-Substituted Cruciforms: Synthesis and Metallochromic Properties

#### 4.1 Introduction

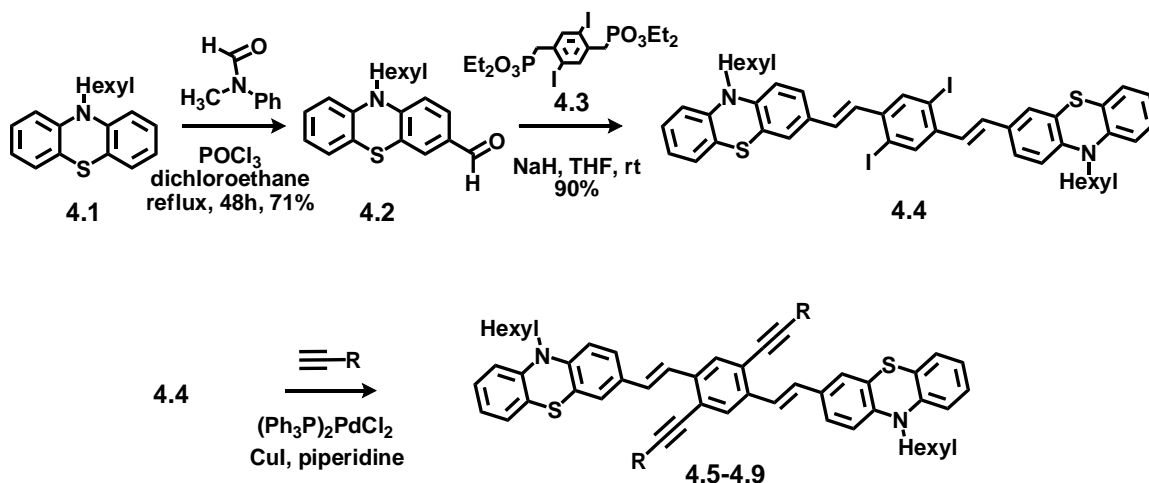
Previous examinations of XFs as responsive fluorophores have focused on compounds containing pyridine and/or dialkylamino groups as metal binding sites.<sup>1</sup> These initial examinations explored the fundamental photophysical behavior and sensory potential of these cores. With these basic lessons in hand, we proceeded to expand our library of XFs by incorporating phenothiazine heterocycles on the cruciform periphery. As electron rich tricyclic heterocycles, phenothiazines are easily and reversibly oxidized; as strong electron donors, they have found application in electroactive materials possessing donor-acceptor character.<sup>2,3</sup> In this chapter, we report the synthesis, characterization, and metallochromic properties of five phenothiazine-substituted XFs. Phenothiazine-containing systems show promise for the synthesis of metallochromic XFs.

#### 4.2 Results and Discussion

##### 4.2.1. Synthesis.

The robust synthetic protocol employed for the synthesis of XFs permits the construction of almost any conceivable architecture as long as the requisite aldehydes and alkynes are available. Starting from 10-hexyl-10*H*-phenothiazine, Vilsmeier formylation of **4.1** with phosphorus oxychloride and *N*-methylformanilide in 1,2-dichloroethane regioselectively furnishes the aldehyde **4.2** in 71% yield as bright yellow crystals

(Scheme 4.1).<sup>2,3</sup> A subsequent Horner reaction<sup>4</sup> of the diphosphonate **4.3** with the phenothiazine aldehyde **4.2** afforded **4.4** in 90% yield after recrystallization. Palladium-catalyzed coupling of the diiodide **4.4** to different alkynes accessed the phenothiazine-based XFs **4.5-4.9** in 20-61% yield (Figure 4.1).



**Scheme 4.1.** Synthesis of phenothiazine XFs.

The XFs were obtained as yellow-to-red colored crystalline powders that were identified by their characteristic <sup>1</sup>H and <sup>13</sup>C NMR signals. To fully corroborate the presence of the XF-core, diffraction quality specimens of XF **4.5** were obtained. Figure 4.2 shows the structure and the packing of XF **4.5** in the solid state. The bond lengths and bond angles are in excellent agreement with expected values and are very similar to those reported for other XFs.<sup>5</sup> Contrary to some of the other XFs, **4.5** is fully planarized in the solid state and forms tilted stacks, typical for aromatic hydrocarbons, where direct  $\pi$ - $\pi$  stacking between the aromatic systems is avoided.<sup>6</sup> In this packing motif the butyl groups act as molecular insulation.

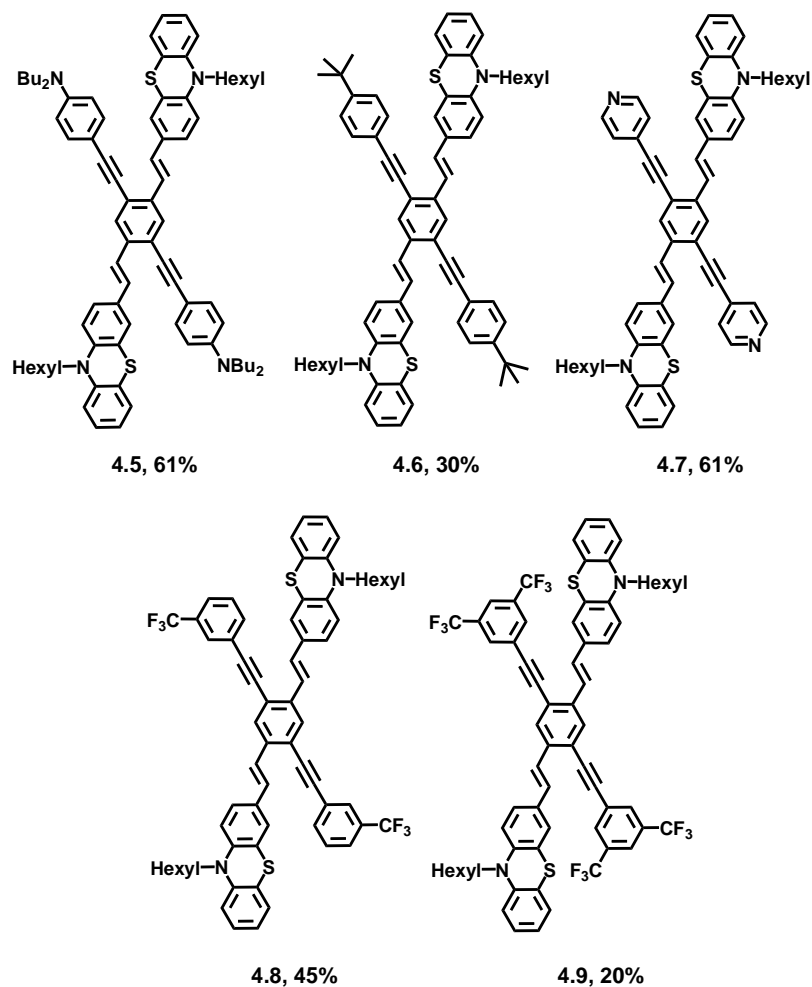


**Figure 4.1.** Synthesized phenothiazine-substituted XFs **4.5-4.9**.

#### 4.2.2. Spectroscopic properties and quantum chemical calculations.

All of the isolated phenothiazine XFs form brightly yellow-orange fluorescent solutions in dichloromethane. Figure 4.3 shows the absorption and emission spectra of XFs of **4.5-4.9** in dichloromethane. The absorption spectra of XF **4.6-4.9** are similar and show a significant charge transfer band at around 430-450 nm and a second more intense absorption at around 325 nm. This charge transfer band is absent in the all-donor-substituted XF **4.5**; it displays a single broad band with a maximum absorption at 392 nm.

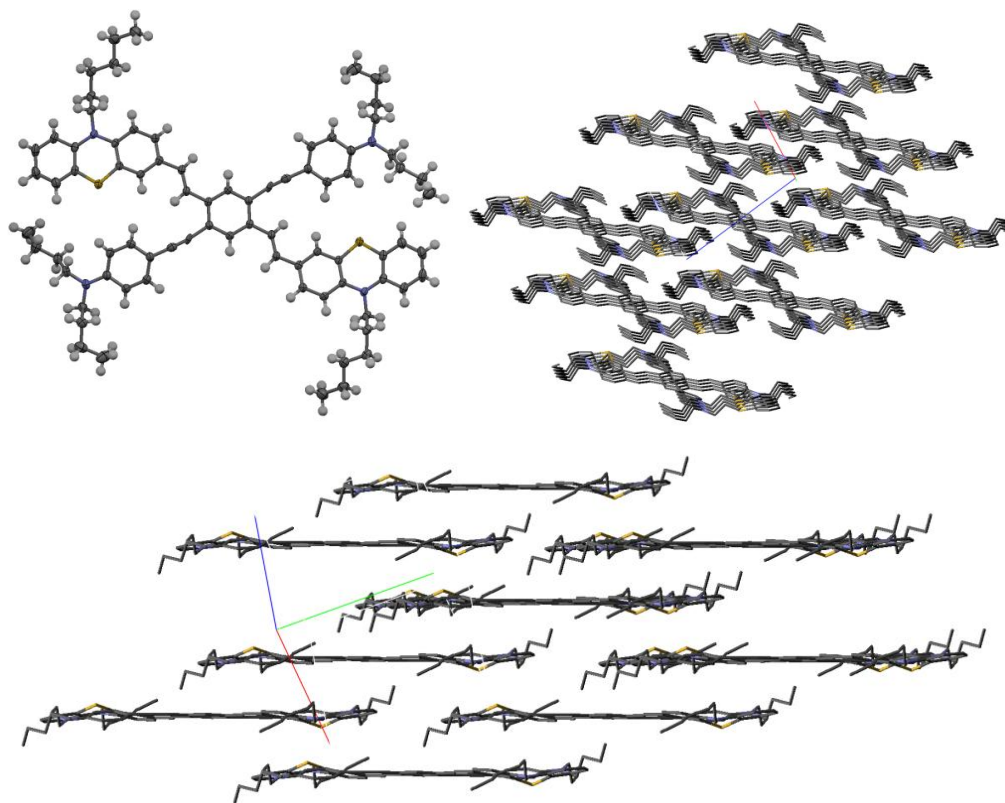


**FIGURE 4.2.** Structure and the packing of XF **4.5** in the solid state. Top left: Molecular structure of **4.5**. Top right: Packing of **4.5** seen along the b-axis. Blue: c-axis, green: b-axis, red: a-axis. Bottom: View of the packing of **4.5** along the planar  $\pi$ -system.

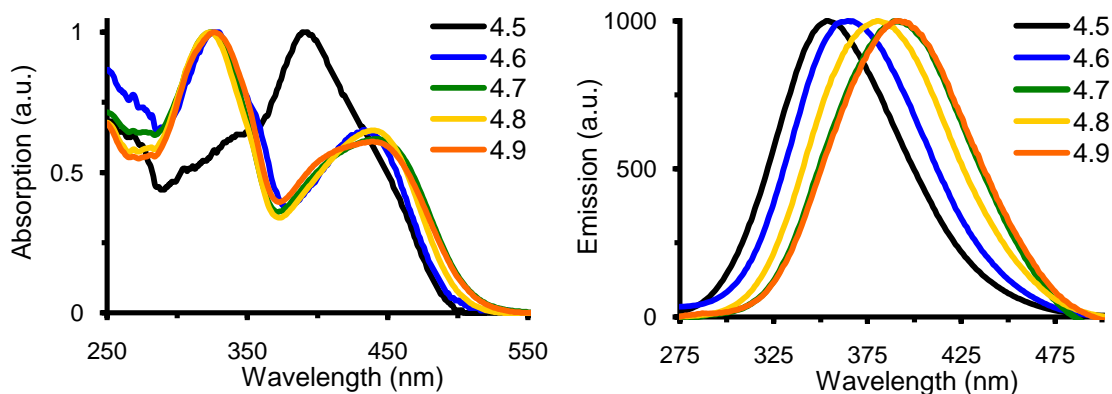


**FIGURE 4.3.** Normalized absorption (top) and emission (bottom) spectra of the XFs **4.5-4.9** in dichloromethane.

**TABLE 4.1.** Spectroscopic and quantum chemical data for the cruciforms **4.5-4.9** in dichloromethane

	<b>4.5</b>	<b>4.6</b>	<b>4.7</b>	<b>4.8</b>	<b>4.9</b>
$\lambda_{\max}$ abs (nm)	392	433	442	437	439
$\lambda_{\max}$ abs (nm) +H <sup>+</sup>	→ <sup>a</sup> 432 (40 eq.) →332 (1000 eq.)	→331 (800 eq)	→422 (2.0 eq.) →349 (1400 eq.)	na	na
$\lambda_{\max}$ emission(nm)	552	563	589	579	590
$\lambda_{\max}$ emission(nm) +H <sup>+</sup>	→577 (40 eq.) →417 (1000 eq.)	→447 (800 eq.)	→q <sup>b</sup> (2.0 eq.) →528 (1400 eq.)	na	na
Stokes Shift (cm <sup>-1</sup> )	7717	5528	5637	5619	6566
$\Phi$	0.53	0.36	0.07	0.25	0.16
HO, LU calc. (eV)	<b>(4.5')</b> -4.46, -1.62	<b>(4.6')</b> -4.74, -1.95	<b>(4.7')</b> -4.91, -2.32	na	na
Band gap calc. (eV)	<b>(4.5')</b> 2.84	<b>(4.6')</b> 2.79	<b>(4.7')</b> 2.59		

a) arrow (→) depicts addition of increasing amounts of acid. b) q: fluorescence is quenched

The emission spectra of the XFs are broad and featureless and range from 552-590 nm. The donor-substituted XF **4.5** possesses the highest energy emission. Increasing donor-acceptor strength substitution leads to increasing red shift of the fluorescence of the XFs. Table 4.1 shows spectroscopic data for **4.5-4.9** including the quantum yield. Increasing donor-acceptor substitution decreases the quantum yields of the XFs, in good qualitative agreement with the energy gap law.<sup>7</sup> In order to rationalize the charge transfer band present in **4.6-4.9**, we performed quantum chemical calculations (B3LYP/6-31G\*\*//6-31G\*) on smaller model systems **4.5'-4.7'** that omitted the N-hexyl groups on the phenothiazine unit. Figures 4.4 and 4.5 show representations of the HOMO and the LUMO of simplified versions of **4.5-4.7**, viz. **4.5'-4.7'** in their neutral and doubly protonated forms. Figure 4.6 shows the calculated orbital positions.

Our previous analysis has demonstrated that in the case of XFs, HOMO and LUMO can localize on the distyrylbenzene and the arylolethynyl axis respectively, if the transverses are donor and acceptor substituted.<sup>1</sup> It was of interest to see if the same type of “disjoint” orbital arrangement could also be observed in representative phenothiazine-functionalized cruciforms **4.5-4.7**. Inspection of the FMOs of **4.5'-4.7'** shows that there is some spatial separation between the frontier orbitals but not as significant as in the case of simpler XFs such as **4.10** and **4.11** (Figure 4.7). In the donor-substituted **4.5'** we do not observe spatial separation of the FMOs. Only in **4.7'** is clear FMO separation enforced by the substituents; the bis(vinylphenothiazine)benzene axis in **4.7'** is electron rich whereas the bis(pyridylethynyl)benzene axis has an electron accepting character. While **4.5'** and **4.6'** have a more congruent orbital structure,<sup>1</sup> it might be possible to induce the “diagonalization” of the FMOs of the C-class XFs **4.5** and **4.6** upon protonation and/or addition of metal salts. We therefore computationally investigated the protonation of **4.5'-4.7'** (Figure 4.5). In the case of **4.6'**, protonation of the phenothiazines leads to a species with a disjoint FMO structure. The HOMO of **4.6'-2H<sup>+</sup>** is located on the bis(arylolethynyl) axis while the LUMO is located on the axis containing the protonated phenothiazines. While these calculations forecast a dramatically different FMO structure, they do not predict an increase in the band gap upon protonation (Figure 4.6). However, this level of theory may not be sufficient to project spectroscopic changes. In **4.5**, we expect that the alkyranilines would be protonated preferentially. As a consequence we computed **4.5'-2H<sup>+</sup>**, in which the aniline nitrogens in **4.5'** are protonated. In the case of **4.7'**, we investigated the protonation of the pyridine units and also protonation of the phenothiazines.

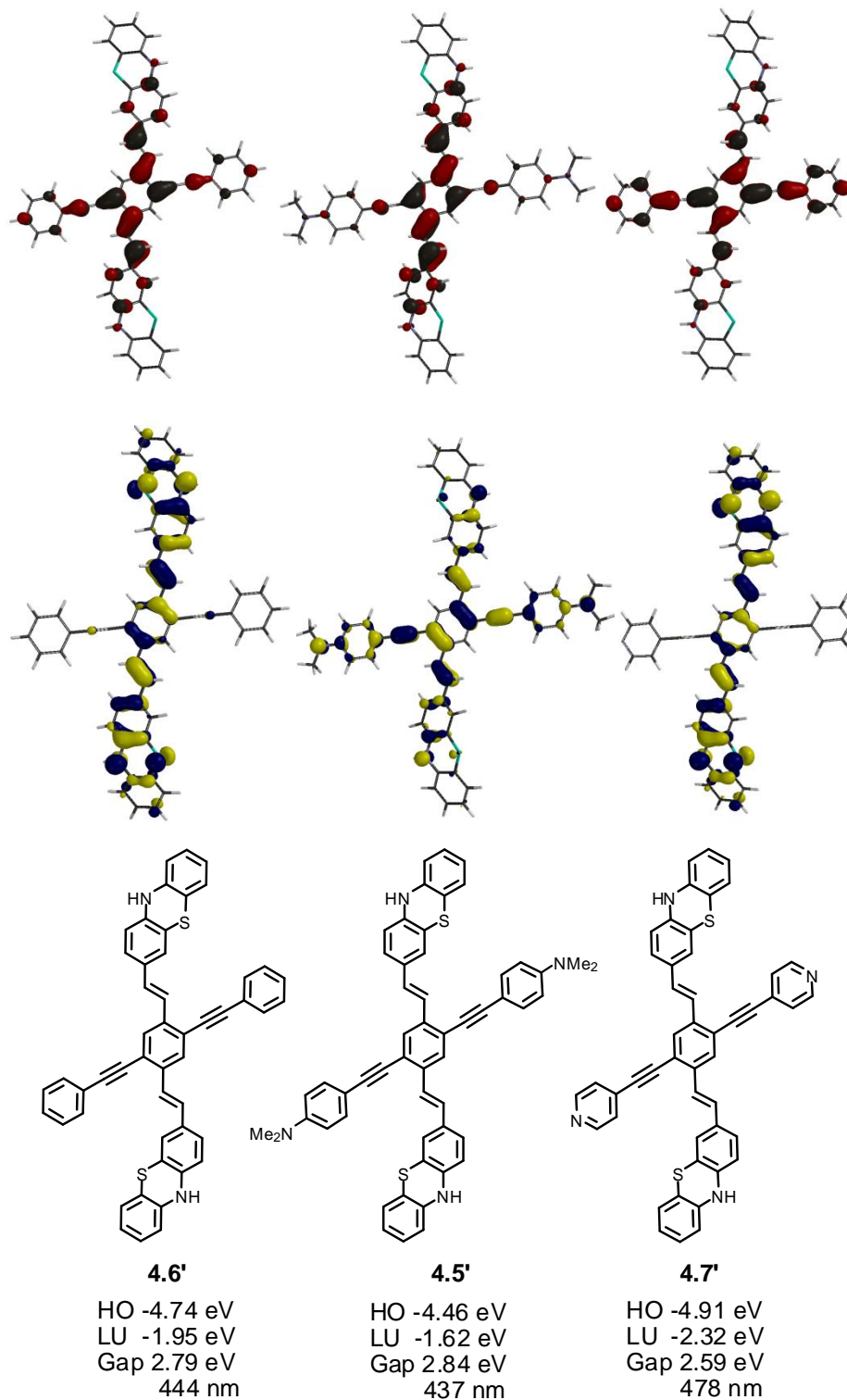


**FIGURE 4.4.** Molecular orbital plots (LUMOs, Top; HOMOs, Bottom) of cruciforms **4.5'**-**4.7'**. The calculations were performed using B3LYP/6-31G\*\*/6-31G\* as implemented on SPARTAN.

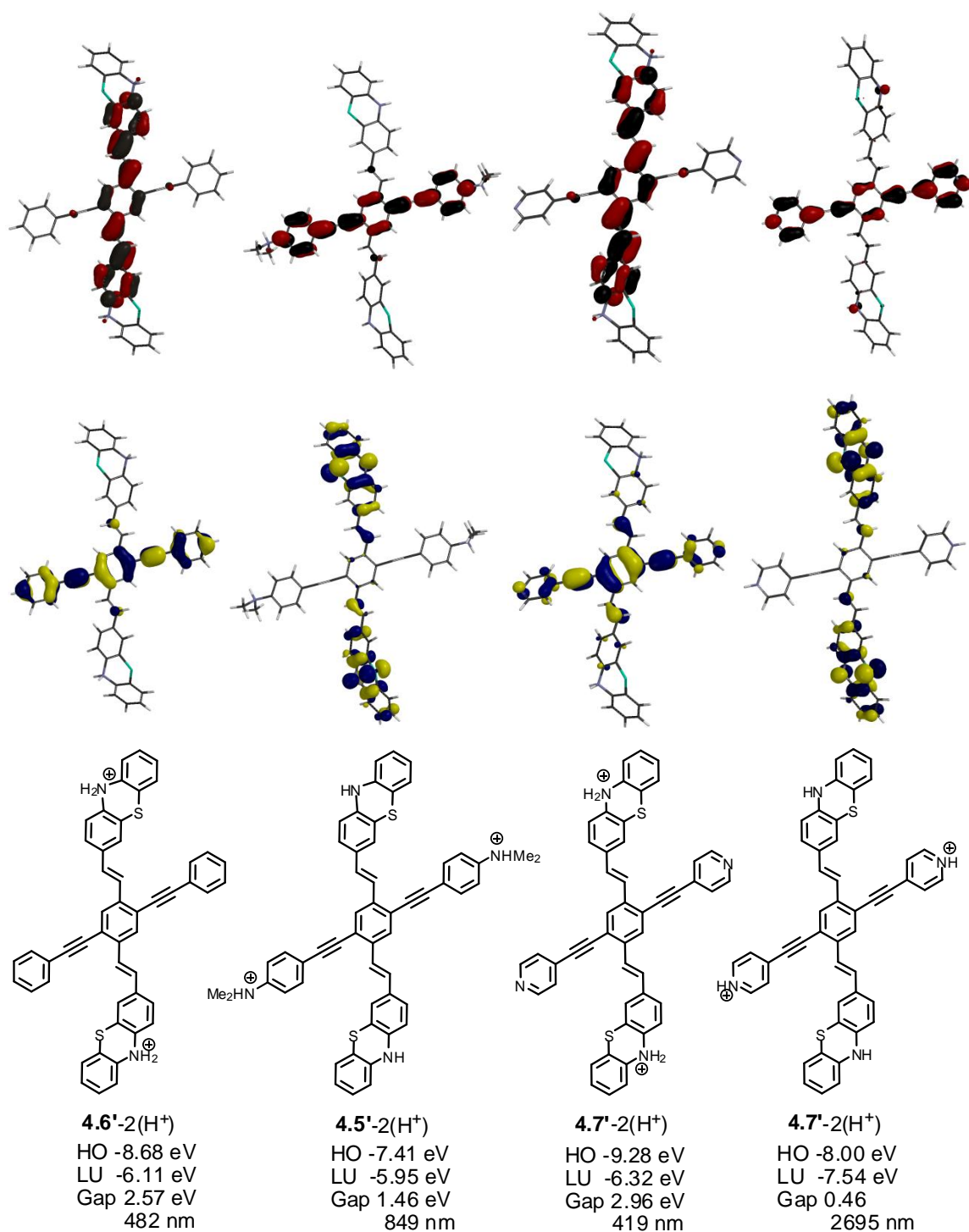


**FIGURE 4.5.** Molecular orbital plots (LUMOs, Top; HOMOs, Bottom) of the bisprotonated species **4.5'-2(H<sup>+</sup>)**, **4.6'-2(H<sup>+</sup>)**, and **4.7'-2(H<sup>+</sup>)**. The calculations were performed using B3LYP/6-31G\*\*//6-31G\* as implemented on SPARTAN.

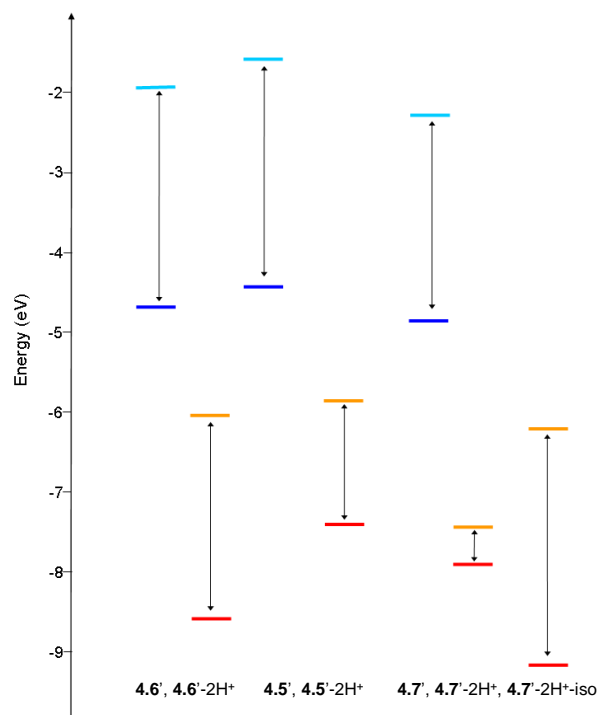


**Figure 4.6.** Absolute HOMO-LUMO positions from (B3LYP/6-31G\*\*//6-31G\*) calculations.

In the case of **4.5'**, which is all donor substituted, protonation of the aniline nitrogens leads to a decrease in the HOMO-LUMO gap and the development of a disjoint orbital structure, in which the anilinium ions are the acceptors and the phenothiazine-containing axis localizes the HOMO. When the phenothiazine units of **4.7** are protonated, the HOMO is localized on the bis(pyridinylethynyl)benzene axis, while the LUMO is localized on the axis that contains the protonated phenothiazines. A blue shift of the emission is expected (and found experimentally, *vide infra*), due to the increase in the HOMO-LUMO gap by removing the donor character from the phenothiazine-transverse. Upon protonation of the pyridine, the already pronounced spatial HOMO-LUMO separation in **4.7'** is further amplified and becomes extreme to such a point that there is no Franck-Condon overlap between the FMOs anymore. At the same time, the HOMO-LUMO gap shrinks to 0.46 eV.

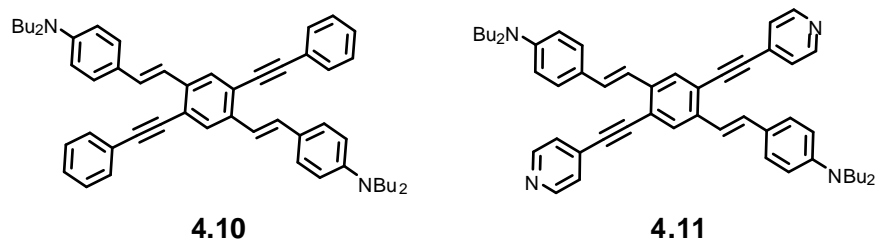


**Figure 4.7.** Structure of XFs **4.10** and **4.11**.

#### **4.2.3. Titration studies of 4.5-4.7 using trifluoroacetic acid in dichloromethane.**

To see if the qualitative predictions of the quantum chemical calculations were correct we performed titration studies on **4.5-4.7**. Generally, the protonation of phenothiazine forms oxidized radical cations.<sup>3,8</sup> In our hands (vide infra) protonation with a strong acid leads to a spectroscopic behavior that is best interpreted by partial oxidation but mostly simple multiple protonation of the phenothiazine nuclei. We investigated the absorption and the emission of **4.5-4.7** in the presence of increasing amounts of trifluoroacetic acid in dichloromethane. The spectra of the titration experiments are shown in Figures 4.8-4.10. The simplest case is that of **4.6** (Figure 4.9), where only the phenothiazine groups are present as basic sites. Upon addition of up to 40 equivalents of TFA there is no change in the absorption spectrum and only a small decrease in fluorescence intensity. After addition of 250 equivalents of TFA, there are two bands of approximately equal height visible in the emission spectrum. One is the original band recorded at 563 nm, while the second band is a blue-shifted feature at 447 nm. Upon increasing the amount of TFA, the absorption feature located at 433 nm decreases and a somewhat blue shifted maximum develops at 331 nm. After the addition of 1000 equivalents of TFA, the protonation is complete and only the blue emitting feature at 447 nm remains. In the absorption spectra, a band grows in at around 590 nm

upon exposure of **4.6** to large amounts of TFA under air. We see this secondary peak developing at 550-600 nm in all of the phenothiazine-XFs when they are exposed to a large excess of TFA in air. This absorption band is most probably a consequence from some oxidation of the XFs to the respective radical cations on each of the phenothiazine sites. The oxidation of phenothiazines in acidic solution is not uncommon and has been discussed.<sup>8</sup> However, complete oxidation of the XF is unlikely, as we have a strong blue fluorescence that is located at higher energy than the absorption maximum for the secondary band in absorption. In addition, a phenothiazine radical cation would in all probability be non-fluorescent. The presence of some percentage of radical cations is supported by the massive broadening of the proton NMR signals which additionally are severely downfield shifted.

Overall, this spectroscopic behavior can be interpreted by considering the FMO arrangement of **4.6**. Upon protonation of the phenothiazine rings, the HOMO of **4.6** is substantially stabilized while the LUMO is less affected. As a consequence, the observed blue shift in emission and the disappearance of the absorption feature at 433 nm is not unexpected. These spectroscopic properties are similar to those reported for the dibutylamino-XF **4.10**, only that the corresponding transitions in **4.10** are red-shifted and that the protonation of the phenothiazine units is considerably more difficult than that of the dibutylanilines in **4.10**. Our inability to forecast the increase in the HOMO-LUMO gap of **4.6** upon protonation using the model compound **4.6'** using a B3LYP/631G\*\*//6-31G\* calculation is probably due to the relatively low level of theory we have to use in these relatively large molecules.

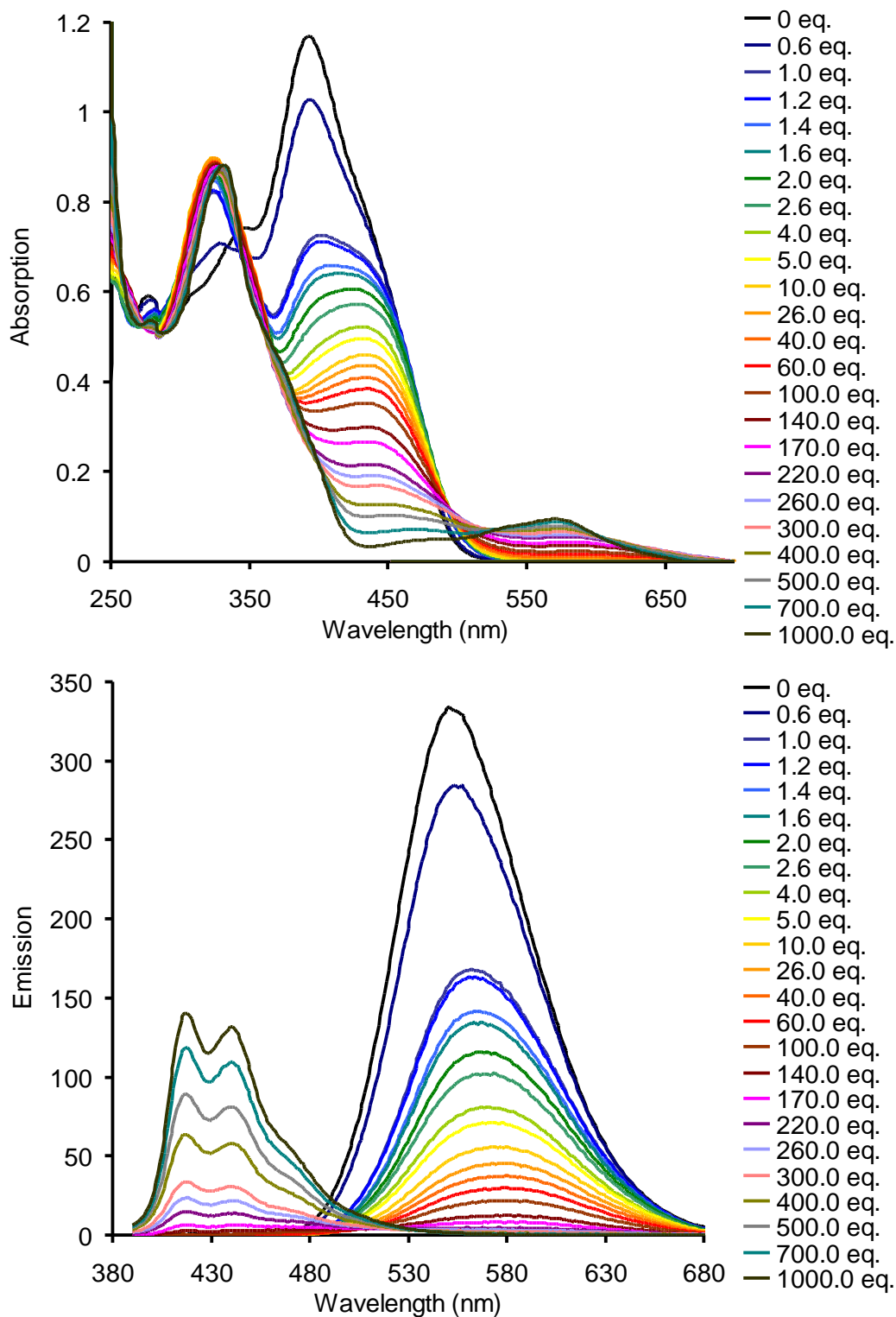


**Figure 4.8.** Absorption and emission spectra of XF 4.5 in the presence of increasing amounts of TFA.

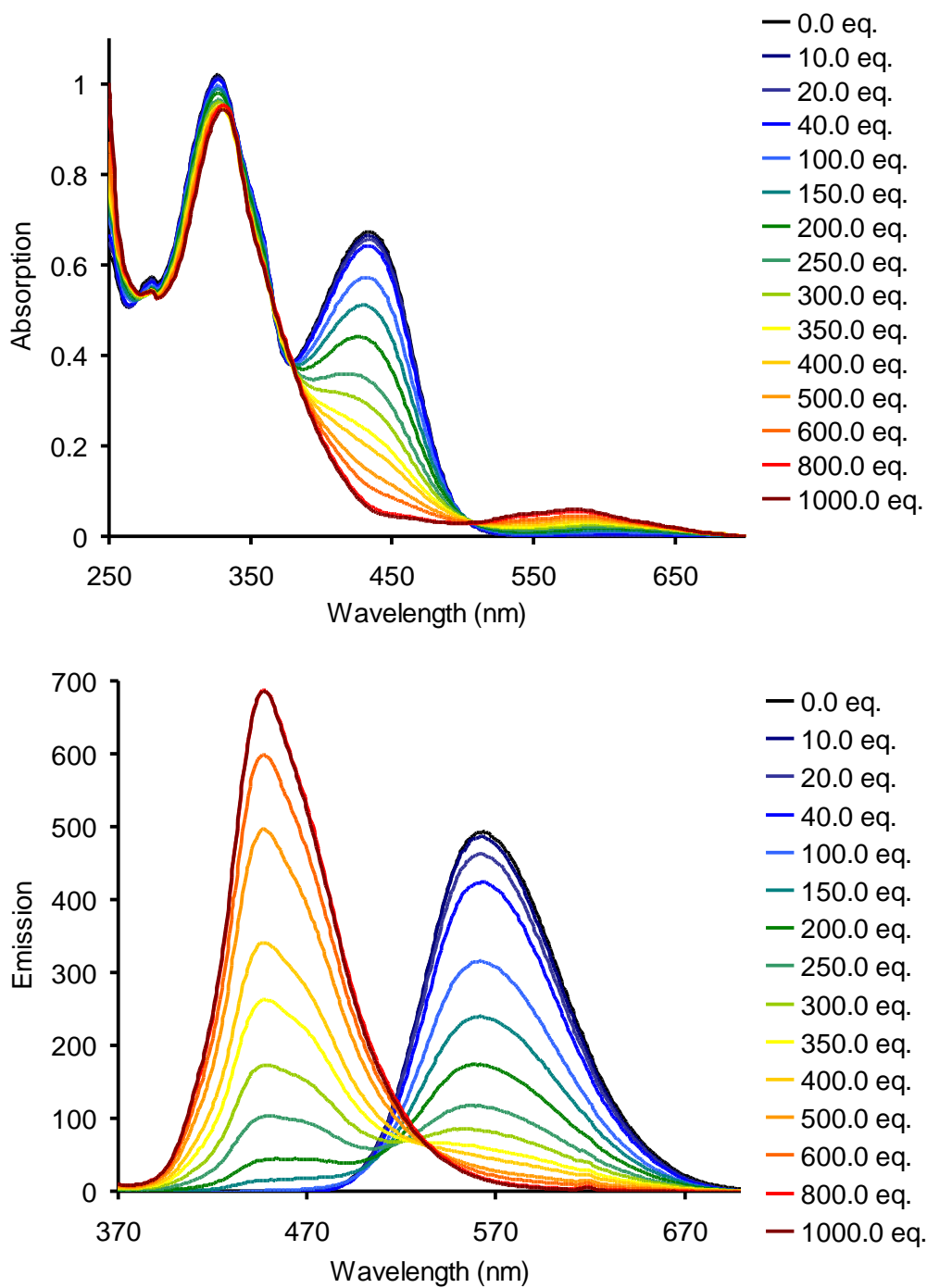


**Figure 4.9.** Absorption and emission spectra of XF 4.6 in the presence of increasing amounts of TFA.

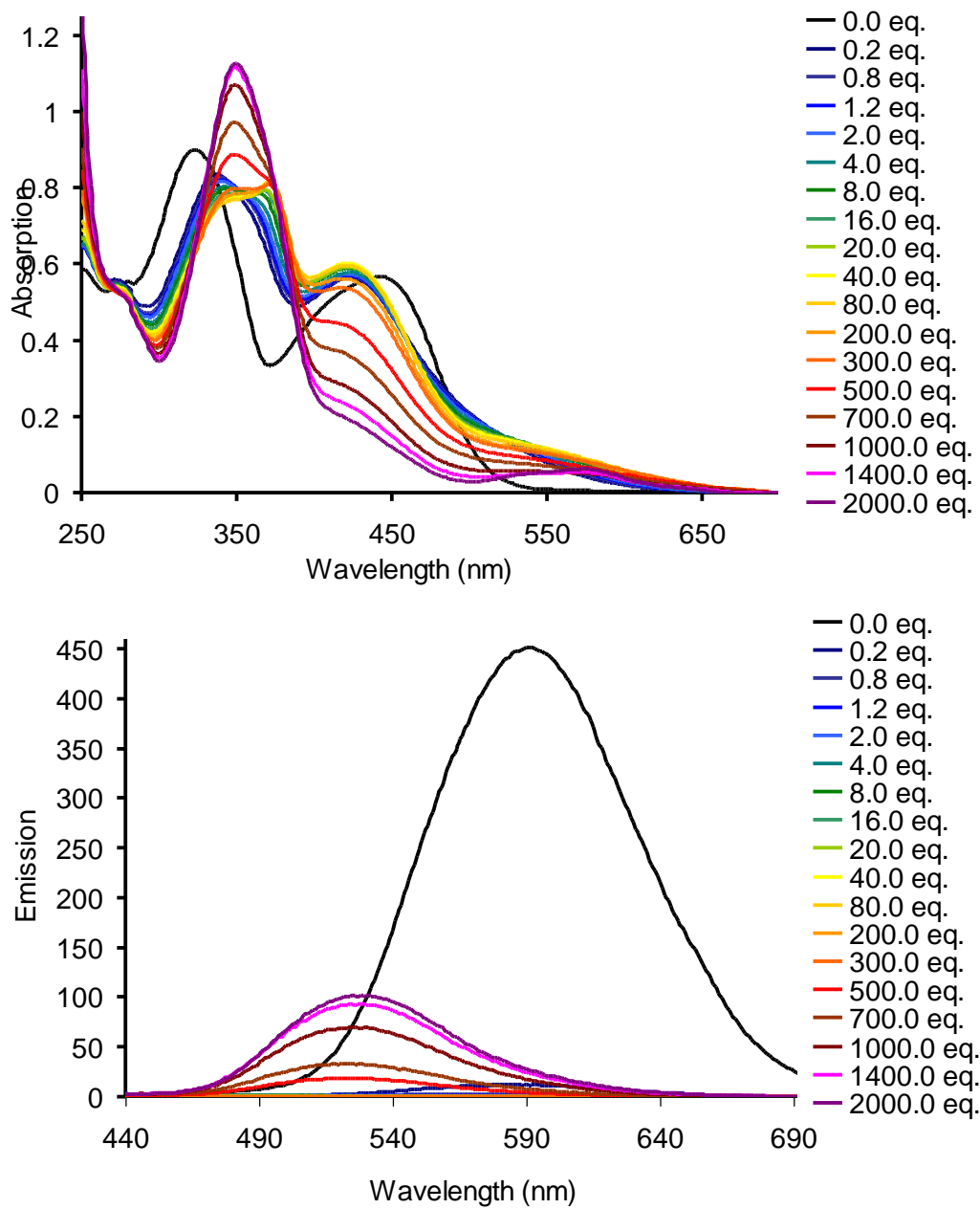


**Figure 4.10.** Absorption and emission spectra of XF 4.7 in the presence of increasing amounts of TFA.

After addition of 10 equivalents of TFA to a solution of **4.5**, the feature recorded at 392 nm diminishes in intensity and centers at 432 nm (Figure 4.8). At the same time we observe a shift in the emission from 552 nm to 577 nm. We attribute these changes to the protonation of the dibutylaniline moieties in **4.5**. Under these conditions we transform **4.5** into **4.5-2H<sup>+</sup>**, a donor-acceptor species with a disjoint FMO structure and a decreased band gap. Upon addition of considerably more TFA (1000 equivalents), the phenothiazine units are also protonated. Both the absorption and the emission are blue shifted as the HOMO is now stabilized by the protonation of the phenothiazine nuclei, yet the LUMO does not seem to be affected. Again, the broad feature that emerges at around 600 nm in the absorption spectrum is attributed to the partial oxidation of the phenothiazine units under these conditions.

In the case of **4.7** the neutral compound displays an absorption at 442 nm (Figure 4.10). Addition of up to 40 equivalents of TFA leads to a red shift in absorption that is characterized by a shoulder/tail at 550 nm and a sharp peak at 422 nm. We assign this signature to the doubly pyridine-protonated XF **4.7**. Upon further addition of TFA the shoulder disappears and a feature at 350 nm dominates the absorption spectrum. The main emission of **4.7** at 589 nm is quenched after the addition up to 100 equivalents of TFA. Upon addition of more TFA a new blue shifted emission is observed at 528 nm. We assume that first the pyridine units are protonated, leading to a species with a very low band gap, as the LUMO is stabilized by protonation. This species is non-fluorescent as there apparently are effective paths available for non-radiative excited state deactivation, in line with the energy gap law.<sup>7</sup> Upon further addition of TFA the phenothiazine units are likewise protonated, stabilizing the HOMO. The result is an all

acceptor-substituted species with congruent FMOs displaying an increased HOMO-LUMO gap. The **4.7**-4H<sup>+</sup> tetracation is fluorescent and would be best described as a class C cruciform.

#### 4.2.4 Interaction of the XFs with metal salts.

The study of the interaction of **4.5-4.7** with TFA was illuminating: Absorption and emission of the XFs are manipulated by protonation. It was of interest if similar effects could be elicited by the addition of metal cations to the XFs. We investigated both the absorption and the emission of **4.5-4.9** in the presence of Mg<sup>2+</sup>, Zn<sup>2+</sup>, and Ca<sup>2+</sup> in form of their triflates in dichloromethane solution. From prior experience we are expecting that the binding affinity for the anilines, pyridines and the phenothiazines would be Mg<sup>2+</sup>>Zn<sup>2+</sup>>>Ca<sup>2+</sup>.<sup>1</sup> Zinc complexes with promazine hydrochlorides had been proposed by Gowda et al. The coordination of zinc chloride with the phenothiazinyl sulfur was inferred from shifts of C-S-valence bands in the IR spectra.<sup>9</sup> However, prominent effects in the electronic spectra of the complexes were not observed.

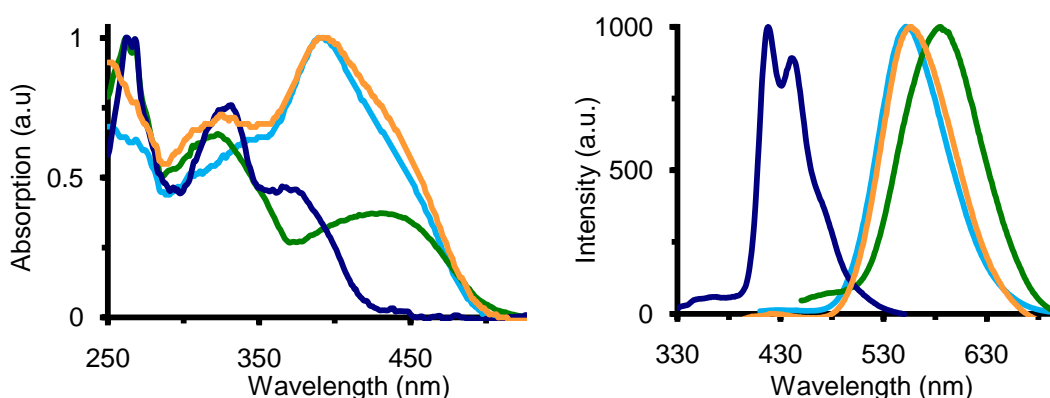


**Figure 4.11.** Normalized absorption and emission spectra of XF **4.5** (light blue trace) in the presence of different metal cations (Zn<sup>2+</sup> = green trace, Mg<sup>2+</sup> = dark blue trace, Ca<sup>2+</sup> = orange trace).

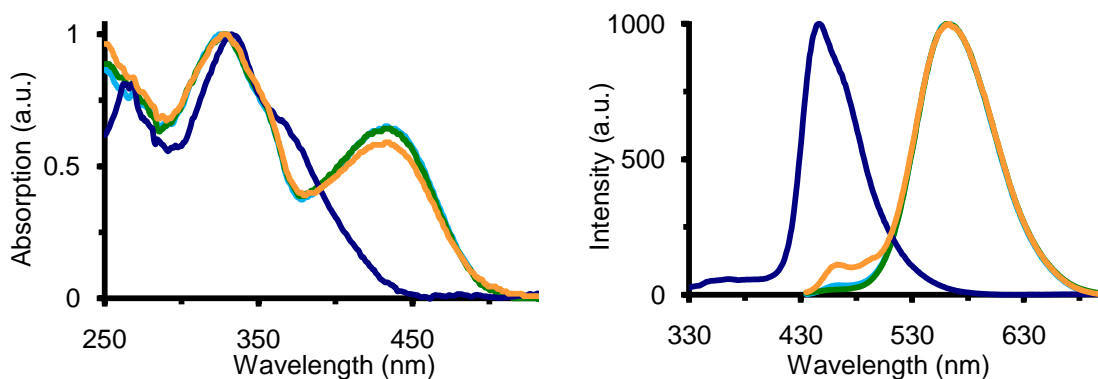


**Figure 4.12.** Normalized absorption and emission spectra of XF 4.6 (light blue trace) in the presence of different metal cations ( $\text{Zn}^{2+}$  = green trace,  $\text{Mg}^{2+}$  = dark blue trace,  $\text{Ca}^{2+}$  = orange trace).

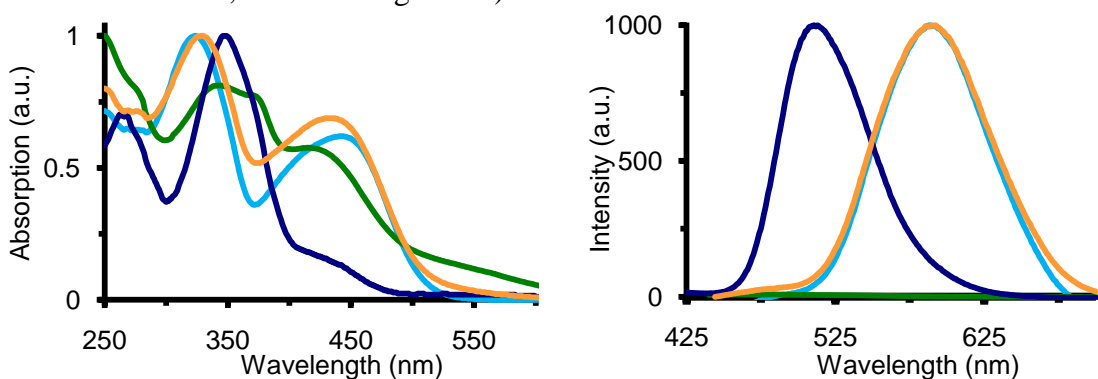


**Figure 4.13.** Normalized absorption and emission spectra of XF 4.7 (light blue trace) in the presence of different metal cations ( $\text{Zn}^{2+}$  = green trace,  $\text{Mg}^{2+}$  = dark blue trace,  $\text{Ca}^{2+}$  = orange trace).

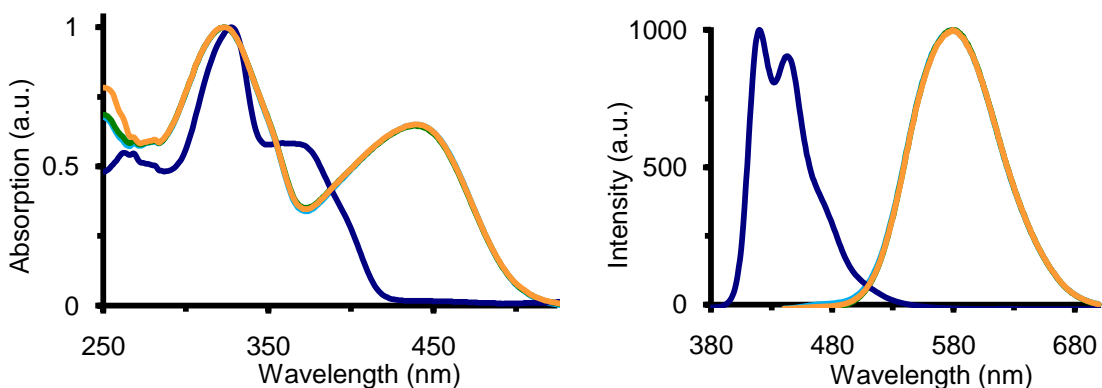


**Figure 4.14.** Normalized absorption and emission spectra of XF 4.8 (light blue trace) in the presence of different metal cations ( $\text{Zn}^{2+}$  = green trace,  $\text{Mg}^{2+}$  = dark blue trace,  $\text{Ca}^{2+}$  = orange trace).

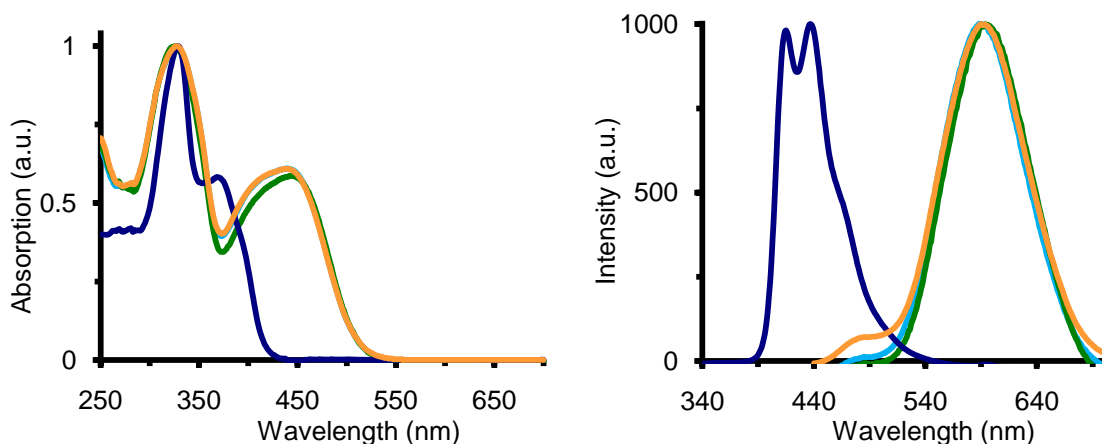


**Figure 4.15.** Normalized absorption and emission spectra of XF **4.9** (light blue trace) in the presence of different metal cations ( $\text{Zn}^{2+}$  = green trace,  $\text{Mg}^{2+}$  = dark blue trace,  $\text{Ca}^{2+}$  = orange trace).

The exposure of **4.5** to  $\text{Ca}(\text{OTf})_2$  in dichloromethane (Figure 4.11, Table 4.2) elicits a vanishingly small bathochromic shift in absorption and emission, probably due to weak binding. In the case of  $\text{Zn}(\text{OTf})_2$ , a striking red shift in both absorption and emission is observed, while  $\text{Mg}(\text{OTf})_2$  causes a blue shift in both emission and absorption. The differences in the spectroscopic behavior can be easily explained if one assumes that  $\text{Zn}(\text{OTf})_2$  binds to the dibutylanilines but does *not* bind to the phenothiazine nuclei, transforming the donor XF **4.5** into a donor-acceptor XF with a decreased band gap. The arylethynyl transverse localizes the LUMO after zinc coordination, while the HOMO is still localized on the phenothiazine-bearing axis. The binding affinity of  $\text{Mg}(\text{OTf})_2$  is sufficiently high to coordinate not only to the dibutylanilines but also to the phenothiazine nuclei, transforming the donor-substituted XF **4.5** into an all-acceptor-substituted XF with an increased band gap. In this case, the HOMO is more stabilized than the LUMO to give the blue emitting species.

**Table 4.2.** Spectroscopic data of **4.5-4.9** in the presence of divalent metal ions in dichloromethane.

	<b>4.5</b>	<b>4.6</b>	<b>4.7</b>	<b>4.8</b>	<b>4.9</b>
$\lambda_{\max}$ abs (nm)	392	433	442	437	439
$\lambda_{\max}$ abs (nm) + Zn <sup>2+</sup>	431	433	412	440	444
$\lambda_{\max}$ abs (nm) + Mg <sup>2+</sup>	369 sh 330	371 sh 332	431 sh 348	362 328	371 329
$\lambda_{\max}$ abs (nm) + Ca <sup>2+</sup>	392	433	437	440	439
$\lambda_{\max}$ emission (nm)	552	563	589	579	590
$\lambda_{\max}$ emission (nm) + Zn <sup>2+</sup>	586	561	Quenched	579	594
$\lambda_{\max}$ emission (nm) + Mg <sup>2+</sup>	418 441	447	513	420 443	415 437
$\lambda_{\max}$ emission (nm) + Ca <sup>2+</sup>	557	564	592	579	590

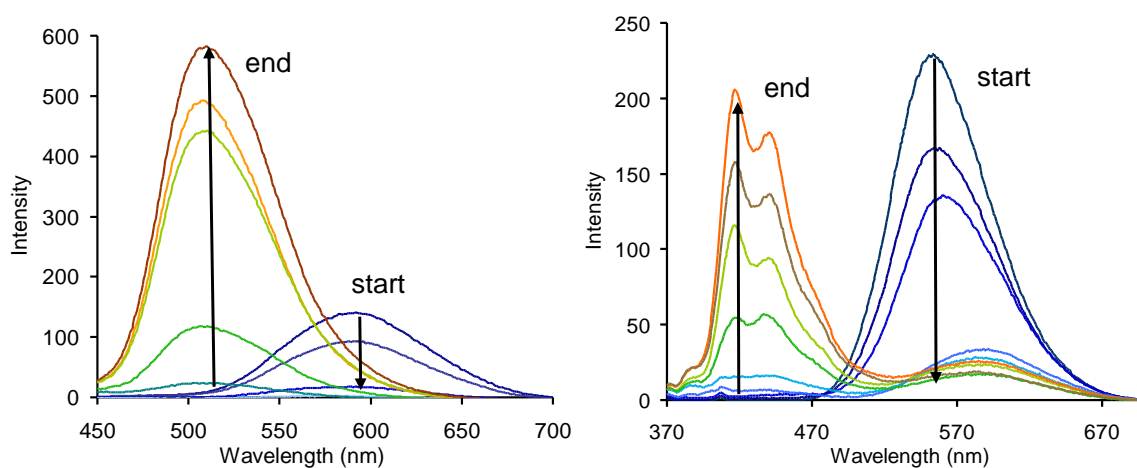


**Figure 4.16.** Left: Interaction of **4.7** with increasing amount of Mg(OTf)<sub>2</sub>. Right: Interaction of XF **4.5** with increasing amounts of Mg(OTf)<sub>2</sub>. Arrows show increasing concentration of Mg(OTf)<sub>2</sub>

In the case of **4.6** (Figure 4.12),  $\text{Ca}(\text{OTf})_2$  and  $\text{Zn}(\text{OTf})_2$  give insignificant responses, while coordination of  $\text{Mg}(\text{OTf})_2$  induces blue shift in both absorption and emission. XF **4.6** is a model compound for both **4.5** and **4.7** in the sense that it only contains the phenothiazine moieties and therefore displays an easier to interpret change in photophysics upon metal salt coordination. In the cases of **4.8** and **4.9**, which are in effect only acceptor-substituted variants of **4.7**, the same coordination pattern as in **4.6** is observed with all three metal triflates.

The XF **4.7** is structurally reminiscent of the donor-acceptor XF **4.11**. Are the same spectroscopic effects observed in **4.7**? In **4.11**, we find a blue shift in both emission and absorption when treating with either  $\text{Zn}(\text{OTf})_2$  or  $\text{Mg}(\text{OTf})_2$ .<sup>1</sup> Upon addition of an excess of these salts, we see a second, bathochromic shift that leads to a green emissive species as the end point. We contend that the dibutylanilines are coordinated first, leading to a stabilization of the HOMO. The subsequent coordination of the metal salt to the pyridines stabilizes the LUMO. Figure 4.13 shows the exposure of **4.7** to metal triflates:  $\text{Ca}(\text{OTf})_2$  unsurprisingly does not coordinate. Upon addition of  $\text{Zn}(\text{OTf})_2$ , we see a red shifted but very broad absorption that is tailing beyond 600 nm, *while the emission of this species is quenched*. Upon addition of  $\text{Mg}(\text{OTf})_2$  to the solution of **4.7**, a significant blue shift is observed both in absorption and emission. The spectral changes induced by  $\text{Mg}(\text{OTf})_2$  are very similar to those observed upon addition of an excess of TFA to **4.5-4.7**, while the spectral changes observed upon addition of  $\text{Zn}(\text{OTf})_2$  to the cruciforms resemble those observed upon protonation of the non-phenothiazine nitrogens.

The behavior of **4.7** when compared to **4.11** is inverted with respect to the coordination ability of the ligands on the XF transverses. In **4.7**, the pyridines coordinate

stronger than the phenothiazines, and the addition of  $\text{Zn}(\text{OTf})_2$  leads to a highly disjoint XF with a very small HOMO-LUMO gap. The decrease of the Franck-Condon overlap in combination with the energy gap law<sup>7</sup> leads to a disallowed HOMO-LUMO transition; radiationless deactivation of the excited state occurs and quenching is observed. In the case of the stronger coordinating  $\text{Mg}(\text{OTf})_2$ , all four binding sites are occupied by metal ions and an all-acceptor-substituted class C XF with a strong emission in the green results. To exclude the possibility that  $\text{Mg}(\text{OTf})_2$  does only coordinate with two of the four sites, we performed a titration of **4.7**, which is shown in Figure 4.16 (left). Upon addition of a small amount of a saturated solution of  $\text{Mg}(\text{OTf})_2$  to the XF, the fluorescence is quenched. Upon addition of more  $\text{Mg}(\text{OTf})_2$ , a strong emission centered at 512 nm develops. The same type of titration can also be performed with **4.5**, as shown in Figure 4.16 (right). Here also the fluorescence red shifts and weakens considerably when a small amount of a  $\text{Mg}(\text{OTf})_2$  is added, suggesting that only the dialkylaniline units are coordinated. Upon further addition of  $\text{Mg}(\text{OTf})_2$ , the expected blue emission appears as all four sites are coordinated. Our results suggest contrary to literature claims that  $\text{Zn}^{2+}$  does not strongly coordinate to phenothiazine, even if zinc triflate is used in a weakly coordinating solvent such as dichloromethane.<sup>9</sup>

### 4.3. Conclusions

To expand the diversity of functionality of cruciform fluorophores, we prepared and examined XFs **4.5-4.9** containing phenothiazine moieties on the arylenevinylene transverse. Depending upon their substitution pattern, these XFs show either class C (congruent) or class D (disjoint) FMOs.<sup>1</sup> Exposure of these XFs to either trifluoroacetic

acid or to metal salts leads to strong chromic effects in absorption and in emission.<sup>10</sup> A small panel of these XFs (Figure 4.17) allows to visualize the observed metallochromic effects and demonstrates that such simple responsive fluorophores can discern zinc from magnesium ions in dichloromethane without the interference of calcium ions. The coordinative ability of  $\text{Ca}^{2+} < \text{Zn}^{2+} < \text{Mg}^{2+}$  explains the observed changes in emission and absorption. Quantum chemical model calculations support the observed trends. When compared to XFs such as **4.10** or **4.11**, the incorporation of the aniline nitrogens into the phenothiazine framework decreases their basicity and metal coordinating ability as would be expected from simple hybridization and resonance arguments. The herein presented XFs display a significantly different pattern of metallochromicity as compared to those observed in **4.10** and **4.11**.

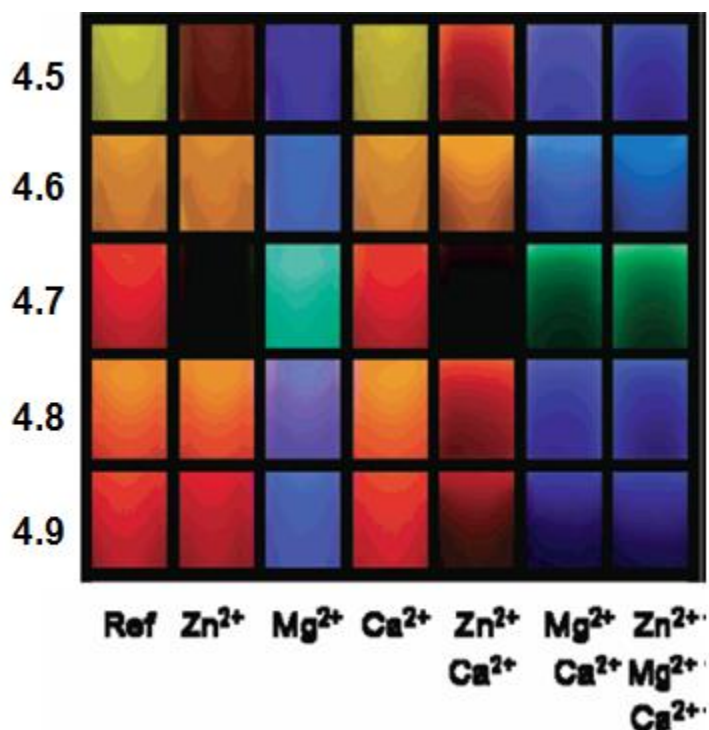


**Figure 4.17.** Exposure of the XFs **4.5-4.9** to different metal ions in dichloromethane. The picture is taken on a black background using a hand-held UV lamp ( $\lambda_{\text{max}} \text{ex} = 365 \text{ nm}$ ) and represents the metallochromic properties of the XFs in emission quite well.

This work has been published in the *Journal of Organic Chemistry*:

Hauck, M.; Schönhaber, J.; Zuccherro, A. J.; Hardcastle, K. I.; Müller, T. J. J.; Bunz, U.

H. F. Phenothiazine cruciforms: synthesis and metallochromic properties. *J. Org. Chem.* **2007**, *72*, 6714-6725.

#### 4.4. Experimental

**General Methods.** All chemicals and solvents were purchased from commercial sources and were used without further purification unless otherwise specified. Column chromatography was performed using Standard Grade silica gel 60 Å, 32-63 µm (Sorbent Technologies) and the specified eluent. All IR spectra were obtained using a Shimadzu FTIR-8400s spectrometer. <sup>1</sup>H NMR spectra were recorded at 298 K on a 300 or 500 MHz spectrometer. Chemical shifts are reported in parts per million (ppm), using residual solvent as an internal standard. The data is reported as follows: chemical shift, multiplicity (s = singlet, d = doublet, t = triplet, q = quartet, m = multiplet, br = broad), and integration. <sup>13</sup>C HMR spectra were recorded at 300 or 500 MHz, and <sup>13</sup>C chemical shifts (δ) are referenced to residual CHCl<sub>3</sub> at 77.23 ppm. All absorption spectra were collected using a Shimadzu UV-2401PC spectrophotometer. All emission spectra were acquired using a Shimadzu RF-5301PC spectrofluorophotometer. Quantum yields were measured using standard procedures using quinine sulfate, fluorescein, or 2-aminopyridine as standards; all solutions were purged with nitrogen prior to measurement.

**Synthesis of aldehyde 4.2. 10-Hexyl-10H-phenothiazin-3-carbaldehyde.** In a dry, nitrogen flushed 500 ml three-necked flask, 14.1 g (0.05 mol) of 10-Hexyl-10H-

phenothiazine and 7.16 g (0.053 mol) N-Methylformanilid were solved in 200 ml of absolute 1,2-Dichlorethane. The reaction was cooled to 0°C and 8.43 g (0.055 mol) POCl<sub>3</sub> solved in 6 ml 1,2-Dichlorethane was added. The reaction was refluxed for two days and then cooled to room temperature. Then 200 ml of a saturated solution of sodium acetate was added and the reaction was stirred for two hours. The layers were separated and the aqueous layer was extracted with ether (3x). The combined organic layers were dried with magnesium sulfate and the solvents were removed in vacuo. The product was purified by column-chromatography (SiO<sub>2</sub>, n-Hexane/Ether 4:1). 11.4 g (0.037 mol, 73 %) as a light yellow oil. <sup>1</sup>H-NMR (300 MHz, Acetone-*d*<sub>6</sub>): δ = 0.81-0.87 (m, 3H), 1.24-1.32 (m, 4H), 1.40-1.51 (m, 2 H), 1.74-1.86 (m, 2H), 4.01 (t, *J* = 7.1 Hz, 2 H), 6.96-7.25 (m, 5H), 7.59 (d, *J* = 1.9 Hz), 1H), 7.72 (dd, *J* = 8.5 Hz, *J* = 1.9 Hz, 1H), 9.82 (s, 1H). <sup>13</sup>C-NMR (75.5 MHz, Aceton-*d*<sub>6</sub>): δ = 15.2, 24.2, 28.0, 28.4, 33.1, 49.3, 117.3, 118.3, 125.4, 126.5, 129.1, 129.5, 129.6, 131.8, 133.4, 145.5, 152.4, 191.4. EI-MS (70 eV, *m/z* (%)): 312 (20), 311 ([M]<sup>+</sup>, 100), 241 (12), 240 ([M-C<sub>5</sub>H<sub>11</sub>]<sup>+</sup>, 80), 227 (17) 226 ([M-C<sub>6</sub>H<sub>13</sub>]<sup>+</sup>, 77), 208 (28), 198 (24), 28 (15).

**Synthesis of diiodide 4.4.** **3,3'-(1*E*,1'*E*)-2,2'-(2,5-diiodo-1,4-phenylene)bis(ethene-2,1-diyl)bis(10-hexyl-10*H*-phenothiazine).** An oven-dried Schlenk flask cooled under nitrogen atmosphere was charged with dry THF (50 mL), diphosphonate **4.3** (788 mg, 1.25 mmol) and NaH (33.0 mg, 1.38 mmol) until the solution turned a purple-red color. Aldehyde **4.2** (973 mg, 3.13 mmol) was added to the stirred mixture. The color changed to orange and a solid precipitated. The reaction mixture was stirred over night at room temperature. The reaction was quenched with water. Dichloromethane (200 mL) was added and extracted five times with brine, dried over magnesium sulphate. The solvent

was evaporated under reduced pressure. The resulting solid was crystallized from dichloromethane/hexanes yielding (1.06 g, 1.12 mmol, 90 %) of bright orange crystals of **4.4**. MP: 178-180°C. <sup>1</sup>H-NMR (300 MHz, CD<sub>2</sub>Cl<sub>2</sub>): δ = 0.85-0.91 (m, 6H), 1.28-1.34 (m, 8 H), 1.39-1.48 (m, 4 H), 3.85 (t, 4 H, J = 7.2 Hz), 6.83-6.95 (m, 8H), 7.04 (d, 2 H, J = 16.0 Hz), 7.12 (dd, 2H, J = 1.5 Hz, J = 7.6 Hz), 7.14-7.19 (m, 2 H), 7.29-7.34 (m, 4 H), 8.06 (s, 2 H). <sup>13</sup>C-NMR (75.5 MHz, CD<sub>2</sub>Cl<sub>2</sub>): δ = 14.2, 23.0, 26.9, 27.1, 31.8, 47.9, 100.6, 115.7, 115.8, 122.8, 124.2, 125.16, 125.17, 125.4, 126.8, 127.6, 127.7, 128.8, 131.3, 136.3, 140.8, 145.0, 145.6. IR (KBr): ν [cm<sup>-1</sup>] 2953 (m), 2927 (m), 2854 (w), 1625 (m), 1599 (m), 1575 (m), 1495 (m), 1467 (s), 1443 (s), 1404 (w), 1364 (w), 1335 (w), 1290 (w), 1247 (m), 1208 (w), 1041 (m), 955 (m), 746 (m). UV/Vis (CH<sub>2</sub>Cl<sub>2</sub>): λ<sub>max</sub> (ε) 250 nm (60000), 276 nm (39000), 328 nm (36000), 424 nm (50000). Emission (CH<sub>2</sub>Cl<sub>2</sub>): λ<sub>max</sub> 578 nm. MS (FAB<sup>+</sup>) (m/z (%)): 945 (M-H<sup>+</sup>, 66), 944 (M<sup>+</sup>, 100), 899 (10), 898 (13), 896 (13), 873 (10), 860 (14), 859 (17). HR-MS: Calc. for C<sub>46</sub>H<sub>46</sub>I<sub>2</sub>N<sub>2</sub>S<sub>2</sub> 944.1192, Found: 944.1168.

**Synthesis of XF 4.5. 4,4'-(2,5-bis((E)-2-(10-hexyl-10H-phenothiazin-3-yl)vinyl)-1,4-phenylene)bis(ethyne-2,1-diyl)bis(N,N-dibutylbenzenamine).** In an oven dried Schlenk tube cooled under nitrogen atmosphere, **4.4** (300 mg, 0.317 mmol) was dissolved in dry THF (8 mL), piperidine (1 mL) and ethanol (2 mL) and combined with PdCl<sub>2</sub>(PPh<sub>3</sub>)<sub>2</sub> (4.5 mg, 6.4 μmol, 2 mol %) and CuI (2.4 mg, 13 μmol, 4 mol %). N,N-Dibutyl-4-((trimethylsilyl)ethynyl)aniline (241 mg 0.799 mmol) and potassium hydroxide (157 mg 2.80 mmol) were added and the reaction was started with a heat gun. Salts started to precipitate immediately. The reaction mixture was stirred overnight at room temperature. The crude mixture was diluted with dichloromethane and washed three

times with water, three times with brine, and once with aqueous ammonia hydroxide. The organic phase was dried with magnesium sulfate and evaporated under reduced pressure. The product was purified by column chromatography hexanes/ethyl acetate (9:1) and crystallization from dichloromethane/hexanes to give **4.5** (223 mg, 0.19 mmol, 61 %) as orange crystals suitable for crystallographic analysis. MP: 162-166°C. <sup>1</sup>H-NMR (300 MHz, CD<sub>2</sub>Cl<sub>2</sub>): δ = 0.86-0.92 (m, 6 H), 1.00 (t, 12 H, J = 7.3 Hz), 1.26-1.49 (m, 20 H), 1.55-1.69 (m, 8H), 1.74-1.88 (m, 4 H), 3.29-3.38 (m, 8 H), 3.86 (t, 4 H, J = 7.1 Hz), 6.68 (d, 4H, J = 8.7 Hz), 6.88-6.93 (m, 6 H), 7.10-7.20 (m, 6 H), 7.32-7.41 (m, 4 H), 7.50 (d, 4 H, J = 8.5 Hz), 7.57 (d, 2 H, J = 16.3 Hz), 7.82 (s, 2 H). <sup>13</sup>C-NMR (75.5 MHz, CD<sub>2</sub>Cl<sub>2</sub>): δ = 14.1, 20.2, 23.0, 26.9, 27.1, 29.7, 31.8, 47.9, 51.0, 86.2, 97.5, 108.6, 111.6, 115.75, 115.77, 122.6, 122.7, 124.4, 125.1, 125.5, 126.3, 127.57, 127.60, 128.3, 129.0, 132.3, 133.1, 133.2, 136.9, 145.18, 145.19, 148.6. IR (KBr): ν [cm<sup>-1</sup>] 2955 (s), 2929 (s), 2869 (m), 2858 (m), 2192 (m), 1604 (s), 1521 (s), 1496 (m), 1465 (m), 1445 (s), 1402 (m), 1367 (m), 1336 (m), 1289 (m), 1247 (m), 1223 (m), 1193 (m), 812 (m), 746 (m). UV/Vis (CH<sub>2</sub>Cl<sub>2</sub>): λ<sub>max</sub> (ε) 252 nm (40000), 278 nm (36000), 312 nm (45000), 348 nm (56000), 392 nm (90000), 450 nm (47000). Emission (CH<sub>2</sub>Cl<sub>2</sub>): λ<sub>max</sub> (ε) 532 nm. MS (FAB<sup>+</sup>) (m/z (%)): 1149 (24), 1148 (56), 1147 (M-H<sup>+</sup>, 95), 1146 (M<sup>+</sup>, 100), 1145 (34). HR-MS: Calc.: for C<sub>78</sub>H<sub>90</sub>N<sub>4</sub>S<sub>2</sub> 1146.6607, Found: 1146.6631.

**Synthesis of XF 4.6. 3,3'-(1E,1'E)-2,2'-(2,5-bis((4-tert-butylphenyl)ethynyl)-1,4-phenylene)bis(ethene-2,1-diyl)bis(10-hexyl-10H-phenothiazine).** An oven-dried

Schlenk flask cooled under nitrogen atmosphere was charged with dry THF (5 mL) and piperidine (3 mL); diiodide **4.4** (200 mg, 0.211 mmol) was dissolved and combined with PdCl<sub>2</sub>(PPh<sub>3</sub>)<sub>2</sub> (3.0 mg, 4.2 μmol, 2 mol %) and CuI (1.6 mg 8.4 μmol, 4 mol %). The

reaction mixture was stirred for 15 min. before 1-*tert*-butyl-4-ethynylbenzene (83.1 mg 0.53 mmol) was added. After a few minutes salts started to precipitate. The reaction was stirred at room temperature overnight. The crude reaction mixture was diluted with water, the organic phase was washed three times with water, two times with brine and two times with 5% aqueous ammonia hydroxide solution, dried with magnesium sulfate and concentrated under vacuum. The product was first purified via column chromatography and then via recrystallization from dichloromethane/hexanes yielding **4.6** (63.0 mg, 0.06 mmol, 30 %) as a yellow powder. MP: 216-218°C. <sup>1</sup>H-NMR (300 MHz, CD<sub>2</sub>Cl<sub>2</sub>): δ = 0.85-0.92 (m, 6H), 1.28-1.40 (m, 24 H), 1.40-1.49 (m, 4H), 1.81 (td, 4H, J = 7.6 Hz, J = 14.8 Hz), 3.86 (t, 4H, J = 7.2 Hz), 6.84 -6.96 (m, 6H), 7.10-7.23 (m, 6H), 7.32-7.40 (m, 4H), 7.50-7.62 (m, 6H), 7.87 (s, 2H). <sup>13</sup>C-NMR (75.5 MHz, CD<sub>2</sub>Cl<sub>2</sub>): δ =14.1, 23.0, 26.9, 27.1, 31.3, 31.8, 35.2, 47.9, 87.5, 96.0, 115.8, 120.3, 122.4, 122.8, 124.0, 124.4, 125.2, 125.6, 125.9, 126.0, 126.4, 127.59, 127.64, 128.8, 129.6, 131.6, 132.0, 137.5, 145.1, 145.4, 152.5. IR (KBr): ν [cm<sup>-1</sup>] 2985 (m), 2929 (m), 2867 (w), 2858 (w), 1629 (m), 1603 (w), 1575 (w), 1515 (w), 1497 (w), 1466 (s), 1444 (s), 1364 (w), 1335 (w), 1269 (m), 1248 (w), 959 (w), 746 (w), 562 (w). UV/Vis (CH<sub>2</sub>Cl<sub>2</sub>): λ<sub>max</sub> (ε) 242 nm (48000), 280 nm (37000), 328 nm (89000), 358 (60000), 343 nm (60000). Emission (CH<sub>2</sub>Cl<sub>2</sub>): λ<sub>max</sub> 562 nm. MS (FAB<sup>+</sup>) (m/z (%)): 1008 (22), 1007 (48), 1006 (M-H<sup>+</sup>, 81), 1005 (M<sup>+</sup>, 100), 1004 (22), 921 (10), 919 (13). HR-MS: Calc. for C<sub>70</sub>H<sub>72</sub>N<sub>2</sub>S<sub>2</sub> 1004.5137, Found:1004.5092.

**Synthesis of XF 4.7. 3,3'-(1*E*,1'*E*)-2,2'-(2,5-bis(pyridin-4-ylethynyl)-1,4-phenylene)bis(ethene-2,1-diyl)bis(10-hexyl-10*H*-phenothiazine).** In an oven dried Schlenk tube cooled under nitrogen atmosphere **4.4** (300 mg, 0.317 mmol) was dissolved

in dry THF (6 mL) and piperidine (1 mL) and combined with PdCl<sub>2</sub>(PPh<sub>3</sub>)<sub>2</sub> (4.5 mg, 6.4 μmol, 2 mol %) and CuI (2.4 mg, 13 μmol, 4 mol %). 4-((Triisopropylsilyl)ethynyl)pyridine (208 mg, 0.80 mmol) was added via syringe and the reaction was started with the addition of tetrabutylammonium fluoride solution (230 mg, 0.88 mmol, 1 M in THF). Salts started to precipitate immediately and the color changed from bright orange to red/brown. The reaction mixture was stirred over night at room temperature. The crude mixture was diluted with dichloromethane and washed three times with water, three times with brine and once with aqueous ammonia hydroxide solution. The organic phase was dried with magnesium sulfate and evaporated under reduced pressure. The product was purified by recrystallization from dichloromethane/hexanes yielding **4.7** (176 mg, 0.20 mmol, 61 %) as an orange-red solid. MP: 186-190°C. <sup>1</sup>H-NMR (300 MHz, CD<sub>2</sub>Cl<sub>2</sub>): δ = 0.84-0.93 (m, 6H), 1.25-1.36 (m, 8H), 1.38-1.50 (m, 4H), 1.74-1.86 (m, 4H), 3.85 (t, 4H, J = 7.1 Hz), 6.84-6.97 (m, 6H), 7.09-7.21 (m, 6H), 7.29-7.37 (m, 4H), 7.40-7.51 (m, 6H), 7.88 (s, 2H), 8.64 (s, 4H). <sup>13</sup>C-NMR (75.5 MHz, CD<sub>2</sub>Cl<sub>2</sub>): δ = 14.1, 23.0, 26.9, 27.1, 31.8, 47.9, 92.1, 93.2, 115.8, 115.9, 122.0, 122.9, 123.2, 124.3, 125.3, 125.6, 125.7, 126.5, 127.6, 127.7, 129.3, 130.4, 131.2, 131.6, 137.9, 145.0, 145.7, 150.3. IR (KBr): ν [cm<sup>-1</sup>]: 3553 (s), 3548 (s), 3511 (s), 3495 (s), 3456 (s), 3447 (s), 3442 (s), 3436 (s), 3431 (s), 3426 (s), 3420 (s), 3267 (m), 2967 (m), 2957 (w), 2928 (m), 2857 (w), 2207 (w), 1628 (m), 1591 (s), 1575 (w), 1497 (m), 1467 (s), 1443 (w), 1249 (m). UV/Vis (CH<sub>2</sub>Cl<sub>2</sub>): λ<sub>max</sub> (ε) 250 nm (43000), 300 nm (58000), 326 nm (78000), 440 nm (51000). Emission (CH<sub>2</sub>Cl<sub>2</sub>): λ<sub>max</sub> 590 nm. MS (FAB<sup>+</sup>) (m/z (%)): 897 (28), 896 (54), 895 (M-H<sup>+</sup>, 100), 894 (M<sup>+</sup>, 90), 893 (17), 810 (15). HR-MS: Calc.: for C<sub>60</sub>H<sub>54</sub>N<sub>4</sub>S<sub>2</sub> 894.3790, Found: 894.3802.

**Synthesis of XF 4.8.** 3,3'-(1*E*,1'*E*)-2,2'-(2,5-bis((3-(trifluoromethyl)phenyl)ethynyl)-1,4-phenylene)bis(ethene-2,1-diyl)bis(10-hexyl-10*H*-phenothiazine). In oven dried Schlenk tube cooled under nitrogen atmosphere **4.4** (300 mg, 0.317 mmol) was dissolved in dry THF (7 mL), piperidine (1 mL), ethanol (2 mL) and combined with PdCl<sub>2</sub>(PPh<sub>3</sub>)<sub>2</sub> (4.5 mg, 6.4 μmol, 2 mol %) and CuI (2.4 mg, 13 μmol, 4 mol %). Trimethyl((3-(trifluoromethyl)phenyl)ethynyl)silane (194 mg, 0.801 mmol) and potassium hydroxide (157 mg, 2.80 mmol) were added and the reaction was started with a heating gun. Salts started to precipitate immediately. The reaction mixture was stirred over night at room temperature. The crude mixture was diluted with dichloromethane and washed three times with water, three times with brine and once with aqueous ammonia hydroxide solution. The organic phase was dried with magnesium sulfate and evaporated under reduced pressure. The product was purified by crystallization from dichloromethane/hexanes yielding **4.8** (148 mg, 0.14 mmol, 45 %) as an orange solid. MP: 208-210°C. <sup>1</sup>H-NMR (500 MHz, THF-d<sub>8</sub>): δ = 0.86-0.91 (m, 6H), 1.28-1.34 (m, 8H), 1.43-1.51 (m, 4H), 1.81 (td, 4H, J = 7.5 Hz, J = 14.8 Hz), 3.92 (t, 4H, J = 7.1 Hz), 6.89 (dt, 2H, J=1.0Hz, J=7.5 Hz), 6.94-6.97 (m, 4 H), 7.09 (dd, 2H, J=1.5 Hz, J=7.6 Hz), 7.11-7.15 (m, 2H), 7.34 (d, 2H, J=16.3 Hz), 7.40 (d, 2H, J = 1.9 Hz), 7.42 (dd, 2H, J=1.9 Hz, J=8.5 Hz), 7.59 (d, 2H, 16.3 Hz), 7.66 (t, 2H, J = 7.8 Hz), 7.74 (d, 2H, J = 7.9 Hz), 7.89 (d, 2H J = 7.7 Hz), 7.99 (s, 2 H), 8.02 (s, 2H). <sup>13</sup>C-NMR: Due to the very limited solubility of **4.8** only an incomplete dataset could be obtained: δ = 14.5, 23.7, 27.6, 28.0, 32.6, 48.3, 90.3, 94.8, 116.57, 116.60, 122.9, 123.4, 124.0, 125.4, 125.5, 126.3, 126.4, 127.1, 128.19, 128.23, 129.2, 129.9, 130.6, 131.3, 131.9, 132.1, 132.4, 132.9, 136.0, 138.7, 146.0, 146.5. IR (KBr): ν [cm<sup>-1</sup>] 2958 (w), 2930 (w), 1632 (m), 1602 (w), 1575

(w), 1496 (w), 1468 (m), 1443 (w), 1333 (w), 1247 (m), 1168 (m), 1129 (m), 800 (w), 746 (w), 694 (w). UV/Vis (CH<sub>2</sub>Cl<sub>2</sub>):  $\lambda_{max}$  ( $\epsilon$ ) 250 nm (46000), 326 nm (81000), 340 nm (68000), 440 nm (54000). Emission (CH<sub>2</sub>Cl<sub>2</sub>):  $\lambda_{max}$  ( $\epsilon$ ) 579 nm. MS (FAB<sup>+</sup>) (m/z (%)): 1031 (21), 1030 (52), 1029 (M-H<sup>+</sup>, 89), 1028 (M<sup>+</sup>, 100), 1027 (15), 957 (12), 944 (14), 943 (19), 942 (17), 941 (40), 940 (58), 939 (39), 938 (40). HR-MS: Calc.: for C<sub>64</sub>H<sub>55</sub>F<sub>6</sub>N<sub>2</sub>S<sub>2</sub> 1029.3711, Found: 1029.3722.

**Synthesis of XF 4.9. 3,3'-(1E,1'E)-2,2'-(2,5-bis((3,5-bis(trifluoromethyl)phenyl)ethynyl)-1,4-phenylene)bis(ethene-2,1-diyl)bis(10-hexyl-10H-phenothiazine).**

An oven-dried Schlenk flask, cooled under nitrogen atmosphere was charged with dry THF (2 mL), piperidine (1 mL) and ethanol (1 mL); potassium hydroxide (94.0 mg, 1.68 mmol), ((3,5-bis(trifluoromethyl)phenyl)ethynyl)trimethylsilane (149 mg, 0.480 mmol) and **4.4** (150 mg, 0.158 mmol) were added to the flask and were combined with PdCl<sub>2</sub>(PPh<sub>3</sub>)<sub>2</sub> (2.2 mg, 3.2  $\mu$ mol, 2 mol %) and CuI (1.2 mg, 6.4  $\mu$ mol, 4 mol %). The reaction mixture was heated to dissolve the diiodide completely. The reaction was stirred at room temperature overnight. The crude reaction mixture was diluted with dichloromethane and washed with brine and two times with 5% aqueous ammonia hydroxide solution, dried with magnesium sulfate and concentrated under vacuum. The product was purified via crystallization from dichloromethane/toluene yielding **4.9** (38.0 mg, 0.03 mmol, 20 %) as a sparingly soluble yellow powder. MP: 240-242°C. <sup>1</sup>H-NMR (300 MHz, THF-d<sub>8</sub>):  $\delta$  = 0.88-0.96 (m, 6H), 1.30-1.40 (m, 8H), 1.45-1.55 (m, 4H), 1.79-1.89 (m, 4H), 3.95 (t, 4H, J = 7.0 Hz), 6.89-7.03 (m, 6H), 7.10-7.20 (m, 4 H), 7.37 (d, 2H, J=16.2 Hz), 7.43-7.49 (m, 4H), 7.62 (d, 2H, J=16.3 Hz), 8.11 (s, 2H), 8.13 (s, 2H), 8.32 (s, 4H). IR (KBr):  $\nu$  [cm<sup>-1</sup>] 2932 (w), 1630 (m), 1497 (w), 1486 (s), 1445 (w), 1373

(s), 1280 (s), 1248 (w), 1182 (m), 1137 (s), 894 (w), 746 (w), 698 (w), 684 (w). UV/Vis (CH<sub>2</sub>Cl<sub>2</sub>):  $\lambda_{max}$  ( $\epsilon$ ) 252 nm (42000), 328 nm (70000), 414 nm (40000), 440 nm (43000). Emission (CH<sub>2</sub>Cl<sub>2</sub>):  $\lambda_{max}$  ( $\epsilon$ ) 595 nm. MS (FAB<sup>+</sup>) (m/z (%)): 1165 (M-H<sup>+</sup>, 85), 1164 (M<sup>+</sup>, 100), 1163 (15). - HR-MS: Calc.: for C<sub>66</sub>H<sub>52</sub>F<sub>12</sub>N<sub>2</sub>S<sub>2</sub> 1164.3380, Found: 1164.3342. <sup>13</sup>C-NMR: Due to the insolubility of the cruciform <sup>13</sup>C-NMR could not be obtained.

**Absorption and Emission Spectra of 4.5-4.9.** Dilute solutions of cruciforms **4.5-4.9** were prepared in spectroscopic grade dichloromethane purchased from OmniSolv. Solid triflate salts (zinc, magnesium, and calcium) were added to the cruciform solutions and samples were allowed to equilibrate overnight before taking optical measurements. All absorption spectra were collected using a Shimadzu UV-2401PC spectrophotometer; emission spectra were acquired using a Shimadzu RF-5301PC spectrofluorophotometer. Absorption and emission spectra were normalized to 1.00 and 1000 respectively.

**Solution Photographs.** Photographs were taken of the solutions used for optical measurements to qualitatively demonstrate the changes in fluorescence observed upon the exposure to metal triflates. Photographs were taken in front of a black background under illumination at 365 nm using a Canon EOS 30D digital camera equipped with a Canon EFS 18-55mm zoom lens.

**Titration of 4.5-4.7 with Trifluoroacetic Acid in Dichloromethane.** Solutions of **4.5-4.7** were prepared using spectroscopic grade dichloromethane purchased from OmniSolv. A solution of **4.5** (0.0135 mM) was prepared by dissolving **4.5** (30.9 mg, 0.0027 mmol) in dichloromethane (200.0 mL). A solution of **4.6** (0.0135 mM) was prepared by dissolving **4.6** (27.1 mg, 0.0027 mmol) in dichloromethane (200.0 mL). A solution of **4.7** (0.0135 mM) was prepared by dissolving **4.7** (24.1 mg, 0.0027 mmol) in

dichloromethane (200.0 mL). All absorption spectra were collected using a Shimadzu UV-2401PC spectrophotometer; emission spectra were acquired using a Shimadzu RF-5301PC spectrofluorophotometer. Increasing equivalents of trifluoroacetic acid (purchased from Acros) were added to solutions of **4.5-4.7** using Eppendorf Reference variable volume pipettors.

**Response of 4.5-4.9 Towards Combinations of Metal Cations.** Cruciforms **4.5-4.9** in CH<sub>2</sub>Cl<sub>2</sub> were exposed to mixtures of calcium, magnesium, and zinc triflate. Solutions were allowed to equilibrate overnight at which point photographs were taken to qualitatively demonstrate the changes in fluorescence observed upon the exposure to metal triflate mixtures. Photographs were taken in front of a black background under illumination at 365 nm using a Canon EOS 30D digital camera equipped with a Canon EFS 18-55mm zoom lens.

#### 4.5. References and Notes

1. (a) Wilson, J. N.; Bunz, U. H. F. Switching of intermolecular charge-transfer in cruciforms: metal ion sensing. *J. Am. Chem. Soc.* **2005**, *127*, 4124-4125. (b) Zuccherro, A. J.; Wilson, J. N.; Bunz, U. H. F. Cruciforms as functional fluorophores: response to protons and selected metal ions. *J. Am. Chem. Soc.* **2006**, *128*, 11872-11881.
2. (a) Bucci, N.; Müller, T. J. J. Synthesis and electronic properties of (oligo)phenothiazine-ethynyl-hydro-C-60 dyads. *Tetrahedron Lett.* **2006**, *47*, 8329-8332. (b) Bucci, N.; Müller, T. J. J. First syntheses and electronic properties of (oligo)phenothiazine-C-60 dyads. *Tetrahedron Lett.* **2006**, *47*, 8323-8327. (c) Sailer, M.; Nonnenmacher, M.; Oeser, T.; Müller, T. J. J. Synthesis and electronic properties of 3-acceptor-substituted and 3,7-bisacceptor-substituted phenothiazines. *Eur. J. Org. Chem.* **2006**, 423-435. (d) Kramer, C. S.; Müller, T. J. J. Synthesis and electronic properties of alkynylated phenothiazines. *Eur. J. Org. Chem.* **2003**, 3534-3548.

3. Krishna, R. M.; Kurshev, V.; Kervan, L. Photoinduced charge separation of phenothiazine derivatives in layered zirconium phosphate at room temperature. *Phys. Chem. Chem. Phys.* **1999**, *11*, 2833-2840.
4. Horner, L.; Hoffmann, H.; Wippel, H. G.; Klahre, G. Phosphororganische verbindungen .20. Phosphinoxyde als olefinierungsreagenzien. *Chem. Ber.* **1959**, *92*, 2499-2505.
5. Wilson, J. N.; Josowicz, M.; Wang, Y.; Bunz, U. H. F. Cruciform  $\pi$ -systems: hybrid phenylene-ethynylene/phenylene-vinylene oligomers. *Chem. Commun.* **2003**, 2962-2963.
6. Hunter, C. A.; Sanders, J. K. M. The nature of pi-pi interactions. *J. Am. Chem. Soc.* **1990**, *112*, 5525-5534.
7. (a) Tolbert, L. M.; Nesselroth, S. M.; Netzel, T. L.; Raya, N.; Stapleton, M. Substituent effects on carbanion photophysics – 9-arylfluorenyl anions. *J. Phys. Chem.* **1992**, *96*, 4492-4496. (b) Englman, R.; Jortner, J. Energy gap law for radiationless transitions in large molecules. *Molecular Physics* **1970**, *18*, 145-154. (c) Caspar, J. V.; Meyer, T. J. Application of the energy-gap law to nonradiative, excited-state decay. *J. Phys. Chem.* **1983**, *87*, 952-957.
8. Pankratov, A. N.; Uchaeva, I. M.; Stepanov, A. N. Chemical and electrochemical oxidation of phenothiazine. *Can. J. Chem.* **1993**, *71*, 674-677.
9. Gowda, N. M. M.; Pacquette, H. L.; Kim, D.-H.; Jayaram, B. Coordination compounds of zinc(II) and N-alkylphenothiazines: Synthesis and characterization. *J. Mol. Struct.* **1996**, *382*, 129-135.
10. (a) Henary, M. M.; Wu, Y.G.; Fahrni, C. J. Zinc(II)-selective ratiometric fluorescent sensors based on inhibition of excited-state intramolecular proton transfer. *Chemistry Eur. J.* **2004**, *10*, 3015-3025. (b) Pond, S. J. K.; Tsutsumi, O.; Rumi, M.; Kwon, O.; Zojer, E.; Bredas, J. L.; Marder, S. R.; Perry, J. W. Metal-ion sensing fluorophores with large two-photon absorption cross sections: Aza-crown ether substituted donor-acceptor-donor distyryl benzenes. *J. Am. Chem. Soc.* **2004**, *126*, 9291-9306.

## CHAPTER 5

### Synthesis and Characterization of Water-Soluble XFs

#### 5.1. Introduction

Metalloresponsive fluorophores<sup>1,2</sup> and chromophores are of scientific and practical interest to detect metal cations in compartmentalized biological systems such as (eukaryotic) cells.<sup>3-7</sup> Metal cations with prominent biological functions in cells are iron, copper, zinc, magnesium, and calcium but also vanadium and manganese.<sup>8,9</sup> A second area of interest for metalloresponsive fluorophores is the detection of environmentally harmful metals such as lead and mercury.<sup>10-13</sup> Both of these divergent fields may use similar design principles for their metallo-phores, yet there are marked differences. For environmental sensing, a successful metalloresponsive fluorophore would need high binding constants to ensure detection limits in the ppb range. It is not clear if metalloresponsive fluorophores can detect environmental pollutants such as mercury ions at levels that are merely elevated but not (yet) toxic. For fluorophores reporting metal ions in cells the sensitivity issue is less severe. The *local* concentration of a specific metal cation can be high in cellular compartments presenting pools of free metal ions.<sup>14</sup> An example is that of zinc ions in neuron slices, which are detected by metalloresponsive fluorophores.<sup>4,15</sup>

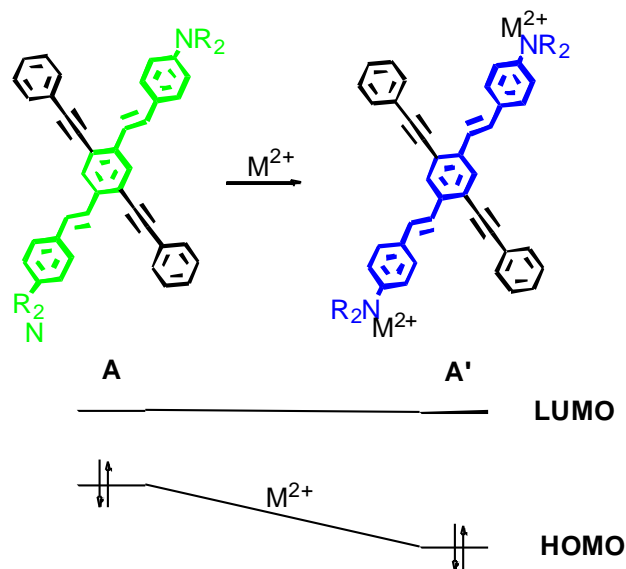
While metallofluorophores have advanced, their design can still be improved. High quantum yield in water, robust ratiometric response to metals with large changes of wavelengths and manipulation of absorption and emission wavelengths are only partially solved problems. In addition, some metallo-fluorophores are not well soluble in water;

cell staining experiments have to be performed by pre-dissolving these fluorophores in DMSO, adding water, and then incubating cells with these dyes. This technique will almost certainly lead to aggregation or even more interesting/worse to nanocrystal formation of the employed fluorophores.<sup>4</sup> Nanocrystals can be endocytized into cell compartments and may persist there, with all accompanying problems for a successful sensing experiment. These factors make it imperative to carefully investigate fluorescent metal sensors in vitro to understand their photophysical properties before undertaking more complex in vivo cell studies.

Clearly, the design of novel water soluble metalloresponsive probes is a critical challenge. Previous examinations have examined XFs and explored their potential as ratiometric probes in organic environs, demonstrating the potential of XFs to exhibit large sensory responses. Exposure of a dibutylamino substituted XF, such as **5.8**, to metal cations results in large hypsochromic shifts in emission that are convincingly explained by stabilization of their HOMO, which is localized on the bis(aminostyryl) axis, through the addition of a positive charge.

Here, we report our investigation of XFs of the type **A** (Scheme 5.1) to understand their photophysics and expand this concept to water soluble cruciforms **5.5-5.7** containing phenylimidobisacetic acid, APTRA<sup>27</sup> or benzo-EDTA receptor units. We investigate the pH dependant photophysical properties of **5.5-5.7** in absorption and emission and compared them with the photophysical properties of the XF **5.8**. The results are surprising, as the presence of the anionic charges from the iminobisacetic acid units modulate the photophysical properties of **5.5-5.7** as compared to **5.8**. A fundamental

change in the interaction paradigm between fluorophores and metal cations is observed when going from **5.8** to **5.5-5.7**.



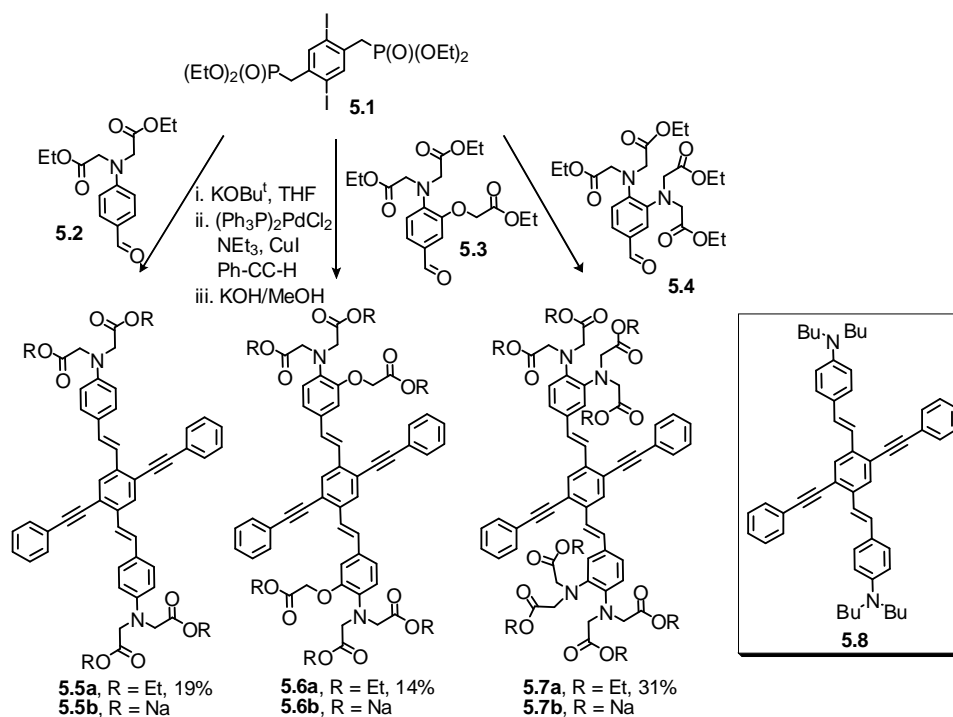
**Scheme 5.1.** Interaction of cruciform fluorophores with metal cations.

## 5.2. Results and Discussion

### 5.2.1. Synthesis of XFs.

The literature known aldehydes **5.2-5.4**<sup>28</sup> are obtained from aniline, *ortho*-aminophenol and *ortho*-phenylenediamine by heating with ethyl bromoacetate in the presence of potassium carbonate in acetone. The esters are subjected to a Vilsmeier formylation and **5.2-5.4**<sup>28</sup> are exposed to a mixture of **5.1**<sup>29</sup> and potassium *tert*-butoxide in THF to give partially saponified distyryl-diiodobenzenes (Scheme 5.2). The intermediates were not characterized but reacted with phenylacetylene under standard Sonogashira coupling conditions, isolating **5.5a-5.7a** after careful chromatography; **5.5a-5.7a** were fully characterized by NMR and IR spectroscopies as well as mass

spectrometry. The ester groups in **5.5a-5.7a** were cleaved under Zempelen conditions to give the sodium salts **5.5b-5.7b** in 87-95% yield after removal of methanol in vacuo; the yellow powders of **5.5b-5.7b** dissolve easily in water. For the photophysical investigations, **5.5b-5.7b** were taken up in aqueous phosphate buffer (100 mmol) and titrated to a pH of 7.0.



**Scheme 5.2.** Synthesis of cruciforms **5.5-5.7** by a combination of Horner and Sonogashira methods.

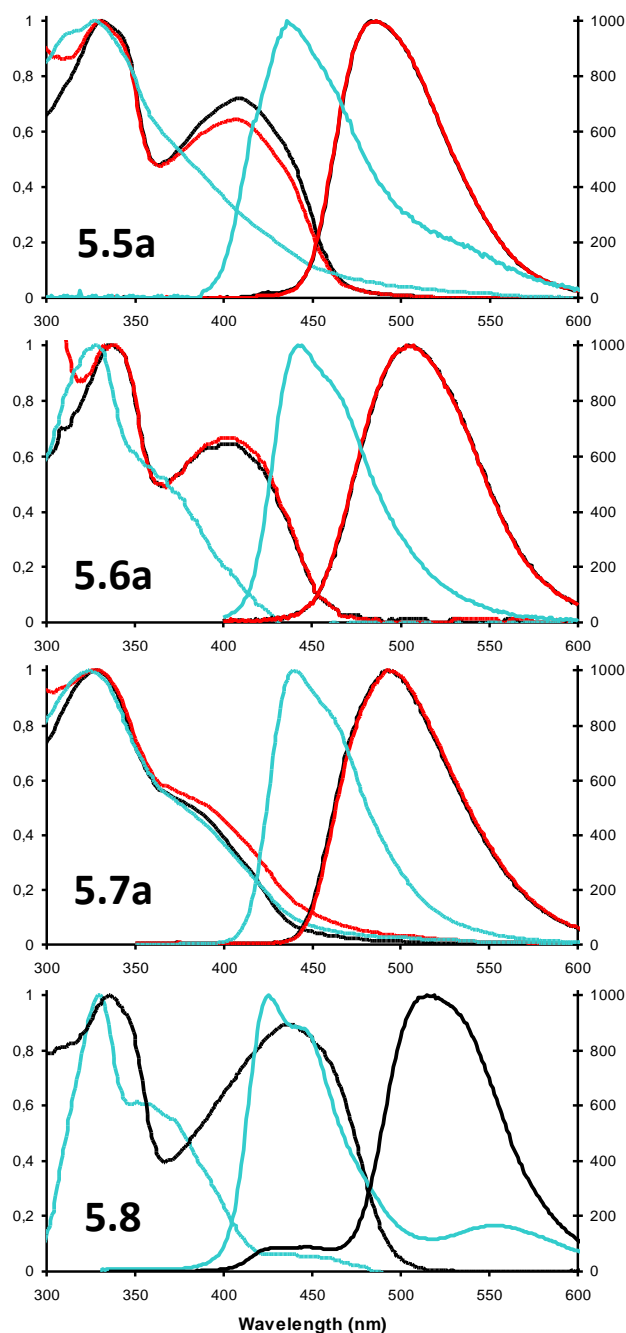
### 5.2.2. Spectroscopic properties of cruciforms **5a-7a** and **8** in dichloromethane.

Figure 5.1 and Table 5.1 show the absorption and emission spectra of **5.5a-5.7a** and **5.8** in dichloromethane before and after the addition of trifluoroacetic acid. We investigated the influence of the acetic acid groups on the photophysics of the XFs without the complications arising from ionic charges and working in water, facilitating

comparison with the model XF **5.8**: The attachment of the ester groups shifts the absorption spectra of **5.5a-5.7a** to the blue when compared to the absorption spectrum of **5.8**. The effect is strongest in **5.7a** where the distinct low energy band visible in **5.8** at 440 nm is reduced in **5.7a** to a shoulder at 394 nm. Addition of triethylamine does not appreciably change the absorption spectrum of **5.7a**, ruling out ground state protonation as a factor for the loss of the low-energy band. In **5.5a** and **5.6a** the low energy feature is blue shifted when compared to the absorption of **5.8**. The emission spectrum of **5.5a** (486 nm) is similar to that of **5.8**, while that of **5.6a** is slightly *red*-shifted to 506 nm. Under neutral conditions the emission spectrum of **5.7a** is *blue*-shifted to 438 nm and shows a distinct vibronic shoulder. Upon addition of triethylamine, the spectra of **5.5a**, **5.6a**, **5.7a** and **5.8** do not change.

**Table 5.1.** Absorption and emission data of XFs **5.5a-5.7a** and **5.8** in CH<sub>2</sub>Cl<sub>2</sub>, 1 μmolL<sup>-1</sup> concentration of XF, in neutral, acid and basic conditions.

CH <sub>2</sub> Cl <sub>2</sub>	<b>5.5a</b>	<b>5.6a</b>	<b>5.7a</b>	<b>5.8</b>
absorption (nm)	333, 411	338, 405	328	336, 440
emission (nm)	486	506	494	518
TFA added absorption (nm)	330	329	326	331
TFA added emission (nm)	439	443	442	427, 558
NEt <sub>3</sub> added absorption (nm)	332, 409	338, 404	329	N/A
NEt <sub>3</sub> added emission (nm)	486	505	495	N/A



**Figure 5.1.** Normalized absorption and emission spectra of **5.5a**, **5.6a**, **5.7a**, and **5.8** in CH<sub>2</sub>Cl<sub>2</sub> (black traces) and after addition of 50  $\mu$ L (0.66 mmol; 66 mmol<sup>-1</sup>;  $6.6 \times 10^4$  equivalents) of trifluoroacetic acid (TFA, blue traces **5.5a**, **5.6a**, **5.7a**, **5.8**) or 50  $\mu$ L (0.36 mmol, 36 mmol<sup>-1</sup>;  $3.6 \times 10^4$  equivalents) of triethylamine (red traces **5.5a**, **5.6a**, **5.7a**). For **5.5a** and **5.6a**, the triethylamine and dichloromethane traces in emission are perfectly overlapping, so that only the red trace is visible. The spectra are taken at a concentration of 1  $\mu$ mol<sup>-1</sup> XF.

Upon addition of acid, **5.8** shows the well-documented blue shift in absorption and emission.<sup>16</sup> This shift is due to a stabilization of the HOMO (Scheme 5.1) effected by the protonation of the two dibutylamino-groups. The LUMO energy is not affected by the protonation. The same effects as for **5.8** are observed for **5.5a**, **5.6a**, and **5.7a** upon protonation (Figure 5.1). Disappearance of the low energy transition is coupled with a blue shift in emission. In the case of **5.7a** the absorption spectra do not change noticeably upon either addition of acid or base.

The electron withdrawing acetic acid groups attached to the aniline nitrogen(s) exert a moderate inductive effect on the overall distyrylbenzene subunit in **5.5-5.7** and should stabilize their HOMO energy. The general blue shift in emission of **5.5a-5.7a**, with respect to the emission of **5.8**, is difficult to explain. It is significant in **5.5a** but small in **5.6a**. This shift might be due to the de-stabilization of the excited state of **5.5a** by the *meta*-positioned ether group. Upon addition of amine, neither the absorption nor the emission spectra of **5.5a** or **5.6a** change, being practically superimposable (Figure 1). Upon addition of trifluoroacetic acid, **5.8** displays a 124 nm blue shift in absorption under disappearance of the charge transfer band (CT-band) and an 94 nm blue shift in emission. In **5.5a** and **5.6a**, we see qualitatively similar behavior in absorption, i.e. a loss of the CT-band and a blue shift in emission, but this is less distinct in **5.5a** and **5.6a** than in **5.8**. Again, we presume that particularly in **5.6a** the excited state of the protonated species is stabilized. In the case of **5.7a** we see only the slightest change in absorption upon addition of acid or triethylamine, but in emission we observe a shift from 503 nm to 442 nm when going from an amine-added solution to one to which trifluoroacetic acid has been added.

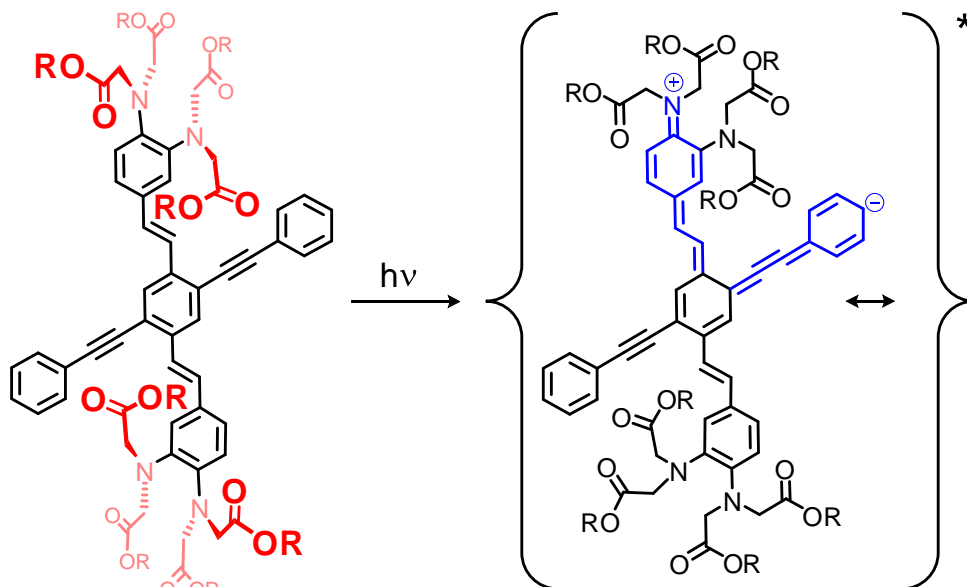


**Figure 5.2.** Proposed excited state planarization of **5.7**.

The lack of change in the absorption spectrum combined with a significant blue shift in emission upon protonation in **5.7a** suggests excited state planarization as possible explanation;<sup>30</sup> **5.7a** carries two amine groups per styryl unit. Their high steric congestion forces them into a perpendicular (with respect to the plane of the aromatic system) orientation, and deconjugates the free electron pair. Upon going into the first excited state, quinoidal resonance structures will show an increased contribution (Figure 5.2) and force the *para* positioned amine (*para* with respect to the central benzene ring) into planarity. Different quinoidal resonance structures are possible, and a representative one is shown in Figure 5.2. The secondary phenyleneethynylene arm is a convenient acceptor for the negative charge generated when drawing a closed-shell quinoidal resonance structure. The exact electron distribution in the excited state of **5.7a** is difficult to determine, but this simple resonance argument explains the experimental data.

### 5.2.3. Spectroscopic properties of cruciforms **5.5b-5.7b** in water.

In Figure 5.3, the absorption and emission spectra of **5.5b-5.7b** in 100 mmol phosphate buffer are displayed. Overlaid are the absorption and emission spectra of **5.8** in dichloromethane. The absorption spectra of **5.5b** and **5.6b** in water are different from those of **5.5a** and **5.6a** in dichloromethane. The charge transfer band (CT-band) is significantly reduced; the Uv-vis spectrum of **5.7a** in water is similar to that of **5.7b** in dichloromethane. A qualitative explanation assumes the repulsion of like (negative) charges leads to deplanarization of the amine groups in **5.5b** and **5.6b** with respect to the  $\pi$ -system of the distyrylbenzene. Enhanced intramolecular hydrogen bonding between the carboxylic acids, the carboxylates and the anilines leads to a hydrogen-bonded network, preferring a conformation in which the free electron pairs of the aniline nitrogens of **5.5b** and **5.6b** are twisted out of the plane of the distyrylbenzene unit. In the emission spectra this effect is less pronounced; the emission spectra of **5.5b** and **5.6b** in dilute solution are red shifted as compared to that of **5.8**. However, in the case of **5.7b** the emission is centered around 450 nm, suggesting that the combination of both the steric hindrance and electrostatic repulsion decouples the amino groups electronically from the distyrylbenzene skeleton.

The absorption spectra of **5.5b** and **5.7b** are concentration independent, while the absorption spectrum of **5.6b** changes with concentration (Figure 5.4). At low concentration (light green,  $5 \mu\text{molL}^{-1}$ ) the CT-band is not visible, while at  $100 \mu\text{molL}^{-1}$  the CT-band is prominent at 393 nm; the concentration dependent change in the absorption spectra of **5.6b** suggests a ground state interaction of two or more molecules

of **5.6b**, either acting by mechanical/electrostatic agglomeration-induced planarization or the formation of electronic aggregates.

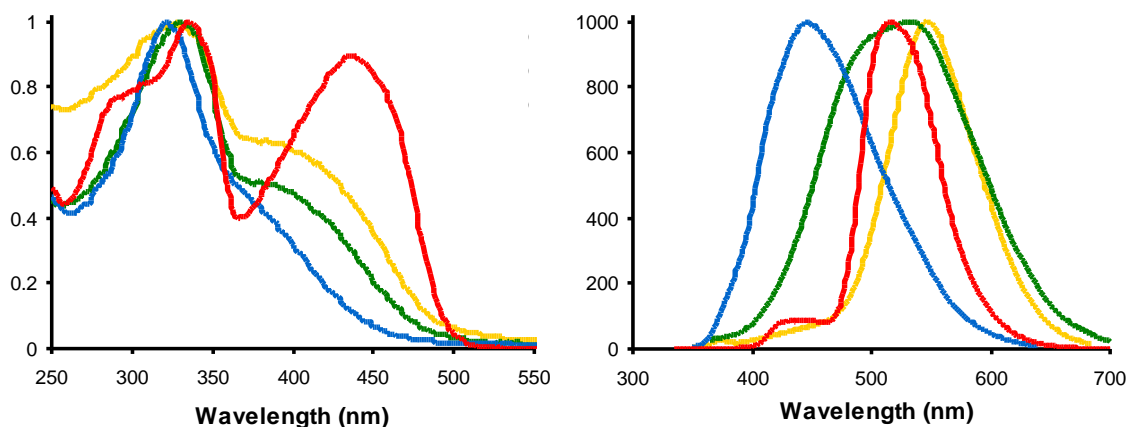


**Figure 5.3.** Overlaid normalized absorption and emission spectra of **5.5b**, **5.6b**, and **5.7b** in phosphate buffered ( $100 \text{ mmolL}^{-1}$ ) aqueous solution and **5.8** in  $\text{CH}_2\text{Cl}_2$  as  $10 \text{ }\mu\text{molL}^{-1}$  solutions.

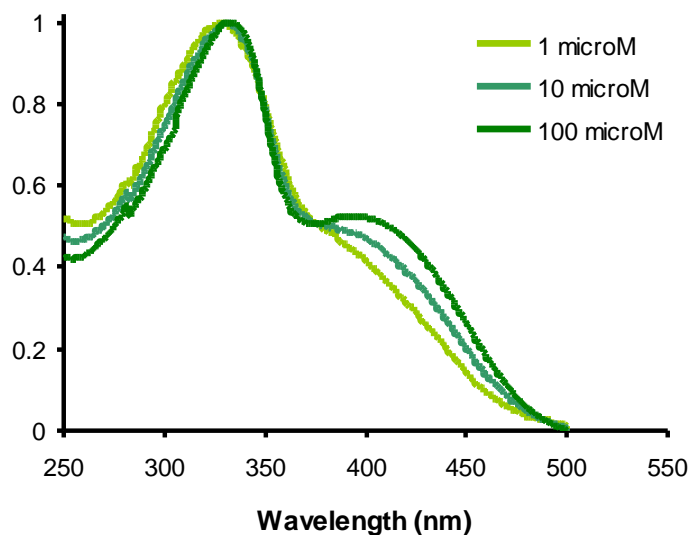


**Figure 5.4.** Absorption spectra of **5.6b** at concentrations of 1, 10 and  $100 \text{ }\mu\text{molL}^{-1}$  concentration in phosphate buffered ( $100 \text{ mmolL}^{-1}$ ) aqueous solution.

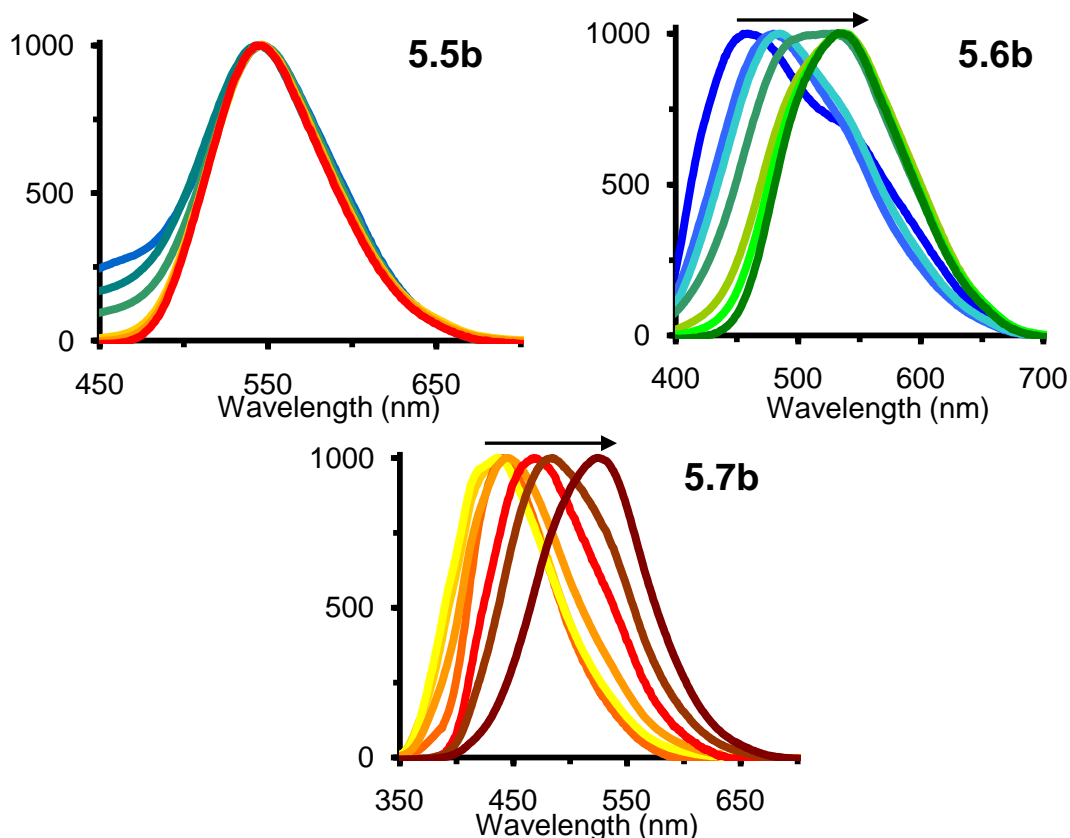


**Figure 5.5.** Emission of **5.5b** (top left), **5.6b** (top right), and **5.7b** (bottom) in phosphate buffer ( $100 \text{ mmolL}^{-1}$ ) at 1, 2, 5, 10, 25, 50 and  $100 \text{ }\mu\text{molL}^{-1}$  concentrations. The arrow displays increasing concentration of the respective cruciform.

The concentration effects in emission are more pronounced. For **5.5b** no concentration-dependent change in emission is recorded, but both **5.6b** and **5.7b** experience a significant shift in emission when increasing their concentration from  $1 \text{ }\mu\text{molL}^{-1}$  to  $100 \text{ }\mu\text{molL}^{-1}$ . While the emission of **5.6b** red-shifts from 458 to 537 nm, that of **5.7b** changes from 439 to 524 nm. This concentration dependence suggests excimeric species in **5.6b** and **5.7b** but not in **5.5b**. Both **5.6b** and **5.7b** show blue-shifted emission bands at low concentrations that in **5.8** would be indicative for metal binding, protonation, or twisting around the aniline nitrogen. As we work in buffered solution at pH 7.0, protonation of the aniline nitrogen is rejected. To exclude self-absorption effects

in the case of **5.6b** we performed fluorescence measurements in a triangular cuvette, and the obtained spectra are identical to those we recorded for **5.6b** in regular cuvettes.

The fluorescence quantum yields of **5.5b-5.7b** in water are low at physiological pH (Table 5.2); the XF **5.7b** shows the highest quantum yield ( $\Phi = 4.4\%$ ) in water. While **5.6b** is almost non-fluorescent, **5.5b** displays a  $\Phi$  of 0.8%. While these quantum yields are somewhat disappointing, they are not unusual for organic chromophores in aqueous solution. Water as a highly polar solvent stabilizes excited zwitterionic CT-states which will then efficiently deactivate.

We investigated the emission profiles of **5.5b-5.7b** with respect to different excitation wavelengths. While both **5.5b** and **5.7b** show only minute changes in their emission spectra, XF **5.6b** experiences significant modulation upon modulating the excitation wavelength; indeed there is a significant wavelength dependency of the excitation spectra (Figure 5.6, right).

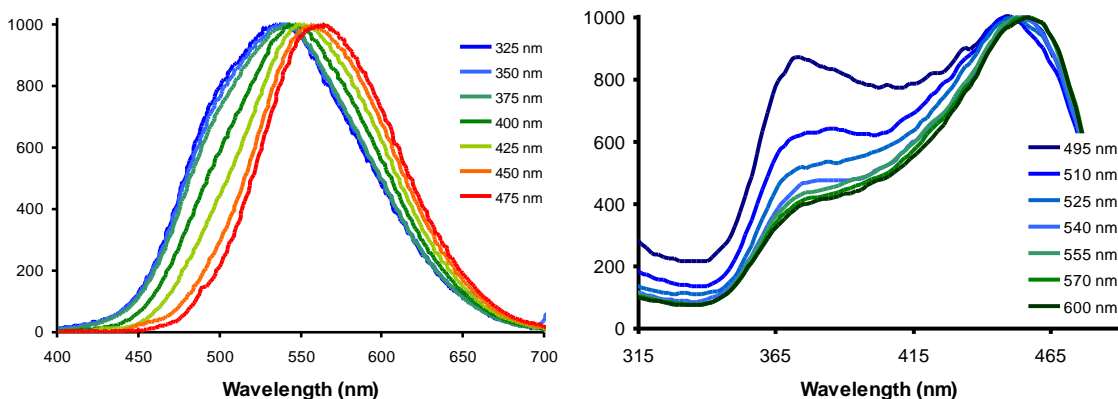


**Figure 5.6.** Left: Emission spectra of **5.6b** under excitation at 325, 350, 375, 400, 425, 450, and 475 nm at  $50\ \mu\text{molL}^{-1}$  concentration in phosphate buffered ( $100\ \text{mmolL}^{-1}$ ) aqueous solution. Scattering peaks and peaks due to lamp profile are subtracted out. Right: Normalized excitation spectra of **5.6b** at different wavelengths. At an increasing excitation wavelength the feature at 465 nm increases.

**Table 5.2.** Absorption and emission data of XFs **5.5b-5.7b** in water (phosphate buffer, 100 mmolL<sup>-1</sup>, pH = 7.0, 10 μmolL<sup>-1</sup> concentration of XF).

H <sub>2</sub> O pH 7.0	<b>5.5b</b>	<b>5.6b</b>	<b>5.7b</b>
Absorption (nm)	328	329	322
Emission (nm)	546	531	446
Stokes Shift (cm <sup>-1</sup> )	12172	11563	8634
Φ (%)	0.8	<0.5	4.4
ε (l mol <sup>-1</sup> cm <sup>-1</sup> )	53500	48000	54000

We explain this behavior as a consequence of co-planarization of the amine groups in XF **5.6b**. If we irradiate at low wavelengths (high energy) the non-planarized molecules are preferentially excited and emission from non-planarized excited states is observed. If irradiated at lower frequencies only planarized molecules are excited and therefore preferred emission from planar XFs **5.6b** is observed as a result. We presume that in **5.6b**, in the ground state, there is a thermal distribution of planarized and non-planarized forms of the XFs, leading to the wavelength dependant emission spectra. In **5b**, **8** and **7b** on the other hand, there is either the mostly planarized form (**5b**, **8**) or the predominantly twisted form (**7b**) present. The propensity for the twisting of the aniline unit is a function of the increasing steric hindrance and the electrostatic repulsion of the negative charges when going from **5b** to **7b**. The APTRA-type XF **6b** seems intermittent in its ability to planarize. However, the emission spectra taken from very dilute solutions suggest that isolated **6b** is preferentially in its twisted form as it is blue emissive. We examined the ionic strength dependency of the emissive properties of **6b** and **7b** by addition of a large excess of KClO<sub>4</sub> and did not see any effect on fluorescence

wavelength or intensity. Metal sensing with ligand systems such as **6b** or **7b** will probably not work by the same mechanism that we have found to be operative for **8**, but instead possibly by breakup of aggregates (vide infra).

#### **5.2.4. Investigation of the pH dependency of absorption and emission in 5.5b-5.7b.**

As **5.5b-5.7b** have acidic and basic functionalities, their pH-dependent photophysical properties were of great interest. Figure 7 displays absorption and emission spectra of **5.5b-5.7b** under neutral (pH 7.0), basic (pH 14) and acidic (pH 1.6) conditions. The spectra are taken at a  $5 \mu\text{molL}^{-1}$  concentration of the respective XF, with exception of the black traces marked with a red asterisk. These spectra were taken at  $100 \mu\text{molL}^{-1}$  concentration of XF for comparison. Upon addition of acid, the fluorescence of **5.5b** is greatly reduced but blue-shifted to 506 nm. We attribute the blue shift to the protonation of the aniline nitrogen, leading to a significant stabilization of the HOMO. At a pH of 1.6, however, not only the aniline units but also the carboxylic acid units are protonated. In the structurally similar phenyl imidobisacetic acid the pKa's are 6.4, 4.6, 3.5 and 3.0.<sup>31</sup> In absorption, the expected blue shift and a loss of the CT-band is observed, similar as reported for the model compound **5.8**. In the case of **5.6b**, protonation leads to quenching of the fluorescence of the XF. In absorption, the pH-dependent changes are subtle. Blue shifts and intensity reductions of the CT-bands of XFs are recorded.

In **5.7b** the absorption is almost pH independent, but the emission red-shifts upon protonation from 437 nm to 476 nm, while at pH 14 the emissive maximum is at 440 nm, i.e. blue, suggesting deplanarization of the aniline lone pairs. The red shift in emission at pH 1.6 might be due to partial planarization in the excited state, enabled by

the removal of the electrostatic repulsion between the formerly negatively charged acetate (now acetic acid) groups.

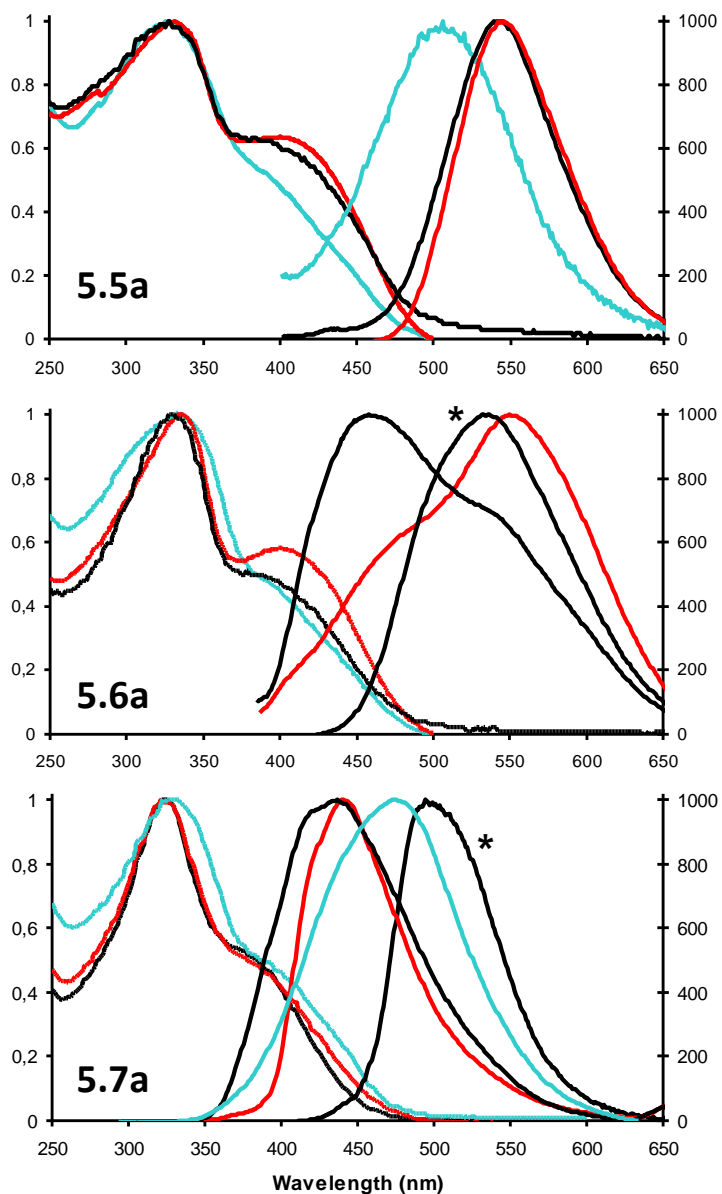


**Figure 5.7.** Normalized absorption and emission spectra of **5.5b** (top), **5.6b** (middle), and **5.7b** (bottom) under neutral (black pH 7.0), acidic (blue pH 1.6), and basic (red pH 14) conditions. The concentration of the XFs was  $5 \mu\text{molL}^{-1}$ . For the starred black lines, the XF concentration was  $100 \mu\text{molL}^{-1}$ .

This hypothesis is borne out by the significant red shift of the emission spectra of both **5.6b** and **5.7b** upon a pH increase. This shift is concentration independent, which excludes excimer formation or other intermolecular mechanisms for the red shift in the emission of **5.6b** and **5.7b**. Again, **5.5b** as sterically less encumbered species does not show significant emission shifts upon going from neutral buffered into basic solution.

### 5.2.5. Metal-responsive properties of 5.5b-5.7b in aqueous buffered solution.

The most enticing aspect of water soluble chromophores and fluorophores is their interaction with metal cations under physiological conditions. Questions of the quantity and distribution of pools of free transition metal cations such as zinc or copper in cells are connected with neurophysiological function and disease states of the central nervous system and the brain. Zinc cations are suspected to play a role in the formation of plaques; enhanced levels of  $\text{Zn}^{2+}$  ions is found in the brains of deceased Alzheimer patients.<sup>15,32</sup>

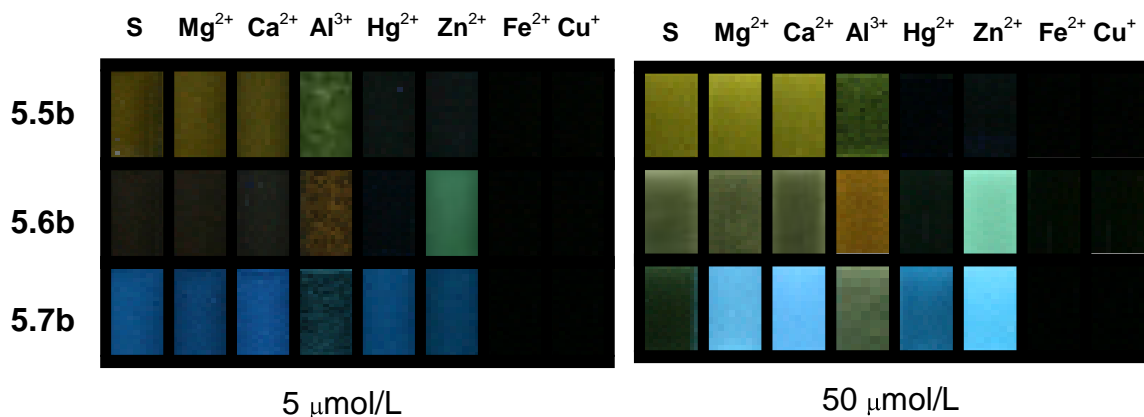


**Figure 5.8.** Qualitative results of the sensing of metal cations ( $0.4 \text{ mmolL}^{-1}$ ) by the three XFs **5.5b-5.7b** in PIPES solution.

**Table 5.3.** Emissive lifetime data of cruciforms **5.5b-5.7b** (pH 7.0 phosphate buffer, 100 mmolL<sup>-1</sup>).

XF	Concentration ( $\mu\text{M}$ )	Metal	$\lambda_{\text{max}}$ emission (nm)	$\tau$ (ns)
<b>5.7b</b>	2		450	2.4
	5		460	2.6
	50		531	1.2
	100		531	1.4
	5	Zn <sup>2+</sup>	455	2.7
	50	Zn <sup>2+</sup>	455	2.5
<b>5.6b</b>	2		446	1.5
	5		446	1.4
	50		519	0.8
	100		530	0.7
	5	Zn <sup>2+</sup>	471	1.8
	50	Zn <sup>2+</sup>	471	1.6
<b>5.5b</b>	2		546	0.8
	5		546	0.8
	50		546	0.8
	100		546	0.8
	5	Zn <sup>2+</sup>	535	0.9
	50	Zn <sup>2+</sup>	535	0.9

With the water soluble XFs **5.5b-5.7b** in hand and armed with the knowledge gained from the investigation of the model XF **5.8** and its interaction with metal cations,<sup>16b,d</sup> we exposed the XFs **5.5b-5.7b** to different metal salts (0.4 mmolL<sup>-1</sup> metal salt, XF either 5  $\mu\text{molL}^{-1}$  and 50  $\mu\text{molL}^{-1}$ ). We performed these experiments in PIPES buffer (100 mmolL<sup>-1</sup>, Figure 5.8). The XF **5.5b** is quenched upon addition of Hg<sup>2+</sup>, Cu<sup>2+</sup> and Zn<sup>2+</sup>, while for **5.6b** its color changes upon exposure to Zn<sup>2+</sup>. Using a 50  $\mu\text{molL}^{-1}$  solution of XF gives a significantly enhanced emissive response. For **5.6b**, Mg<sup>2+</sup> and Ca<sup>2+</sup> cations respond weakly but Hg<sup>2+</sup> and Cu<sup>2+</sup> effectively quench the fluorescence of

**5.6b.** Zinc ions induce a significant color shift – from orange to blue, while  $\text{Al}^{3+}$  increases the fluorescence intensity. The XF **5.7b** ( $50 \mu\text{molL}^{-1}$ ) experiences an increase in fluorescence for the addition of  $\text{Mg}^{2+}$ ,  $\text{Ca}^{2+}$ ,  $\text{Hg}^{2+}$  and  $\text{Zn}^{2+}$ , while  $\text{Al}^{2+}$ ,  $\text{Fe}^{3+}$ , and  $\text{Cu}^{2+}$  do not lead to a change in the emission at all. If we perform the experiments in a solution  $5 \mu\text{molL}^{-1}$  in XF, only  $\text{Fe}^{3+}$  and  $\text{Cu}^{2+}$  quench the fluorescence of **5.7b**, other metal cations do not have an effect on the fluorescence.

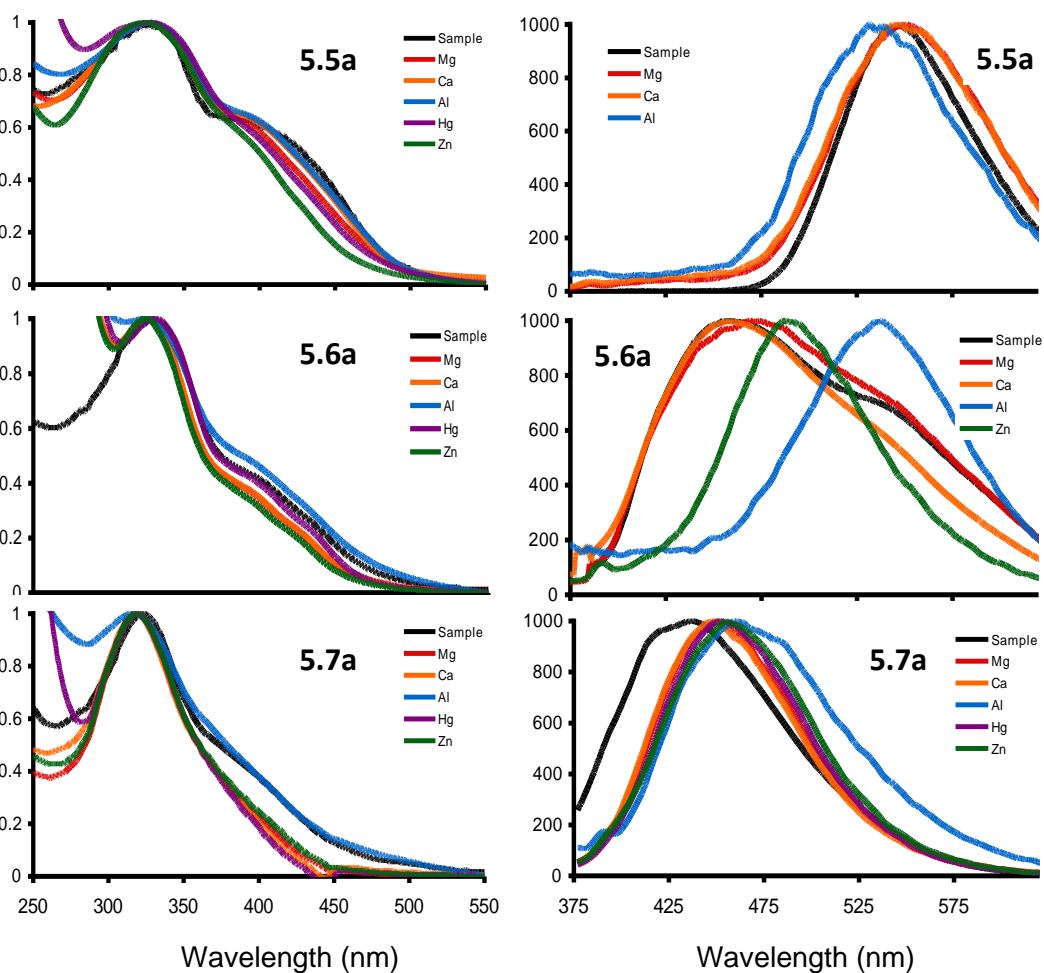


**Figure 5.9.** Interaction of metal cations ( $\text{Mg}^{2+}$ ,  $\text{Ca}^{2+}$ ,  $\text{Al}^{3+}$ ,  $\text{Hg}^{2+}$ ,  $\text{Zn}^{2+}$ ;  $0.4 \text{ mmolL}^{-1}$ ) with the three XFs **5b-7b** at  $5 \mu\text{molL}^{-1}$  concentration in aqueous PIPES solution at pH 7.2. Normalized absorption spectra are displayed on the left, normalized emission spectra are displayed on the right.

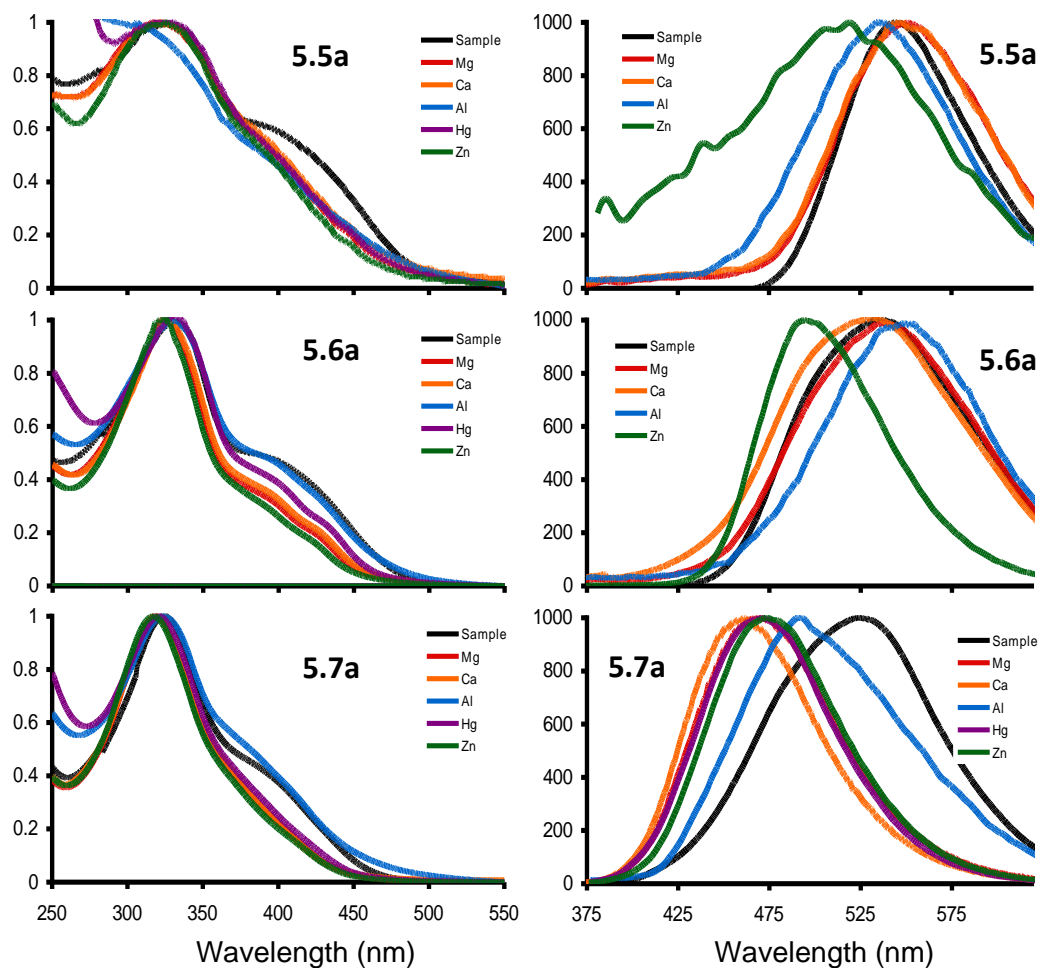


**Figure 5.10.** Interaction of metal cations ( $\text{Mg}^{2+}$ ,  $\text{Ca}^{2+}$ ,  $\text{Al}^{3+}$ ,  $\text{Hg}^{2+}$ ,  $\text{Zn}^{2+}$ ;  $0.4 \text{ mmolL}^{-1}$ ) with the three XFs **5b-7b** at  $50 \text{ } \mu\text{molL}^{-1}$  concentration in aqueous PIPES solution at pH 7.2. Normalized absorption spectra are displayed on the left, normalized emission spectra are displayed on the right.

Figures 5.9 and 5.10 display the accompanying spectra to the pictorial description in Figure 5.8. Important points are gleaned from Figures 5.8-5.10 and Table 5.3, where the emissive lifetimes of XFs **5.5b-5.7b** at different concentrations and in the presence and the absence of zinc ions are on display. The three seemingly similar compounds **5.5b-5.7b** feature metallo-reactivities that are dependent upon their concentration, particularly in the case of **5.6b** and **5.7b**. At  $5 \text{ } \mu\text{mol}$  concentrations, XF **5.6b** does not

show any metal reactivity; however, at a concentration of  $50 \mu\text{molL}^{-1}$  the metalloreactivity, particularly to zinc, is noticeable. A shift from yellow-orange to blue occurs in the fluorescence. In solutions of **5.6b** at  $50 \mu\text{molL}^{-1}$  concentration, excimers persist, leading to a red shifted, excimeric emission (Table 5.3) complemented by a decrease of the emissive lifetime from 1.5 ns to 0.8 ns. Upon addition of zinc cations, but not upon the addition of  $\text{Ca}^{2+}$  or  $\text{Mg}^{2+}$ , the blue fluorescence of the monomeric species is restored and the emissive lifetime is increased to 1.6 ns, suggesting either the suppression, or the breakup of excimeric species of **5.6b** by zincation.

We see a similar effect in **5.7b**, which is weakly fluorescent at a  $50 \mu\text{mol}$  concentration. The addition of mercury, magnesium, calcium or zinc cations leads to a strong increase in fluorescence intensity but without a large shift in emission wavelengths. Investigation of the emissive lifetimes of **5.7b** in dilute (Table 5.3,  $\tau = 2.4$  ns) and concentrated ( $\tau = 1.2$  ns) solution before and after the addition of zinc ions to a concentrated solution of **5.7b** ( $\tau = 2.4$  ns) suggests the formation and disruption/suppression of excimers as the mechanism of metalloresponsivity of **5.7b**; however, the ‘excimers’ formed from **5.7b** are self-quenching and almost non-fluorescent instead of red shifted.

In the case of **5.5b** excimers do not form, and the lifetime does not change, even if we inspect aqueous solutions that are  $100 \mu\text{mol}$  in concentration. The metalloresponsivity of **5.5b** disappoints. The addition of  $\text{Mg}^{2+}$ ,  $\text{Ca}^{2+}$ ,  $\text{Al}^{3+}$  or  $\text{Fe}^{3+}$  cations does not change the fluorescence of **5.5b** at all, while mercury, zinc and copper simply quench the fluorescence of **5.5b**. When investigating **5.5b** in aqueous buffer,  $\text{Zn}^{2+}$ , and  $\text{Hg}^{2+}$  change the absorption of **5.5b**, leading to a modest weakening of the CT-band.

The classic explanation of the change in the absorption spectrum and quenching in the emission spectrum would invoke partial excited state decomplexation,<sup>3,33,34</sup> resulting in species where the metal cation is only loosely bound to the fluorophore but assists in vibrational or otherwise radiationless deactivation of the excited state. However, the complexation of the weakly binding XF **5.8** with zinc or magnesium salts in dichloromethane results in a strong blue shift of the emission, suggesting that, by analogy, excited state decomplexation is not a probable mechanism for the quenching of **5.5b**. We hypothesize that the binding of **5.5b** to Zn<sup>2+</sup> or Hg<sup>2+</sup> ions in aqueous buffered solution will stabilize the excited state. It is coupled to an overtone vibration of water molecules coordinated to either Zn<sup>2+</sup> or Hg<sup>2+</sup> ions and therefore will promote radiationless deactivation of the fluorescence. If we examine the emission of **5.5b-5.7b** in D<sub>2</sub>O as opposed to H<sub>2</sub>O, the fluorescence intensity increases by a factor of 2-4, regardless of the presence or absence of metal cations. While this observation suggests some vibrational coupling of the excited states of **5.5b-5.7b** to suitable overtone vibrations of water, the fluorescence quantum yields in D<sub>2</sub>O are still not very high, suggesting that other factors also play a significant role; however, ionic strength (vide supra) does not seem to be one them.

### 5.3. Conclusions

The water soluble XFs **5.5b-5.7b** were synthesized by a combination of Horner reaction, Sonogashira coupling and subsequent saponification. The photophysical properties of **5.5b-5.7b** and their metalloreactivity were examined and compared to that of the model compound **5.8**. It is noted that the metalloresponsive properties of **5.5b-**

**5.7b** in aqueous buffered solution are fundamentally different from those of the model system **5.8** possessing the same fluorophore core. While the low fluorescence quantum yields for **5.5b-5.7b** in water was not unexpected, the blue shifted emission of **5.6b** and **5.7b** in the absence of metal ions in water was surprising at first but is explained by a combination of electrostatic repulsion of the negatively charged carboxylate groups and the significant steric crowding. In the case of **5.6b**, an attractive zinc-specific response was found, which was based upon the breakup of excimeric species rather than upon the specific binding of the zinc cations to the lone pair of the aniline nitrogen in the APTRA motif of **5.6b**. While APTRA and similar motifs are popular and successful in the detection of metal cations in cellular environs and compartments, they may actually act not by the normally proposed coordination mechanism but also by breakup of aggregates and even, as suggested in the literature, by interaction of intact dye nanoparticles with metal cations after endocytosis into the cell.<sup>4</sup> We note that the investigation of organo-soluble model compounds such as **5.8** is invaluable to understand the innate properties of a metallo-responsive species. The attachment of charged appendages and water as solvent fundamentally changes the fluorescent responses of XFs but is difficult to predict ways. Without the careful investigation of **5.8** in organic solutions, the interpretation of the results obtained for **5.5b-5.7b** in aqueous environs would have been difficult and perhaps misleading.

This work has been published in the *Journal of Organic Chemistry*:

Tolosa, J.; Zuccherro, A. J.; Bunz, U. H. F. Water-soluble cruciforms: response to protons and selected metal ions. *J. Am. Chem. Soc.* **2008**, *130*, 6498-6506.

## 5.4. Experimental

**General Methods.** All chemicals were purchased from Aldrich Chemical, Acros, TCI America, or Fischer Scientific and used without purification unless otherwise specified. Column chromatography was performed using Standard Grade silica gel 60 Å, 32-63 µm (230 x 450 mesh) from Sorbent Technologies and the indicated eluent. Elution of cruciforms was readily monitored using a handheld UV lamp (365 nm). Melting points were obtained using a Mel-Temp apparatus fitted with a Fluke 51<sup>K/J</sup> digital thermometer. All pH measurements were made using a calibrated VWR sympHony SP20 digital pH meter. All IR spectra were obtained using a Simadzu FTIR-8400s spectrometer. Unless otherwise specified, NMR spectra were recorded at 298 K on a Varian Mercury spectrometer (300 MHz). Chemical shifts are reported in parts per million (ppm), using residual solvent (chloroform-*d*) as an internal standard. Data Reported as follows: chemical shift, multiplicity (s = singlet, d = doublet, t = triplet, q = quartet, m = multiplet), coupling constant, and integration. Mass spectral analyses were provided by the Georgia Institute of Technology Mass Spectrometry Facility.

All absorption spectra were collected using a Shimadzu UV-2401PC spectrophotometer. All emission spectra were acquired using a Shimadzu RF-5301PC spectrofluorophotometer. Lifetime data were collected using a Lifespec-ps (Edinburgh Instruments), pulsed diode laser (PicoQuant, 372 nm excitation), and PMT detector (Hamamatsu). Data were fit to single exponential decay so as to optimize chi-squared values. Quantum yields for cruciforms were measured using standard procedures. In all cases, quinine sulfate was used as a standard and all solutions were purged with nitrogen prior to measurement.

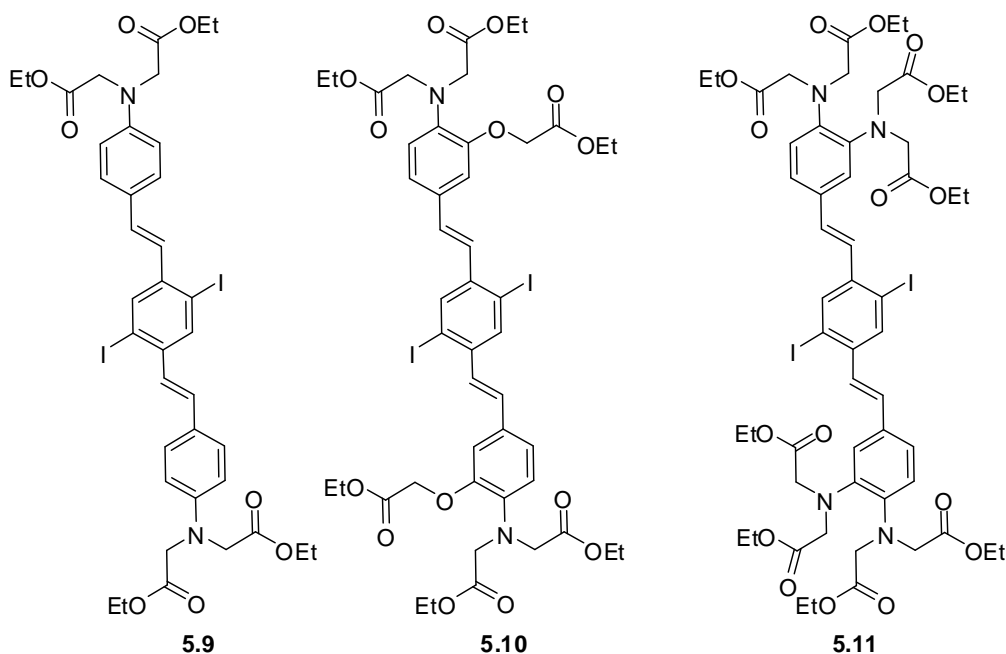
**Synthesis of Cruciform 5.7a (general procedure for all XFs).** A solution of diphosphonate **5.1** (315 mg, 0.5 mmol) and the corresponding aldehyde **5.4** (481 mg, 1 mmol), in dry THF (15 mL) was stirred at 0°C under N<sub>2</sub>. Then, KO<sup>t</sup>Bu (115 mg, 1.05 mmol) was added in small portions in order to prevent hydrolysis of the esters. After the addition the reaction mixture was stirred at this temperature for 30 min until TLC indicated complete reaction of the aldehyde. A saturated solution of NH<sub>4</sub>Cl (10 mL) was added to quench the reaction and the mixture was extracted with dichloromethane (3 x 20 mL). The combined organic phases were washed with water and brine and dried over MgSO<sub>4</sub>. The solvent was then evaporated in vacuo. The crude mixture was dissolved in 6 mL of a mixture of dry THF / NEt<sub>3</sub> 2:1 and PdCl<sub>2</sub>(PPh<sub>3</sub>)<sub>2</sub> (2%) and CuI (2%) were added to the solution. The mixture was stirred for 10 min at room temperature under N<sub>2</sub>. Phenylacetylene (160 mg, 1.56 mmol) was added, the reaction was warmed to 50 °C and stirred at that temperature overnight. The reaction mixture was poured into water and extracted with dichloromethane (3 x 15 mL). The combined organic phases were collected, dried over MgSO<sub>4</sub> and evaporated after filtration. The crude mixture was purified by column chromatography (hexane / ethyl acetate 4:1 to 5:2) isolating **5.7a** as an orange solid (yield 31 %). MP: 169-170 °C. <sup>1</sup>H-NMR (300Mz, CDCl<sub>3</sub>): δ = 1.17 (t, 12H, *J* = 7.2 Hz); 1.19 (t, 12H, *J* = 7.2 Hz); 4.09 (c, 8H, *J* = 7.2 Hz); 4.11 (c, 8H, *J* = 7.2 Hz); 4.32 (s, 8H); 4.33 (s, 8H); 7.03 (d, 2H, *J* = 8.4 Hz, Ar-H); 7.16 (d, 2H, *J* = 16 Hz, A from AB); 7.20 (d, 2H, *J* = 7.2 Hz, Ar-H); 7.27 (broad s, 2H); from 7.32 to 7.44 (m, 6H); 7.54 (d, 2H, *J* = 16 Hz, B from AB); 7.65 (dd, 4H, *J*<sub>1</sub> = 1.8 Hz, *J*<sub>2</sub> = 7.2 Hz, Ar-H); 7.86 (s, 2H). <sup>13</sup>C-NMR (75MHz, CDCl<sub>3</sub>): δ = 171.1, 171.0, 141.8, 141.7, 137.5, 132.3, 11.9, 130.6, 128.7, 124.2, 123.5, 122.2, 122.0, 121.7, 120.6, 95.7, 88.2, 60.9, 52.7, 52.6, 14.4.

IR:  $\nu$  [ $\text{cm}^{-1}$ ] = 2358.8, 2331.8, 1735.8, 1195.8. MS (ESI): 1231 ( $\text{M-H}^+$ ). HRMS: Calc: 1231.5482, Found: 1231.5492. Elemental Analysis: C, 68.01; H, 6.13; N, 4.83 (calc. C, 68.28; H, 6.38; N, 4.55).

**Synthesis of Cruciform 5.5a.** Synthesized using the general procedure described above with aldehyde **5.2** instead of **5.4**. In this case, the pure compound was obtained by column chromatography (hexane / ethyl acetate 4:1 to 5:2). **5.5a** was obtained as a yellow solid (yield = 19 %). MP: 144-145°C.  $^1\text{H-NMR}$  (300 MHz,  $\text{CDCl}_3$ ):  $\delta$  = 1.27 (t, 12H,  $J$  = 7.2 Hz); 4.15 (s, 4H); 4.21 (c, 8H,  $J$  = 7.2 Hz); 6.61 (d, 4H,  $J$  = 8.7 Hz, Ar-H); 7.16 (d, 2H,  $J$  = 16 Hz, A from AB); 7.36 to 7.49 (m, 12H, including B from AB); 7.55 to 7.63 (m, 4H); 7.84 (s, 2H).  $^{13}\text{C-NMR}$  (75 MHz,  $\text{CDCl}_3$ ):  $\delta$  = 170.7, 147.7, 137.3, 131.6, 130.1, 128.4, 128.1, 128.0, 127.7, 123.3, 122.3, 121.7, 120.0, 112.6, 95.1, 88.1, 61.3, 53.5, 14.2. IR:  $\nu$  [ $\text{cm}^{-1}$ ] = 2360.7, 2341.4, 1745.5, 1737.7, 1604.7, 1521.7, 1375.1, 1188.0. MS (ESI): 857 ( $\text{M-H}^+$ ). HRMS: Calc: 857.3745, Found: 857.3756. Elemental Analysis: C, 75.45; H, 5.99; N, 3.46 (calc. C, 75.68; H, 6.12; N, 3.27).

**Synthesis of Cruciform 5.6a.** Synthesized using the general procedure described above with aldehyde **5.3** instead of **5.4**. Yield 15 %. MP: 102-105°C.  $^1\text{H-NMR}$  (300 MHz,  $\text{CDCl}_3$ ):  $\delta$  = 1.24 (t, 18H,  $J$  = 7.2 Hz); from 4.1 to 4.3 (m, 20H); 4.67 (s, 4H); 6.89 (d, 2H,  $J$  = 8.4 Hz, Ar-H); 7.04 (d, 2H,  $J$  = 1.8 Hz, Ar-H); 7.15 (dd, 2H,  $J_1$  = 1.8 Hz,  $J_2$  = 7.2 Hz, Ar-H); 7.16 (d, 2H,  $J$  = 16 Hz, A from AB); 7.32 to 7.44 (m, 6H); 7.50 (d, 2H,  $J$  = 16 Hz, B from AB); 7.60 to 7.64 (m, 4H); 7.86 (s, 2H).  $^{13}\text{C-NMR}$  (75 MHz,  $\text{CDCl}_3$ ):  $\delta$  = 171.2, 168.7, 149.6, 139.6, 137.2, 131.6, 131.6, 130.0, 128.6, 128.5, 128.5, 123.9, 123.1, 122.0, 121.6, 119.6, 112.8, 95.4, 87.8, 66.3, 61.2, 60.8, 53.8, 52.6, 14.2, 14.2. IR:  $\nu$  [ $\text{cm}^{-1}$ ] = 2360.7, 2335.6, 1747.5, 1737.7, 1524.0, 1197.7, 1168.8, 1027.9. MS (ESI): 1061

(M-H<sup>+</sup>). HRMS: Calc: 1061.4385, Found: 1061.4375. Elemental Analysis: C, 70.03; H, 6.12; N, 2.46 (calc. C, 70.17; H, 6.08; N, 2.64).



**Isolation of intermediate 5.9.** After a Horner reaction of **5.1** with aldehyde **5.2** (see above), a saturated solution of NH<sub>4</sub>Cl (10 mL) was added to quench the reaction and the mixture was extracted with dichloromethane (3 x 20 mL). The combined organic phases were washed with water and brine and dried over MgSO<sub>4</sub>. The crude mixture was purified by column chromatography ethyl acetate / hexane (2:7), isolating **5.9** as a yellow solid (yield = 23 %). MP: 98-101°C. <sup>1</sup>H-NMR (300 MHz, CDCl<sub>3</sub>): δ = 1.27 (t, 12H, *J* = 7.2 Hz); 4.15 (s, 4H); 4.21 (c, 8H, *J* = 7.2 Hz); 6.60 (d, 4H, *J* = 8.7 Hz, Ar-H); 6.86 (d, 2H, *J* = 16 Hz, A from AB); 6.97 (d, 2H, *J* = 16 Hz, B from AB); 7.41 (d, 2H, *J* = 8.7 Hz, Ar-H); 8.00 (s, 2H). <sup>13</sup>C-NMR (75 MHz, CDCl<sub>3</sub>): δ = 170.8, 148.2, 140.8, 136.0, 131.9, 128.5, 127.4, 127.2, 112.8, 100.4, 61.5, 53.8, 14.5. IR: ν [cm<sup>-1</sup>] = 2358.8, 1733.9, 1604.7, 1519.8, 1186.1.

**Isolation of intermediate 5.10.** After a Horner reaction of **5.1** with aldehyde **5.3**, a saturated solution of  $\text{NH}_4\text{Cl}$  (10 mL) was added to quench the reaction and the mixture was extracted with dichloromethane (3 x 20 mL). The combined organic phases were washed with water and brine and dried over  $\text{MgSO}_4$ . The crude mixture was purified by column chromatography from ethyl acetate / hexane (1:5 to 1:3), isolating **5.10** as a green oil (yield = 21 %).  $^1\text{H-NMR}$  (300 MHz,  $\text{CDCl}_3$ ):  $\delta$  = 1.24 (t, 18H,  $J$  = 7.2 Hz); from 4.1 to 4.3 (m, 20H); 4.67 (s, 4H); from 6.90 to 6.97 (m, including A from AB, 4H); 7.02 (d, 2H,  $J$  = 16 Hz, B from AB); 7.04 (s, 2H); 7.12 (d, 2H,  $J$  = 7.2 Hz); 7.99 (s, 2H).  $^{13}\text{C-NMR}$  (75 MHz,  $\text{CDCl}_3$ ):  $\delta$  = 171.3, 168.9, 147.1, 141.3, 140.9, 135.2, 131.6, 128.5, 127.4, 127.2, 121.2, 112.8, 100.4, 66.3, 61.1, 60.8, 53.7, 52.8, 14.3, 14.2. IR:  $\nu$  [ $\text{cm}^{-1}$ ] = 2358.8, 1733.9, 1604.7, 1519.8, 1186.1.

**Isolation of intermediate 5.11.** After a Horner reaction of **5.1** with aldehyde **5.4** (see above), a saturated solution of  $\text{NH}_4\text{Cl}$  (10 mL) was added to quench the reaction and the mixture was extracted with dichloromethane (3 x 20 mL). The combined organic phases were washed with water and brine and dried over  $\text{MgSO}_4$ . The crude mixture was purified by column chromatography ethyl acetate / hexane (1:3), isolating **5.11** as a yellow solid (yield = 41 %). MP: 136-138°C.  $^1\text{H-NMR}$  (300 MHz,  $\text{CDCl}_3$ ):  $\delta$  = 1.21 (t, 24H,  $J$  = 7.2 Hz); 4.12 (c, 8H,  $J$  = 7.2 Hz); 4.13 (c, 8H,  $J$  = 7.2 Hz); 4.33 (s, 8H); 4.34 (s, 8H); 6.85 (d, 2H,  $J$  = 16 Hz, A from AB); 7.01 (d, 2H,  $J$  = 16 Hz, B from AB); 7.02 (d, 2H,  $J$  = 8 Hz, Ar-H); from 7.14 to 7.21 (m, 4H); 7.99 (s, 2H).  $^{13}\text{C-NMR}$  (75 MHz,  $\text{CDCl}_3$ ):  $\delta$  = 170.8, 141.7, 141.4, 140.6, 136.0, 132.0, 131.5, 129.0, 121.6, 121.5, 120.6, 100.2, 60.6, 52.4, 52.4, 14.2, 14.1. IR:  $\nu$  [ $\text{cm}^{-1}$ ] = 2343.5, 1733.9, 1506.3, 1174.6, 1028.0, 970.1.

**Synthesis of saponified XFs 5.5b, 5.6b and 5.7b.** In all cases, a suspension of the ester (60 mg, 0.049 mmol) and NaOH (120 mg, 3 mmol) in methanol was refluxed overnight and then transferred into a freezer. A precipitate formed overnight which was filtered and washed with cold methanol and copious hexanes. Solids obtained were completely soluble in water. **5.5b** (brown solid, yield = 91 %); **5.6b** (brown solid, yield = 87 %), **5.7b** (yellow solid, yield = 95 %).

### 5.5. References and Notes

1. Henary, M. M.; Wu, Y.G.; Fahrni, C. J. Zinc(II)-selective ratiometric fluorescent sensors based on inhibition of excited-state intramolecular proton transfer. *Chemistry Eur. J.* **2004**, *10*, 3015-3025.
2. (a) Wang, B.; Wasielewski, M. R. Design and synthesis of metal ion-recognition-induced conjugated polymers: An approach to metal ion sensory materials. *J. Am. Chem. Soc.* **1997**, *119*, 12-21. (b) Bangcuyo, C. G.; Rampey-Vaughn, M. E.; Quan, L. T.; Angel, S. M.; Smith, M. D.; Bunz, U. H. F. Quinoline-containing, conjugated poly(aryleneethynylene)s: Novel metal and H<sup>+</sup>-responsive materials. *Macromolecules* **2002**, *35*, 1563-1568. (c) Pautzsch, T.; Klemm, E. Ruthenium-chelating poly(heteroaryleneethynylene)s: Synthesis and properties. *Macromolecules* **2002**, *35*, 1569-1575.
3. Pond, S. J. K.; Tsutsumi, O.; Rumi, M.; Kwon, O.; Zojer, E.; Bredas, J. L.; Marder, S. R.; Perry, J. W. Metal-ion sensing fluorophores with large two-photon absorption cross sections: Aza-crown ether substituted donor-acceptor-donor distyryl benzenes. *J. Am. Chem. Soc.* **2004**, *126*, 9291-9306.
4. Lim, N. C.; Freake, H. C.; Bruckner, C. Illuminating zinc in biological systems. *Chem. Eur. J.* **2005**, *11*, 38-49.
5. Pearce, D. A.; Jotterand, N.; Carrico, I. S.; Imperiali, B. Derivatives of 8-hydroxy-2-methylquinoline are powerful prototypes for zinc sensors in biological systems. *J. Am. Chem. Soc.* **2001**, *123*, 5160-5161.
6. (a) Burdette, S. C.; Walkup, G. K.; Spingler, B.; Tsien, R. Y.; Lippard, S. J. Fluorescent sensors for Zn<sup>2+</sup> based on a fluorescein platform: Synthesis, properties and intracellular distribution. *J. Am. Chem. Soc.* **2001**, *123*, 7831-7841. (b) Walkup, G. K.; Burdette, S. C.; Lippard, S. J.; Tsien, R. Y. A new cell-permeable fluorescent probe for Zn<sup>2+</sup>. *J. Am. Chem. Soc.* **2000**, *122*, 5644-5645.

7. (a) Hirano, T.; Kikuchi, K.; Urano, Y.; Higuchi, T.; Nagano, T. Highly zinc-selective fluorescent sensor molecules suitable for biological applications. *J. Am. Chem. Soc.* **2000**, *122*, 12399-12400. (b) Hirano, T.; Kikuchi, K.; Urano, Y.; Nagano, T. Improvement and biological applications of fluorescent probes for zinc, ZnAFs. *J. Am. Chem. Soc.* **2002**, *124*, 6555-6562. (c) Komatsu, K.; Kikuchi, K.; Kojima, H.; Urano, Y.; Nagano, T. Selective zinc sensor molecules with various affinities for  $Zn^{2+}$ , revealing dynamics and regional distribution of synaptically released  $Zn^{2+}$  in hippocampal slices. *J. Am. Chem. Soc.* **2005**, *127*, 10197-10204. (d) Kawabata, E.; Kikuchi, K.; Urano, Y.; Kojima, H.; Odani, A.; Nagano, T. Design and synthesis of zinc-selective chelators for extracellular applications. *J. Am. Chem. Soc.* **2005**, *127*, 818-819.
8. (a) Hofer, A. M.; Machen, T. E. Technique for In Situ Measurement of Calcium in Intracellular Inositol 1,4,5-Triphosphate-Sensitive Stores Using the Fluorescent Indicator MAG-FURA-2. *Proc. Nat. Acad. Sci.* **1993**, *90*, 2598-2602. (b) Sensi, S. L.; Canzoniero, L. M. T.; Yu, S. P.; Ying, H. S.; Koh, J. Y.; Kerchner, G. A.; Choi, D. W. Measurement of intracellular free zinc in living cortical neurons: Routes of entry. *J. Neuroscience* **1997**, *17*, 9554-9564. (c) Zhao, M. D.; Hollingworth, S.; Baylor, S. M. Properties of tri- and tetracarboxylate  $Ca^{2+}$  indicators in frog skeletal muscle fibers. *Biophys. J.* **1996**, *70*, 896-916. (d) Metten, B.; Smet, M.; Boens, N.; Dehaed, W. Synthesis of APTRA derivatives as building blocks for low-affinity fluorescent  $Ca^{2+}$  indicators. *Synthesis* **2005**, 1838-1844.
9. (a) Zhou, Z.; Fahrni, C. J. A Fluorogenic Probe for the Copper(I)-Catalyzed Azide-Alkyne Ligation Reaction: Modulation of the fluorescence emission via (3)(n, $\pi^*$ )-(1)( $\pi$ , $\pi^*$ ) inversion. *J. Am. Chem. Soc.* **2004**, *126*, 8862-8863. (b) Yang, L. C.; McRae, R.; Henary, M. M.; Patel, R.; Lai, B.; Vogt, S.; Fahrni, C. J. Imaging of the intracellular topography of copper with a fluorescent sensor and by synchrotron x-ray fluorescence microscopy. *Proc. Nat. Acad. Sci.* **2005**, *102*, 11179-11184. (c) Cody, J.; Fahrni, C. J. Fluorescence Sensing Based on Cation-Induced Conformational Switching: Copper-selective modulation of the photoinduced intramolecular charge transfer of a donor-acceptor biphenyl fluorophore. *Tetrahedron* **2004**, *60*, 11099-11107. (d) Corradini, R.; Dossena, A.; Galaverna, G.; Marchelli, R.; Panagia, A.; Sartor, G. Fluorescent chemosensor for organic guests and copper(II) ion based on dansyldiethylenetriamine-modified beta-cyclodextrin. *J. Org. Chem.* **1997**, *62*, 6283-6289.
10. Kim, I.-B.; Dunkhorst, A.; Gilbert, J.; Bunz, U. H. F. Sensing of lead ions by a carboxylate-substituted PPE: Multivalency effects. *Macromolecules* **2005**, *38*, 4560-4562.
11. Kim, I.-B.; Erdogan, B.; Wilson, J. N.; Bunz, U. H. F. Sugar-poly(*para*-phenylene ethynylene) conjugates as sensory materials: Efficient quenching by  $Hg^{2+}$  and  $Pb^{2+}$  ions. *Chem. Eur. J.* **2004**, *10*, 6247-6254.

12. (a) Chen, C. T.; Huang, W. P. A highly selective fluorescent chemosensor for lead ions. *J. Am. Chem. Soc.* **2002**, *124*, 6246-6247. (b) Aragoni, M. C.; Arca, M.; Demartin, F.; Devillanova, F. A.; Isaia, F.; Garau, A.; Lippolis, V.; Jalali, F.; Papke, U.; Shamsipur, M.; Tei, L.; Yari, A.; Verani, G. Fluorometric chemosensors. Interaction of toxic heavy metal ions Pb-II, Cd-II, and Hg-II with novel mixed-donor phenanthroline-containing macrocycles: Spectrofluorometric, conductometric, and crystallographic studies. *Inorg. Chem.* **2002**, *41*, 6623-6632.
13. (a) Thomas, S. W.; Joly, G. D.; Swager, T. M. Chemical sensors based on amplifying fluorescent conjugated polymers. *Chem. Rev.* **2007**, *107*, 1339-1386. (b) Ono, A.; Togashi, H. Highly selective oligonucleotide-based sensor for mercury(II) in aqueous solutions. *Angew. Chem.* **2004**, *43*, 4300-4302. (c) Kim, Y. H.; Youk, J. S.; Moon, S. Y.; Choe, J. I.; Chang, S. K. Hg<sup>2+</sup>-selective fluorogenic chemosensor derived from 8-aminoquinoline. *Chem. Lett.* **2004**, *33*, 702-703. (d) Nolan, E. M.; Lippard, S. J. A "Turn-On" fluorescent sensor for the selective detection of mercuric ion in aqueous media. *J. Am. Chem. Soc.* **2003**, *125*, 14270-14271.
14. (a) Grynkiewicz, G.; Poenie, M.; Tsien, R. Y. A new generation of Ca<sup>2+</sup> indicators with greatly improved fluorescence properties. *J. Biol. Chem.* **1985**, *260*, 3440-3450. (b) Minta, A.; Kao, J. P. Y.; Tsien, R. Y. Fluorescent indicators for cytosolic calcium based on rhodamine and fluorescein chromophores. *J. Biol. Chem.* **1989**, *264*, 8171-8178. (c) Zhang, J.; Campbell, R. E.; Ting, A. Y.; Tsien, R. Y. Creating new fluorescent probes for cell biology. *Nature Rev. Cell Biol.* **2002**, *3*, 906-918.
15. (a) Kay, A. R.; Neyton, J.; Paoletti, P. A startling role for synaptic zinc. *Neuron* **2006**, *52*, 572-574. (b) Budde, T.; Minta, A.; White, J. A.; Kay, A. R. Imaging free zinc in synaptic terminals in live hippocampal slices. *Neuroscience* **1997**, *79*, 347-358. (c) Snitsarev, V.; Budde, T.; Stricker, T. P.; Cox, J. M.; Krupa, D. J.; Geng, L.; Kay, A. R. Fluorescent detection of Zn<sup>2+</sup>-rich vesicles with zinquin: Mechanism of action in lipid environments. *Biophys. J.* **2001**, *80*, 1538-1546. (d) Suh, S. W.; Jensen, K. B.; Jensen, M. S.; Silva, D. S.; Kesslak, P. J.; Danscher, G.; Frederickson, C. J. Histochemically-reactive zinc in amyloid plaques, angiopathy, and degenerating neurons of Alzheimer's diseased brains. *Brain Res.* **2000**, *852*, 274-278.
16. (a) Wilson, J. N.; Bunz, U. H. F. Switching of intermolecular charge-transfer in cruciforms: metal ion sensing. *J. Am. Chem. Soc.* **2005**, *127*, 4124-4125. (b) Zuccherro, A. J.; Wilson, J. N.; Bunz, U. H. F. Cruciforms as functional fluorophores: response to protons and selected metal ions. *J. Am. Chem. Soc.* **2006**, *128*, 11872-11881.
17. Wilson, J. N.; Hardcastle, K. I.; Josowicz, M.; Bunz, U. H. F. Synthesis and electronic properties of bis-styryl substituted trimeric arylenethynyls. Comparison of cruciforms with *iso*-cruciforms. *Tetrahedron.* **2004**, *60*, 7157-7167.
18. Wilson, J. N.; Smith, M. D.; Enkelmann, V.; Bunz, U. H. F. Cruciform  $\pi$ -systems: effect of aggregation on emission. *Chem. Commun.* **2004**, 1700-1701.

19. Hauck, M.; Schönhaber, J.; Zuccherro, A. J.; Hardcastle, K. I.; Müller, T. J. J.; Bunz, U. H. F. Phenothiazine cruciforms: synthesis and metallochromic properties. *J. Org. Chem.* **2007**, *72*, 6714-6725.
20. Wilson, J. N.; Josowicz, M.; Wang, Y.; Bunz, U. H. F. Cruciform  $\pi$ -systems: hybrid phenylene-ethynylene/phenylene-vinylene oligomers. *Chem. Commun.* **2003**, 2962-2963.
21. Brombosz, S. M.; Zuccherro, A. J.; Phillips, R. L.; Vazquez, D.; Wilson, A.; Bunz, U. H. F. Terpyridine-based cruciform-Zn<sup>2+</sup> complexes as anion-responsive fluorophores. *Org. Lett.* **2007**, *22*, 4519-4522.
22. (a) McGrier, P. L.; Solntsev, K. M.; Miao, S.; Tolbert, L. M.; Miranda, O. R.; Rotello, V. M.; Bunz, U. H. F. Hydroxycruciforms: amine-responsive fluorophores. *Chem. Eur. J.* **2008**, *14*, 4503-4510. (b) McGrier, P. L.; Solntsev, K. M.; Schönhaber, J.; Brombosz, S. M.; Tolbert, L. M.; Bunz, U. H. H. Hydroxy-cruciforms. *Chem. Commun.* **2007**, 2127-2129.
23. (a) Gerhardt, W. W.; Zuccherro, A. J.; Wilson, J. N.; South, C. R.; Bunz, U. H. F.; Weck, M. Supramolecular cruciforms. *Chem. Commun.* **2006**, 2141-2143. (b) Gerhardt, W. W.; Zuccherro, A. J.; South, C. R.; Bunz, U. H. F.; Weck, M. Controlling polymer properties through dynamic metal-ligand interactions: supramolecular cruciforms made easy. *Chem. Eur. J.* **2007**, *13*, 4467-4474.
24. (a) Kang, H.; Facchetti, A.; Jiang, H.; Cariati, E.; Righetto, S.; Ugo, R.; Zuccaccia, C.; Macchioni, A.; Stern, C. L.; Liu, Z.; Ho, S.-T.; Brown, E. C.; Ratner, M. A.; Marks, T. J. Ultralarge hyperpolarizability twisted pi-electron system electro-optic chromophores: Synthesis, solid-state and solution-phase structural characteristics, electronic structures, linear and nonlinear optical properties, and computational studies. *J. Am. Chem. Soc.* **2007**, *129*, 3267-3286. (b) Kang, H.; Evmenenko, G.; Dutta, P.; Clays, K.; Song, K.; Marks, T. J. X-shaped electro-optic chromophore with remarkably blue-shifted optical absorption. synthesis, characterization, linear/nonlinear optical properties, self-assembly, and thin film microstructural characteristics. *J. Am. Chem. Soc.* **2006**, *128*, 6194-6205. (c) Hu, K.; Zhu, P. W.; Yu, Y.; Facchetti, A.; Marks, T. J. Self-assembled electrooptic thin films with remarkably blue-shifted optical absorption based on an X-shaped chromophore. *J. Am. Chem. Soc.* **2004**, *126*, 15974-15975.
25. (a) Klare, J. E.; Tulevski, G. S.; Sugo, K.; de Picciotto, A.; White, K. A.; Nuckolls, C. Cruciform pi-systems for molecular electronics applications. *J. Am. Chem. Soc.* **2003**, *125*, 6030-6031. (b) Klare, J. E.; Tulevski, G. S.; Nuckolls, C. Chemical reactions with upright monolayers of cruciform pi-systems. *Langmuir.* **2004**, *20*, 10068-10072. (c) Florio, G. M.; Klare, J. E.; Pasamba, M. O.; Werblowsky, T. L.; Hyers, M.; Berne, B. J.; Hybertsen, M. S.; Nuckolls, C.; Flynn, G. W. Frustrated Ostwald ripening in self-assembled monolayers of cruciform pi-systems. *Langmuir.* **2006**, *22*, 10003-10008. (d) Tang, J.; De Poortere, E. P.; Klare, J. E.; Nuckolls, C.;

- Wind, S. J. Single-molecule transistor fabrication by self-aligned lithography and in situ molecular assembly. *Microelectron. Eng.* **2006**, *83*, 1706-1709.
26. (a) Marsden, J. A.; Miller, J. J.; Shirtcliff, L. D.; Haley, M. M. Structure-property relationships of donor/acceptor-functionalized tetrakis(phenylethynyl)benzenes and bis(dehydrobenzoannuleno)benzenes. *J. Am. Chem. Soc.* **2005**, *127*, 2464-2476. (b) Spitler, E. L.; Shirtcliff, L. D.; Haley, M. M. Dynamic proton-induced two-stage emission switching in donor-functionalized bis(dehydrobenzo[n]annuleno)benzenes and 1,2,4,5-tetrakis(phenylethynyl)benzene. *J. Org. Chem.* **2007**, *72*, 86-96. (c) Slepko, A. D.; Hegmann, F. A.; Tykwinski, R. R.; Kamada, K.; Ohta, K.; Marsden, J. A.; Spitler, E. L.; Miller, J. J.; Haley, M. M. *Opt. Lett.* **2006**, *31*, 3315-3317. (d) Spitler, E. L.; Haley, M. M. Dynamic proton-induced two-stage emission switching in donor-functionalized bis(dehydrobenzo[n]annuleno)benzenes and 1,2,4,5-tetrakis(phenylethynyl)benzene. *Tetrahedron.* **2008**, *64*, 11469-11474.
27. London, R. E. Methods for measurement of intracellular magnesium – NMR and fluorescence. *Ann. Rev. Physiol.* **1991**, *53*, 241-258.
28. (a) Wang, J.; Qian, X. A series of polyamide receptor based PET fluorescent sensor molecules: Positively cooperative  $Hg^{2+}$  ion binding with high sensitivity. *Org. Lett.* **2006**, *17*, 3721-3724. (b) Wang, J. B.; Qian, X. H.; Cui, J. N. Detecting  $Hg^{2+}$  ions with an ICT fluorescent sensor molecule: Remarkable emission spectra shift and unique selectivity. *J. Org. Chem.* **2006**, *71*, 4308-4311.
29. Wilson, J. N.; Windscheif, P. M.; Evans, U.; Myrick, M. L.; Bunz U. H. F. Band gap engineering of poly(*p*-phenyleneethynylene)s: Cross-conjugated PPE-PPV hybrids. *Macromolecules* **2002**, *35*, 8681-8683.
30. (a) Sluch, M. I.; Godt, A.; Bunz, U. H. F.; Berg, M. A. Excited-state dynamics of oligo(*p*-phenyleneethynylene): Quadratic coupling and torsional motions. *J. Am. Chem. Soc.* **2001**, *123*, 6447-6448. (b) Liu, L. T.; Yaron, D.; Berg, M. A. Electron-phonon coupling in phenyleneethynylene oligomers: A nonlinear one-dimensional configuration-coordinate model. *J. Phys. Chem. C* **2007**, *111*, 5770-5782.
31. Sanchiz, J.; Dominguez, S.; Mederos A.; Brito, F.; Arrieta J. M. Tetramethyl carboxylic acids derived from *o*-phenylenediamines as sequestering agents for iron(III): Thermodynamic studies. X-ray crystal structure of sodium aqua(4-chloro-1,2-phenylenediamine-*N,N,N',N'*-tetraacetato)ferrate(III)-water (1/1.5). *Inorg. Chem.* **1997**, *36*, 4108-4114, and references therein.
32. Burdette, S. C.; Lippard S. J. ICCC34 - golden edition of coordination chemistry reviews. Coordination chemistry for the neurosciences. *Coord Chem. Rev.* **2001**, *216*, 333-361.
33. (a) Fery-Forgues, S.; Le Bris, M.-T.; Guette, J.-P.; Valeur, B. Ion-responsive fluorescent compounds .1. Effect of cation binding on photophysical properties of a

- benzoquinone derivative linked to monoaza-15-crown-5. *J. Phys. Chem.* **1988**, *92*, 6233-6237. (b) Bourson, J.; Valeur, B. Ion-responsive fluorescent compounds .2. Cation-steered intramolecular charge transfer in a crowned merocyanine. *J. Phys. Chem.* **1989**, *93*, 3871-3876. (c) Rurack, K.; Rettig, W.; Resch-Genger, U. Unusually high cation-induced fluorescence enhancement of a structurally simple intrinsic fluoroionophore with a donor-acceptor-donor constitution. *Chem. Commun.* **2000**, 407-408. (d) Bricks, J. L.; Slominskii, J. L.; Kudinova, M.; Tolmachev, A. I.; Rurack, K.; Resch-Genger, U.; Rettig, W. Syntheses and photophysical properties of a series of cation-sensitive polymethine and styryl dyes. *J. Photochem. Photobiol. A* **2000**, *132*, 193-208.
34. (a) Das, S.; Thomas, K. G.; Thomas, K. J.; Kamat, P. V.; George, M. V. Photochemistry of squaraine dyes .8. Photophysical properties of crown-ether squaraine fluoroionophores and their metal complexes. *J. Phys. Chem.* **1994**, *98*, 9291-9296. Marcotte, N.; Fery-Forgues, S.; Lavabre, D.; Marguet, S.; Pivovarenko, V. G. Spectroscopic study of a symmetrical bis-crown fluoroionophore of the diphenylpentadienone series. *J. Phys. Chem. A* **1999**, *103*, 3163-3170. Marcotte, N.; Plaza, P.; Lavabre, D.; Fery-Forgues, S.; Martin, M. M. Calcium photorelease from a symmetrical donor-acceptor-donor bis-crown-fluoroionophore evidenced by ultrafast absorption spectroscopy. *J. Phys. Chem. A* **2003**, *107*, 2394-2402.

## CHAPTER 6

### Supramolecular Cruciforms

#### 6.1. Introduction

Because of their electrical, optical, and redox properties, conjugated and fluorescent molecules are candidates for integration into electro-optical and light-emitting devices (LEDs).<sup>1-6</sup> These functional materials can be based on small molecules, oligomers, or polymers, each with distinct advantages. Small molecules are monodisperse and are easier to purify and characterize. On the other hand, polymers and oligomers are polydisperse. However, polymeric systems are desirable owing to their good mechanical and film forming properties, rendering them amenable to solution processing.<sup>7</sup> Supramolecular polymeric systems based on the assembly of monomeric units via noncovalent interactions introduce an additional level of control. Such materials have the potential to combine the processability and mechanical properties of a traditional polymeric system without the long-range defects and functional group intolerance of covalent polymerization methodologies.<sup>8</sup> Self-assembled materials are dynamic systems with reversible interactions that are responsive to environmental stimuli, permitting the adjustment of polymeric properties for specific applications.

Intense research in this area has yielded new supramolecular polymeric materials based on conjugated building blocks with novel applications ranging from tissue engineering<sup>9</sup> to electronic applications.<sup>10</sup> We are interested in preparing functional and solution processable materials with tailorable physical and optical properties. To accomplish this, we envisage a discrete toolbox of supramolecular monomers that can be

polymerized via noncovalent interactions. By readily exchanging monomer components we can augment the final properties of the materials to fit a specific need via a simple assembly step, minimizing or obviating more costly and time consuming synthetic steps.

Recently, Rowan and Weder have used metal-ligand interactions to form supramolecular fluorescent phenylene-ethynylene coordination polymers that can be easily processed into films and fibers.<sup>11-14</sup> We rationalized that cruciforms could similarly be employed as fluorescent monomer building blocks in functional supramolecular assemblies.<sup>15-26</sup>

The photophysical properties and tunability of XFs make them attractive for use as building blocks in supramolecular assemblies. In addition, the 2-dimensional nature of these chromophores conveys a distinct advantage: one axis can be substituted to drive non-covalent assembly of the fluorophores while the second axis remains available to tune the optical properties of the XF and/or control solubility. As such, XFs suitably functionalized for assembly are ditopic ligands inherently equipped for linear supramolecular assembly.

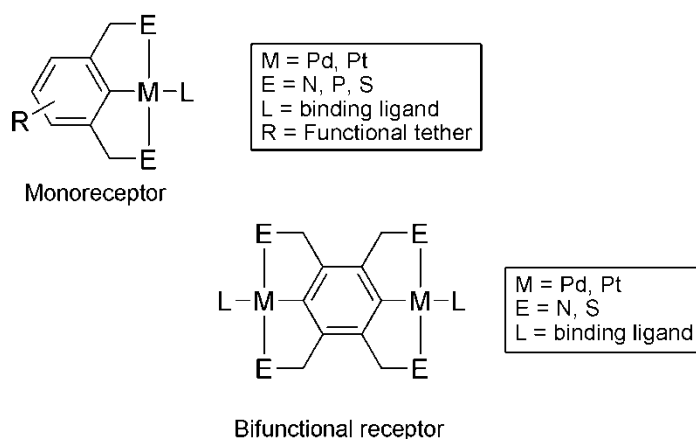


**Figure 6.1.** Examples of mono- and bimetallic pincer complexes as supramolecular synthons in which E is a neutral two-electron donor and L can be a functional recognition unit.

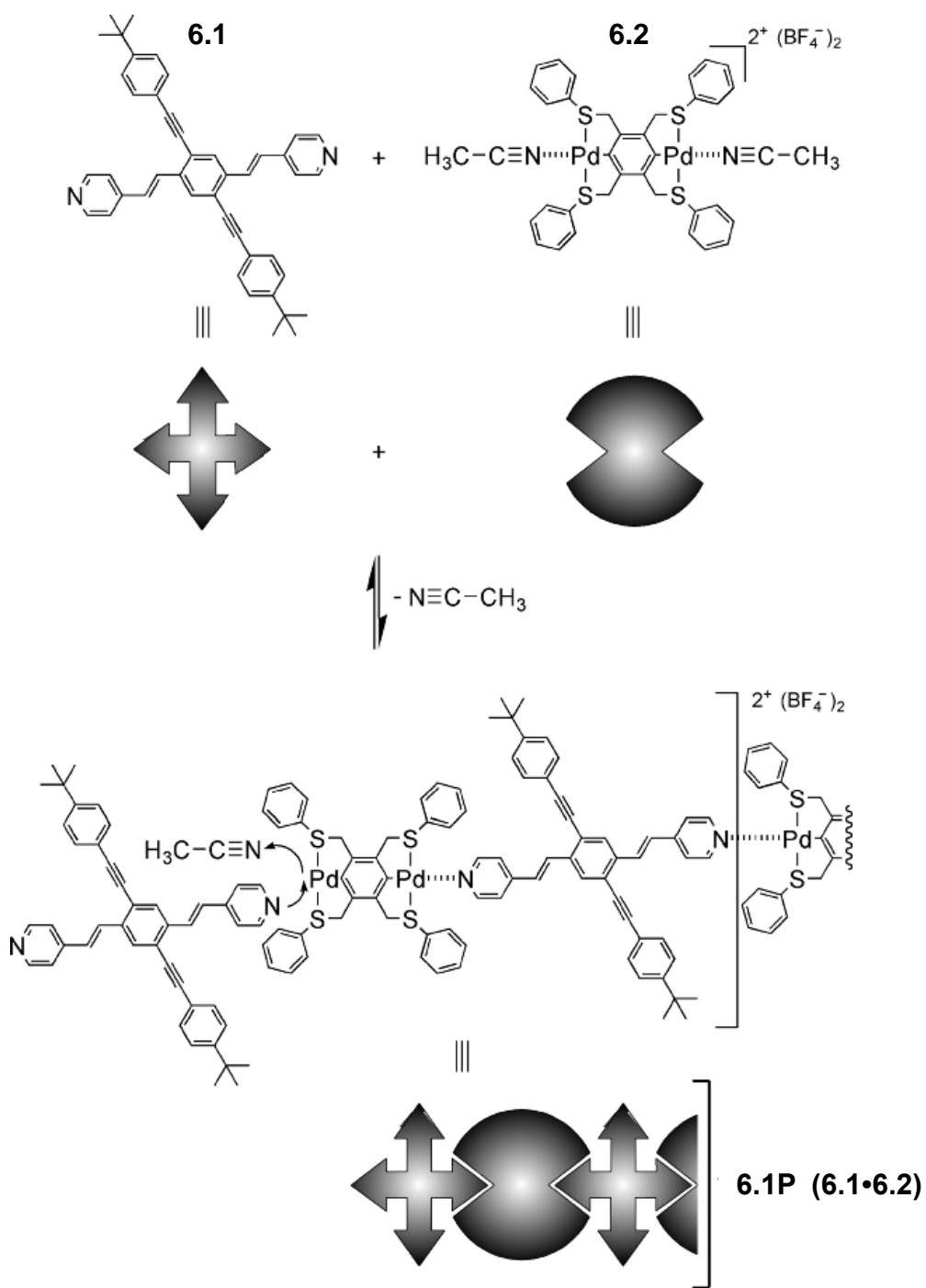
We decided to employ ditopic metal complexes to assemble XFs via metal coordination. Metallated pincer complexes are often employed in metal coordination owing to their chemo-activated coordination, which is both fast and quantitative.<sup>27-39</sup> Monoreceptor pincer complexes are tridentate species composed of a central aromatic core with a carbon-metal bond (C) flanked by two neutral donor atoms (E), giving these ligands an ECE nomenclature (Figure 6.1). Cyclometallation of these ligands with a Pd or Pt salt creates a square planar metal complex, which can coordinate basic ligands upon activation.<sup>40-41</sup> A second cyclometallation *para* to the first results in bifunctional bis-metallated pincer complexes.<sup>42-45</sup> These pincer complexes can be activated by the removal of the fourth ligand – generally a halide atom – through the addition of a suitable silver salt (AgBF<sub>4</sub>, AgOTf, AgNO<sub>3</sub>). This leads to the abstraction of the halide atom by Ag<sup>+</sup> (precipitating AgX<sub>(s)</sub>), leaving a cationic complex with open coordination sites and non-coordinating counterions. The coordination strength of these pincers can be varied by exploiting several common classes of ligands (nitriles < pyridines < thioureas < phosphines).

One could envision a toolbox of XFs and pincer complexes combined to generate highly tunable fluorescent supramolecular assemblies. The fluorescence of these assemblies could be tuned by varying the substituents conjugated into the XF  $\pi$ -system. Varying the metal in the pincer complex as well as the XFs mode of coordination provides the ability to tune the K<sub>a</sub>, permitting the adjustment of the polymeric properties of the assemblies.

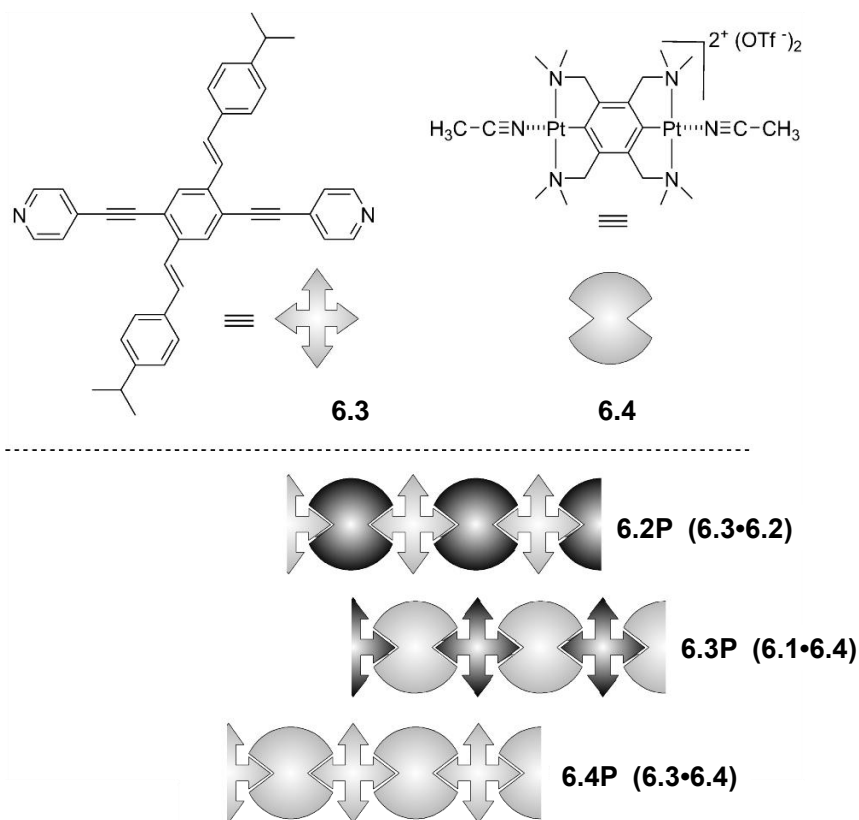
To examine the potential of this strategy, we elected to perform some proof-of-principle experiments. We rationalized that pyridyl-substituted cruciforms could be

assembled into supramolecular aggregates using metal coordination via Pd- and Pt-pincer complexes. For our first experiments, we chose to use bis-pincer complex **6.2** to illicit main-chain assembly of XF **6.1** (Scheme 6.1). **6.2** has been used previously to generate pyrazine and pyridyl coordination polymers. Pyridyl cruciform **6.1** contains two terminal pyridine moieties, i.e. it serves as a bifunctional ligand that can easily displace the acetonitrile-coordinated bis-pincer complex **6.2**, generating supramolecular complex **6.1P** in a simple step. Subsequently, we expanded our study by investigating the self-assembly behavior of pyridyl arylolethynylene cruciform **6.3** and the bis-platinated pincer complex **6.4** (Scheme 6.2).

Coordinating cruciforms through a pyridyl unit on either the styryl or arylolethynylene XF axis to either a bis-Pd or bis-Pt pincer complex provides a library of related polymers having a range of physical and optical properties. The four building blocks **6.1** – **6.4** should allow for a fine-tuning of the association constants and ultimately the polymer properties. The  $K_a$  value of the metal-pyridyl ligand interaction of each cruciform is expected to vary depending on the *para* substituent, which is an alkenyl group in **6.1** or an alkynyl group in **6.3**. This electronic effect has been shown to fit the Hammett equation using the  $\sigma^+$  constant<sup>46</sup> of the *para* substituent.<sup>27</sup> Furthermore, Pt pincer complexes are known to have a significantly stronger association in comparison to Pd pincer complexes, allowing us to also control the association via the metal center.<sup>47</sup> Therefore, the uniqueness of each metal-ligand interaction within these structurally related supramolecular materials should lead to polymers with a set of properties that can be easily controlled.



**Scheme 6.1.** Coordination polymer **6.1P**, a fluorescent supramolecular assembly formed through the coordination of XF **6.1** with bis-Pd pincer **6.2**.



**Scheme 6.2.** Pyridyl XF **6.3**, bis-Pt pincer complex **6.4**, and the three additional supramolecular assemblies (**6.2P-6.4P**) synthesized using monomers **6.1-6.4**.

## 6.2. Results and Discussion

Monomers **6.1-6.4** were synthesized according to published literature procedures.<sup>15, 20, 42-45</sup> In **6.2** and **6.4**, acetonitrile molecules are coordinated to the metal centers of each respective pincer complex. The weaker coordination of nitriles leads to a spontaneous and quantitative exchange of the acetonitriles for the pyridyl-functionalized cruciform ligands to give **6.1P-6.4P** in excellent yields. Self-assembly is accomplished by combining the bis-metallated pincer complexes with the XF of choice. For solubility purposes all of our physical characterization studies were carried out in DMF with the exception of fluorescence studies, which were performed in a  $\text{CHCl}_3/\text{DMSO}$  mixture.

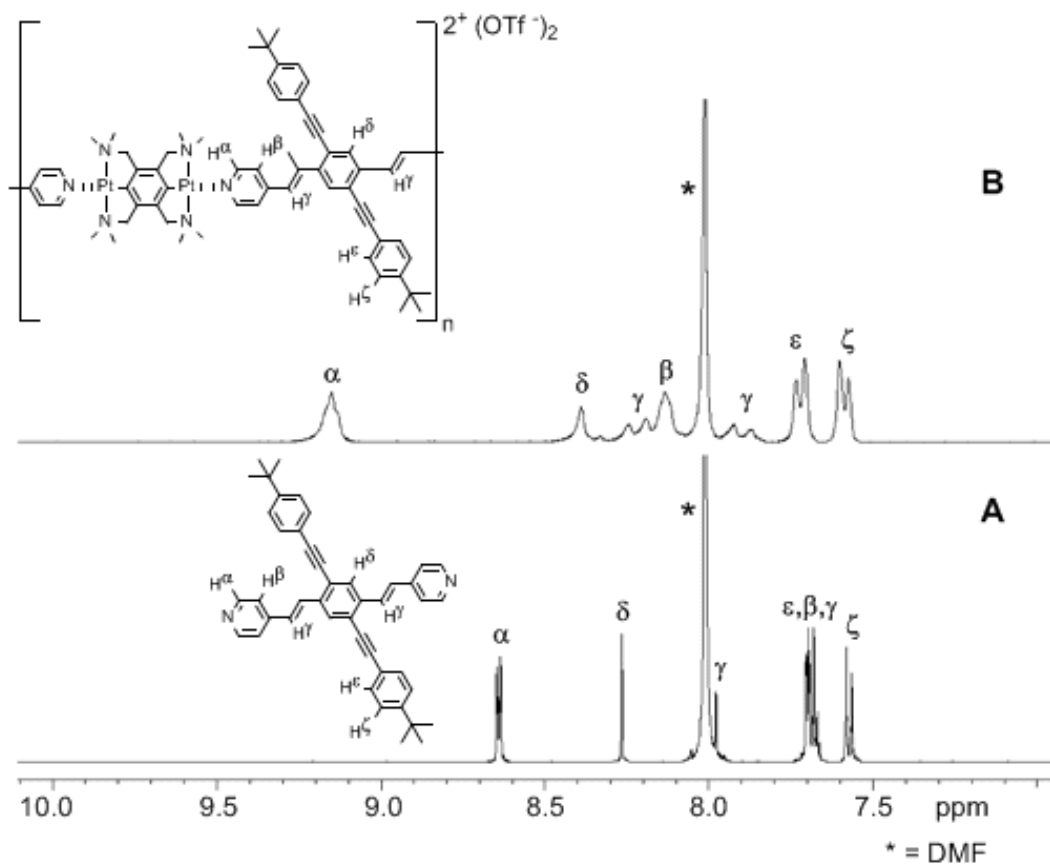


**Figure 6.2.** Stacked  $^1\text{H}$  NMR spectra ( $d_7$ -DMF) of the aromatic region depicting supramolecular assembly of **6.1** and **6.4**. A: XF **6.1** (0.006 M). B: 1:1 mixture of **6.1** and **6.4** yielding supramolecular polymer **6.3P** (0.006 M).

Using  $^1\text{H}$  NMR spectroscopy, the self-assembly was monitored by shifts of diagnostic signals pre- and post-coordination in  $d_7$ -DMF. Both **6.2** and **6.4** showed shifts characteristic of quantitative metal-coordination events. The doublet at  $\delta=8.65$  ppm, representative of the  $\alpha$ -pyridyl protons of cruciform **6.1**, showed a quantitative upfield shift to  $\delta=8.50$  ppm after coordination to **6.2** and a quantitative downfield shift to  $\delta=9.21$  ppm after coordination to **6.4**. In the case of XF **6.3**, the  $\alpha$ -pyridyl protons signal has an upfield shift from  $\delta=8.80$  to 8.63 ppm after coordination to **6.2**, and a downfield shift to  $\delta=9.35$  ppm after coordination to **6.4**.<sup>48</sup> We observed a broadening of all the signals for

**6.1P-6.4P**, which is typical for polymers. As an example, Figure 6.2 shows the formation of **6.3P**, focusing on the aromatic region of **6.1** before and after coordination to **6.4** in  $d_7$ -DMF. The quantitative shifts of every proton along the distyryl axis are shown; protons further from the coordinated pyridyl nitrogen have smaller shifts as they experience less of an electronic perturbation. Additionally, the unaffected doublet of doublets labeled  $\epsilon$  and  $\zeta$  in the spectra clearly shows the electronically decoupled nature of the cross-conjugated arylethynylene axis.

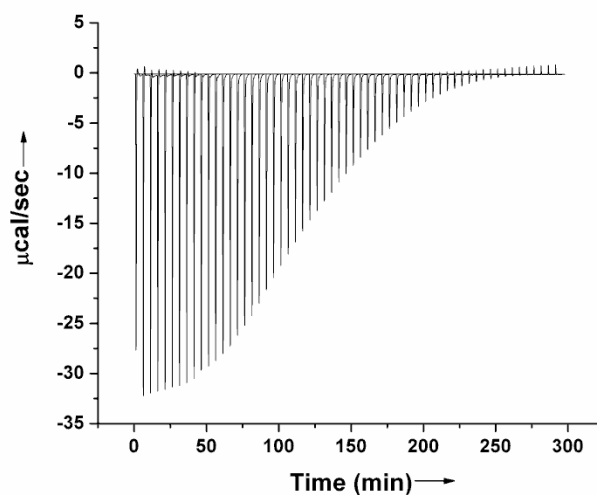


**Figure 6.3.** Isotherm generated from the titration of **6.4** into **6.1** in DMF to yield **6.3P**.

We quantified the strength of our metal-ligand interactions using isothermal titration calorimetry (ITC) to provide a complete thermodynamic characterization, which is calculated from the measured enthalpy of binding. For our experiments we assumed that the  $K_a$  value of our interaction is independent of the polymer length, that is,  $K_{\text{average}} \approx K_1 \approx K_n$ . By titrating a solution of each bismetallated pincer complex in DMF (10 mM) into a solution of each XF in DMF (1 mM) at 22 °C an isotherm is generated, from which

a  $K_a$  ( $K_{\text{average}}$ ) value is calculated. All titrations were carried out in triplicate to validate the reported  $K_a$  values. Furthermore, all showed a hyperbolic shape characteristic of a weaker dynamic on/off binding event as shown in Figure 6.3 for the isotherm of **6.3P** (see Table 6.1).

**Table 6.1.** ITC  $K_a$  values and approximate degree of polymerization (DP) of each supramolecular complex.

Complex	$K_a$ [ $\text{M}^{-1}$ ]	Maximum DP <sup>[a]</sup>
<b>6.1P</b>	$5.7 (\pm 1.6) \times 10^3$	14
<b>6.2P</b>	$2.1 (\pm 0.5) \times 10^3$	10
<b>6.3P</b>	$44.3 (\pm 5.4) \times 10^3$	53
<b>6.4P</b>	$15.2 (\pm 2.9) \times 10^3$	31
<b>6.2•Pyr</b>	$6.0 (\pm 0.5) \times 10^3$	-
<b>6.4•Pyr</b>	$60.0 (\pm 7.8) \times 10^3$	-
<b>6.1•6.5</b>	$9.8 (\pm 3.2) \times 10^3$	-
<b>6.1•6.6</b>	$53.0 (\pm 4.8) \times 10^3$	-

[a] Maximum DP  $\approx (K_a[\text{monomer}])^{1/2}$ , based on a total 1:1 (A/B) monomer concentration of 0.033 M in DMF.

The polymer  $K_a$  values were higher when using **6.4** than **6.2** by approximately an order of magnitude. Literature reports indicate that the Pt-based coordination using pincer complexes is significantly stronger than using their palladium analogues,<sup>47</sup> which is in accordance with our results. The range of association strengths available for coordination events involving cruciforms can be used to control the properties of our system. However, the assumption that  $K_a = K_{\text{average}}$  must first be validated. To this end, we carried out small molecule binding studies to pincer complexes **6.2** and **6.4** and to XF **6.1**, in which the  $K_a$  values were measured and compared to  $K_a$  ( $K_{\text{average}}$ ) values measured

for the coordination polymer. For pincer complexes **6.2** and **6.4** we measured the  $K_a$  values upon the coordination of pyridine, and for XF **6.1** we measured the  $K_a$  values upon the coordination of monotopic Pd and Pt pincer complexes **6.5** and **6.6**, respectively, all in DMF (Figure 6.4).

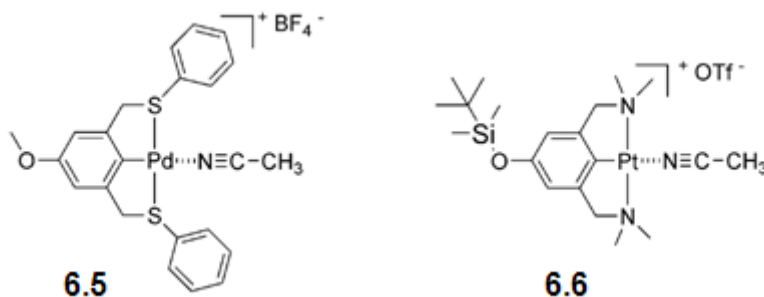


**Figure 6.4.** Monotopic Pd pincer complex **6.5** and monotopic Pt pincer complex **6.6**.

The close agreement of the small model  $K_a$  values to the polymeric  $K_a$  values strengthens the notion that the assumption  $K_a = K_{\text{average}}$  is valid. We obtain a set of DP values after inserting these  $K_a$  values into the multistage open association (MSOA) model equation.<sup>49-51</sup>

After confirming and quantifying the self-assembly of each of our systems using <sup>1</sup>H NMR spectroscopy and ITC, we subsequently characterized the polymer properties. Owing to the weaker  $K_a$  values of our materials in DMF, size-exclusion chromatography proved unreliable for determining their molecular weights and polydispersities. Therefore, we analyzed the materials by viscometry using a Cannon-Ubbelohde semi-micro type viscometer. Initially, we demonstrated the molecular weight dependence of **6.1P** based on monomer feed ratios in DMF, with a maximum relative viscosity ( $\eta_r$ ) at a stoichiometric equivalence of **6.1** and **6.2**.<sup>26</sup> This can be interpreted as the longest possible length of the polymers in solution, assuming maximum coordination. Deviation

from a 1:1 monomer feed ratio led to chain termination and a less viscous solution as the length of the supramolecular polymer decreased.

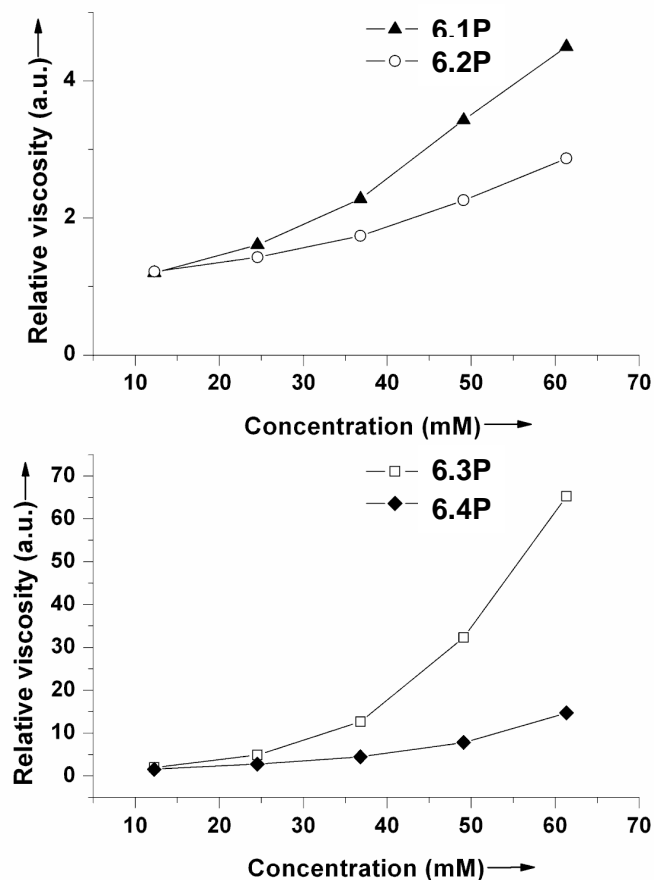


**Figure 6.5.** Top: Plot of relative viscosity of bis-Pd pincer complexed materials **6.1P** and **6.2P**. Bottom: Plot of relative viscosity of bis-Pt pincer complexed materials **6.3P** and **6.4P** in DMF.

Next, we investigated the  $\eta_r$  at different concentrations in DMF. A linear increase in  $\eta_r$  is generally expected as one increases the concentration of a covalent polymer solution. However, because our metal-ligand interactions are more favored at higher concentrations, a nonlinear increase should be observed. Figure 6.5 details our viscometry results. The expected nonlinear increase is seen for all of our materials. Our viscosity measurements are also in accordance with the  $K_a$  values determined by ITC.

The solution of **6.3P** is 70 times more viscous than pure DMF, and both bis-Pt-pincer complexed polymeric solutions **6.3P** and **6.4P** significantly more viscous than the bis-Pd-pincer complexed polymeric solutions **6.1P** and **6.2P**. Polymers **6.1P** and **6.3P**, coordinate to the metal through the more electron-rich pyridyl groups on the distyryl axis and have a higher relative viscosity as compared to the polymers formed from XF **6.3**, which coordinates along the less electron-releasing arylethynylene axis.

The viscosity results illustrate the inherent control over the polymer properties in our supramolecular system. By simply switching one monomeric component with an alternate one from our supramolecular toolbox, we can effectively tune the DP and thus the viscosity.

We also examined the luminescent properties of these supramolecular materials. We used fluorescence spectroscopy, comparing the emissions of **6.1P-6.4P** to that of their small-molecule analogues. Unlike the characterizations of our polymer physical properties, spectroscopic studies in DMF were not possible as the self-assembly was not readily observed at the dilute concentrations necessary for fluorescence measurements. As a result, we conducted all spectroscopic studies in a mixture of CHCl<sub>3</sub>/DMSO (95:5).<sup>52</sup> For each supramolecular material we observed red-shifted emissions compared to the uncoordinated cruciforms. We also observed a decrease in fluorescence intensity for each material proportional to the measured  $K_a$  values of each metal-ligand interaction. The results of this study are summarized in Figure 6.6 and Tables 2 and 3, and the spectra are included here as Figures 6.7-6.15.

Uncoordinated **6.1** possesses a vibrant blue emission at 445 nm (Figure 6.6). Upon the titration of 2.0 equivalents of **6.2**, a bathochromic shift (445→515 nm) is

observed (Figure 6.7). If a large excess (15.0 equivalents) of **6.2** is added, a subsequent hypsochromic shift (515→485 nm) results. In order to rationalize these changes in emission, we performed a similar emission study coordinating monotopic Pd pincer complex **6.5** to **6.1** (Figure 6.8). In the case of this model system, we observed a similar bathochromic shift (445→491 nm) during the titration of **6.5**.

**Table 6.2.** Summary of the changes in emission observed upon the addition of increasing equivalents of **6.2** or **6.4** to **6.1** or **6.3**. The concentration of XF in all samples was 0.0445 mM in a mixture of CHCl<sub>3</sub> and DMSO (95:5).

Supramolecular complex	Cruciform Emission (nm)	Supramolecular complex Emission (nm) <sup>[a]</sup>	Excess Pincer Emission (nm) <sup>[a]</sup>	Solid State Emission (nm)
<b>1P</b>	445	515 (2.0 eq.)	485 (15.0 eq.)	520
<b>2P</b>	455	560 (3.6 eq.)	512 (20.0 eq.)	544
<b>3P</b>	445	542 (1.4 eq.)	N.A.	N.A.
<b>4P</b>	455	510 (3.0 eq.)	504 (15.0 eq.)	504

[a] Parentheses refer to the number of equivalents of ditopic pincer complex added to achieve shift.

**Table 6.3.** Summary of the changes in emission observed upon the addition of **6.5** or **6.6** to **6.1** or **6.3**. The concentration of the cruciform in all samples was 0.0445 mM in a mixture of CHCl<sub>3</sub>: DMSO (95:5).

Supramolecular complex	Cruciform Emission (nm)	Supramolecular complex Emission (nm)
<b>15</b>	445	491
<b>35</b>	455	507
<b>16</b>	445	540
<b>36</b>	455	515

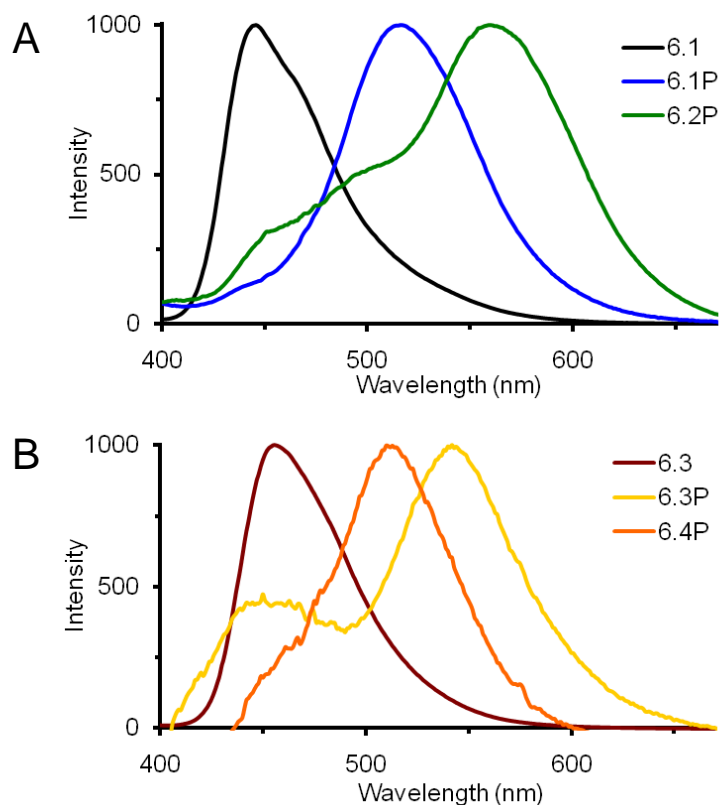


**Figure 6.6.** Normalized emission of XFs **6.1** and **6.3**, and  $\lambda_{\text{max}}$  of the furthest redshifted emissions of polymers **6.1P-6.4P** (precipitation seen at these maximum DPs) all at 0.0445mM. A) Emission of XF **6.1** (black trace), and Pd coordination polymers **6.1P** (blue trace) and **6.3P** (green trace). B) Emission of XF **6.3** (maroon trace), and Pt coordination polymers **6.2P** (yellow trace) and **6.4P** (orange trace).

These emission shifts can be explained by the orthogonal arrangement of the frontier molecular orbitals in our cruciforms. Coordination in these cruciforms is along the LUMO axis. As corroborated in the  $^1\text{H}$  NMR, the HOMO axis is largely unaffected. Therefore, the LUMO is destabilized and the energy band-gap in all our systems decreases resulting in the observed bathochromic shifts.

This effect partially explains the change in emission observed upon the titration of **6.2** into **6.1**. During the early stages of the titration, coordination results in the assembly of polymer **6.1P** with an increasing DP. This material has limited solubility in the

chloroform:DMSO mixture used for fluorescent measurements leading to aggregation, which was visually observed in the samples by clouding and formation of a precipitate. We have previously investigated cruciform aggregates and polymorphs in the solid-state observing differences in their emissive behavior,<sup>18</sup> and we attribute the red-shifted emission to 515 nm at 2 equivalents of **6.2** from both the LUMO stabilization and aggregation effects. This conclusion is further supported by the solid-state emission of **6.1P** at 520 nm (dropcast film from a 1:2 mixture of **6.1** and **6.2**, Figure 6.9). However, upon the addition of 15 equivalents of **6.2**, an excess of pincer complex, the formation of smaller end-capped oligomers, *e.g.* **6.2-6.1-6.2** complexes, is favored. Unlike the highly charged polymer **6.1P**, these smaller species are soluble in CHCl<sub>3</sub>, and therefore the emission appears at a slightly lower wavelength (485 nm) from the initial uncoordinated cruciform. This is similar to the emission observed from the soluble model complex formed upon the addition of monotopic **6.5** to **6.1** (491 nm) solely representing the emission change from the stabilization of the LUMO after self-assembly.

We observed a similar trend for the self-assembly of **6.2P**, detecting a bathochromic shift (455→560 nm) during the beginning stages of the titration of pincer complex **6.2** (3.6 equivalents) into **6.3** (Figure 6.10); further addition of **6.2** (20.0 equivalents) results in a blue-shift (560→512 nm). Once again, we see a substantial bathochromic shift resulting from complexation with **6.2** as well as aggregation of the growing polymers. This results in a red-shifted emission similar to that observed for **6.2P** in the solid state (544 nm). Addition of 20 equivalents of **6.2** leads to the formation of soluble oligomers emitting at 512 nm. Again this is comparable to the emission observed upon the addition of monotopic **6.5** (507 nm) to **6.3** (Figure 6.11).

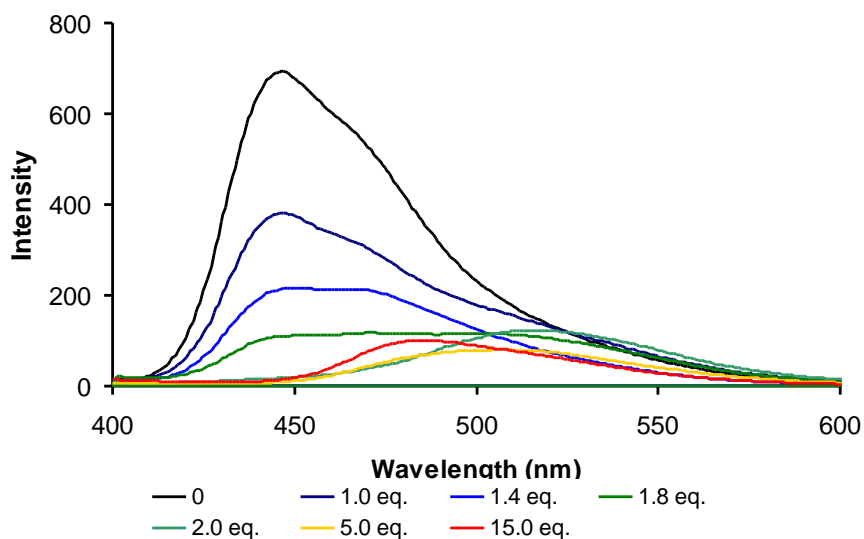


**Figure 6.7.** Emission spectra of **6.1** upon the addition of increasing equivalents of **6.2**. Selected traces are included here for the sake of clarity.

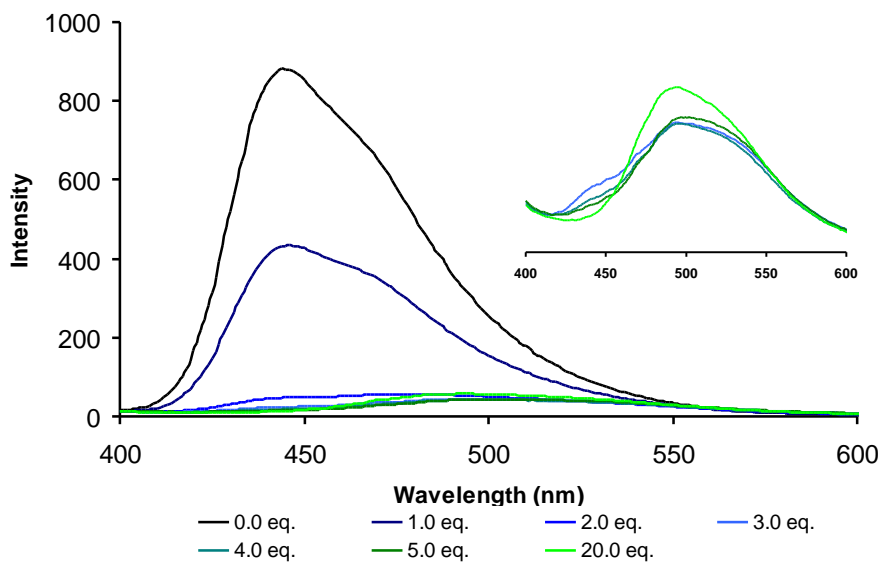


**Figure 6.8.** Emission spectra of **6.1** upon the addition of increasing equivalents of mono-Pd-pincer **6.5**. Selected traces are included here for the sake of clarity.

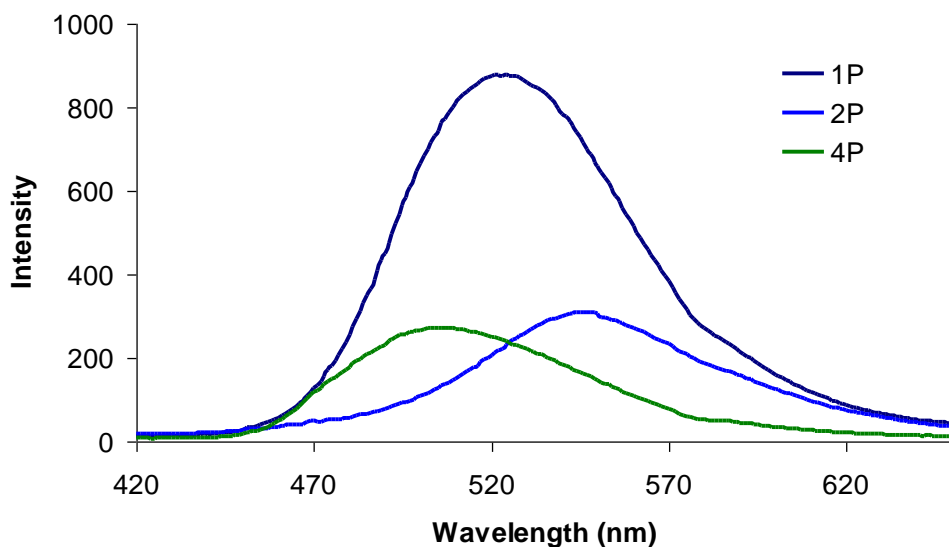


**Figure 6.9.** Emission of thin films of polymers **6.1P**, **6.2P**, and **6.4P** after the baseline-subtraction of a glass slide.

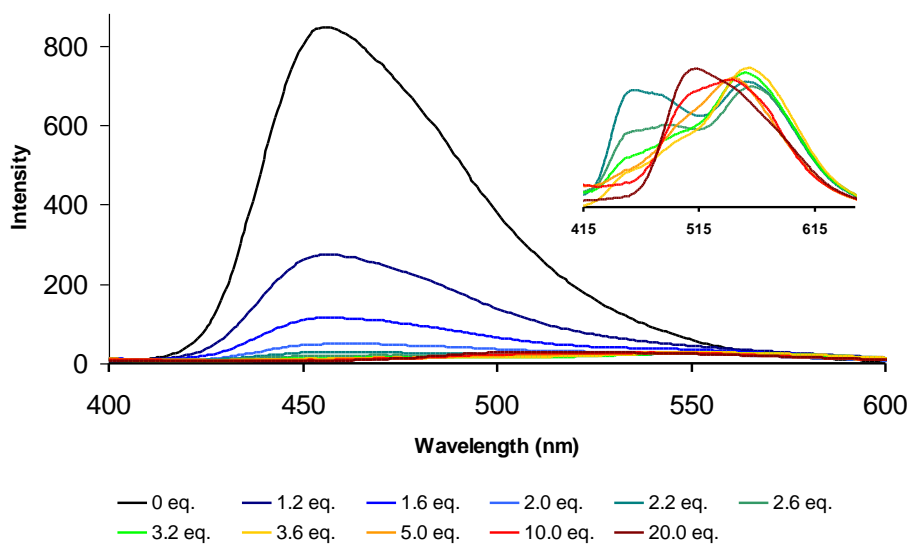


**Figure 6.10.** Emission spectra of **6.3** upon the addition of increasing equivalents of **6.2**. Selected traces are included here for the sake of clarity.

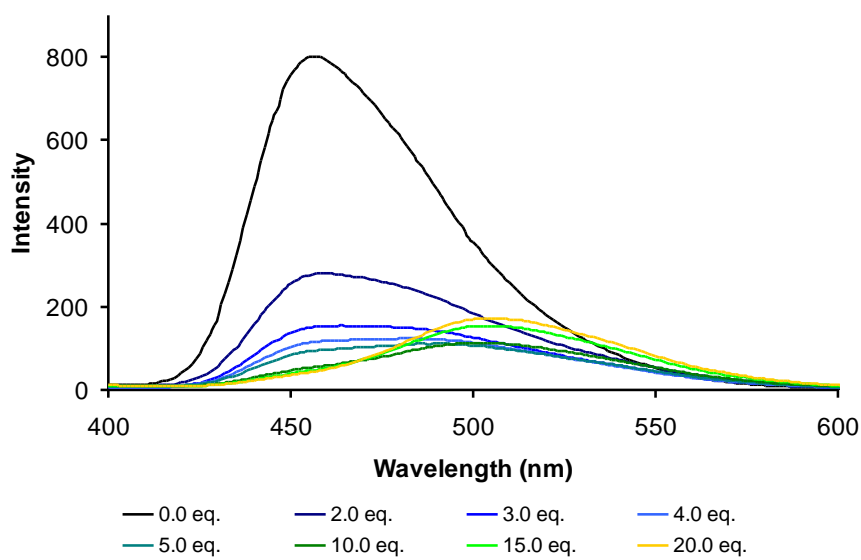


**Figure 6.11.** Emission spectra of **6.3** upon the addition of increasing equivalents of mono-Pd-pincer **6.5**. Selected traces are included here for the sake of clarity.

Changes in the optical properties of **6.1** and **6.3** are also observed upon assembly with bis-Pt pincer complex **6.4**. In the case of **6.3**, a bathochromic shift (455→510 nm) is observed upon the addition of 3.0 equivalents of **6.4** (Figure 6.12). This emission is consistent with the observed solid state emission of 504 nm. Further addition of **6.4** (15.0 equivalents) results in a small blue-shift (510→504 nm) corresponding to short-chain soluble oligomers. This emission is consistent with the emission observed for the model complex formed from cruciform **6.3** and monotopic Pt pincer **6.6** (515 nm, Figure 6.13). Assembly of **1** with **4** also resulted in a bathochromic shift (445–542 nm) upon the addition of 1.4 equivalents of **4** (Figure 6.14). However, further fluorescence measurements at higher equivalents of pincer complex could not be made due to near baseline fluorescence intensity. Limited intensity also prevented the measurement of the solid state emission of **3P**.

The decrease in fluorescence intensity observed upon the self-assembly of each material also occurred in other cruciform coordination studies. We previously demonstrated that upon exposure to protons or metal cations, cruciforms **6.1** and **6.3** experience a sharp decrease in fluorescence quantum yield.<sup>16</sup> This effect is greater for protonation than for binding to metal cations, suggesting that a greater positive charge at the pyridine nitrogen result in a greater decrease in fluorescence intensity. We suggest that binding of a proton or metal at the pyridyl nitrogen results in a stronger vibronic coupling between the ground and excited states, in addition the heavy atom effect exerted by the Pt-pincer complex. Therefore, as the binding increases, non-radiative relaxation pathways from the excited state to the ground state become more accessible resulting in a decreased fluorescence intensity.

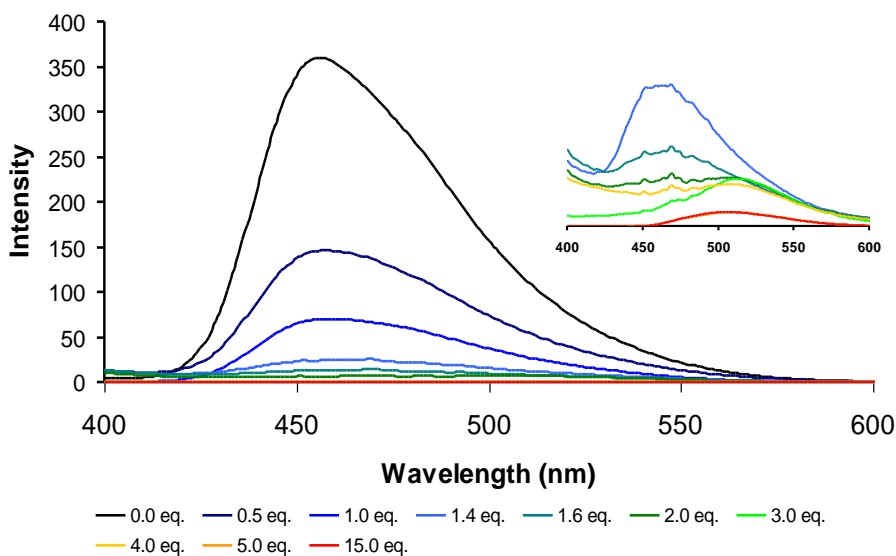


**Figure 6.12.** Emission spectra of **6.3** upon the addition of increasing equivalents of **6.4**. Selected traces are included here for the sake of clarity.

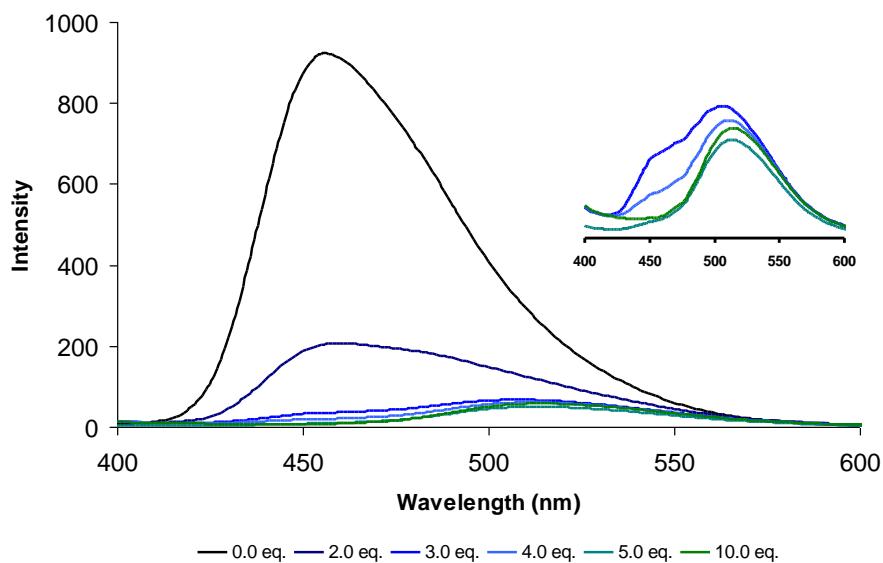


**Figure 6.13.** Emission spectra of **6.3** upon the addition of increasing equivalents of mono-Pt-pincer **6.6**. Selected traces are included here for the sake of clarity.

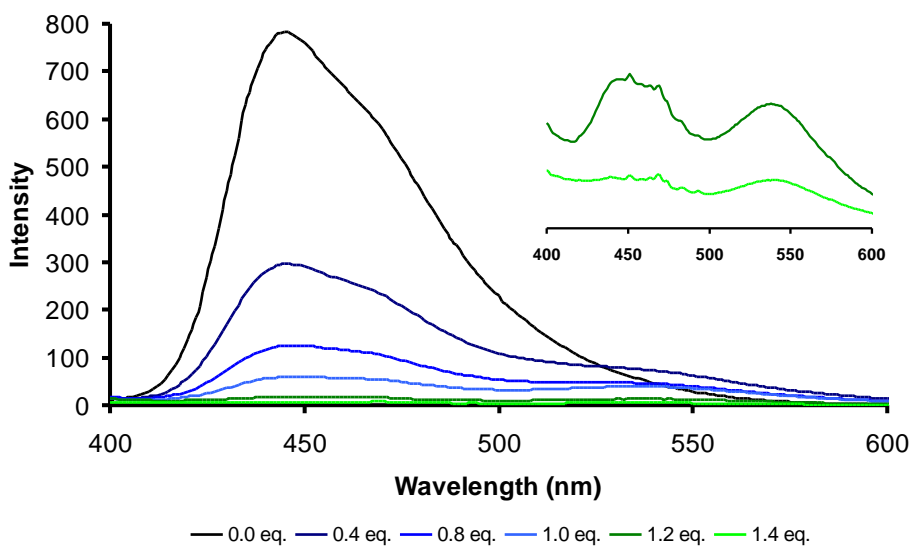


**Figure 6.14.** Emission spectra of **6.1** upon the addition of increasing equivalents of **6.4**. Selected traces are included here for the sake of clarity. Residual fluorescence was observed at 542 nm upon further addition of **6.4**; however, it could not be measured due to near baseline fluorescence intensity.

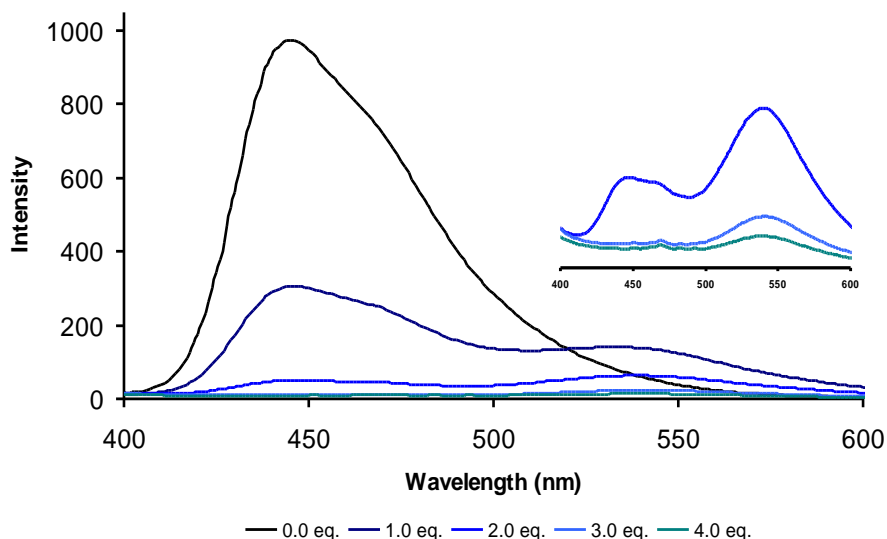


**Figure 6.15.** Emission spectra of **6.1** upon the addition of increasing equivalents of mono-Pt-pincer **6.6**. Selected traces are included here for the sake of clarity.

### 6.3. Conclusions

In summary we have assembled four new supramolecular polymers by coordinating pyridyl functionalized cruciforms **6.1** and **6.3** to either a ditopic bis-Pd or bis-Pt pincer complex. The fast and quantitative self-assembly process was characterized by  $^1\text{H}$  NMR spectroscopy, and the association strength of each metal-ligand interaction was evaluated using ITC. From these values, approximate degrees of polymerization were calculated. This data indicate that the pyridyl distyryl-Pt coordination is the strongest and the pyridyl ethynyl-Pd interaction is the weakest. The polymeric properties in solution were characterized using viscometry, the results from which complement the association strengths calculated from ITC, in which **6.3P** is the most viscous and **6.2P** is the least viscous. Finally, the luminescent properties were measured using fluorescence spectroscopy. The emissions of the supramolecular materials were significantly red-

shifted from their uncoordinated cruciforms. The fluorescence intensity increased in the order **6.3P** < **6.1P** < **6.2P** < **6.4P**, *inversely proportional to their association strength*.

By developing, expanding, and studying the building blocks available for self-assembly, the strategy employed herein allows for the design and synthesis of a class of novel functional organometallic polymers with predictable and tunable properties from a discrete set of monomers, circumventing problems associated with traditional covalent polymer synthesis. Each component in this system is amenable to further functionalizations and modification giving us a virtually unlimited pool of monomers to investigate and exploit.

Future work in this area could focus on coordinating and investigating cruciforms with different substitution patterns to expand the physical and optical property ranges in the final polymers. Additionally, efforts should focus on improving the fluorescence quantum yields and solubility of the polymers via synthetic modifications to both monomeric constituents.

This work has been published in *Chemistry – A European Journal* and *Chemical Communications*:

Gerhardt, W. W.; Zuccherro, A. J.; South, C. R.; Bunz, U. H. F.; Weck, M. Controlling polymeric properties through dynamic metal-ligand interactions: Supramolecular cruciforms made easy. *Chem. Eur. J.* **2007**, *13*, 4467-4474.

Gerhardt, W. W.; Zuccherro, A. J.; Wilson, J. N.; South, C. R.; Bunz, U. H. F.; Weck, M. Supramolecular cruciforms. *Chem. Commun.* **2006**, 2141-2143.

## 6.4. Experimental

**General Methods.** All chemicals were purchased from Aldrich Chemical, Acros, or Fisher Scientific and used as received unless otherwise specified. NMR spectra were recorded at 298 K on a Varian Mercury spectrometer ( $^1\text{H}$  = 300 MHz,  $^{13}\text{C}$  NMR = 75 MHz). Chemical shifts are reported in parts per million (ppm), using residual solvent as an internal standard. Data reported as follows: chemical shift, multiplicity (s = singlet, d = doublet, t = triplet, q = quartet, dd = doublet of doublets, m = multiplet, br = broad), coupling constants, and integration. The synthesis of XFs and metallated pincer complexes was conducted according to previously

**General procedures for ITC characterization of coordination complexes.** All measurements were made on a Microcal VP-ITC Microcalorimeter at 22 °C in anhydrous DMF degassed under reduced pressure.

**Bis-metallated pincer complex:cruciform.** The bis-metallated pincer complex in DMF (10 mM) was titrated (5  $\mu\text{L}$  injections over 10 sec followed by an equilibration period) into a DMF solution of the cruciform (1 mM). A reference run of each bis-metallated pincer complex solution titrated into pure DMF was subtracted from each measurement to account for the heat of dilution. Each experiment was done in triplicate to validate all  $K_a$  values.

**Monotopic pincer complex:cruciform.** The monotopic metallated pincer complex in DMF (20 mM) was titrated (5  $\mu\text{L}$  injections over 10 sec followed by an equilibration period) into a DMF solution of the cruciform (1 mM). A reference run of each monotopic metallated pincer complex solution titrated into pure DMF was subtracted from each measurement to account for the heat of dilution. Each experiment was done in

triplicate to validate all  $K_a$  values. The reverse addition was also carried out to corroborate the data by titrating a DMF cruciform solution (10 mM) into a DMF monotopic metallated pincer complex solution (1 mM) under identical conditions.

**Bis-metallated pincer complex:pyridine.** The bis-metallated pincer complex solution in DMF (10 mM) was titrated (5  $\mu$ L injections over 10 sec followed by an equilibration period) into a DMF solution of anhydrous pyridine (1 mM). A reference run of each bis-metallated pincer complex solution titrated into pure DMF was subtracted from each measurement to account for the heat of dilution. Each experiment was done in triplicate to validate all  $K_a$  values. The reverse addition was also carried out to corroborate the data by titrating a DMF anhydrous pyridine solution (20 mM) into a DMF bis-metallated pincer complex solution (1 mM) under identical conditions.

**Viscometry.** All studies were carried out in HPLC grade DMF, in a Cannon-Ubbelohde semi-micro type viscometer No. 100 L182, timed with a stopwatch at 25 °C. Initial solutions of each supramolecular material (0.033 mM) at a 1:1 stoichiometric ratio were prepared by dissolving 0.033  $\mu$ mol of each component in DMF (1 mL) in the viscometer, sonicating the sample for 10 min, incubating it for 10 min, and then acquiring three efflux times. Then the solution within the viscometer was diluted to 0.025, 0.018, 0.012, and 0.006 mM; between each measurement of these concentrations, the solutions were equilibrated and the efflux times measured in triplicate.

**Optical Spectra.** All samples for spectroscopic measurement were prepared using spectroscopic grade solvents purchased from OmniSolv. All fluorescence spectra were recorded on a Shimadzu RF-5301PC spectrofluorophotometer and acquired in a triangular quartz cuvette to minimize spectral artifacts (specifically self absorption).

Solutions were mixed such that the final concentration of cruciform in all samples measured was 0.0445 mM in a mixture of CHCl<sub>3</sub> and DMSO (95:5) as described below. All solution volumes were measured using Eppendorf *Reference* variable volume pipettors. Significant noise was present due to near baseline fluorescence intensity in some cases. In addition, scattering peaks were present. A spectra of the triangular cuvette filled with solvent was obtained and subtracted to minimize scattering artifacts. Corrected and uncorrected spectra are included in the Supporting Information of Reference 25.

**Procedure for the preparation of XF 6.1:bis-Pd-pincer 6.2 solutions for fluorescence spectroscopy.** A stock solution of **6.1** (1.78 mM) was prepared by dissolving **6.1** (106.2 mg, 0.178 mmol) in CHCl<sub>3</sub> (100.0 mL). A stock solution of bis-Pd-pincer **6.2** (0.0177 M) was prepared by dissolving **6.2** (92.0 mg, 0.086 mmol) in 5.0 mL DMSO. Individual solutions were then prepared as outlined in Table 6.4.

**Table 6.4.** Preparation of spectroscopic solutions of **6.1•6.2**.

Equivalents of <b>6.2</b>	Stock Solution <b>6.1</b> (μL)	Stock Solution <b>6.2</b> (μL)	DMSO (μL)	CHCl <sub>3</sub> (μL)
0.0	100	0	200	3700
1.0	100	10	190	3700
1.4	100	14	186	3700
1.6	100	16	184	3700
1.8	100	18	182	3700
2.0	100	20	180	3700
3.0	100	30	170	3700
4.0	100	40	160	3700
5.0	100	50	150	3700
10.0	100	100	100	3700
15.0	100	150	50	3700
20.0	100	200	0	3700

**Procedure for the preparation of XF 6.3:bis-Pd-pincer 6.2 solutions for fluorescence spectroscopy.** A stock solution of **6.3**(1.78 mM) was prepared by dissolving **6.3** (101.0 mg, 0.178 mmol) in CHCl<sub>3</sub> (100.0 mL). A stock solution of bis-Pd-pincer **6.2** (0.0177 M) was prepared by dissolving **6.2** (92.0 mg, 0.086 mmol) in 5.0 mL DMSO. Individual solutions were then prepared as outlined in Table 6.5.

**Table 6.5.** Preparation of spectroscopic solutions of **6.3•6.2**.

Equivalents of <b>6.2</b>	Stock Solution <b>6.3</b> (μL)	Stock Solution <b>6.2</b> (μL)	DMSO (μL)	CHCl <sub>3</sub> (μL)
0.0	100	0	200	3700
1.0	100	10	190	3700
1.2	100	12	188	3700
1.6	100	16	184	3700
2.0	100	20	180	3700
2.2	100	22	178	3700
2.6	100	26	174	3700
3.0	100	30	170	3700
3.2	100	32	168	3700
3.6	100	36	164	3700
4.0	100	40	160	3700
5.0	100	50	150	3700
10.0	100	100	100	3700
15.0	100	150	50	3700
20.0	100	200	0	3700

**Procedure for the preparation of XF 6.1:bis-Pt-pincer 6.4 solutions for fluorescence spectroscopy.** A stock solution of XF **6.1** (1.78 mM) was prepared by dissolving **6.1** (106.2 mg, 0.178 mmol) in CHCl<sub>3</sub> (100.0 mL). A stock solution of bis-Pt-pincer **6.4** (0.0177 M) was prepared by dissolving **6.4** (95.7 mg, 0.086 mmol) in 5.0 mL DMSO. Individual solutions were then prepared as outlined in Table 6.6.

**Procedure for the preparation of XF 6.3:bis-Pd-pincer 6.4 solutions for fluorescence spectroscopy.** A stock solution of **6.3**(1.78 mM) was prepared by dissolving **6.3** (101.0 mg, 0.178 mmol) in CHCl<sub>3</sub> (100.0 mL). A stock solution of bis-Pt-pincer **6.4** (0.0177 M) was prepared by dissolving **6.4** (95.7 mg, 0.086 mmol) in 5.0 mL DMSO. Individual solutions were then prepared as outlined in Table 6.7.

**Table 6.6.** Preparation of spectroscopic solutions of **6.1•6.4**.

Equivalents of <b>6.4</b>	Stock Solution <b>6.1</b> (μL)	Stock Solution <b>6.4</b> (μL)	DMSO (μL)	CHCl <sub>3</sub> (μL)
0.0	100	0	200	3700
0.4	100	4	196	3700
0.8	100	8	192	3700
1.0	100	10	190	3700
1.2	100	12	188	3700
1.4	100	14	186	3700
2.0	100	20	180	3700
3.0	100	30	170	3700
4.0	100	40	160	3700
5.0	100	50	150	3700
10.0	100	100	100	3700
15.0	100	150	50	3700
20.0	100	200	0	3700

**Table 6.7.** Preparation of spectroscopic solutions of **6.3•6.4**.

Equivalents of <b>6.4</b>	Stock Solution <b>6.3</b> (μL)	Stock Solution <b>6.4</b> (μL)	DMSO (μL)	CHCl <sub>3</sub> (μL)
0.0	100	0	200	3700
0.5	100	5	195	3700
1.0	100	10	190	3700
1.4	100	14	186	3700
1.6	100	16	184	3700
1.8	100	18	182	3700
2.0	100	20	180	3700
3.0	100	30	170	3700
4.0	100	40	160	3700
5.0	100	50	150	3700
10.0	100	100	100	3700
15.0	100	150	50	3700
20.0	100	200	0	3700

**Procedure for the preparation of XF 6.1:mono-Pd-pincer 6.5 solutions for fluorescence spectroscopy.** A stock solution of cruciform **6.1** (1.78 mM) was prepared by dissolving **6.1** (106.2 mg, 0.178 mmol) in CHCl<sub>3</sub> (100.0 mL). A stock solution of mono-Pd-pincer **6.5** (0.0177 M) was prepared by dissolving **6.5** (51.9 mg, 0.086 mmol) in 5.0 mL DMSO. Individual solutions were then prepared as outlined in Table 6.8.

**Table 6.8.** Preparation of spectroscopic solutions of **6.1•6.5**.

Equivalents of <b>6.5</b>	Stock Solution <b>6.1</b> (μL)	Stock Solution <b>6.5</b> (μL)	DMSO (μL)	CHCl <sub>3</sub> (μL)
0.0	100	0	200	3700
1.0	100	10	190	3700
2.0	100	20	180	3700
3.0	100	30	170	3700
4.0	100	40	160	3700
5.0	100	50	150	3700
20.0	100	200	0	3700

**Procedure for the preparation of XF 6.1:mono-Pt-pincer 6.6 solutions for fluorescence spectroscopy.** A stock solution of **6.1** (1.78 mM) was prepared by dissolving **6.1** (106.2 mg, 0.178 mmol) in CHCl<sub>3</sub> (100.0 mL). A stock solution of mono-Pt-pincer **6.6** (0.0177 M) was prepared by dissolving **6.6** (62.6 mg, 0.086 mmol) in 5.0 mL DMSO. Individual solutions were then prepared as outlined in Table 6.9.

**Table 6.9.** Preparation of spectroscopic solutions of **6.1•6.6**.

Equivalents of <b>6.6</b>	Stock Solution <b>6.1</b> (μL)	Stock Solution <b>6.6</b> (μL)	DMSO (μL)	CHCl <sub>3</sub> (μL)
0.0	100	0	200	3700
1.0	100	10	190	3700
2.0	100	20	180	3700
3.0	100	30	170	3700
4.0	100	40	160	3700

**Procedure for the preparation of XF 6.3:mono-Pd-pincer 6.5 solutions for fluorescence spectroscopy.** A stock solution of **6.3** (1.78 mM) was prepared by dissolving **6.3** (101.0 mg, 0.178 mmol) in CHCl<sub>3</sub> (100.0 mL). A stock solution of mono-Pd-pincer **6.5** (0.0177 M) was prepared by dissolving **6.5** (51.9 mg, 0.086 mmol) in 5.0 mL DMSO. Individual solutions were then prepared as outlined in Table 6.10.

**Table 6.10.** Preparation of spectroscopic solutions of **6.3•6.5**.

Equivalents of <b>6.5</b>	Stock Solution <b>6.3</b> (μL)	Stock Solution <b>6.5</b> (μL)	DMSO (μL)	CHCl <sub>3</sub> (μL)
0.0	100	0	200	3700
2.0	100	20	180	3700
3.0	100	30	170	3700
4.0	100	40	160	3700
5.0	100	50	150	3700
10.0	100	100	100	3700
15.0	100	150	50	3700
20.0	100	200	0	3700

**Procedure for the preparation of XF 6.3:mono-Pt-pincer 6.6 solutions for fluorescence spectroscopy.** A stock solution of cruciform **6.3** (1.78 mM) was prepared by dissolving **6.3** (101.0 mg, 0.178 mmol) in CHCl<sub>3</sub> (100.0 mL). A stock solution of mono-Pt-pincer **6.6** (0.0177 M) was prepared by dissolving **6.6** (62.6 mg, 0.086 mmol) in 5.0 mL DMSO. Individual solutions were then prepared as outlined in Table 6.11.

**Solid-State Emission Spectra.** Solid-state emission spectra were obtained for **1P**, **2P**, and **4P** (spectra for **3P** could not be obtained due to baseline fluorescence intensity). Solutions were dropcast onto glass slides and dried under a flow of air. Emission spectra were acquired on a Shimadzu RF-5301PC spectrofluorophotometer. The spectra of the glass slides were subtracted to remove minor scattering effects.

**Table 6.11.** Preparation of spectroscopic solutions of **6.3•6.6**.

Equivalents of <b>6.6</b>	Stock Solution <b>6.3</b> ( $\mu\text{L}$ )	Stock Solution <b>6.6</b> ( $\mu\text{L}$ )	DMSO ( $\mu\text{L}$ )	$\text{CHCl}_3$ ( $\mu\text{L}$ )
0.0	100	0	200	3700
2.0	100	20	180	3700
3.0	100	30	170	3700
4.0	100	40	160	3700
5.0	100	50	150	3700
10.0	100	100	100	3700

**Solution Photographs.** Photographs were taken of the solutions used for optical measurements to qualitatively demonstrate the changes in fluorescence observed upon assembly. The concentration of cruciform in all samples measured was 0.0445 mM in a mixture of  $\text{CHCl}_3$  and DMSO (95:5). Photographs were taken under illumination at 365 nm using a Canon EOS 30D digital camera equipped with a Canon EFS 18-55mm zoom lens. These solution photographs are published in the Supporting Information of Reference 25.

## 6.5. References and Notes

1. Wegner, K.; Müllen, K. *Electronic Materials: The Oligomer Approach*. **1996**, Wiley-VCH, Weinheim, Germany.
2. Kraft, A.; Grimsdale, A. C.; Holmes, A. B. Electroluminescent conjugated polymers - Seeing polymers in a new light. *Angew. Chem. Int. Ed.* **1998**, *37*, 402-428.
3. Dimitrakopoulos, C. D.; Malenfant, P. R. L. Organic thin film transistors for large area electronics. *Adv. Mater.* **2002**, *14*, 99-117.
4. Mitschke, U.; Bäuerle, P. The electroluminescence of organic materials. *J. Mater. Chem.* **2000**, *10*, 1471-1507.
5. Shirota, Y. Organic materials for electronic and optoelectronic devices. *J. Mater. Chem.* **2000**, *10*, 1-25.

6. McCullough, R. D. The chemistry of conducting polythiophenes. *Adv. Mater.* **1998**, *10*, 93-116.
7. Friend, R. H.; Gymer, R. W.; Holmes, A. B.; Burroughes, J. H.; Marks, R. N.; Taliani, C.; Bradley, D. D. C.; Dos Santos, D. A.; Brédas, J.-L.; Lögdlund, M.; Salaneck, W. R. Electroluminescence in conjugated polymers. *Nature* **1999**, *397*, 121-128.
8. Dobrawa, R.; Lysetska, M.; Ballester, P.; Grüne, M.; Würthner, F. Fluorescent supramolecular polymers: Metal directed self-assembly of perylene bisimide building blocks. *Macromolecules* **2005**, *38*, 1315-1325.
9. Dankers, P. Y. W.; Harmsen, M. C.; Brouwer, L. A.; Van Luyn, M. J. A.; Meijer, E. W. A modular and supramolecular approach to bioactive scaffolds for tissue engineering. *Nature Mater.* **2005**, *4*, 568-574.
10. Chang, M. H.; Hoeben, F. J. M.; Jonkheijm, P.; Schenning, A. P. H. J.; Meijer, E. W.; Silva, C.; Herz, L. M. Influence of mesoscopic ordering on the photoexcitation transfer dynamics in supramolecular assemblies of oligo-p-phenylenevinylene. *Chem. Phys. Lett.* **2006**, *418*, 196-201.
11. Iyer, P. K.; Beck, J. B.; Weder, C.; Rowan, S. J. Synthesis and optical properties of metallo-supramolecular polymers. *Chem. Commun.* **2005**, 319-321.
12. Knapton, D.; Rowan, S. J.; Weder, C. Synthesis and properties of metallo-supramolecular poly(*p*-phenylene ethynylene)s. *Macromolecules* **2006**, *39*, 651-657.
13. Beck, J. B.; Ineman, J. M.; Rowan, S. J. Metal/ligand-induced formation of metallo-supramolecular polymers. *Macromolecules* **2005**, *38*, 5060-5068.
14. Kokil, A.; Yao, P.; Weder, C. Organometallic networks based on 2,2'-bipyridine-containing poly(*p*-phenylene ethynylene)s. *Macromolecules* **2005**, *38*, 3800-3807.
15. Wilson, J. N.; Bunz, U. H. F. Switching of intermolecular charge-transfer in cruciforms: metal ion sensing. *J. Am. Chem. Soc.* **2005**, *127*, 4124-4125.
16. Zuccherro, A. J.; Wilson, J. N.; Bunz, U. H. F. Cruciforms as functional fluorophores: response to protons and selected metal ions. *J. Am. Chem. Soc.* **2006**, *128*, 11872-11881.
17. Wilson, J. N.; Hardcastle, K. I.; Josowicz, M.; Bunz, U. H. F. Synthesis and electronic properties of bis-styryl substituted trimeric arylenethynylenes. Comparison of cruciforms with *iso*-cruciforms. *Tetrahedron.* **2004**, *60*, 7157-7167.

18. Wilson, J. N.; Smith, M. D.; Enkelmann, V.; Bunz, U. H. F. Cruciform  $\pi$ -systems: effect of aggregation on emission. *Chem. Commun.* **2004**, 1700-1701.
19. Hauck, M.; Schönhaber, J.; Zuccherro, A. J.; Hardcastle, K. I.; Müller, T. J. J.; Bunz, U. H. F. Phenothiazine cruciforms: synthesis and metallochromic properties. *J. Org. Chem.* **2007**, *72*, 6714-6725.
20. Wilson, J. N.; Josowicz, M.; Wang, Y.; Bunz, U. H. F. Cruciform  $\pi$ -systems: hybrid phenylene-ethynylene/phenylene-vinylene oligomers. *Chem. Commun.* **2003**, 2962-2963.
21. Brombosz, S. M.; Zuccherro, A. J.; Phillips, R. L.; Vazquez, D.; Wilson, A.; Bunz, U. H. F. Terpyridine-based cruciform-Zn<sup>2+</sup> complexes as anion-responsive fluorophores. *Org. Lett.* **2007**, *22*, 4519-4522.
22. McGrier, P. L.; Solntsev, K. M.; Miao, S.; Tolbert, L. M.; Miranda, O. R.; Rotello, V. M.; Bunz, U. H. F. Hydroxycruciforms: amine-responsive fluorophores. *Chem. Eur. J.* **2008**, *14*, 4503-4510.
23. McGrier, P. L.; Solntsev, K. M.; Schönhaber, J.; Brombosz, S. M.; Tolbert, L. M.; Bunz, U. H. F. Hydroxy-cruciforms. *Chem. Commun.* **2007**, 2127-2129.
24. Tolosa, J.; Zuccherro, A. J.; Bunz, U. H. F. Water-soluble cruciforms: Response to protons and selected metal ions. *J. Am. Chem. Soc.* **2008**, *130*, 6498-6506.
25. Gerhardt, W. W.; Zuccherro, A. J.; South, C. R.; Bunz, U. H. F.; Weck, M. Controlling polymeric properties through dynamic metal-ligand interactions: Supramolecular cruciforms made easy. *Chem. Eur. J.* **2007**, *13*, 4467-4474.
26. Gerhardt, W. W.; Zuccherro, A. J.; Wilson, J. N.; South, C. R.; Bunz, U. H. F.; Weck, M. Supramolecular cruciforms. *Chem. Commun.* **2006**, 2141-2143.
27. van Manen, H.-J.; Nakashima, K.; Shinkai, S.; Kooijman, H.; Spek, A. L.; van Veggel, F. C. J. M.; Reinhoudt, D. N. Coordination chemistry of SCS Pd-II pincer systems. *Eur. J. Inorg. Chem.* **2000**, 2533-2540.
28. Pollino, J. M.; Weck, M. Supramolecular side-chain functionalized polymers: Synthesis and self-assembly behavior of polynorbornenes bearing (PdSCS)-S-II pincer complexes. *Synthesis* **2002**, 1277-1285.
29. Pollino, J. M.; Stubbs, L. P.; Weck, M. One-step multifunctionalization of random copolymers via self-assembly. *J. Am. Chem. Soc.* **2004**, *126*, 563-567.
30. Pollino, J. M.; Weck, M. Tandem catalysis and self-assembly: A one-pot approach to functionalized polymers. *Org. Lett.* **2002**, *4*, 753-756.

31. Higley, M. N.; Pollino, J. M.; Hollembeak, E.; Weck, M. A modular approach toward block copolymers. *Chem. Eur. J.* **2005**, *11*, 2946-2953.
32. Huck, W. T. S.; Van Veggel, F. C. J. M.; Reinhoudt, D. N. Self-assembly of hyperbranched spheres. *J. Mater. Chem.* **1997**, *7*, 1213-1219.
33. Huck, W. T. S.; Prins, L. J.; Fokkens, R. H.; Nibbering, N. M. M.; van Veggel, F. C. J. M.; Reinhoudt, D. N. Convergent and divergent noncovalent synthesis of metallodendrimers. *J. Am. Chem. Soc.* **1998**, *120*, 6240-6246.
34. Stiriba, S.-E.; Slagt, M. Q.; Kautz, H.; Gebbink, R. J. M. K.; Thomann, R.; Frey, H.; van Koten, G. Synthesis and supramolecular association of immobilized NCN-pincer platinum(II) complexes on hyperbranched polyglycerol supports. *Chem. Eur. J.* **2004**, *10*, 1267-1273.
35. Kersey, F. R.; Yount, W. C.; Craig, S. L. Single-molecule force spectroscopy of bimolecular reactions: System homology in the mechanical activation of ligand substitution reactions. *J. Am. Chem. Soc.* **2006**, *128*, 3886-3887.
36. Friggeri, A.; van Manen, H.-J.; Auletta, T.; Li, X.-M.; Zapotoczny, S.; Schönherr, H.; Vancso, G. J.; Huskens, J.; van Veggel, F. C. J. M.; Reinhoudt, D. N. Chemistry on surface-confined molecules: An approach to anchor isolated functional units to surfaces. *J. Am. Chem. Soc.* **2001**, *123*, 6388-6395.
37. Gerhardt, W. W.; Weck, M. Investigations of metal-coordinated peptides as supramolecular synthons. *J. Org. Chem.*, **2006**, *71*, 6333-6341.
38. Guillena, G.; Rodríguez, G.; Albrecht, M.; van Koten, G. Covalently bonded platinum(II) complexes of alpha-amino acids and peptides as a potential tool for protein labeling. *Chem. Eur. J.* **2002**, *8*, 5368-5376.
39. Guillena, G.; Rodríguez, G.; van Koten, G. Palladium(II) pincer complexes of alpha-amino acids: towards the synthesis of catalytically active artificial peptides. *Tetrahedron Lett.* **2002**, *43*, 3895-3898.
40. Albrecht, M.; van Koten, G. Platinum group organometallics based on "Pincer" complexes: Sensors, switches, and catalysts. *Angew. Chem. Int. Ed.* **2001**, *40*, 3750-3781.
41. Slagt, M. Q.; Rodríguez, G.; Grutters, M. M. P.; Gebbink, R. J. M. K.; Klopper, W.; Jenneskens, L. W.; Lutz, M.; Spek, A. L.; van Koten, G. Synthesis and properties of para-substituted NCN-pincer palladium and platinum complexes. *Chem. Eur. J.* **2004**, *10*, 1331-1344.

42. Loeb, S. J.; Shimizu, G. K. H. Dimetallated thioether complexes as building blocks for organometallic coordination polymers and aggregates. *J. Chem. Soc., Chem. Commun.* **1993**, 1395-1397.
43. Loeb, S. J.; Shimizu, G. K. H.; Wisner, J. A. Mono- versus dipalladation of the durene-based tetrathioether ligand 1,2,4,5-(tBuSCH(2))(4)C<sub>6</sub>H<sub>2</sub> center dot structures of [PdCl((tBuSCH(2))(4)C<sub>6</sub>H)] and [Pd-2((tBuSCH(2))(4)C-6)(MeCN)(2)][BF<sub>4</sub>](2). *Organometallics* **1998**, *17*, 2324-2327.
44. Steenwinkel, P.; James, S. L.; Grove, D. M.; Kooijman, H.; Spek, A. L.; van Koten, G. Double cyclometalation via carbon-silicon bond cleavage by palladium(II) acetate. X-ray structure of a cationic 1,4-dipalladated benzene ring and selective synthesis of heterobimetallic 1,4-phenylene-bridged platinum(II)-palladium(II) complexes. *Organometallics* **1997**, *16*, 513-515.
45. Steenwinkel, P.; Kooijman, H.; Smeets, W. J. J.; Spek, A. L.; Grove, D. M.; van Koten, G. Intramolecularly stabilized 1,4-phenylene-bridged homo- and heterodinuclear palladium and platinum organometallic complexes containing N,C,N-coordination motifs; eta 1-SO<sub>2</sub> coordination and formation of an organometallic arenium ion complex with two Pt-C sigma-bonds. *Organometallics* **1998**, *17*, 5411-5426.
46. Brown, H. C.; Okamoto, Y. Directive effects in aromatic substitution .30. Electrophilic substituent constants. *J. Am. Chem. Soc.* **1958**, *80*, 4979-4987.
47. Yount, W. C.; Loveless, D. M.; Craig, S. L. Small-molecule dynamics and mechanisms underlying the macroscopic mechanical properties of coordinatively cross-linked polymer networks. *J. Am. Chem. Soc.* **2005**, *127*, 14488-14496.
48. The directionally opposite shift of the  $\alpha$ -pyridyl cruciform signal observed in the <sup>1</sup>H NMR spectrum upon coordination to the bis-Pd pincer complex **2** relative to the shift after coordination to the bis-Pt pincer complex **4** is a result of an overlap of the pyridyl protons with the thiophenyl ring currents of the bis-Pd pincer complex **2**, see reference 27.
49.  $DP \approx (K[\text{monomer}])^{1/2}$
50. Ciferri, A. Supramolecular polymerizations. *Macromol. Rapid Commun.* **2002**, *23*, 511-529.
51. Dobraawa, R.; Würthner, F. Metallosupramolecular approach toward functional coordination polymers. *J. Polym. Sci., Part A: Polym. Chem.* **2005**, *43*, 4981-4995.
52. Owing to the highly dilute CHCl<sub>3</sub>/DMSO solvent mixture we did not observe the expected polymerization at a metal/ligand stoichiometry of 1:1. Putative high-molecular-weight polymers, which precipitated out of solution were not seen until an

excess of the pincer complex was titrated into the cruciform solution. As the  $K_a$  value increased, precipitation of the respective complex occurred closer to the expected 1:1 stoichiometry.

## CHAPTER 7

### Cruciform-Silica Hybrid Materials

#### 7.1. Introduction

Functional chromophores and fluorophores are attractive as sensory and responsive materials in biology, materials science, organic electronics and analytical chemistry.<sup>1</sup> For deployment in biological applications such as the targeted staining of cell compartments, water soluble fluorophores appended with binding elements are highly desirable and necessary. To enable charge transport for applications in organic electronics, chromophores/fluorophores must be capable of forming high quality, ordered thin films. For many environmental and biodiagnostic sensory applications, it is desirable if the fluorophores or chromophores utilized for analysis are immobilized – temporarily or permanently – on a solid support. Such solid supports can either be just a scaffold for the dye(s) under consideration, or they can perform secondary functions such as suppressing aggregation/excimer formation or aiding in preconcentration of analytes. An elegant example of this approach is the work by Rakow and Suslick, who investigated the response of an array of immobilized porphyrin dyes towards a battery of different analytes.<sup>2</sup> The success of their colorimetric approach was rooted in the immobilization of their dyes onto hydrophobic silanized silica gel which helped to pre-concentrate gaseous or liquid analytes either from the gas phase or from the aqueous phase onto their solid support, where it could react with the dye under consideration.

As fluorophore cores possessing spatially separated FMOs, 1,4-distyryl-2,5-bisarylethynylbenzenes<sup>3-5</sup> display exceptionally large red or blue shifts in absorption and

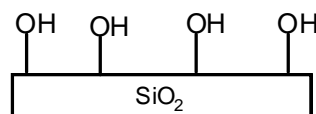
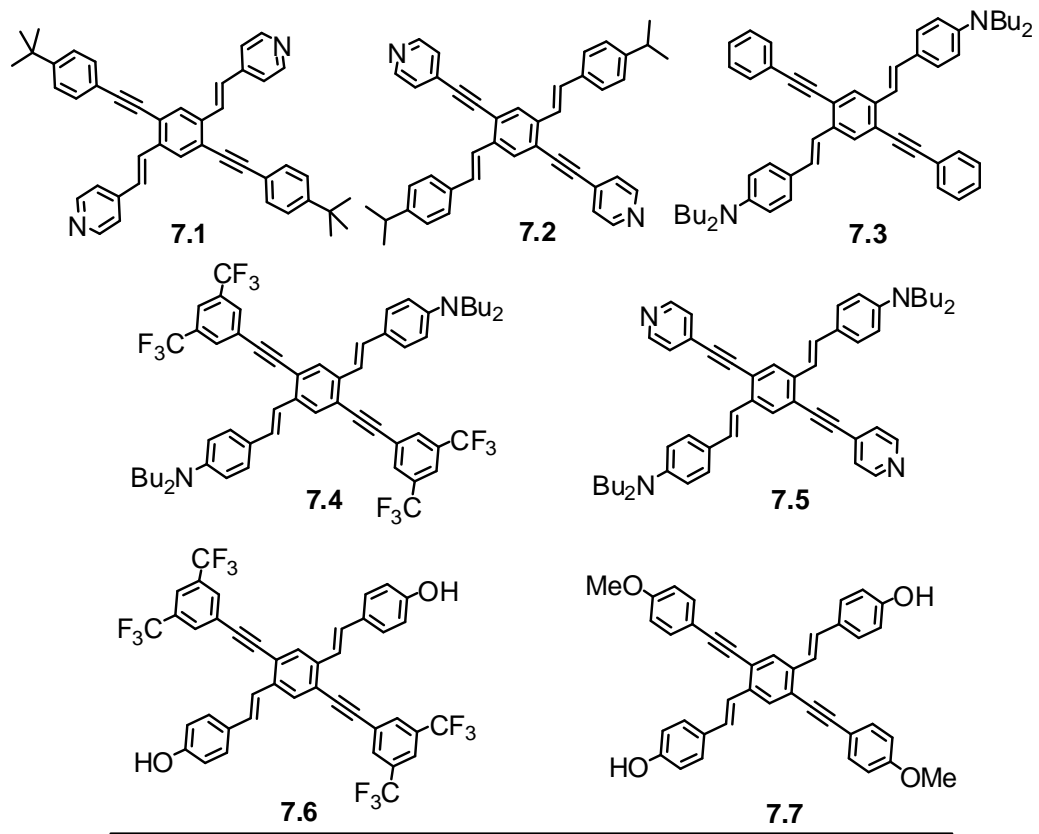
emission upon exposure to acids or metal salts. Specifically, coordination of metal cations to XFs results in either red- or blue-shifted emission if pyridines or dialkylanilines are incorporated.<sup>3a,b</sup> If both are present, a two-stage mechanism, where there is first a blue shift followed by a red shift is observed that results from the complexation of an XF such as **7.5** with increasing amounts of zinc or magnesium ions. If we incorporate hydroxyl groups into the  $\pi$ -system of these functional fluorophores, we observe fluorescence shifts upon deprotonation. These compounds can also serve as fluorescent probes for the differentiation of amine bases.<sup>5</sup>

We elected to examine the interaction of XFs **7.1-7.7** with mesoporous SBA-15 silica materials **A-D** containing acidic sites (**A**), basic sites (**B**), hydrophobic trimethylsilyl sites (**C**), and bare, unfunctionalized silica containing silanols (**D**) (Scheme 7.1). We investigate the resulting cruciform-silica hybrid materials by optical and fluorescent spectroscopies. It was of great interest to examine the interactions between the various XFs and the different mesoporous silica samples, establish what emission responses would be observed, whether support of XFs on silica would allow the XFs to maintain their fluorescence properties in the solid state, and if these solid-state adsorbed XFs could be used to detect amines or organic acids in the gas phase.

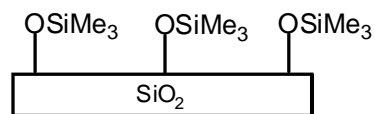
## **7.2. Results and Discussion**

### **7.2.1. Synthesis of mesoporous silica supports.**

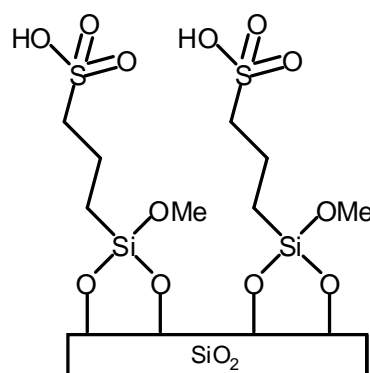
Mesoporous silica SBA-15 was identified as a good candidate for a porous host material.<sup>6</sup> SBA-15 can be easily prepared via block copolymer templating methods and the size of the mesopores can be controlled. In this work, SBA-15 with an average pore



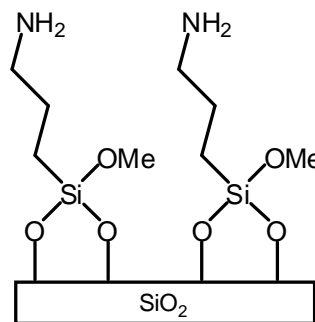
Bare Silica (D)



Capped Silica (C)  
Loading (mmol/g) = 1.030



Sulfonic Acid Silica (A)  
Loading (mmol/g) = 0.030



Basic Silica (B)  
Loading (mmol/g) = 1.458

**Scheme 7.1.** Structure of XFs **7.1-7.7** and a schematic representation of the surface functionality of silicas **A-D**.

diameter of 57 Å and a surface area of ~700 m<sup>2</sup>/g was prepared via standard methods.<sup>7</sup> After calcination to remove the block copolymer template, the material was functionalized by standard silane grafting techniques to introduce Lewis basic aminopropyl groups,<sup>8</sup> Brønsted acidic sulfonic acid groups,<sup>9</sup> or hydrophobic trimethylsilyl groups.<sup>10</sup> Changes in surface properties were verified by nitrogen physisorption and thermogravimetric analysis.

### **7.2.2. Spectroscopic properties of the cruciforms 7.1-7.7 in the presence of microstructured functionalized silica supports.**

XF<sub>s</sub> 7.1-7.7 emit vibrantly in organic solutions. We have detailed their sensory responses towards metal cations, protons, and amines.<sup>3a-b, 5</sup> Emissions of the XF<sub>s</sub> in the solid state are generally red shifted, broadened, and less intense, limiting their potential use as sensory materials in the solid state (Figure 7.1). A possible method to overcome these limitations is to employ the fluorophore immobilized on a solid support for potential environmental and biodiagnostic applications. Solid supports serve as scaffolds for the dye(s) under consideration; they may also suppress aggregation/excimer formation or preconcentrate analytes.

XF<sub>s</sub> 7.1-7.7 were dissolved in toluene and dry mesoporous silica was added. The resulting suspensions were incubated in the dark for 24 hours, at which point the samples were photographed under UV light (ex = 365 nm) to qualitatively examine the resulting fluorescence of the cruciform-silica hybrid materials. As Figure 7.2 shows, the solid silica settled to the bottom of the vials and was highly fluorescent. To more quantitatively assess the fluorescent of these XF-silica hybrid materials, we recorded the fluorescence spectra of suspensions of these hybrid materials in toluene using a triangular

cuvette to minimize scattering (Figure 7.3 and Table 7.1). When compounds **7.1-7.7** are exposed to capped silica, the emission of the XF-silica hybrids ranges from 424 (XF 7) to 548 (XF 4) nm. In addition, the intensity and shape of the observed emissions are reminiscent of those observed in solution, not those observed in the solid state. Thus, mesoporous SBA-15 silica appears to be a promising platform to enhance and/or modulate XF fluorescence.

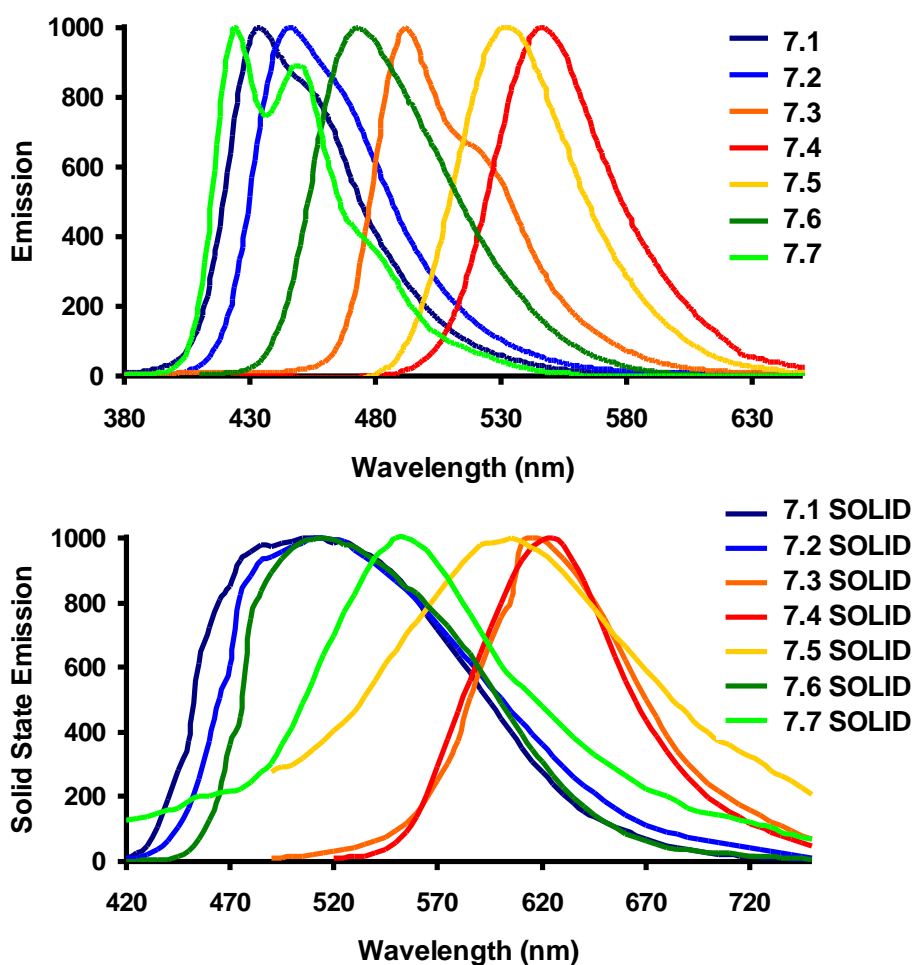


**Figure 7.1.** Normalized emission spectra of **7.1-7.7** in toluene (top) and the solid state (bottom). In the solid state, spectra are broadened, redshifted, and of dramatically decreased intensity compared to in solution. Spectra of XFs in the solid state are noisy due to scattering off of the powdered solid as well as relatively low fluorescence intensity.

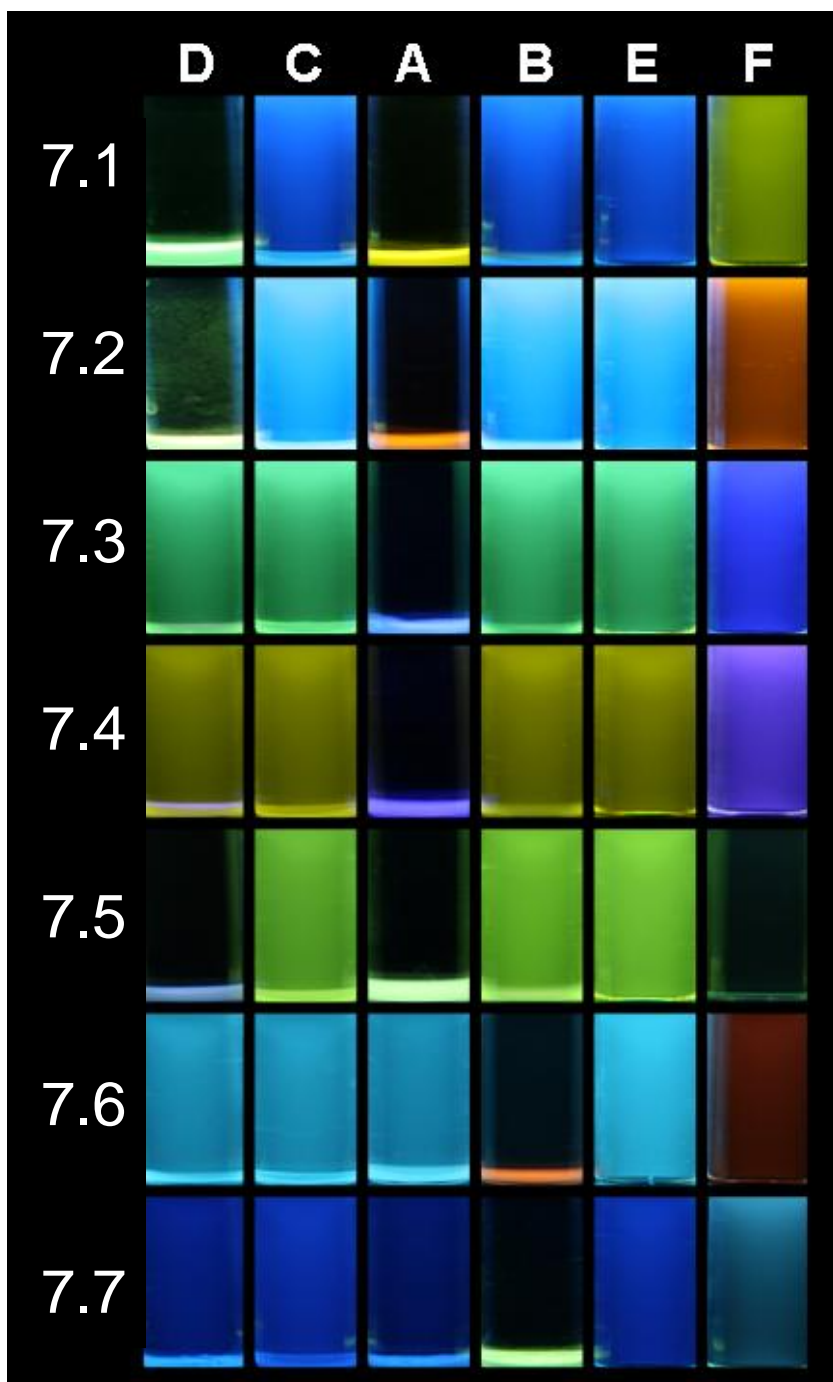


**Figure 7.2.** Vials containing XFs **7.1-7.7** in toluene incubated with silicas (**D** = Bare silica, **C** = Capped Silica, **A** = Acidic Silica, **B** = Basic Silica) for 24 hours. For comparison, column **F** shows XFs **7.1-7.7** in toluene exposed to trifluoroacetic acid (**7.1-7.5**) or *n*-hexylamine (**7.6, 7.7**). Column **E** shows XFs **7.1-7.7** in a toluene solution. Photos were taken under blacklight (ex = 365 nm) and photographed using a Canon EOS Digital Camera equipped with an EFS 18-55mm lens.

**Table 7.1.** Tabulated emission data of XFs **7.1-7.7** in the solid state, solution, and complexed with functionalized silica. For reference, emissions of **7.1-7.7** upon exposure to trifluoroacetic acid and n-hexylamine in toluene solution are included. All  $\lambda_{\text{max}}$  emission values are reported in nm.

XF	Solid	Toluene	Bare	Capped	Acidic	Basic	TFA	Hexylamine
<b>7.1</b>	515	434	508	434	537	434	530	n/a
<b>7.2</b>	515	446	513	446	555	446	555	n/a
<b>7.3</b>	615	492	426, 492	492	427	492	424	n/a
<b>7.4</b>	625	547	428, 547	548	433	546	432	n/a
<b>7.5</b>	605	531	468	531	523	531	532	n/a
<b>7.6</b>	515	473	475	475	473	476, 550	n/a	561
<b>7.7</b>	550	424	425	424	426	513	n/a	454, 497

XF<sub>s</sub> **7.1-7.5** – all of which possess Lewis base moieties – show large shifts in fluorescence upon exposure to acidic silica. These shifts can be rationalized by assuming protonation of **7.1-7.5** occurs upon exposure to the sulfonic acid moieties present on these silica particles. We have previously established that upon donor and/or acceptor substitution, XF<sub>s</sub> can display spatially separated FMOs. In the case of **7.1** and **7.2**, the LUMO is localized primarily on the acceptor-substituted axis of the molecule while the HOMO resides on the ‘non-substituted’ branch of the XF. Upon protonation of the pyridine, the LUMO is stabilized while the HOMO remains largely unaffected, resulting in large bathochromic shifts in **7.1** (434 to 537 nm) and **7.2** (446 to 555 nm) in emission (Figure 7.4, A).

In the case of **7.3** and **7.4**, we observe large hypsochromic shifts upon protonation. Upon incubation with acidic silica, we observe blue shifts in the emission of **7.3** (492 to 427 nm) and **7.4** (547 to 433 nm). This is a consequence of the FMO structure of these donor/acceptor-substituted XF<sub>s</sub>. In XF<sub>s</sub> **7.3** and **7.4**, the HOMO is

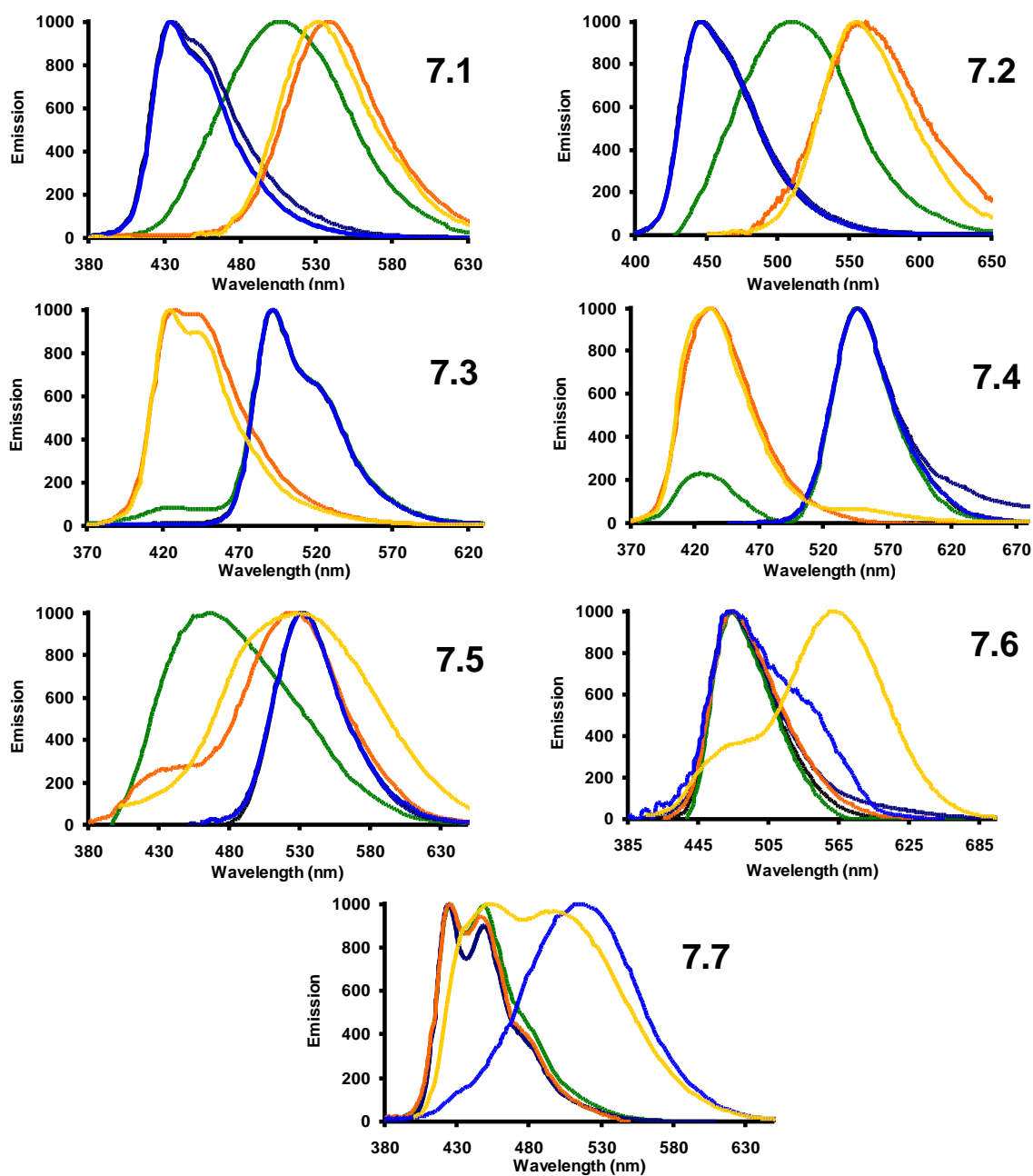


**Figure 7.3.** Normalized emission spectra of **7.1-7.7** supported on bare (green), capped (dark blue), acidic (orange), and basic (light blue) silica. For comparison, the emission of XFs **7.1-7.7** in toluene (black), **7.1-7.5** with trifluoroacetic acid (yellow), and **7.6-7.7** with *n*-hexylamine (yellow) are shown in black. Spectra were taken of the suspended silica particles in toluene using a triangular cuvette. Emission maxima are shown in Table 7.1.

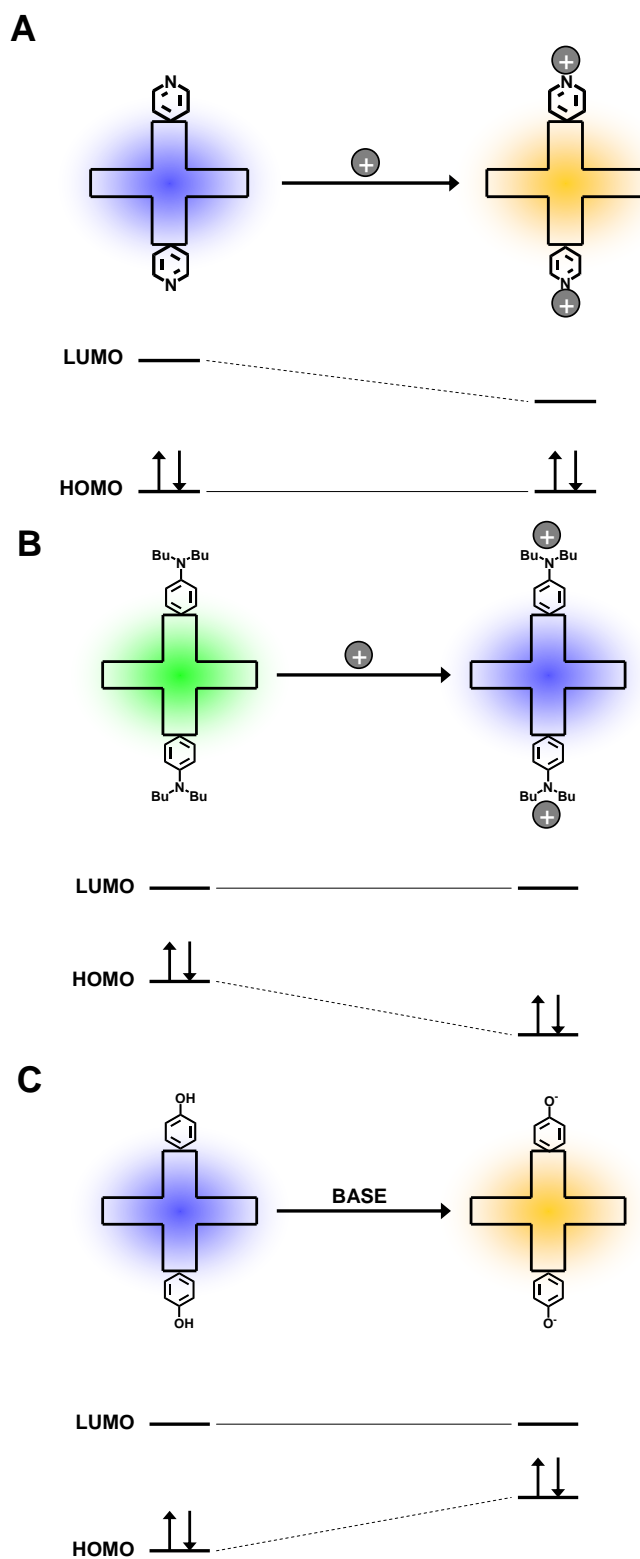


**Figure 7.4.** Schematic representation of the effect of protonation upon the FMOs and emission of XFs **7.1** (A, top left) and **7.3** (B, top right). C (bottom) shows the effect of deprotonation on the FMOs and emission of **7.6**.

localized on the electron-rich distyryl axis of the XF while the LUMO lies on the arylolethynyl arms. Protonation of the alkyylaniline functionalities stabilizes the HOMO while the LUMO remains unaffected, resulting in a blue shift (Figure 7.4, B).

We also observe a small blue shift (531-523 nm) upon incubation of **7.5** with acidic silica. We are able to rationalize this slight blue shift as the consequence of the two-stage fluorescence response previously observed upon reaction of **7.5** with trifluoroacetic acid.<sup>3a-b</sup> In the case of **7.5**, the HOMO lies on the donor-substituted distyryl axis of **7.5**, while the LUMO is localized primarily on the arylolethynyl branch of the XF. Upon exposure to acidic silica, the protonation of all four nitrogens stabilizes both the HOMO and the LUMO, resulting in a slight net blue shift. As the digital photograph indicates, the toluene supernatant was completely non-fluorescent upon incubation of **7.1-7.5** with **A**, presumably because the acidic support adsorbs all the basic XFs from solution. In all cases, the emissions observed for complexes of **7.1-7.5** with **A** are similar to emissions recorded upon addition of excess trifluoroacetic acid to **7.1-7.5**; **7.6** and **7.7** show no change in emission upon exposure to **A**. This can be rationalized by assuming that the hydroxy functionalities present in these XFs do not react with the acidic functional groups of the silica particles. As a result, the emission of the resulting composites are roughly identical to the emissions observed upon complexation with capped silica.

Upon exposure of **7.1-7.7** to basic silica, an opposite response is observed. The composites of Lewis basic substituted XFs **7.1-7.5** with basic silica **B** display the same emission as **7.1-7.5** with **C**. This is readily rationalized by assuming that the basic surface functionality of **B** does not interact with these XFs and affect the photophysics of

**7.1-7.5.** In the case of **7.6** and **7.7**, the chromophores possess hydroxy substituents which interact with the amino-functionalized surface of **B**. We have previously reported that hydroxy-functionalized XFs such as **7.6** and **7.7** can display shifts in emission upon exposure to amines and other bases. Similar effects are observed here upon complexation of **7.6** and **7.7** with **B**. Reaction with **B** deprotonates the hydroxy functionalities, destabilizing the HOMO of **7.6** and **7.7** while the LUMO remains relatively unperturbed (Figure 7.4, C). As a result, bathochromic shifts are observed upon complexation of hydroxy-functionalized XFs with **B**. In the case of **7.6**, a large redshift is readily visible in Figure 2; this is observed as a large shoulder in the emission of **7.6•B** centered near 550 nm. Some of the unreacted XF **7.6** also remains in the silica, which appears dominant due to the relatively low emission intensity of the sample as well as the higher quantum yield of the blue species relative to the red species. Upon exposure of **7.7** to **B**, we observe a similar redshift from 424 nm to 513 nm.

Complexation of XFs **7.1-7.7** with bare silica **D** also generates fluorescent hybrid materials. The surface chemistry of **D** is mildly acidic; therefore, one might expect to observe similar responses to those observed for the sulfonic acid functionalized silica **A**. Upon exposure of **7.6** and **7.7** to bare silica, solids are formed which retain the fluorescence of **7.6** and **7.7** in solution. As in the case of **A**, no large shifts in emission are observed upon formation of **7.6•D** and **7.7•D**. In the case of the complex of **7.3** with **D**, we observe little change in emission qualitatively. Spectroscopic examination of **7.3•D** reveals a small amount of a blueshifted species present in the hybrid material at 426 nm, corresponding to the emission of the protonated XF **7.3**. However, the majority of the XF is deposited in the complex as the native unprotonated **7.3**, responsible for the

dominant emission at 492 nm. A similar result is observed in the case of **7.4•D**. Here we observe a dominant emission at 547 nm originating from unprotonated **7.4**; however, a small blueshifted band is observed at 428 nm, contributed by protonated **7.4**.

Upon reaction of XF **7.5**, containing both alkylamino substituents and pyridyl substituents, with bare silica particles, we observe a large hypsochromic shift from 531 nm to 468 nm. This emission is attributed to the bisprotonated state of **7.5** and is consistent with the emission observed in previous titrations of **7.5** with trifluoroacetic acid. When **7.1** and **7.2** are exposed to bare silica, bathochromic shifts are observed upon formation of hybrids **7.1•D** and **7.2•D**. In the case of **7.1**, a shift from 434 to 508 nm is observed; in **7.2**, the emission shifts from 446 to 513 nm. These bathochromic shifts are consistent with an interaction which stabilizes the LUMOs of the XFs while leaving the HOMOs unperturbed (i.e. protonation); however, the magnitude of the shift is considerably smaller in both cases as compared with shifts observed upon addition of sulfonic-acid functionalized silica or trifluoroacetic acid. We attribute this to hydrogen bond formation rather than true protonation. It is interesting to note that while the alkylamino functionalities are considerably more basic than the pyridine moieties, the experimental results suggest that protonation of the pyridine nitrogens in **7.1•D** and **7.2•D** appears more favorable than protonation of the alkylamino nitrogens in **7.3•D** and **7.4•D**. We attribute this to the steric effects of the dibutyl chains which limit the interaction of the aniline nitrogens with the silica surface.

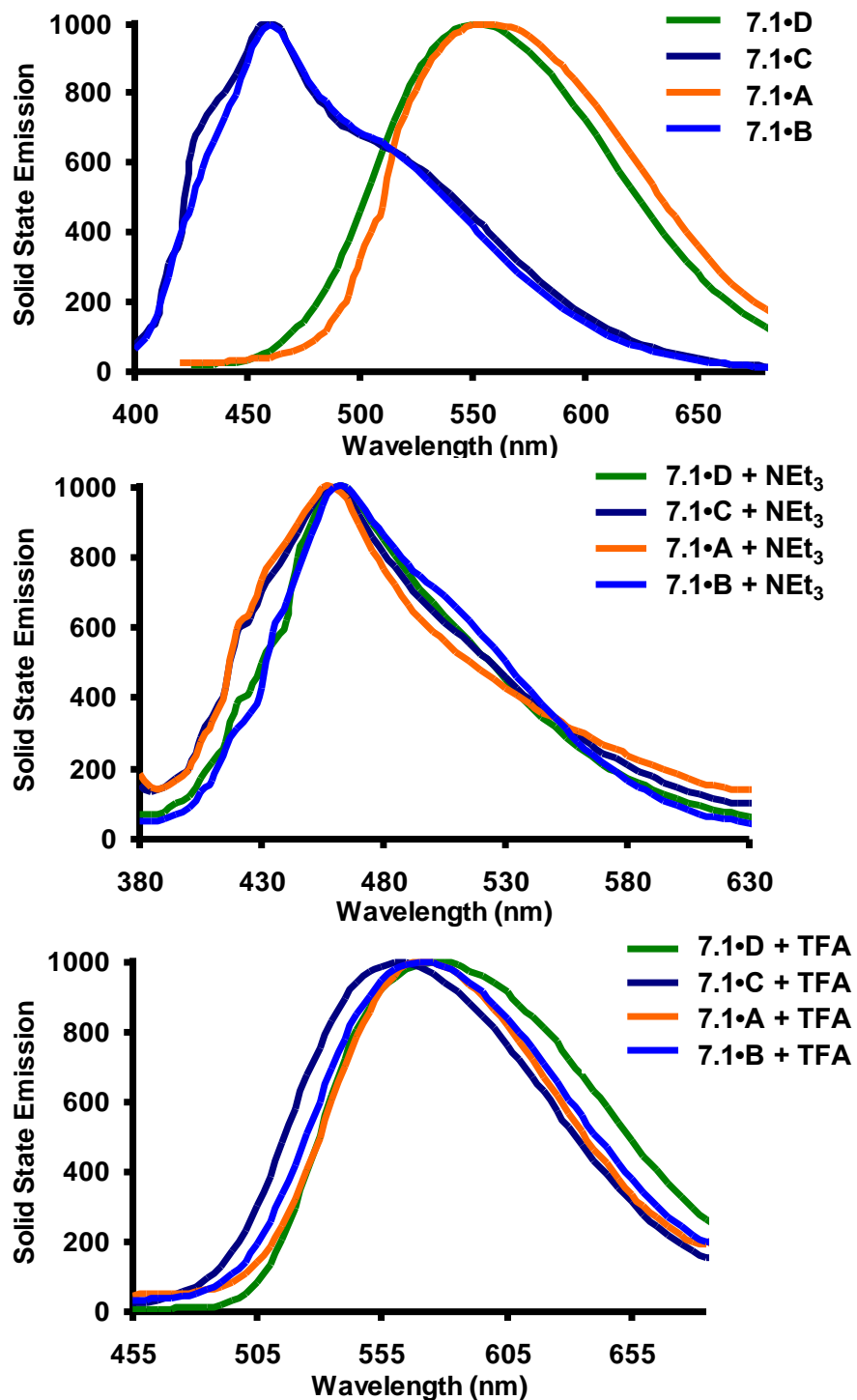


**Figure 7.5.** Fluorescence response of 7.1 supported on functionalized silica scaffold upon exposure to vapor analytes. The top spectra displays the emission of 7.1 supported on bare (green), capped (dark blue), acidic (orange), and basic (blue) silicas. Upon exposure to  $\text{NEt}_3$  (middle) and trifluoroacetic acid (bottom) vapors, notable fluorescence responses are observed.

### **7.2.3. Sensory responses of XF-functionalized silica microstructures towards representative volatile organic compounds (VOCs).**

Functionalized mesoporous silica microstructures provide an attractive platform for the solid-phase support of XFs. We were anxious to assess the potential of these fluorophores to respond to the presence of vapor-phase analytes. We exposed **7.1** supported on all four functionalized silicas to representative vapor phase analytes of interest. This proof-of-principle sensing experiment was conducted using dried XF-silica hybrids. After incubation of the desired XF dye with the functional silica scaffold of choice, evaporation of the solvent in vacuo yields dry, vibrantly fluorescent solids (Figure 7.5, A).

Figure 7.5 shows the responses observed upon exposure of **7.1** (A) to triethylamine (B) and trifluoroacetic acid (C) vapors. In the dry solid state, the hybrid materials resulting from the exposure of XF **7.1** to both basic and capped silica display emissions of approximately 460 nm. Incorporation of **7.1** into/onto bare and acidic particles generates materials with emissions of 550 and 555 nm respectively. Upon exposing these solids to  $\text{NEt}_3$  vapors for five minutes, large hypsochromic shifts in the emission of the acidic and bare hybrid materials are observed while the emission of the capped and basic materials remain largely unchanged; the result is nearly identical emissions of between 460 and 465 nm for all materials. Upon exposure to trifluoroacetic acid, a large red shift in the emission of the capped and basic hybrid materials is observed. However, the emission of the acidic and bare composites remain largely intact, resulting similar emissions – ranging from 560 to 580 nm – in all four cases.

These responses can be rationalized by considering the protonation states of XF **7.1** when deposited on silica scaffolds and when exposed to vapor-phase analytes. The emissions of hybrids **7.1•C** and **7.1•B** centered at 460 nm indicate the presence of the nonprotonated XF **7.1**. Emissions of 550 and 555 nm recorded for **7.1•D** and **7.1•A** respectively correspond to the expected protonated form of **7.1**. Upon exposure to ambient  $\text{NEt}_3$  vapors, we observe large bathochromic shifts in **7.1•A** and **7.1•D** while the emissions of the capped and basic hybrids remain unchanged; after exposure, the emissions of all four species appear between 460 and 465 nm. This can be explained by assuming exposure to  $\text{NEt}_3$  vapor causes the deprotonation of **7.1** supported in/on **7.1•A** and **7.1•D**, restoring their emission to the native form. A similar but opposite effect is observed upon exposure to trifluoroacetic acid vapors. Upon exposure, the bathochromic shift is observed in the case of **7.1•B** (460-570 nm) and **7.1•C** (460-560 nm) while acidic and bare hybrids of **7.1** remain unchanged. This finding is consistent with the protonation of **7.1** in the basic and capped hybrids, resulting in the observed redshift in these samples.

The shifts observed upon exposure of these XF-silica hybrids are not readily reversed upon incubation of the reacted solids under a flow of air. Over 1 hour, no reversal of these shifts is observed in the emission spectra of the reacted hybrids. In this application, the silica scaffolds serve two functions. First, the porous particles preserve the desirable solution properties of the XFs in the solid state hybrids, rendering them potentially useful for a wider variety of environmental and biodiagnostic assays. In addition, the functionality of these particles modulates the photophysics of the XFs as

well as their reactivity towards the simple VOCs employed in this proof-of-principle assay.

### 7.3. Conclusions

Microstructured mesoporous silica possessing varied functionalities were successfully employed as scaffolds for the support of XFs. Whereas crystalline XFs frequently display weak emission in the solid state, immobilization of XFs in/on these particles yields solids which retain the highly fluorescent character of the parent cruciforms. Functionality integrated into the silica scaffold can be utilized to modulate the photophysical behavior of the incorporated dyes. The resulting XF-silica hybrid materials display reactivity towards representative amines and organic acids which is modulated by the functionalization present on the silica scaffold. Future contributions will more thoroughly examine the potential of silica-supported XFs – as well as the hybrid materials generated from the XFs metallated and protonated analogues – as fluorescent dyes for the detection of a variety of volatile organic compounds. Such materials may prove useful in the future development of fluorescent differential sensory arrays for the detection of VOCs in the gas phase as well as in aqueous solution.

This work has been published in *Chemistry – An Asian Journal*:

Zucchero, A. J.; Shiels, R. A.; McGrier, P. L.; To, M. A.; Jones, C. W.; Bunz, U. H. F. Cruciform-Silica Hybrid Materials. *Chem. Asian. J.* **2009**, *4*, 262-269.

### 7.4. Experimental

**General Methods.** All chemicals were purchased from Aldrich Chemical, Acros, TCI America, or Fischer Scientific and used without purification unless otherwise specified. Column chromatography was performed using Standard Grade silica gel 60 Å, 32-63 µm

(230 x 450 mesh) from Sorbent Technologies and the indicated eluent. Elution of cruciforms was readily monitored using a handheld UV lamp (365 nm). Melting points were obtained using a Mel-Temp apparatus fitted with a Fluke 51K/J digital thermometer. All IR spectra were obtained using a Simadzu FTIR-8400s spectrometer. Unless otherwise specified, NMR spectra were recorded at 298 K on a Varian Mercury spectrometer (300 MHz). Chemical shifts are reported in parts per million (ppm), using residual solvent (chloroform-*d*) as an internal standard. Data Reported as follows: chemical shift, multiplicity (s = singlet, d = doublet, t = triplet, q = quartet, m = multiplet), coupling constant, and integration. Mass spectral analyses were provided by the Georgia Institute of Technology Mass Spectrometry Facility.

All absorption spectra were collected using a Shimadzu UV-2401PC spectrophotometer. The emission spectra of solutions and suspensions were acquired using a Shimadzu RF-5301PC spectrofluorophotometer or a PTI QuantaMaster spectrofluorophotometer outfitted with a xenon arc lamp and series 814 PMT detector. To minimize scattering, spectra of silica suspensions were obtained using a triangular cuvette. Scattering peaks were removed by subtracting a fluorescence spectra of suspended silica with no added fluorophores from all spectra. Solid state emission spectra of XFs and dried functionalized silica materials were acquired using a Spectra Max M2 plate reader from Molecular Devices.

**Synthesis of Mesoporous Silica Materials.** SBA-15 was prepared similarly to reported literature procedures.<sup>7</sup> A copolymer template of poly(ethylene oxide)-block-poly(propylene oxide)-block-poly(ethylene oxide) (18 g) was dissolved in a solution of  $\text{CHCl}_3$  (103.5 g) and deionized water (477 g). Tetraethyl orthosilicate (38.4 g) was added

to the solution which was subsequently stirred for 20 h at 35 °C, heated to 80 °C, and held for 24 h at 80 °C. At the end of this period, the reaction was quenched with deionized water, and the solid was filtered and washed with several portions of deionized water to remove residual copolymer and give SBA-15 as a white powder. The material was dried for 3 h at 50 °C and then calcined as follows: ramp to 200 °C at 1.2 °C/min, hold at 200 °C for 1 h, ramp to 550 °C at 1.2 °C/min, and hold at 550 °C for 6 h. The calcined SBA-15 was then heated under vacuum at 200 °C for three hours and yielded approximately 12 g of SBA 15. Nitrogen physisorption experiments showed the material to have a BET surface area of 687 m<sup>2</sup>/g and a BJH adsorption pore diameter of 57 Å.

**Synthesis of capped SBA-15.** In order to remove surface silanol groups and reduce surface acidity, 1,1,1,3,3,3-hexamethyldisilazane (1.0 g) was added to a solution of calcined SBA 15 (1.0 g) in hexanes. The solution was stirred overnight and then filtered. The solid material was washed with copious amounts of hexanes and dried under vacuum at 50 °C. Thermogravimetric analysis indicated a capping of 1.6 mmol silanols/g SiO<sub>2</sub>. Nitrogen physisorption experiments showed the material to have a BET surface area of 332 m<sup>2</sup>/g and a BJH adsorption pore diameter of 49 Å.

**Synthesis of sulfonic acid functionalized SBA-15.** The sulfonic acid functionalized SBA-15 was prepared similarly to reported literature procedures.<sup>8</sup> 3-mercaptopropyltrimethoxysilane (1.0 g) was added to a solution of calcined SBA 15 (1.0 g) in toluene. The solution was stirred overnight and then filtered. The solid material was washed with copious amounts of toluene and hexanes and dried under vacuum at 50 °C. Thermogravimetric analysis indicated a loading of 0.57 mmol SH/g SiO<sub>2</sub>. The residual surface silanols groups on the thiol functionalized SBA-15 were capped by adding the

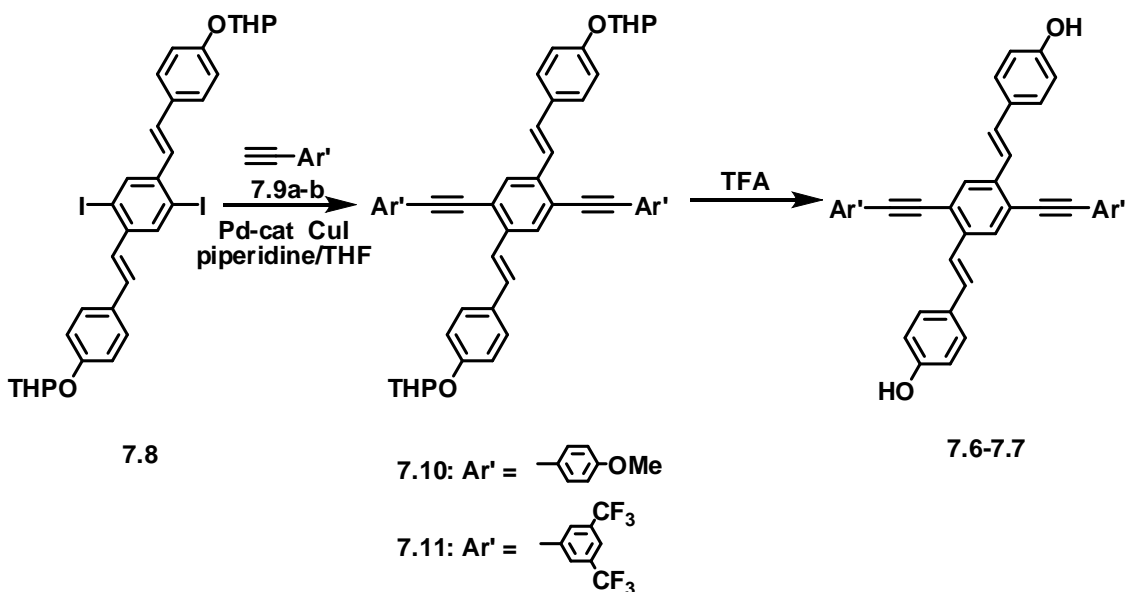
material (1.0 g) to 1,1,1,3,3,3-hexamethyldisilazane (1.0 g) in hexanes and stirring overnight. The capped, thiol functionalized material was then filtered, washed with hexanes, and dried under vacuum at 50 °C. Thermogravimetric analysis indicated a capping of 0.55 mmol silanols/g SiO<sub>2</sub>. Finally, the capped, thiol functionalized material (1.0 g) was oxidized by adding it to a solution of methanol (10 g) and 30% H<sub>2</sub>O<sub>2</sub> (20 g). The solution was stirred overnight and filtered. The solid material was washed with deionized water and dried under vacuum at 50 °C. Nitrogen physisorption experiments showed the material to have a BET surface area of 450 m<sup>2</sup>/g and a BJH adsorption pore diameter of 50 Å.

**Synthesis of amine functionalized SBA-15.** The amine functionalized SBA-15 was prepared similarly to reported literature procedures.<sup>11, 12</sup> 3-aminopropyltrimethoxysilane (1.0 g) was added to a solution of calcined SBA 15 (1.0 g) in toluene. The solution was stirred overnight and then filtered. The solid material was washed with copious amounts of toluene and hexanes and dried under vacuum at 50 °C. Thermogravimetric analysis indicated a loading of 1.7 mmol NH<sub>2</sub>/g SiO<sub>2</sub>. Nitrogen physisorption experiments showed the material to have a BET surface area of 180 m<sup>2</sup>/g and a BJH adsorption pore diameter of 38 Å.

**Silica material characterization.** Thermogravimetric analyses (TGA) were conducted on a Netzsch STA409. Samples were heated from 30 °C to 900 °C at 10 °C/min under an air blanket. The organic loading was determined from weight loss occurring between 200 °C and 750 °C. Nitrogen physisorption measurements were performed on a Micromeritics ASAP 2010 at 77 K. SBA-15 samples were degassed at 150 °C under vacuum overnight prior to analysis, and functionalized SBA-15 samples were degassed at

50 °C under vacuum overnight prior to analysis. Analysis of the porosity of the organic-inorganic hybrid materials before and after XF adsorption showed minimal loss of porosity, indicating that the XFs adsorbed primarily on the outer surface of the particles or in the pore mouths.

**Synthesis of XFs 7.6 and 7.7.** Scheme 7.2 outlines the general synthetic approach used to obtain XFs 7.6 and 7.7. From the previously reported distyrylbenzene 7.8,<sup>5</sup> Sonogashira coupling is utilized to affix the arylethynyl substituents. Incorporation of hydroxy functionality requires tetrahydropyran (THP) protection of 4-hydroxybenzaldehyde prior to the Horner olefination used to synthesize 7.8. Following the Sonogashira coupling, deprotection with trifluoroacetic acid readily yields 7.6 and 7.7 from their THP-protected precursors (7.10 and 7.11) in 88% and 91% respectively.



**Scheme 7.2.** Synthetic pathway providing access to XFs 7.6-7.7.

**Synthesis of compound 7.10.** **7.8** (0.335 g, 0.456 mmol) was combined with **7.9a**<sup>4</sup> (0.181 g, 1.37 mmol), (PPh<sub>3</sub>)<sub>2</sub>PdCl<sub>2</sub> (5 mg, 7.1 μmol), CuI (5 mg, 33 μmol) and dissolved in THF (50 mL) and piperidine (5 mL) in a nitrogen purged Schlenk flask. The solution was degassed, capped with a septum and allowed to stir at room temperature for 24 h. The product was extracted with dichloromethane (100 mL), washed three times with water (100 mL), dried with magnesium sulfate and reduced until a yellow powder formed, which was purified by recrystallization adding hot chloroform and an excess of hexanes, yielding a yellow powder. Yield: 77%. MP: 209 °C. IR: 2933, 2847, 2206, 1603, 1512, 1244, 1172, 1035, 961 cm<sup>-1</sup>. <sup>1</sup>H NMR (500 MHz, CDCl<sub>3</sub>): δ = 7.87 (s, 2H, Ar-H), 7.57 (d, 4H, Ar-H, J<sub>H,H</sub> = 9 Hz), 7.56 (d, 2H, C=C-H, J<sub>H,H</sub> = 16.5 Hz), 7.53 (d, 4H, Ar-H, J<sub>H,H</sub> = 9 Hz), 7.24 (d, 2H, C=C-H, J<sub>H,H</sub> = 16.5 Hz), 7.11 (d, d, 4H, Ar-H, J<sub>H,H</sub> = 9 Hz), 6.95 (d, 4H, Ar-H, J<sub>H,H</sub> = 9 Hz), 5.49 (s, 2H, α-C-H), 3.94 (m, 2H, ε-C-H), 3.88 (s, 6H, Ar-OMe), 3.66 (m, 2H, ε-C-H), 2.04 (m, 2H, β-C-H), 1.91 (m, 4H, γ-C-H) 1.71 (m, 4H, δ-C-H), 1.64 (m, 2H, β-C-H). <sup>13</sup>C NMR (500 MHz, CDCl<sub>3</sub>): δ = 160.24, 157.41, 137.54, 133.46, 131.45, 130.29, 128.80, 128.31, 124.42, 122.48, 117.13, 115.79, 114.57, 96.72, 95.75, 87.23, 62.47, 55.77, 30.74, 25.62, 19.15.

**Synthesis of compound 7.11.** **7.8** (0.450 g, 0.613 mmol) was combined with **7.9b**<sup>4</sup> (0.572 g, 1.84 mmol), (PPh<sub>3</sub>)<sub>2</sub>PdCl<sub>2</sub> (5 mg, 7.1 μmol), CuI (5 mg, 33 μmol), KOH (0.500 g, 8.90 mmol) and dissolved in piperidine (5 mL), EtOH (10 mL) and THF (25 mL) in a nitrogen purged Schlenk flask. The solution was degassed, capped with a septum and allowed to stir at room temperature for 24 h. The product was extracted with dichloromethane (100 mL), washed three times with water (100 mL), dried with magnesium sulfate and reduced until a yellow powder formed, which was purified by

chromotography eluting with 70:30 dichloromethane and hexanes, yielding 252 mg of yellow crystals. Yield: 53%. *MP*: 242 °C. *IR*: 2929, 2852, 2214, 1507, 1374, 1280, 1245, 1181, 1130  $\text{cm}^{-1}$ .  $^1\text{H NMR}$  (500 MHz,  $\text{CDCl}_3$ ):  $\delta$  = 8.05 (s, 4H, Ar-H), 7.94 (s, 2H, Ar-H), 7.90 (s, 2H, Ar-H), 7.53 (d, 2H, Ar-H,  $J_{\text{H,H}} = 8.5$  Hz), 7.49 (d, 2H, C=C-H,  $J_{\text{H,H}} = 16.5$  Hz), 7.27 (d, 2H, C=C-H,  $J_{\text{H,H}} = 16.5$  Hz), 7.11 (d, 4H, Ar-H,  $J_{\text{H,H}} = 8.5$  Hz), 5.49 (s, 2H,  $\alpha$ -C-H), 3.95 (m, 2H,  $\epsilon$ -C-H), 3.65 (m, 2H,  $\epsilon$ -C-H), 2.05 (m, 2H,  $\beta$ -CH), 1.91 (m, 4H,  $\gamma$ -C-H) 1.72 (m, 4H,  $\delta$ -C-H), 1.65 (m, 2H,  $\beta$ -C-H).  $^{13}\text{C NMR}$  (500 MHz,  $\text{CDCl}_3$ ):  $\delta$  = 157.87, 138.25, 132.65 (m), 131.76, 131.58, 130.80, 129.36, 128.41, 126.60, 125.78, 124.43 123.26, 122.26, 121.84, 117.24, 96.71, 92.82, 91.60, 62.53, 30.71, 25.59, 19.10

**Synthesis of XF 7.6. 7.10** (0.095 g, 0.166 mmol) was dissolved in dichloromethane (50 mL) and trifluoroacetic acid (2 mL) was added into a 100 mL round bottom flask kept in a dry ice acetone bath. The solution was allowed to stir at -78 °C for 2h and then thawed to room temperature. The reaction mixture was washed three times with water (100 mL), dried with magnesium sulfate, filtered and reduced until a dark green powder was formed. The powder was recrystallized by dissolving in hot chloroform and adding an excess amount of hexanes, yielding dark green crystals (83.6 mg). Yield: 88%. *MP*: 228 °C. *IR*: 3357, 2915, 2834, 2198, 1603, 1512, 1244, 1170, 958  $\text{cm}^{-1}$ .  $^1\text{H NMR}$  (500 MHz,  $\text{THF}-d_8$ ):  $\delta$  = 8.42 (s, 2H, Ar-OH), 7.88 (s, 2H, Ar-H), 7.53 (d, 4H, Ar-H,  $J_{\text{H,H}} = 9$  Hz), 7.51 (d, 2H, C=C-H,  $J_{\text{H,H}} = 16.5$  Hz), 7.44 (d, 4H, Ar-H,  $J_{\text{H,H}} = 9$  Hz), 7.29 (d, 2H, C=C-H,  $J_{\text{H,H}} = 16.5$  Hz), 6.96 (d, 4H, Ar-H,  $J_{\text{H,H}} = 8.5$  Hz), 6.75 (d, 4H, Ar-H,  $J_{\text{H,H}} = 8.5$  Hz), 3.82 (s, 6H, Ar-OMe).  $^{13}\text{C NMR}$  (500 MHz,  $\text{THF}-d_8$ ):  $\delta$  = 160.59, 158.42, 137.53, 133.13,

130.77, 129.30, 128.35, 128.30, 122.52, 122.33, 115.86, 115.67, 114.43, 95.51, 86.92, 54.99. *MS (EI, 70-SE) (C<sub>40</sub>H<sub>30</sub>O<sub>4</sub>):* m/z = 574.

**Synthesis of XF 7.7.** **7.11** (0.095 g, 0.166 mmol) was dissolved in dichloromethane (50 mL) and trifluoroacetic acid (2 mL) was added into a 100 mL round bottom flask kept in a dry ice acetone bath. The solution was allowed to stir at -78 °C for 2h and then thawed to room temperature. The reaction mixture was extracted with diethyl ether (100 mL), washed three times with water (100 mL), dried with magnesium sulfate, filtered and reduced until an orange powder was formed. The powder was recrystallized by dissolving in hot methanol, yielding yellow crystals (76.4 mg). Yield: 91%. *MP:*292 °C. *IR:* 3356, 2923, 2858, 2213, 1606, 1514, 1373, 1280, 1126 cm<sup>-1</sup>. *<sup>1</sup>H NMR (500 MHz, THF-d<sub>8</sub>):* δ = 8.53 (s, 2H, Ar-H), 8.30 (s, 4H, Ar-H), 8.12 (s, 2H, Ar-OH), 8.09 (s, 2H, Ar-H), 7.57 (d, 2H, C=C-H, J<sub>H,H</sub> = 16.5 Hz), 7.52 (d, 4H, Ar-H, J<sub>H,H</sub> = 8.5 Hz), 7.39 (d, 2H, C=C-H, J<sub>H,H</sub> = 16.5 Hz), 6.81 (d, 4H, Ar-H, J<sub>H,H</sub> = 8 Hz). *<sup>13</sup>C NMR (500 MHz, THF-d<sub>8</sub>):* δ = 157.03, 136.50, 130.18 (m), 127.17, 126.90, 126.67, 125.04, 124.19, 122.88, 120.71, 120.47, 119.81, 119.62, 118.58 114.07, 90.70, 89.65.

## 7.5. References and Notes

1. (a) Pond, S. J. K.; Tsutsumi, O.; Rumi, M.; Kwon, O.; Zojer, E.; Bredas, J. L.; Marder, S. R.; Perry, J. W. Metal-ion sensing fluorophores with large two-photon absorption cross sections: Aza-crown ether substituted donor-acceptor-donor distyryl benzenes. *J. Am. Chem. Soc.* **2004**, *126*, 9291-9306. (b) Wang, B.; Wasielewski, M. R. Design and synthesis of metal ion-recognition-induced conjugated polymers: An approach to metal ion sensory materials. *J. Am. Chem. Soc.* **1997**, *119*, 12-21. (c) Bangcuyo, C. G.; Rampey-Vaughn, M. E.; Quan, L. T.; Angel, S. M.; Smith, M. D.; Bunz, U. H. F. Quinoline-containing, conjugated poly(aryleneethynylene)s: Novel metal and H<sup>+</sup>-responsive materials. *Macromolecules* **2002**, *35*, 1563-1568. (d) Pautzsch, T.; Klemm, E. Ruthenium-chelating poly(heteroaryleneethynylene)s: Synthesis and properties. *Macromolecules* **2002**, *35*, 1569-1575. (e) Nielsen, M. B.; Diederich, F. Conjugated oligoenynes based on the diethynylethene unit. *Chem. Rev.* **2005**, *105*, 1837-1867. (f) Kivala, M.; Diederich, F. Acetylene-derived strong

- organic acceptors for planar and nonplanar push-pull chromophores. *Acc. Chem. Res.* **2009**, *42*, 235-248. (g) Iyer, P. K.; Beck, J. B.; Weder, C.; Rowan, S. J. Synthesis and optical properties of metallo-supramolecular polymers. *Chem. Commun.* **2005**, 319-321. (h) Knapton, D.; Rowan, S. J.; Weder, C. Synthesis and properties of metallo-supramolecular poly(*p*-phenylene ethynylene)s. *Macromolecules* **2006**, *39*, 651-657. (i) Beck, J. B.; Ineman, J. M.; Rowan, S. J. Metal/ligand-induced formation of metallo-supramolecular polymers. *Macromolecules* **2005**, *38*, 5060-5068.
2. (a) Rakow, N. A.; Suslick, K. S. A colorimetric sensor array for odour visualization. *Nature* **2000**, *406*, 710-713. (b) Rakow, N. A.; Sen, A.; Janzen, M. C.; Ponder, J. B.; Suslick, K. S. Molecular recognition and discrimination of amines with a colorimetric array. *Angew. Chem. Int. Ed.* **2005**, *44*, 4528-4532. (c) Suslick, K. S.; Rakow, N. A.; Sen, A. Colorimetric sensor arrays for molecular recognition. *Tetrahedron* **2004**, *60*, 11133-11138. (d) M. C. Janzen, J. B. Ponder, D. P. Bailey, C. K. Ingison, K. S. Suslick. *Anal. Chem.* **2006**, *78*, 3591-3600. (e) Zhang, C.; Suslick, K. S. A colorimetric sensor array for organics in water. *J. Am. Chem. Soc.* **2005**, *127*, 11548-11549. (f) Zhang, C.; Suslick, K. S. Colorimetric sensor array for soft drink analysis. *J. Agric. Food Chem.* **2007**, *55*, 237-242. (g) Zhang, C.; Bailey, D. P.; Suslick, K. S. Colorimetric sensor arrays for the analysis of beers: A feasibility study. *J. Agric. Food Chem.* **2006**, *54*, 4925-4931.
3. (a) Wilson, J. N.; Bunz, U. H. F. Switching of intermolecular charge-transfer in cruciforms: metal ion sensing. *J. Am. Chem. Soc.* **2005**, *127*, 4124-4125. (b) Zuccherro, A. J.; Wilson, J. N.; Bunz, U. H. F. Cruciforms as functional fluorophores: response to protons and selected metal ions. *J. Am. Chem. Soc.* **2006**, *128*, 11872-11881. (c) Tolosa, J.; Zuccherro, A. J.; Bunz, U. H. F. Water-soluble cruciforms: response to protons and selected metal ions. *J. Am. Chem. Soc.* **2008**, *130*, 6498-6506. (d) Brombosz, S. M.; Zuccherro, A. J.; Phillips, R. L.; Vazquez, D.; Wilson, A.; Bunz, U. H. F. Terpyridine-based cruciform-Zn<sup>2+</sup> complexes as anion-responsive fluorophores. *Org. Lett.* **2007**, *22*, 4519-4522. (e) Hauck, M.; Schönhaber, J.; Zuccherro, A. J.; Hardcastle, K. I.; Müller, T. J. J.; Bunz, U. H. F. Phenothiazine cruciforms: synthesis and metallochromic properties. *J. Org. Chem.* **2007**, *72*, 6714-6725. (f) Wilson, J. N.; Hardcastle, K. I.; Josowicz, M.; Bunz, U. H. F. Synthesis and electronic properties of bis-styryl substituted trimeric aryleneethynylenes. Comparison of cruciforms with *iso*-cruciforms. *Tetrahedron.* **2004**, *60*, 7157-7167. (g)
4. (a) Wilson, J. N.; Josowicz, M.; Wang, Y.; Bunz, U. H. F. Cruciform  $\pi$ -systems: hybrid phenylene-ethynylene/phenylene-vinylene oligomers. *Chem. Commun.* **2003**, 2962-2963. (b) Gerhardt, W. W.; Zuccherro, A. J.; Wilson, J. N.; South, C. R.; Bunz, U. H. F.; Weck, M. Supramolecular cruciforms. *Chem. Commun.* **2006**, 2141-2143. (c) Gerhardt, W. W.; Zuccherro, A. J.; South, C. R.; Bunz, U. H. F.; Weck, M. Controlling polymer properties through dynamic metal-ligand interactions: supramolecular cruciforms made easy. *Chem. Eur. J.* **2007**, *13*, 4467-4474.

5. (a) McGrier, P. L.; Solntsev, K. M.; Miao, S.; Tolbert, L. M.; Miranda, O. R.; Rotello, V. M.; Bunz, U. H. F. Hydroxycruciforms: amine-responsive fluorophores. *Chem. Eur. J.* **2008**, *14*, 4503-4510. (b) McGrier, P. L.; Solntsev, K. M.; Schönhaber, J.; Brombosz, S. M.; Tolbert, L. M.; Bunz, U. H. H. Hydroxy-cruciforms. *Chem. Commun.* **2007**, 2127–2129.
6. Zhao, D.; Feng, J.; Huo, Q.; Melosh, N.; Fredrickson, G. H.; Chmelka, B. F.; Stucky, G. D. Triblock copolymer syntheses of mesoporous silica with periodic 50 to 300 angstrom pores. *Science* **1998**, *279*, 548-552.
7. Zhao, D.; Huo, Q.; Feng, J.; Chmelka, B. F.; Stucky, G. D. Nonionic triblock and star diblock copolymer and oligomeric surfactant syntheses of highly ordered, hydrothermally stable, mesoporous silica structures. *J. Am. Chem. Soc.* **1998**, *120*, 6024-6036.
8. Yokoi, T.; Yoshitake, H.; Tatsumi, T. Synthesis of amino-functionalized MCM-41 via direct co-condensation and post-synthesis grafting methods using mono-, di- and tri-amino-organoalkoxysilanes. *J. Mater. Chem.* **2004**, *14*, 951-957.
9. (a) Van Rhijn, W. M.; De Vos, D. E.; Sels, B. F.; Bossaert, W. D. Sulfonic acid functionalised ordered mesoporous materials as catalysts for condensation and esterification reactions. *Chem. Commun.* **1998**, 317-318. (b) Wilson, B. C.; Jones, C. W. A recoverable, metal-free catalyst for the green polymerization of epsilon-caprolactone. *Macromolecules* **2004**, *37*, 9709-9714.
10. Anwander, R.; Nagl, I.; Widenmeyer, M.; Engelhardt, G.; Groeger, O.; Palm, C.; Röser, T. Surface characterization and functionalization of MCM-41 silicas via silazane silylation. *J. Phys. Chem. B* **2000**, *104*, 3532-3544.
11. Stein, A.; Melde, B. J.; Schroden, R. C. Hybrid inorganic-organic mesoporous silicates - Nanoscopic reactors coming of age. *Adv. Mater.* **2000**, *12*, 1403-1419.
12. Kallury, K. M. R.; Macdonald, P. M.; Thompson, M. Effect of surface-water and base catalysis on the silanization of silica by (aminopropyl)alkoxysilanes studied by x-ray photoelectron spectroscopy and C-13 cross-polarization magic-angle-spinning nuclear magnetic resonance. *Langmuir* **1994**, *10*, 492-499.

## CHAPTER 8

### Conclusions and Future Directions

#### 8.1. Summary and Conclusions

Moving beyond one-dimensional molecular wire-type fluorophores to two-dimensional ‘X-shaped’ materials provides access to conjugated architectures with unexpected and exciting properties.<sup>1</sup> 1,4-distyryl-2,5-bis(arylethynyl)benzenes represent a prime example of such a novel conjugated architecture. XFs have been employed as building blocks in supramolecular coordination assemblies<sup>2</sup> and used as switches in molecular electronics;<sup>3</sup> however, their FMO-architecture makes XFs particularly attractive for sensing applications as demonstrated in the case of metal ions<sup>4</sup> and amines.<sup>5</sup>

This thesis outlines our preliminary investigation of XFs, including their synthesis, investigation of their photophysical properties, and evaluation of their sensory responses. This began with the synthesis of a series of XFs and a thorough investigation of their properties (Chapter 2). To fully understand and appreciate the subtleties of these cruciform chromophores and lay the groundwork for future study, we synthesized a series of donor-, acceptor-, and donor-acceptor substituted XFs and examined their steady state photophysical properties. The observed photophysics can be explained by the position and the spatial arrangement of the FMOs in these fluorophores.

Analysis of the electronic structure of XFs revealed that donor and acceptor substitution results in compounds possessing FMOs spatially disjoint from one another; in these cases the HOMO and LUMO localize on the ‘orthogonal’ arms of XFs. Given this FMO arrangement, we rationalized that it should be possible to address HOMO and

LUMO independently upon introduction of a suitable analyte. To examine the responsivity achievable using this molecular architecture, we exposed a representative series of XFs – all of which are functional chromophores with incorporated basic nitrogens – to metal cations and acid. These studies demonstrated the ability of cross-conjugated XF cores to register substantial sensory responses.

Previous examinations of XFs as responsive fluorophores focused on compounds containing pyridine and/or dialkylamino groups as metal binding sites. With the lessons of Chapters 2 and 3 in hand, we proceeded to expand our library of XFs by incorporating phenothiazine heterocycles on the cruciform periphery. In Chapter 4, we report the synthesis, characterization, and metallochromic properties of five phenothiazine-substituted XFs.

In Chapter 5, we report the synthesis and characterization of a series of water soluble cruciforms containing phenylimidobisacetic acid, APTRA, or benzo-EDTA receptor units. We investigate the pH dependant photophysical properties of these XFs in absorption and emission and compare them with the photophysical properties of organosoluble alkylamino XFs. The results are surprising, as the presence of the anionic charges from the iminobisacetic acid units modulate the photophysical properties of these water soluble phores. In addition, a fundamental change in the interaction paradigm between fluorophores and metal cations is observed when going from alkylamino-functionalized XFs in organic solution to XFs in aqueous environments.

Chapter 6 outlines the use of pyridyl functionalized XFs as supramolecular synthons. We explored the assembly of two pyridyl functionalized XFs with ditopic bis-Pd or bis-Pt pincer complexes to generate four novel supramolecular coordination

polymers. Both the polymer and optical properties of these assemblies were fully characterized, revealing that variation of both XF and metal center generates assemblies with unique polymer and optical properties. The strategy employed herein allows for the design and synthesis of a class of novel functional organometallic polymers with predictable and tunable properties from a discrete set of monomers. Each component in this system is amenable to further functionalizations and modification giving us a virtually unlimited pool of monomers to investigate and exploit.

Finally, in Chapter 7 we employ functionalized mesoporous silica particles as scaffolds for the support of XFs. Whereas crystalline XFs frequently display weak emission in the solid state, immobilization of XFs in/on these particles yields solids which retain the highly fluorescent character of the parent cruciforms. We also demonstrate that the functionality integrated into the silica scaffold can be utilized to modulate the photophysical behavior of the incorporated dyes and that the resulting XF-silica hybrid materials display reactivity towards representative amines and organic acids which is modulated by the functionalization present on the silica scaffold.

These examinations reveal the rich potential of XFs. Substituent-induced FMO separation in XFs provides an opportunity to develop responsive materials; by spatially separating HOMO and LUMO on a conjugated framework, analytes can independently address these FMOs, translating electronic into spatial information; large changes in optical properties result upon analyte recognition. These studies provide a foundation for future access of functional responsive ratiometric cores and demonstrate the importance and unique potential of FMO-separated fluorophores.

More generally, our examination of XFs also highlights the importance of the serendipity in the development of functional materials. Frequently, the structural components and principles developed in diverse research areas serve as the inspiration for the construction of advanced materials. For example, Müllen's examination of the intramolecular [4+2]-cycloaddition reactions of small molecule phenylenevinylenes as well as Vollhardt's exploration of the cyclotrimerization of 1,2-diphenylethyne provided the synthetic underpinnings for the later examination of a wealth of remarkable polycyclic aromatic hydrocarbons.<sup>6</sup> Similarly, our inspiration for XFs architectures arose from earlier examinations of cross-conjugated polymers.

## **8.2. Current and Future Research Directions**

This thesis outlines the examination of a promising new conjugated architecture. The results presented herein speak to the future potential XF specifically; they show potential in materials science applications and exhibit vibrant sensory responses. In a broader sense, this work serves to highlight the potential of FMO-separated conjugated materials and underscore the importance of exploring new conjugated architectures. In light of these results, there are numerous possibilities for future studies (many of which are underway in our laboratories at the current time). A few current and future research directions are briefly outlined below.

### **8.2.1. Expanding the color palate: Achieving new fluorescence responses.**

Figure 8.1 schematically represents the possible responses for pair wise symmetrically substituted XFs. If both positive and negatively charged species are

allowed to interact with functionalized XFs, *eight different electronic responses (A-H) exhibiting unique emission colors will result*. In case **A**, coordination of an electron deficient analyte (i.e. a proton or metal cation) with the HOMO-branch of an XF stabilizes the HOMO, yielding a blue-shifted emission. In **B**, binding to the LUMO-containing axis of the XF elicits a red shift emission. These effects are reversed in cases **D** and **E** where an anion or an electron releasing species interacts with the XF; here, the HOMO or the LUMO are destabilized, leading to a red shift in **D** and an expected quenching in **E**. If all four termini are bound by an analyte (**C** and **F**), only slight net shifts should be visible. In principle, either a blue or a red shift could be observed; however, in the case of **C**, we observe a slight net blue shift, while in **F** we observe a significant red shift.

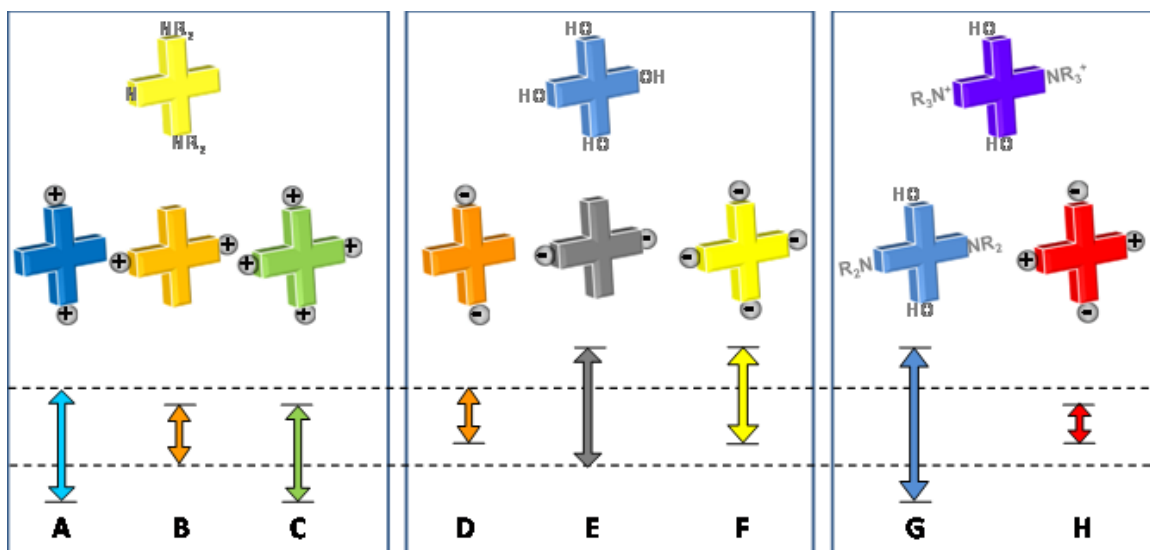


**Figure 8.1.** Schematic representation of the potential sensory responses elicited by the binding of cationic and/or anionic species to symmetrically-functionalized XFs. Eight different binding scenarios are conceivable resulting in five unique fluorescence responses. The dotted lines indicate the position of the frontier molecular orbitals of the parent XF, while the solid lines indicate the changes to the FMOs upon binding of a cation or an anion to the XF.

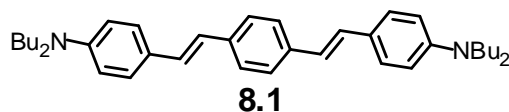
Thusfar, we have successfully constructed and explored cases **A-F**. Future efforts will examine further functionalization of the XF core to achieve the interesting and challenging cases **G** and **H**. In the case of **G**, addition of an electron releasing analyte to the HOMO branch and an electron deficient species to the LUMO branch, the LUMO is destabilized while the HOMO is stabilized and a dramatic blue shift is expected. In **H** we predict the opposite effect where LUMO is stabilized and HOMO is destabilized; emission in the red or near IR will result. These final examples will fully unveil the potential responses which can be registered using XFs. Additional responsive diversity can be introduced with XFs if the distyryl and arylolethynyl branches are asymmetrically substituted. These studies will serve to expand the library of sensory responses achievable using XF cores.

### **8.2.2. Photophysical behavior and sensory responses of distyrylbenzenes and arylolethynylbenzenes: Probing the properties of XF building blocks.<sup>7</sup>**

In order to better understand XF fluorophores, we have begun examining the photophysical behavior and sensory responses of functionalized distyrylbenzenes and arylolethynylbenzenes. In particular, we have begun a detailed examination of the acidochromicity and metallochromicity of bis(4-dibutylaminostyryl)benzene (**8.1**).

Previously, Perry et al. explored the metal binding capabilities of donor-acceptor substituted distyrylbenzenes as two-photon absorbing fluorophores for the detection of metal ions.<sup>8</sup> While these authors did not claim excited state ejection of the bound magnesium cations, they found large blue-shifts in absorption but only miniscule shifts in emission upon complexation with magnesium perchlorate in acetonitrile. These findings,

in combination with similar reports of excited state decomplexation in stilbene dyes, have relegated aminostyryl fluorophores to the sidelines in sensory development.



In contrast, most XFs exhibit spectacular shifts in absorption and emission upon treatment with TFA or metal cations.<sup>4</sup> This is a somewhat surprising result, as XFs are in effect distyrylbenzene derivatives; however, XFs as well seem to be unhampered by excited state decomplexation, which has thus far plagued other stilbene and distyrylbenzene-based fluorophores. This has led us to examine the sensory responses exhibited by **8.1**.

TFA as a model cation provides a uniquely valuable opportunity to quantitatively assess the sensory responses of **8.1**. A detailed study suggests a two-stage response in the absorption and emission of **8.1** upon exposure to TFA (Figure 8.2). Changes in absorption are accompanied by concomitant changes in emission, suggesting that excited state decomplexation will *not* hinder the performance of all amino-styryl based fluorophores if the charge-transfer nature of the excited-state is properly designed. Surprising is the finding of the enhanced photobasicity (or decreased photoacidity) of the monoprotonated species **1H**<sup>+</sup>, which flies in the face of common chemical reasoning and accentuates the dramatic differences between stilbenes, where cation ejection is observed and distyrylbenzenes, where other rules seem to apply.

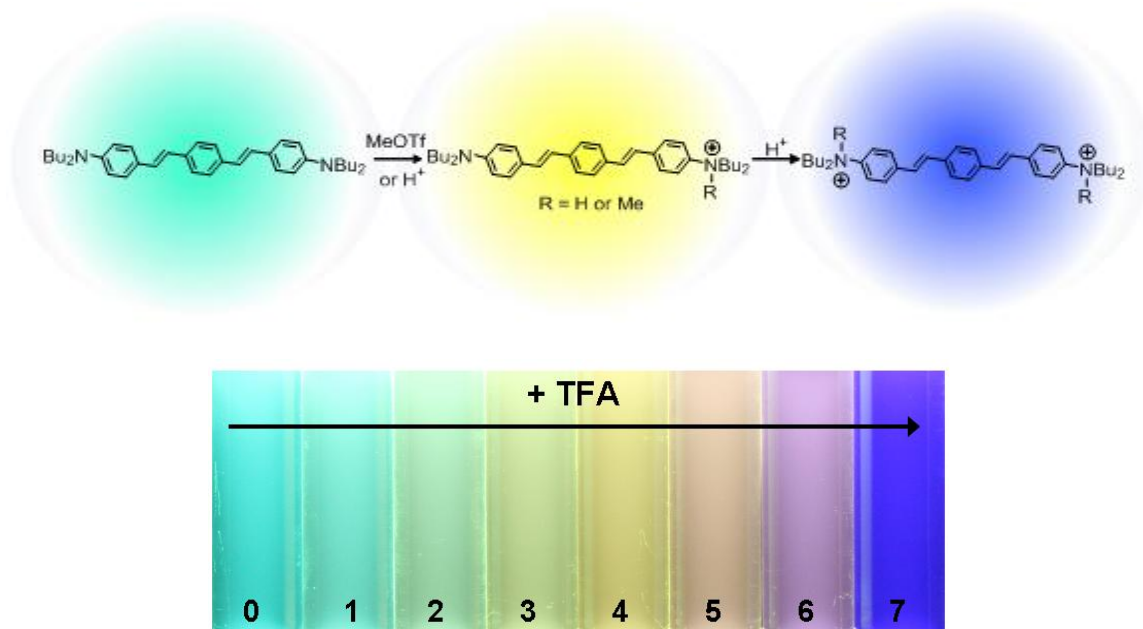


**Figure 8.2.** Top: Serial protonation or methylation of **8.1** and change in its emission color. Bottom: Fluorescence color of **8.1** after addition of TFA in dichloromethane. Samples contain increasing amounts of TFA and are illuminated under blacklight ( $\lambda_{\text{ex}} = 365 \text{ nm}$ ). Solutions were photographed using a Canon EOS Digital Camera equipped with an EFS 18-55mm lens. Spectra of solutions 0-7 are available in Reference 7a.

### 8.2.3. Incorporation of cross-conjugated motifs into water soluble PPEs: Towards red emissive PPEs.

PPEs are an attractive class of conjugated polymers.<sup>9</sup> Their attributes – including high stability and superb photophysical behavior – has led to their deployment in sensory schemes and material science applications. In particular, we have become interested in deploying PPEs in biosensing applications.<sup>10</sup>

PPEs typically possess vibrant blue/blue-green emissions in solution. Though suitable for many applications, the blue emission of PPEs is less than desirable for use in biosensing; the background fluorescence of biological samples limits the efficacy of typical PPEs in these applications. The performance of PPEs in biosensory applications



longer wavelength emitting PPEs. This approach shows potential for the development of next generation PPEs for biosensing applications.

### 8.3. References and Notes

1. (a) Opsitnick, E.; Lee, D. Two-dimensional electronic conjugation: statics and dynamics at structural domains beyond molecular wires. *Chem. Eur. J.* **2007**, *13*, 7040-7049. (b) Galbrecht, F.; Bönningel, T.; Bilge, A.; Scherf, U.; Farrell, T. Cruciform-Conjugated Oligomers. In *Functional Organic Materials – Syntheses, Strategies, and Applications*; Müller, T. J. J., Bunz, U. H. F., Eds.; Wiley-VCH: Heidelberg, **2007**, 83-118.
2. (a) Gerhardt, W. W.; Zuccherro, A. J.; Wilson, J. N.; South, C. R.; Bunz, U. H. F.; Weck, M. Supramolecular cruciforms. *Chem. Commun.* **2006**, 2141-2143. (b) Gerhardt, W. W.; Zuccherro, A. J.; South, C. R.; Bunz, U. H. F.; Weck, M. Controlling polymer properties through dynamic metal-ligand interactions: supramolecular cruciforms made easy. *Chem. Eur. J.* **2007**, *13*, 4467-4474.
3. Grunder, S.; Huber, R.; Horhoiu, V.; González, M. T.; Schönenberger, C.; Calame, M.; Mayor, M. New cruciform structures: towards coordination induced single molecule switches. *J. Org. Chem.* **1997**, *72*, 8337-8344.
4. (a) Wilson, J. N.; Bunz, U. H. F. Switching of intermolecular charge-transfer in cruciforms: metal ion sensing. *J. Am. Chem. Soc.* **2005**, *127*, 4124-4125. (b) Zuccherro, A. J.; Wilson, J. N.; Bunz, U. H. F. Cruciforms as functional fluorophores: response to protons and selected metal ions. *J. Am. Chem. Soc.* **2006**, *128*, 11872-11881. (c) Tolosa, J.; Zuccherro, A. J.; Bunz, U. H. F. Water-soluble cruciforms: response to protons and selected metal ions. *J. Am. Chem. Soc.* **2008**, *130*, 6498-6506. (d) Brombosz, S. M.; Zuccherro, A. J.; Phillips, R. L.; Vazquez, D.; Wilson, A.; Bunz, U. H. F. Terpyridine-based cruciform-Zn<sup>2+</sup> complexes as anion-responsive fluorophores. *Org. Lett.* **2007**, *22*, 4519-4522. (e) Hauck, M.; Schönhaber, J.; Zuccherro, A. J.; Hardcastle, K. I.; Müller, T. J. J.; Bunz, U. H. F. Phenothiazine cruciforms: synthesis and metallochromic properties. *J. Org. Chem.* **2007**, *72*, 6714-6725. (f) Wilson, J. N.; Hardcastle, K. I.; Josowicz, M.; Bunz, U. H. F. Synthesis and electronic properties of bis-styryl substituted trimeric aryleneethynyls. Comparison of cruciforms with *iso*-cruciforms. *Tetrahedron.* **2004**, *60*, 7157-7167. (g) Wilson, J. N.; Josowicz, M.; Wang, Y.; Bunz, U. H. F. Cruciform  $\pi$ -systems: hybrid phenylene-ethynylene/phenylene-vinylene oligomers. *Chem. Commun.* **2003**, 2962-2963.
5. (a) McGrier, P. L.; Solntsev, K. M.; Miao, S.; Tolbert, L. M.; Miranda, O. R.; Rotello, V. M.; Bunz, U. H. F. Hydroxycruciforms: amine-responsive fluorophores. *Chem. Eur. J.* **2008**, *14*, 4503-4510. (b) McGrier, P. L.; Solntsev, K. M.; Schönhaber, J.;

- Brombosz, S. M.; Tolbert, L. M.; Bunz, U. H. H. Hydroxy-cruciforms. *Chem. Commun.* **2007**, 2127–2129.
6. (a) Vollhardt, K. P. C. Transition-metal-catalyzed acetylene cyclizations in organic synthesis. *Acc. Chem. Res.* **1977**, *10*, 1-8. (b) Berresheim, A. J.; Müller, M.; Müllen, K. Polyphenylene nanostructures. *Chem. Rev.* **1999**, *99*, 1747-1785. (c) Watson, M. D.; Fechtenkötter, A.; Müllen, K. Big is beautiful – “Aromaticity” revisited from the viewpoint of macromolecular and supramolecular benzene chemistry. *Chem. Rev.* **2001**, *101*, 1267-1300.
  7. (a) Zuccherro, A. J.; Tolosa, J.; Tolbert, L. M.; Bunz, U. H. F. Bis(4-dibutylaminostyryl)benzene: Spectroscopic behavior upon protonation or methylation. *Chem. Eur. J.* In Press. (b) Brombosz, S. M.; Zuccherro, A. J.; McGrier, P. L.; Bunz, U. H. F. Acidochromicity of bisarylethynylbenzenes: Hydroxy versus dialkylamino substituents. *J. Org. Chem.* In Press.
  8. Pond, S. J. K.; Tsutsumi, O.; Rumi, M.; Kwon, O.; Zojer, E.; Bredas, J. L.; Marder, S. R.; Perry, J. W. Metal-ion sensing fluorophores with large two-photon absorption cross sections: Aza-crown ether substituted donor-acceptor-donor distyryl benzenes. *J. Am. Chem. Soc.* **2004**, *126*, 9291-9306.
  9. Bunz, U. H. F. Poly(aryleneethynylene)s: Syntheses, properties, structures, and applications. *Chem. Rev.* **2000**, *100*, 1605-1644.
  10. (a) Kim, I. B.; Wilson, J. N.; Bunz, U. H. F. Mannose-substituted PPEs detect lectins: A model for Ricin sensing. *Chem. Commun.* **2005**, 1273-1275. (b) Gaylord, B. S.; Heeger, A. J.; Bazan, G. C. DNA detection using water-soluble conjugated polymers and peptide nucleic acid probes. *Proc. Natl. Acad. Sci.* **2002**, *99*, 10954-10957. (c) Kumaraswamy, S.; Bergstedt, T.; Shi, X. B.; Rininsland, F.; Kushon, S.; Xia, W. S.; Ley, K.; Achyuthan, K.; McBranch, D.; Whitten, D. Fluorescent-conjugated polymer superquenching facilitates highly sensitive detection of proteases. *Proc. Natl. Acad. Sci.* **2004**, *101*, 7511-7515. (d) Disney, M. D.; Zheng, J.; Swager, T. M.; Seeberger, P. H. Detection of bacteria with carbohydrate-functionalized fluorescent polymers. *J. Am. Chem. Soc.* **2004**, *126*, 13343-13346. (e) Phillips, R. L.; Miranda, O. R.; You, C.-C.; Rotello, V. M.; Bunz, U. H. F. Rapid and efficient identification of bacteria using gold-nanoparticle-poly(*para*-phenyleneethynylene) constructs. *Angew. Chem. Int. Ed.* **2008**, *47*, 2590-2594.
  11. (a) Zhao, X.; Pinto, M. R.; Hardison, L. M.; Mwaura, J.; Müller, J.; Jiang, H.; Witker, D.; Kleiman, V. D.; Reynolds, J. R.; Schanze, K. S. Variable band gap poly(arylene ethynylene) conjugated polyelectrolytes. *Macromolecules* **2006**, *39*, 6355-6366. (b) Pinto, M. R.; Kristal, B. M.; Schanze, K. S. A water-soluble poly(phenylene ethynylene) with pendant phosphonate groups. Synthesis, photophysics, and layer-by-layer self-assembled films. *Langmuir*, **2003**, *19*, 6523-6533.

12. Wilson, J. N.; Windscheif, P. M.; Evans, U.; Myrick, M. L.; Bunz, U. H. F. Band gap engineering of poly(*p*-phenyleneethynylene)s: cross-conjugated PPE-PPV hybrids. *Macromolecules*. **2002**, *35*, 8681-8683.